CHAIR OF FERROUS METALLURGY
MONTANUNIVERSITAET LEOBEN

Characterization of Ferrous Burden Material for Use in Ironmaking Technologies

Dissertation

by

Dipl.-Ing. Martina B. Hanel

handed in at the Montanuniversitaet Leoben/Chair of Ferrous Metallurgy for attaining the degree of a Doctor of Metallurgical and Mining Sciences

under the supervision of

Univ.-Prof. Dipl.-Ing. Dr. tech. Johannes L. Schenk
(Chair of Ferrous Metallurgy, Montanuniversitaet Leoben)

peer-reviewed by

Univ.-Prof. Dipl.-Ing. Dr. mont. Helmut Antrekowitsch
(Chair of Non-Ferrous Metallurgy, Montanuniversitaet Leoben)

MONTAN
UNIVERSITÄT

Chair of Ferrous Metallurgy
Montanuniversitaet Leoben
Franz-Josef-Straße 18 – 8700 Leoben, Austria

Preface

At this point I wish to thank all the persons and institutions that have supported me, both financially and personally, during my time working at the Chair of Ferrous Metallurgy for making this work possible.

First and foremost I want to express my sincere gratitude to my advisor Prof. Dr. Johannes Schenk for the tremendous support during my research work, his expert guidance and for offering me the chance to prove and improve myself every time anew. Furthermore I wish to thank my co-advisor Prof. Dr. Helmut Antrekowitsch.

Special thanks are also due to Ass.-Prof. Dr. Heinrich Mali for his scientific support and sharing his expertise in a variety of areas, to Kurt Schiefer for his assistance in executing the experimental work and to the entire staff of the Chair of Ferrous Metallurgy for their contribution to this work. Finally, thanks to all my colleagues and friends who made this time so special and memorable.

This work has been performed within the K1-MET metallurgical competence center and is financially supported by the BMVIT, BMW_F and the provinces of Upper Austria, Styria and Tyrol. I also want to sincerely thank the industrial partners Siemens VAI Metals Technologies GmbH, voestalpine Stahl GmbH and voestalpine Stahl Donawitz GmbH for the excellent collaboration during the whole project and personally Franz Hauzenberger, Dipl.-Ing. Hugo Stocker and Dr. Christoph Thaler for their help.

Last but most importantly, I wish to thank my parents for their complete and unconditional support.

Affidavit

I declare in lieu of oath, that I wrote this thesis and performed the associated research work myself, using only literature cited in this volume.

Martina Hanel

13th June 2014

Abstract

The rising demand for steel products with the simultaneous search for a more cost-saving and environmentally friendly operation mode make the efficient use of raw materials a key factor of iron and steel making. In particular, different direct and smelting reduction process routes have been developed and further enhanced as an alternative to the predominant blast furnace route. Within the research work for this thesis, a variety of industrial scale processed lump ferrous burden materials were investigated with the objective of characterizing a raw material's appearance and nature, and subsequently describing its behaviour during the conversion to metallic iron. In order to characterize different ores, pellet brands and sinter samples, testing methodologies and procedures have been developed and executed in different lab scale testing facilities.

The description of a material's ability regarding oxygen release and mechanical performance during reduction was at first executed at standardized process conditions and subsequently at varying conditions related to industrial scale processes concerning temperature and gas composition. These results revealed the applicability of a material for different industrial scale process routes. It was discovered that the investigated lumpy materials behave differently as the testing conditions differ; especially pellet samples showed varying behaviour whereas sinter samples retained their good reducibility performance regardless of the testing conditions. However, the variation of single testing parameters revealed the influence of different gas oxidation potentials as well as the effect of hydrogen addition to the reducing gas mixture.

Combined with the morphological characterization and the structural evolution during reduction, the results contributed to finding a correlation between raw material properties and their performance during the reduction process. It was revealed that though the path of reduction – the gradual reduction of the different oxides proceeds in a layerlike manner from the outer part to the core – remains the same, hydrogen distinctly changes the formation of metallic iron. Moreover, the initial structural appearance of the material and the gangue amount and composition influence the final outcome, just as porosity and slag phase distribution are assumed to severely affect the reduction kinetics.

Kurzfassung

Durch die immer weiter steigende Nachfrage nach Stahlerzeugnissen und dem Ziel einer kostensparenden und umweltfreundlichen Prozessführung ist der effiziente Einsatz von Rohmaterialien ein Schlüsselfaktor der Eisen- und Stahlherstellung. Vor allem die verschiedenen Direktreduktionsverfahren als Alternative zum Hochofenprozess wurden ständig vorangetrieben. Für diese Arbeit wurden verschiedenartige eisenhaltige Einsatzmaterialien in stückiger Form untersucht mit dem Ziel einer Charakterisierung der Rohmaterialeigenschaften und weiterführend der Beschreibung des Verhaltens während der Umwandlung zu metallischem Eisen. Es wurde eine Versuchsmethodik entwickelt, um verschiede Stückerze, Pellet-Sorten und Sinter-Proben anhand von Laborversuchen zu untersuchen.

Dabei konnten Aussagen über die Fähigkeit eines Materials Sauerstoff abzubauen sowie der mechanischen Eigenschaften während des Reduktionsvorgangs unter verschiedenen industrienahen Bedingungen erfolgen. Die Ergebnisse wurden in einer ersten Versuchsserie mittels eines standardisierten Tests dargestellt und weiterführend wurden die Versuchsbedingungen bezüglich Gaszusammensetzung und Temperatur industrienahen Bedingungen angepasst. Die Ergebnisse konnten ein Bild bezüglich der Eignung der der verschiedenen Materialien für unterschiedliche Prozessführungen geben. Es zeigte sich, dass unter veränderten Versuchsbedingungen sich die Einsatzstoffe unterschiedlich Verhalten. Weiters konnte, unter Abwandlung einzelner Versuchsparameter, der Einfluss des Gasreduktionspotentials und des Wasserstoffgehalts der Gasmischung gezeigt werden.

Kombiniert mit der morphologischen Charakterisierung und einer Beschreibung der Gefügeentwicklung während des Reduktionsvorgangs konnten dazu beitragen einen Zusammenhang zwischen Rohmaterialeigenschaften und dem Verhalten während der Reduktion zu finden. Es zeigte sich, dass obwohl das Schema des Reduktionsfortschritts – die schrittweise Reduktion der verschiedenen Oxidationsstufen erfolgt in schalenartiger Form von außen nach innen – gleich bleibt, die Anwesenheit von Wasserstoff jedoch die Ausbildungsform des metallischen Eisens ändert. Ferner verändert die Ausgangsstruktur des Rohmaterials sowie die Schlackenmenge und –zusammensetzung das Reduktionsergebnis. Schließlich ist anzunehmen, dass Parameter wie Porosität und Schlackenverteilung die Reduktionskinetik stark beeinflussen.

Table of Contents

Preface I

Affidavit II

Abstract III

Kurzfassung IV

Table of Contents V

1 Introduction 1

1.1 Objective and Investigations of this Work 1

1.2 Facts and Figures about Iron and Steel Production Routes 2

2 Processing of Lump Ferrous Materials 6

2.1 Usage of Lump Burden Material – Process Routes 6

2.1.1 The Blast Furnace Process 6
2.1.2 Direct Reduction – The MIDREX®-Process 7
2.1.3 Smelting Reduction – The COREX®-Process 9

2.2 General Material Requirements for Lumpy Ferrous Burden 11

2.2.1 Chemical Properties 13
2.2.2 Physical and Mechanical Properties 15
2.2.3 Metallurgical Properties 16

3 Fundamentals of Iron Oxides and Agglomeration Processes 19

3.1 Mining and Beneficiation of Iron Minerals 20

3.2 Characterization of Naturally Occurring Iron Bearing Minerals 20

3.3 Pelletization Processes and Microstructure of Pellets 24

3.4 The Sintering Process and different Sinter Phases 25

4 Fundamentals of Reduction and Metallic Iron Formation 30

4.1 Thermodynamic Aspects of Iron Oxide Reduction 31
  4.1.1 Direct and Indirect Reduction of Iron Ores 33
  4.1.2 Gas Oxidation Degree (GOD) and the Baur-Glaessner Diagram 34
  4.1.3 Definition of Reduction Degree and Metallization Degree 36

4.2 Kinetic Aspects of Iron Oxide Reduction 37
  4.2.1 Simplification of the Reaction - Homogenous Reduction Reaction 37
  4.2.2 Heterogeneous Reduction Reaction – Selection of a Model 38
  4.2.3 Sequence of Reactions and Possible Rate Determining Steps 40
    4.2.3.1 Mass Transport Controlled (Gas Diffusion) 41
    4.2.3.2 Ash Diffusion Controlled (Pore Diffusion) 42
    4.2.3.3 Chemical Reaction Controlled (Boundary Layer Reaction) 44
    4.2.3.4 Summary and Graphical Illustration 45

4.3 Combination of Thermodynamics and Kinetics - Different Types of Metallic Iron Formation 46

5 Literature Review – Influence on Reducibility and Mechanical Properties 48

5.1 Influencing Factors Concerning Reducibility 48
  5.1.1 Temperature 49
  5.1.2 Gas Composition and Reducing Agent 50
  5.1.3 Size of the Particles 51
  5.1.4 Porosity and Pore Size Distribution 53
  5.1.5 Mineralogy 54
  5.1.6 Chemistry 55

5.2 Influencing Factors Concerning Mechanical Properties 56
  5.2.1 Reduction Rate 56
  5.2.2 Temperature and Gas Composition 57
  5.2.3 Porosity 58
  5.2.4 Chemical Composition and Mineralogy 58

5.3 State of the Art – Lab Scale Testing 61

6 Experimental Setup and Testing Facilities 63

6.1 Reducibility Testing - Vertical Reduction Aggregate 63

6.2 Other Lab Testing Equipment and Methods 66
  6.2.1 Rotating Tumbling Drum 66
  6.2.2 Light Microscopic Analysis and Scanning Electron Microscopy 66
  6.2.3 B.ET. – Specific Surface Area Measurement 67
  6.2.4 Chemical Analysis 68
  6.2.5 Definition and Determination of the Loss on Ignition (LOI) 68

7 Methodology of Testing 69

7.1 Calculation of the actual Reduction Degree (RD) 69

7.2 Reducibility Tests – Standardized Testing Procedure 71
  7.2.1 Description of the Evaluation – ISO 4695 71
  7.2.2 Modification of ISO 4695 72

7.3 Reducibility Tests – Industrial Scale Process Conditions 72
  7.3.1 Approach to the BF-Profile 73

7.3.2 BF-Profile – Effect of Initial and Final GOD 74
7.3.3 BF-Profile – Effect of Hydrogen 75
7.3.4 Approach to Direct and Smelting Reduction 76

7.4 Mechanical Testing Procedure 77

8 Raw Material Characterization 79

8.1 Chemical Analysis, LOI and B.E.T. 79

8.2 Morphological Characterization 82
8.2.1 Iron Ores 82
8.2.2 Pellet Brands 85
8.2.3 Sinter Samples 86

9 Experimental Results 89

9.1 Comparison of Different Raw Materials according to ISO 4695 89

9.2 Effect of Parameter Variation – Hematitic Ore 93
9.2.1 Variation of the ISO 4695 – Hydrogen and GOD Influence 93
9.2.2 BF-Profile – Effect of Initial and Final GOD 94
9.2.3 Influence of Pre-reduction Step 95
9.2.4 Effect of Hydrogen Addition on Reduction 96

9.3 Comparison of Different Raw Materials at Industrial Scale Process Conditions 97
9.3.1 Different Iron Ores 97
9.3.2 Pellet Brands 99
9.3.3 Sinter Samples 101

9.4 Mechanical Stability at Industrial Scale Conditions 103

9.5 Morphological Evolution during Reduction 104

9.6 Changes of Metallic Iron Formation – Effect of GOD and Hydrogen 108

9.7 Kinetic Interpretation of the Results 110

10 Conclusion and Outlook 114

10.1 Applicability of the materials in industrial scale processes 114

10.2 Outlook 118

11 References 121

A Appendix I

A-1 List of Figures I

A-2 List of Tables V

A-3 Publications VI

A-4 Curriculum Vitae VIII

1 Introduction

Due to the rising importance of the economic and environmental aspects of ironmaking, one major focus in research activities is the continuous improvement and optimization of prevailing and approved processes including blast furnace, direct and smelting reduction processes, respectively. Whereas the production of hot metal in the blast furnace, as the predominant process, is significantly dependent on metallurgical coke as a source of heat and as a reducing agent, there are increasing attempts to partly bypass this excessively costly and therefore negative circumstance through the usage of coal in the case of smelting reduction technologies and natural gas in the production of direct reduced iron (DRI) in direct reduction processes. In addition, the increasing use of by-products and the interconnected demands to decrease CO_2-emmisions further enhance the requirements on all input materials towards an outstanding spectrum of quality regarding chemical, physical and mechanical properties. Since all iron making routes (with the exception of melting scrap in electric arc furnaces) are based on the reduction of oxidic raw materials, a better understanding of the reaction as it happens inside the furnace or further inside the material, could lead to a variety of benefits. A more specific application of burden material would result in either enhancement of productivity, a more cost saving operation mode, fewer waste products, lower CO_2-emission or, in the best case, a combination of all of these together.

One significant part of this research work deals with the depiction of the behaviour regarding reducibility performance and the mechanical stability of lump iron oxide containing burden material either naturally occurring or artificially agglomerated by pelletizing and sintering. The ability to describe, depict or even predict a material's behaviour during the reducing procedure within an ironmaking process could make the decision regarding the use of a distinct sort of iron carrier easier and more precise and could further contribute to a more efficient, cost saving or environmentally friendly iron making operation.

1.1 Objective and Investigations of this Work

Within this research work raw materials of different origins and mineralogical and structural types were chosen for their best possible applicability in the diverse reduction aggregates of various ironmaking routes. The aim is to describe the materials behaviour during the reduction process and combine those results with the raw material´s properties in order to find a correlation between the raw material structure and the reduction performance.

A literature review concerning the influencing parameters on the reducibility and mechanical stability of a ferrous burden material has been performed, aimed at revealing the complex relationship between process conditions and raw material properties on reducibility and stability. In addition, the determination of appropriate testing conditions led to the use of testing conditions which are comparable both to industrial scale process conditions as well as to standardized testing conditions. In a first approach of characterization all available raw materials, namely different lump ores, pellet brands and sinter samples; were investigated regarding their morphological and structural phenotypes. Whereas ores consist of more or less simple morphology, the complexity increases when investigating pellets. Based on the fact that sinter samples contain up to 25 % additional slag forming phases the variety of different prevailing phases and the inhomogeneity of samples is even higher. Combining this with the fact that any industrial scale process has different conditions and parameters, means combining raw material characteristics and the performance of the material during reduction is a complex issue.

Nevertheless the test results gained are intended to reveal a generally valid correlation between the raw material structure, the standardized testing results and the industrial scale testing procedures. A possibility of predicting the materials behaviour without costly and time consuming testing methods could contribute to an optimized use of the ferrous burden material and enhance productivity. Furthermore, with a better understanding of what actually happens inside the material the pre-step, the preparation and fabrication of the ferrous burden, can be influenced in a way supporting the reduction facility.

1.2 Facts and Figures about Iron and Steel Production Routes

Though iron is the fourth most abundant element in the earth´s crust, metallic or native iron is hardly to be found due to its chemically unstable phenotype and tendency to oxidize at atmospheric conditions. Beginning in ancient times, mankind wanted to make use of the outstanding properties of processed iron and further steel; the hardness and strength, the ductility and finally the optical appearance. After the usage of meteoric iron as jewellery and religious items from 4000 B.C on, the first extraction of iron from oxidic ores is evidenced around 1200 B.C. From the Mediterranean Sea iron production started its triumphal procession, from simplest bloomery furnaces to today’s multitudinous highly developed and sophisticated iron and steel making routes.

In 2012, 1.9 billion tons of iron ore were mined and further processed to 1.1 billion tons of pig iron, 71.1 million tons of direct reduced iron and finally to 1.5 billion tons of crude steel [1,3,4]. Because of the continuous increase in world population and the rising demands brought about by modern standards of living, the need for iron and steel products continues to increase. Within the last 40 years the world crude steel production has almost tripled, from 595 million tons in 1970 up to 1547 million in 2012; in accordance, the average annual growth rate of crude steel production increased from 1.6 to 4.5 %/year when considering the 5-year periods 1970-75 and 2005-10, respectively [1,2]. The constant decrease of that ratio recorded during the first 4 years of the 20th century was caused by the increased recycling rate of steel scrap. A remarkable observation, however, is that since 1940 the hot metal to steel ratio has remained at an almost constant level at around 0.7 (c.f. Figure 1-1) [4].

Figure 1-1 depicts the development in production of crude steel, hot metal and DRI/HBI over the last 35 years. The steady increase of the world’s demand for steel can be seen in the increasing amounts of crude steel, hot metal or DRI/HBI. Still the DRI/HBI production is only a small part, with a portion of up to 70 % of the crude steel production by using the conventional blast furnace process route.

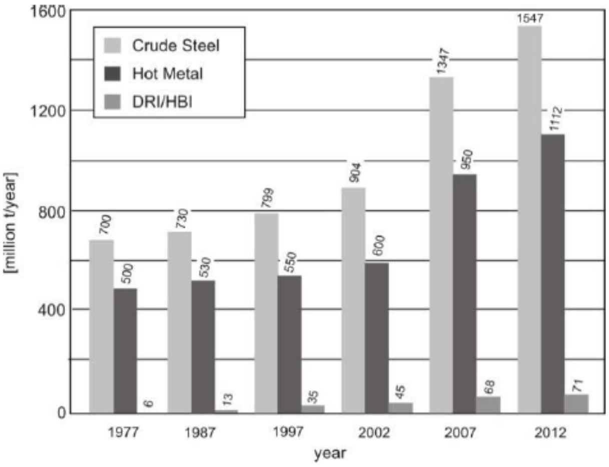

Figure 1-1: Worldwide production of crude steel, hot metal and DRI/HBI [1,2]

The need for metallurgical coal as a raw material for the subsequent coke making, coupled with the need for lumpy iron bearing burden material combined with decreasing availability of metallurgical coal and lump ores make the blast furnace an increasingly costly process. Those negative aspects can be juxtaposed, however, with simultaneous consideration of the local availability of different raw materials; several attempts have been made in the recent decades to produce of hot metal with at least the same quality as from the blast furnace. Depending on the appearance of the iron carrying material used, the type of the reducing agent and the type of furnace the different aggregates can be distinguished.

Generally speaking the production of crude steel as a product from the different raw materials, collectively denominated as “Primary Metallurgy”, can be classified into four major process routes [3–12]:

- The *blast furnace route* uses lump iron ore or ore agglomerates combined with coke as the reducing agent and fossil energy source for the production of the liquid hot metal from iron oxides. This is then further processed to liquid steel in a basic oxygen converter combined with the melting of scrap.
- From of the *direct reduction (DR) process route* direct reduced iron (DRI) or hot briquetted iron (HBI) is produced, mainly as an intermediate product for further processing in either electric furnaces for the production of crude steel or as scrap substitutes within the electric arc furnace. The term direct reduction refers to any process that reduces solid iron oxides to solid metallic iron avoiding the liquid phase; the produced iron sponge can then further be compacted.
- Similar to the blast furnace route, the *smelting reduction (SR) processes* produces liquid hot metal but without the usage of coke. In contrary to the blast furnace, where iron oxides are fully reduced and melted and then further converted to steel in the blast oxygen converter, a smelting reduction facility partly splits up the process of ore reduction and smelting into a two-stage operation mode whereas the subsequent steelmaking process remains the same.
- The method of steelmaking via *electric arc furnaces* is the only route that is not based on the reduction of iron oxides as iron carrier. The main raw material is scrap which is melted, potentially by adding some amounts of DRI or liquid iron, with electrical energy in electric arc furnaces.

Due to the fact that the electric arc furnace route uses few if any iron oxides as a raw material, this process will not be discussed in any further detail in the course this work. In Figure 1-2 a simplified summary of the blast furnace route as well as the alternative steelmaking routes is given by depicting the different (intermediate) products based on their oxygen and carbon contents. Starting from the basis of iron ore with an oxygen content of 30 (high grade ore) to 70 % (low grade ore) the oxygen decreases in each process stage. Due to the reducing conditions in the blast furnace the oxygen is totally removed and furthermore the liquid hot metal is significantly carburized. At the converter process the carbon content is decreases once again by means of oxygen blowing in order to obtain crude steel. The last small portions of oxygen (some

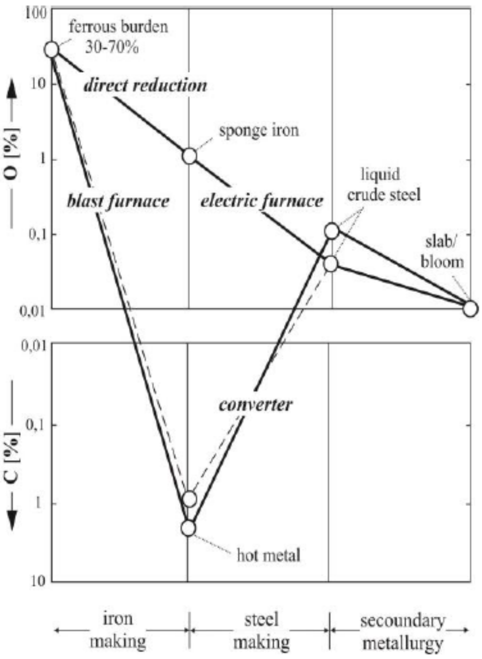

Figure 1-2: Iron making routes [3]

ppm) are removed in the aggregates within the steel plant (secondary metallurgy) before casting the steel to the final product. In contrary to the BF and also the smelting reduction route, within direct reduction aggregates some oxygen remains in the intermediate product to an extent of about 1 % during the reduction to sponge iron. At the downstream process stage, the melting in electric furnaces, the sponge iron is converted to a liquid product. By means of both, the DR and SR route, the final raw steel analysis is in good comparability to the blast furnace product and can subsequently be treated in the steel plant.

The process routes listed can further be sub-classified by different criterions. One significant distinguishing feature is the nature and form, particularly the grain size distribution, of the raw materials. On the one hand the iron carriers can be introduced to the process as fine ores, like in the FINEX® and FINMET®-process for example, or as lump burden material as for a majority of the processes. The reducing agent, as another characteristic parameter, can consist of solid carbon carriers, like coke or coal, or can be brought in the process as a gaseous reductant. Furthermore, the production pathway of the gaseous reducing agent can occur via different procedures, based either on coal (by coal gasification) or based on natural gas (via different ways of gas reforming). Depending on the raw materials, the principle and the design of the facilities can be different for direct reduction as well as smelting reduction production aggregates, comprising fluidized bed facilities, shaft furnaces, rotary kilns and hearth furnaces. The final step of the different smelting reduction processes, the smelting reduction part, can also be distinguished between 'In-bed' and 'In-bath' reactors. Since there are different methods for the preparation and production of the reducing gas, either coal gasification or gas reforming, the gas composition can differ in a wide range of the components CO, CO_2, H_2, H_2O, CH_4 and N_2.

In both cases, ore and reducing agent, the most carefully considered economic aspect is avoiding costly and complex agglomeration steps. By bringing fine iron ore into the process, a pelletization or sintering step can be circumvented. With the use of coal or even gaseous reductants the need of metallurgical coal for coking is diminishing and the coking process can be fully eliminated.

Table 1-I gives a short overview of the most used and important aggregates for the production of direct reduced iron and hot metal. For a more detailed description of these processes as well as other, unlisted, processes, numerous references are given.

Table 1-I: Classification of the most common iron making process routes:

	Iron carrier	Reducing agent	Furnace type	Short process description	Category	References
Blast Furnace	Lump ore, pellets, sinter	Lump coke (partly substituted by PCI, heavy oil, natural gas or waste plastics)	Shaft furnace	Counter current flow of gas and burden material, iron carriers and coke are alternately charged at the upper part of the furnace, hot air is introduced at the tuyere level, periodically tapping of hot metal and slag		[7,8,10, 13–17]
MIDREX®	Lump ore, pellets	Gas (gas reforming of natural gas)	Shaft furnace	Reduction in a shaft furnace, external production of the reduction gas via catalytic gas reforming of methane, DRI has high MD of > 90 %, operating pressure 1.8 bar, temperature maximum 800-900 °C	**Direct reduction**	[2,7,9,13,14,18–20]
HYL Process	Lump ore, pellets	Gas (gas reforming of natural gas)	Shaft furnace	Similar to MIDREX®, Reduction in a shaft furnace, external production of the reduction gas via water gas reforming of methane, MD of > 94 %, operating pressure 5-8 bar, maximum temperature 900 °C		[9,10,13,15,21–24]
FIOR/FINMET® **CICORED®**	Fine ore	Gas (gas reforming of natural gas)	Fluidized bed cascades	3-stages reduction in fluidized bed cascades, one fluidized bed for preheating, Operating temperatures 760-790 °C		[9,10,13,15,19,23–25]
SL/RN DRC	Lump ore, pellets, sinter	Lump coal	Rotary kiln	Reduction in rotary kiln furnaces, first part 'preheating zone' for heating up to 900-1100 °C, further 'metallization zone' for reduction and metallization to MD = 90 % at 1050-1100 °C		[4,5,9,10,13,15]
FASTMET	Fine ore/pellets	Pulverized coal	Rotary hearth furnace	Fine ore and pulverized coal are mixed, consolidated to pellets and fed to the rotary hearth furnace (one or two layers), heating rapidly to 1350 °C reduced via gas produced inside the pellets, MD > 90 %		[5,13,15,26–28]
COREX®	Lump ore, pellets, (sinter)	Gas (reduction shaft) Coal (melter gasifier)	Shaft furnace 'In Bed' smelting	2-stage process, at first pre-reduction of the burden material in a shaft furnace to DRI with gas from the melter gasifier (coal gasification) to a RD of 80 %, further reduction and melting of the DRI in the melter gasifier by coal	**Smelting reduction**	[7,10,23–25,29,30]
FINEX®	Fine ore	Gas (fluidized bed) Coal (melter gasifier)	Fluidized bed 'In Bed' smelting	2-stage process, at first pre-reduction of the fine burden material ina fluidized bed cascade to DRI with gas from the melter gasifier, further reduction and melting of the DRI in the melter gasifier by coal (similar to COREX®-process)		[4,5,10,11,30–32]
Hismelt®	Fine ore	Gas (fluidized bed) Coal (melter gasifier)	Fluidized bed 'In Bath' smelting	Fine ore is injected to the reaction vessel as well as coal and fluxes. Initially designed as horizontal unit, In-Bath process for carbon oxidation and post combustion with oxygen lance		[5,7,15,10,33,34]
DIOS	Fine ore	Gas (fluidized bed) Coal (melter gasifier)	Fluidized bed 'In Bath' smelting	Direct Iron Ore Smelting (DIOS) process, further development of Hismelt®, 2 fluidized bed reactors for preheating and pre-reduction with offgas from melter gasifier		[5,7,10,15,17,25]

2 Processing of Lump Ferrous Materials

Within this research work, the investigation is focused on the examination of lump burden material during reduction at conditions of various ironmaking processes at temperatures up to 1000 °C. To achieve this, ways and means of investigation methods and testing parameters had to be found that cover all the different process routes. The following section gives an overall insight into the three different process routes and furthermore the most prevailing and representative process of each route is described more in detail.

However, all efforts towards a cost and resource saving operation mode are based on an efficient use of raw materials. Since the process conditions for each process route and reduction facility are different, the requirements for lumpy ferrous materials differ. Therefore a summary of general aspects regarding material demands subsequently will be presented, and some special requirements for single processes considered.

2.1 Usage of Lump Burden Material – Process Routes

All processes described use the same kind of raw material, lump iron carriers, that in the end leads to either liquid hot metal or solid sponge iron, both as raw material for further processing. Even though the reduction of iron ore, hence the removal of oxygen, is fundamentally always the same, the path of reduction might differ widely. During the entire reduction process the raw material is confronted with different conditions in terms of gas composition, temperature range and a plurality of mechanical stresses and strains. As a consequence, the requirements on the material for an optimum operation process will differ for each process route. With a better understanding of the operation mode of these processes, their individual assets and drawbacks can be pointed out and as a result the special and unique demands on the raw materials will be highlighted.

2.1.1 The Blast Furnace Process

As the predominant reduction aggregate [3,6–8,14,17], the materials behaviour during the burden´s descent of the shaft (upper) part of the blast furnace is one key element of this research work, a schematic picture of a blast furnace is given in Figure 2-1.

Since the blast furnace is a shaft furnace working in counter current operation, the lump burden material is charged at the upper part of the furnace (blast furnace top) and moves downwards whereas the reducing gas, which is generated by the injection of hot blast through the tuyeres, flows upwards.

The main reactions are the step by step transformation of the solid iron oxide into liquid hot metal by gaseous carbon monoxide (indirect reduction) at the upper part of the furnace as well as by solid carbon (direct reduction) at the lower parts. The simultaneously formed liquid slag at the lower part acts as a collector for most other accompanying elements. During the descent of the charged burden (a mixture of lump iron carriers, fluxes and lump coke) a multitude of processes and reactions take place before the final tapping of the liquid hot metal and slag.

For the sake of simplicity the BF is divided from the top down into different reaction and temperature zones. Right after the charging the material is warmed up to 600 °C at the preheating zone and the mainly hematitic burden is first reduced to magnetite. During the further descent, the ferrous burden is reduced by gaseous CO during the indirect reduction zone and heated up to 1200 °C. From now on the material starts to liquefy, slag is formed and the oxidic burden is finally reduced to metallic iron and subsequently melts. As a result the burden is compressed by the weight of the upper burden material and without the intermediate coke layers the gas flow would no longer be ensured. At the final stages the molten iron droplets pass the liquid slag and are refined in terms of desulphurization before finally being collected in the hearth where the molten iron is periodically tapped.

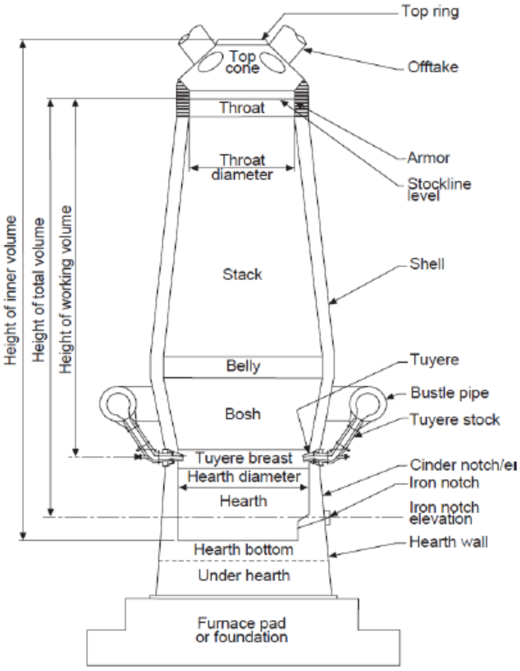

Figure 2-1: Schematic picture of a blast furnace [16]

Since coke is a costly fuel for the blast furnace operation, a lot of measures have been implemented in recent decades [35–38] aimed at decreasing the coke rate by adding alternative fuels. In particular the injection of (hydro-) carbon carriers such as pulverized coal (PCI), heavy oil, natural gas and waste plastics through the tuyeres has been proofed as a suitable method for decreasing the need for coke. The injection of waste plastics has the added benefit of resulting in an increased H_2-content of the reducing gas which is assumed to enhance the reduction rate [39–43]. Consequently, with the reduction of coke as a part of the burden material, the requirements for the ferrous charged material increase. Particularly the mechanical stability is in demand because of the lack of coke as a support column but also the reducibility and softening/dripping and melting properties have to be adapted to these new challenges.

2.1.2 Direct Reduction – The MIDREX®-Process

The term direct reduction refers to the reduction of iron ores to metallic iron, bypassing the molten phase [3,9–13]. The ore is reduced in its solid state by means of various gaseous reducing agents. The iron ore carriers used as a raw material can be either lump or fine and the variety of different processes that made it to industrial scale installation is remarkable (c.f. Figure 2-2). Nevertheless, the product of all those processes is direct reduced iron (DRI) with as high a metallization degree as possible, of usually between 85 to 97 %. The DRI can then further be processed to hot briquetted iron (HBI) by briquetting the sponge iron in its hot condition. The main application for both products, DRI and HBI, is the use as scrap substitution within electric arc furnaces. DRI can also be charged directly from the reduction aggregate into the subsequent steelmaking facility in the hot condition, though this implicates proximity of both plants. The reduction generally takes place at temperatures significantly lower than within the blast furnace, usually at a maximum temperature of about 1000 °C, to ensure that no softening, dipping or melting of the burden material occurs.

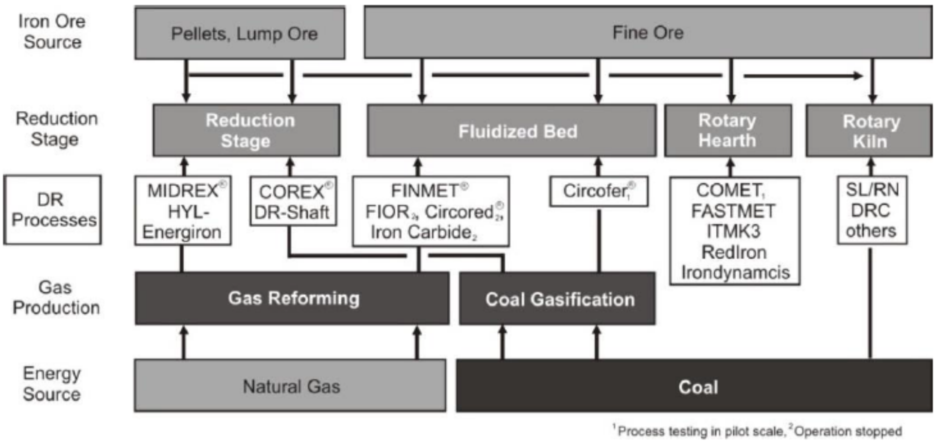
Iron Ore Source
Pellets, Lump Ore
Fine Ore
Reduction Stage
Reduction Stage
Fluidized Bed
Rotary Hearth
Rotary Kiln
DR Processes
MIDREX® HYL- Energiron
COREX® DR-Shaft
FINMET® FIOR₂, Circored®₂, Iron Carbide₂
Circofer¹
COMET₁ FASTMET ITMK3 RedIron Irondynamcis
SL/RN DRC others
Gas Production
Gas Reforming
Coal Gasification
Energy Source
Natural Gas
Coal
¹Process testing in pilot scale, ²Operation stopped

Figure 2-2: Classification of direct reduction processes [11]

The main driving force of the development of direct reduction processes is to avoid complex burden material preparation steps as are necessary for the blast furnace, particularly in terms of the carbon carrier. In addition, it is intended to have smaller and more flexible production units and to use regionally available raw materials by simultaneously producing a product of premium quality and decreasing environmental pollution and CO_2-emissions. Figure 2-2 gives a general overview of the prevailing direct reduction technologies; it illustrates the variety of different applied raw materials, reduction furnace geometries, energy sources and the possibilities of combining them, which are illustrated.

Since the MIDREX®-process is the most applied direct reduction process with a production capacity of 60.4 % of the worldwide produced 74.0 million tons of DRI [1,2], the production procedure and the three different operation units are outlined in Figure 2-3.
The MIDREX®-process is inherently simple, involving three major operation units: gas preheating, natural gas reforming, and iron ore reduction. Over the years, many other direct reduction process concepts have been devised with theoretically lower energy or iron ore consumptions and reduced operating and capital costs, but they proved too complex or expensive in practice, or just did not work. The simplicity of the MIDREX®-process is possible because it uses natural gas as a very clean fuel and agglomerated iron ore, which makes the processing relatively easy if the raw materials requirements are fulfilled.

The operation mode can be summarized as follows. The reduction shaft is charged at the upper part with the raw materials from the bunker system. During its descent through the shaft, the material is reduced in counter current flow with a reducing gas that is produced via catalytic natural gas reforming. After the reforming process the gas consists of 95 % H_2 + CO with a H_2/CO ratio of 1.5-1.6 and is introduced to the shaft at a temperature of 800 to 900 °C. The operational pressure of the shaft furnace is about 1.5 bar_{abs}. A part of the reducing gas leaving the top of the shaft furnace is mixed with natural gas and this gas mixture is fed via the heat recovery system to the catalytic gas reformer [10,31].

Generally speaking, a packed bed reactor with counter-current reactant flows is one of the most efficient means of processing materials. There are two primary reasons: since the reactor (shaft furnace) is filled completely with iron oxide, the volumetric productivity is very high. Additionally, a moving packed bed ensures that each particle of iron oxide experiences the same temperature profile, gas composition and residence time. But it is the same reason - the filling of the shaft furnace without any lump coal as a support column - which requires a very high mechanical stability and a narrow sized grain size distribution in order to guarantee a proper gas flow through the burden.

However, there is also a great deal of flexibility in sources of reductant and MIDREX®-plants can be designed to operate with hydrogen/carbon monoxide ratios of 0.5/1 up to 3.5/1 whereas most MIDREX®-plants use standard natural gas processed in the reformer to create a syngas with a ratio of 1.5/1.

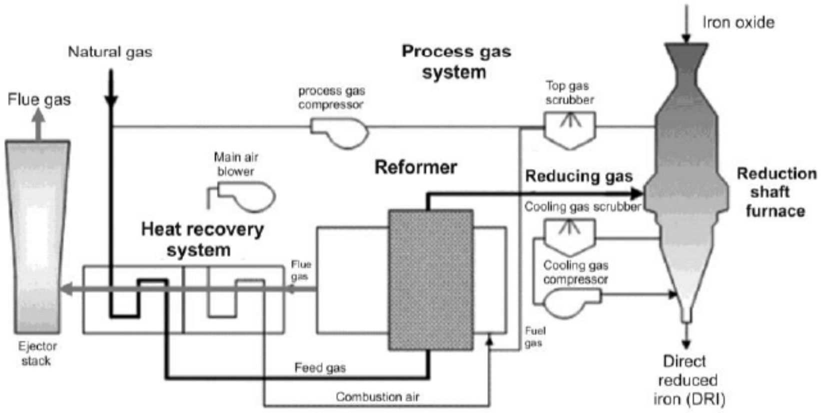
Iron oxide
Natural gas
Process gas system
Flue gas
process gas compressor
Top gas scrubber
Main air blower
Reformer
Reducing gas
Reduction shaft furnace
Heat recovery system
Cooling gas scrubber
Cooling gas compressor
Flue gas
Fuel gas
Ejector stack
Feed gas
Combustion air
Direct reduced iron (DRI)

Figure 2-3: Flow sheet of the MIDREX®-process [31]

For the sake of completeness, it is necessary to mention the second most common process, the HYL/Energion process. The HYL/Energion process is to some extent similar to the MIDREX®-process with the main differences of a higher operational pressure (5-8 bar) and an even higher hydrogen content of the reducing gas (typically 72 %). In 2012 about 16 % of the worldwide DRI production is produced with this process [2].

2.1.3 Smelting Reduction – The COREX®-Process

An characteristic all smelting reduction processes have in common is that they produce hot metal by gasification of coal as an energy source and reducing agent with the superordinate aim of “coke-free” hot metal production [3,5,7,9–12]. Smelting reduction can use coal directly and operate at high temperatures with liquid phase reactions. Though smelting reduction aggregates usually consist of two stages, a reduction and a smelting part, to some extent smelting reduction aggregates can be compared to a blast furnace process, primarily due to a comparability of the hot metal produced. However, the pre-reduction stage of a smelting reduction process can be seen as an integrated direct reduction process and therefore resembles other direct reduction processes. As shown in Figure 2-4, the diversity of different process routes almost as great as for direct reduction plants, a wide range of different combinations of (pre-) reduction stages and smelting stages is possible.

Another demand, besides creating a coke-free process, is to produce hot metal in smaller scale capacities and aggregates and hence to be more flexible. But at the same time there are attempts towards up-scaling facilities for lower investment costs by increasing their capacity.

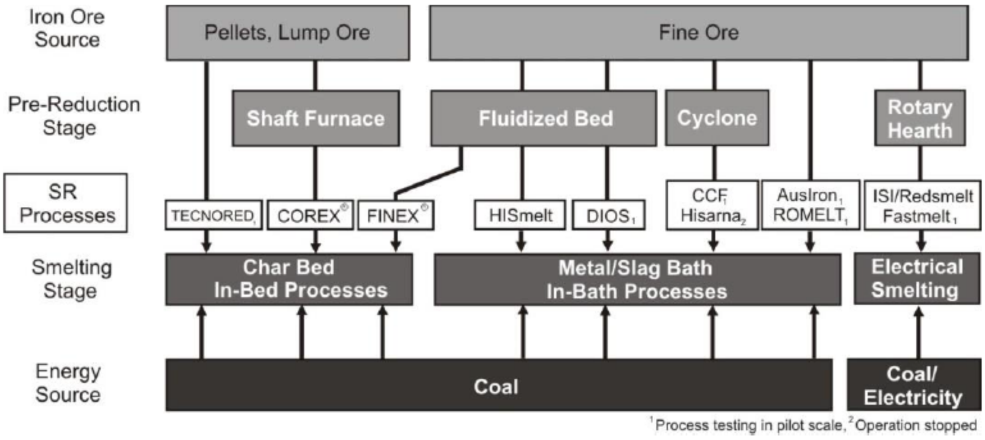
Iron Ore Source
Pellets, Lump Ore
Fine Ore
Pre-Reduction Stage
Shaft Furnace
Fluidized Bed
Cyclone
Rotary Hearth
SR Processes
TECNORED1
COREX®
FINEX®
HISmelt
DIOS1
CCF1 Hisarna2
AusIron1 ROMELT1
ISI/Redsmelt Fastmelt1
Smelting Stage
Char Bed In-Bed Processes
Metal/Slag Bath In-Bath Processes
Electrical Smelting
Energy Source
Coal
Coal/ Electricity
1Process testing in pilot scale, 2Operation stopped

Figure 2-4: Classification of smelting reduction process routes [11]

Besides the FINEX®-process with currently two operating plants, the COREX®-process is the predominant industrial scale applied smelting reduction facility, since there are seven operating plants worldwide. In contrary to most smelting reduction operation units, COREX®-plants are operated with lump charge; reducing gas is generated by gasifying lump coal and some coke (which may be of a quality of inferior to coking coal grade) with oxygen in the melter gasifier. The CO-rich gas generated in the melter gasifier is used for producing DRI from the ferrous burden in the shaft furnace arranged above, comparable to a MIDREX® or HYL/Energion process. After the pre-reduction in the shaft part, the generated direct reduced iron moves downwards to the melter gasifier. There the energy needed to complete the reduction of the DRI and to produce hot metal and slag is provided by partial combustion of the coal. The liquid products are tapped periodically.

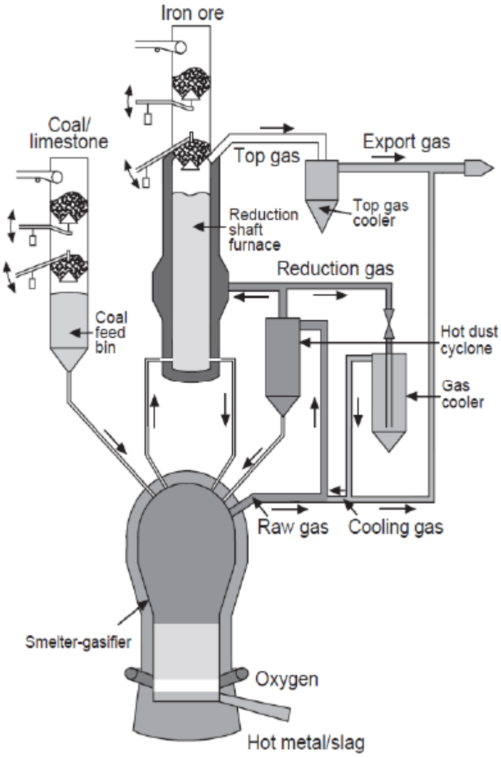
Iron ore
Coal/ limestone
Top gas
Export gas
Reduction shaft furnace
Top gas cooler
Reduction gas
Coal feed bin
Hot dust cyclone
Gas cooler
Raw gas
Cooling gas
Smelter-gasifier
Oxygen
Hot metal/slag

Figure 2-5: Schematic picture of the COREX®-process [9]

In Figure 2-5 the schematic flow sheet of a COREX®-plant is given. In contrary to the MIDREX® shaft furnace, the reducing gas from the melter gasifier has smaller amounts of hydrogen (around 20 %), the temperature is lower at 800-850 °C and the operation pressure is atmospheric. Also the metallization degree of the DRI is distinctly lower at about 75 % (= reduction degree of 80 %) due to the subsequent melting within the same process.

Notwithstanding all the advantageous aspects of alternative routes of ironmaking investigators reached the conclusion that neither one-stage nor two-stage processes can compete with the blast furnace on the amount of carbon consumption per ton of iron produced. Even under ideal conditions, carbon consumption in the two-stage process cannot be any lower that 650 kg/ton hot metal (operation data 900-1000 kg/ton) [10]. That value is still significantly higher than for blast-furnace with 550 kg/ton [44]. However, this statement has to be considered cautiously because on additional consideration of alternative carbon carriers the difference in carbon consumption is comparable between BF smelting reduction.

On comparing the total operating costs for BF and COREX® according to [10] it is given that $ 132.6 per ton of hot metal for BF and $ 128.04 for a COREX® plant (numbers date from 1995).

Once again, this statement has to be looked at critically since the majority of the costs strongly depend on the raw material costs. To this end, lower operational costs always have to be considered in combination with raw material costs.

All these facts; the energy consumption and the significantly higher demands on burden material concerning chemical, mechanical and metallurgical properties indicate that still all the alternative process routes remain an alternative choice for special local applications but cannot fully replace the blast furnace at this moment or in the near future. Investigations need to be continued with respect to all the possible process routes for further enhancing the DRI as well as hot metal production towards a more cost and energy saving operation.

2.2 General Material Requirements for Lumpy Ferrous Burden

All continuous or semi-continuous running processes rely on the availability of a raw material with uniform and homogeneous characteristics. Whatever parameter is considered; mechanical stability, grain size distribution, chemical composition or reducibility properties, the specified values have to be met within some range for guaranteeing a constant product quality. This circumstance can be solved starting with the ore deposit and the subsequent beneficiation and agglomeration process by appropriately mixing and blending the different components.

In Figure 2-6 different aspects of burden material distribution are given. In figure (a) the development of the burden distribution of blast furnace operation over the last 45 years is given, as an average value for Germany. It can be seen that the usage of pellets as a blast furnace feed material started between 1965 and 1975 and further increased until 1995, whereas sinter production stayed almost constant at 60 % over the whole decade.

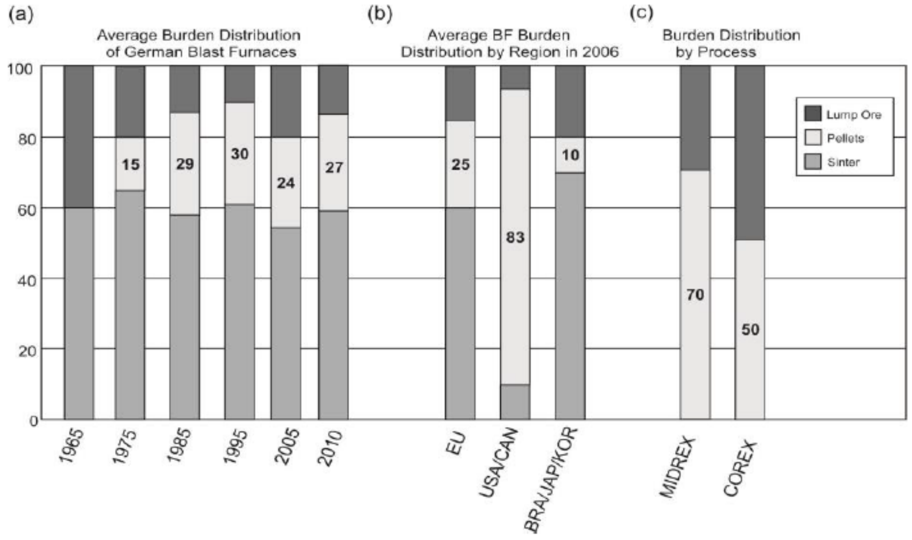

Figure 2-6: Different aspects of ferrous burden distribution [1,2,44,46]

This indicates that due to the lack of availability of appropriate lump iron ores, especially for Germany as a representative example for the rest of Europe, agglomeration processes are of significant importance. On the other hand, the extraordinary regional difference in the use of burden material can be seen in figure (b). The Austrian burden material distribution is in good accordance to the European average; the use of pellets makes up about 20 %. Due to the special situation of the Austrian steel producers regarding the Erzberg ore deposit as a main source of ferrous burden material, in particular the usage of sinter made from the domestic sideritic ore is up to 60 % at some blast furnaces. Otherwise the average of sinter is about 40 % [45].

For direct reduction facilities the burden material consists only of pellets and lump ore (c), for a MIDREX®-facility the portion of lump ore is about 30 % whereas for COREX®-facilities the portion depends on the capacity, from 60 % ore for 1 million tons per year capacity facility decreasing to 40 % ore for a facility with a capacity bigger than 1.5 million tons per year [45].

The three examples given for the production period of 2006 in Figure 2-6 (b) indicate that in contrast to the use of 60 % of sinter in Europe, USA /Canada´s portion is only 10 %. There pellets are the predominant burden material due to their large scale and accordingly modern pellet plants [47]. The Brazilian, Korean and Japanese statistical average in turn shows a usage of sinter by a three quarter majority and only 10 % pellets were used in 2006.

However, there are certain demands and criteria that have to be fulfilled for any burden material, independently of the process. Especially in terms of an economical and cost reducing operation, the total iron content can never be high enough whereas the amount of accompanying elements and gangue material can never be too low. But by considering the different operation routes and reduction facility designs, there are differences concerning the optimal raw material. Particularly between the blast furnace and direct reduction aggregates, due to the great differences in operation mode, there are differences in raw material demands.

Since the blast furnace is a counter current gas-solid reactor in which the solid charge material moves downwards while the hot reducing gas flows upwards, the best possible contact between the solids and the reducing gas is obtained with a most permeable burden, due to kinetic reasons [48,49]. This means not only a high rate of gas flow but also a uniform gas flow distribution without any channelling of the gas. Thereby the blast furnace coke rate can be decreased by increasing reduction rate. In order to prevent channelling effects and guarantee a uniform gas flow, the material´s size and the ability to retain this size despite the mechanical stresses and strains of both, hot and cold conditions, are of outstanding significance. Furthermore the ability to release the chemically bound oxygen quite easily, hence a good reducibility, is required for a cost optimized operation.

The leading direct and smelting reduction processes MIDREX® and COREX® also consist of shaft furnaces which rely on the counter current gas-solid contact, so the principles of restricted burden sizing are similar to that of the blast furnace. However, the fact that the ferrous burden material is the only solid material in these shaft furnaces gives even more weight to the mechanical materials characteristics. Furthermore, the subsequent melting within the electric furnace of the produced DRI and the use as a scrap substituent without any refining by slag, the requirements concerning the portion of gangue material is very restricted. Due to the reduction in the solid phase, and hence the absence of slag as a collector of the gangue and accompanying elements as in the blast furnace process, all the elements and oxides remain within the sponge iron and are further transported to the next processing stages.

From this description, the three major property categories can be derived for a proper characterization of ferrous burden material. First, the material has to meet chemical requirements concerning iron content, gangue amount and concomitant elements. If the ore's natural state does not meet those requirements for acceptable chemistry, it has to be upgraded by concentration processes. The mechanical properties comprise not only the material's grain size distribution but also the ability to maintain a given grain size during the transport and charging processes. At this point, the mechanical and physical properties refer to room temperature conditions. Last but not least the metallurgical properties have to be considered. As a consequence of the desirably low energy consumption that is needed to release the oxygen, the reducibility properties are of specific interest. Also some negative aspects that occur during the heating and reducing processes, namely degradation, swelling and sticking, are defined as part of the metallurgical properties.

The individual description of these three aspects will give an idea about the fact that there will never be any burden material that can fulfil all the requirements to a perfect extent. There is only the possibility of being within a certain range and finding a compromise solution for the overall term quality.

It has been noted, that all these requirements are generally valid for selling those burden materials on the world market. In special cases, for example when an ore deposit is located in close proximity to the steel plant, special and reasonable solutions can and will be found. As an example, the sideritic iron ore from the Erzberg deposit in Austria can never fulfil all (in fact hardly any) of the subsequent enumerated properties and can never keep up with globally traded products. Nevertheless the short and therefore cheap delivery distances and the special way of operating the blast furnace process at the nearby blast furnace redress those negative aspects and even constitute a selective advantage.

2.2.1 Chemical Properties

The first and most important requirement concerning the chemical properties is the iron content of the burden material. In order to ensure a most economical and cost efficient operation mode, the iron content is required to be high. In the case of ores and pellets: at least 60 % of total iron (Fe_{tot}) for blast furnace use, at a maximum possible iron content of 72 % for pure hematite. However, some literatures or specification sheets [50], stipulate 62 % or even 64 % as a minimum value. For the use in direct reduction facilities the iron content has to be even higher (65 % [59] or 67 % [10]). If lump iron ore has a lower iron concentration it cannot be used directly and has to be beneficiated and pre-treated to enrich the iron content. Concerning iron content the demands of the different (direct reduction) process routes are not much different; the more iron inside the material, the less energy is needed for melting, treating and/or separating the non-iron portions.

As a consequence of lower iron content, the amount of accompanying material increases, hence more and more slag is formed and gangue material is within the iron carrier. It is generally intended to keep this amount as low as possible, however for the blast furnace and smelting reduction processes slag and gangue contents are not as restricted as for direct reduction facilities. It can even be said that for direct reduction in a number of ways the chemistry is the key consideration [47].

Generally speaking, for all materials as well as processes, the free moisture content and the loss on ignition (LOI) as CO_2 and H_2O (bonded to the oxide of certain ore types) are undesirable in the feed material because of the extra heat load and increased volume of gas to be handled.

Within the direct reduction facility the primary process is the removal of oxygen without the presence of any molten or liquid phase. By comparison, whenever there is molten slag, the slag formed functions as a collector for a wide range of accompanying elements, oxides and minerals. With the absence of slag all the remaining constitutes stay with the direct reduced iron product but are even increased in concentration due to the removal of oxygen. The nature and level directly affects the process performance and economics of the subsequent electric furnace process or any other process in which the DRI is used.

Two broadly used parameters that reflect the characteristics of the burden material are the total gangue amount and the basicity value for (oxidic) slag components (B_4) and can be understood as the sum of the oxidic parts and the ratio of basic oxides to acidic oxides respectively.

$$gangue\ amount\ = SiO_2 + Al_2O_3 + CaO + MgO$$

and

$$B_4 = \frac{CaO + MgO}{SiO_2 + Al_2O_3}$$

whereby all minerals are understood as wt.-% known from the chemical analysis. As the chemical requirements for the BF and SR processes are more relaxed, the gangue content is restricted to a maximum content of 4 to max. 6 % for lump ores [13,47]. Further contents of up to 7 % are deemed to be acceptable [10]. The plurality of ores has acidic gangue (high SiO_2 contents) and needs to be fluxed during the different processes to attain the desired basicity of the slag. This, as the more acidic gangue material requires more basic flux material, is another reason for desirable low gangue contents.

Regarding pellets there is a distinction between acidic and basic pellets. For acidic pellets (basicity value of 0.1-0.4) the silica content is typically between 4-6 %, basic pellets (basicity around 0.9) have lower SiO_2 contents as this is beneficial in minimizing the total flux. For direct reduction the acid gangue, namely SiO_2 and Al_2O_3, should be as low as possible, preferably below 2 %, acceptable up to 3 %. The basic oxide (namely CaO and MgO) limit is below 3 %. In some cases it can partly displace the purchased flux in steelmaking.

Another criterion is the content of phosphorus and sulphur. As well as phosphorus, sulphur is generally known as a steel parasite and therefore, the contents of both should be as low as possible. Besides other drawbacks, sulphur can lead to red shortness during hot rolling or decreases the weldability of the steel product. In contrast to that, phosphorus increases the tendency of hot tearing and decreases the cold ductility. To avoid the very costly intensive step of desulphurization and dephosphorization by adding lime, care must be taken regarding the raw materials. In case of process routes using natural gas like MIDREX®, attention has to be given to the natural gas. In cases of higher sulphur amounts it has to be desulfurized. For direct reduction the limits are set preferably below 0.030 % for phosphorus and lower than 0.008 % for sulphur [10]. Further the alkali contents have to be considered as they cause swelling and degradation during the reduction process, so their content has to be as low as possible.

As one speciality of the COREX®-process it can be noted that it has a bleed of alkalis in the smelting off gas. This features the COREX®-process over the BF for consumption of high-alkali iron ores [10].

The chemistry for sinters as an artificially created agglomerate/product distinctly differs from the pellet and ore composition. Sinter is not a product that is sold on the world's market and those steel works using sinter for their blast furnace almost always have their own sinter plant onsite. In principle this enables the production of the optimum sinter that is required for each blast furnace, which, depending on a variety of parameters, can differ in a wide range. Concerning basicity, fuel reactant and the amount and composition of flux or slag formers the sintering plants operational parameters can be adapted regarding the furnace operation mode as well as the raw material availability. This makes a general description of sinter chemistry very difficult. Additionally there is the fact that at the sinter plant there is the possibility of using waste material and different portions of sieved fines as returned material; the sinter quality is not constant, and the predominant means of chemically characterizing sinter is to characterize the used raw materials. Since the main raw material of a sinter plant are iron ore fines with a size range of 0-10 mm (whereby 70 % > 0.2 mm) the requirements for these iron ore fines can be compared to the requirements of coarse iron ores regarding the Fe-content, LOI, sulphur, phosphorous and alkali contents. The final sinter as a burden material for the blast furnace typically has up to 25 % of gangue and slag formers, a basicity range between 0.5-3.5 and a FeO content of 5- 15 %. Other literature restricts FeO at a maximum of 6 % [47].

2.2.2 Physical and Mechanical Properties

The physical properties of iron ore feed material include size, size distribution, mechanical strength and degradation. The disintegration tendency, hence the tendency towards disintegration during the early stages of reduction, can either be seen as a physical property or as a metallurgical one, but in the majority of cases it is defined as a metallurgical property and therefore will be described later on. Physical property requirements differ depending on the reactor type, which can be shaft-like furnaces, rotary kilns or rotary hearths. All these (c.f. Table 1-I) use lump burden material. Nevertheless the description of the material demands within this work is considered to refer to the predominant facilities as BF, MIDREX® and COREX®.

It is of extraordinary interest that the burden material can provide adequate bed permeability for the reducing gases to flow upwards. Strength is required to support the weight of the bed and since the ferrous burden is the only solid material present within the direct or smelting reduction shaft furnace, the physical properties are economically important.

The performance of the shaft furnace, as well as the shaft part of the blast furnace, is adversely affected by increased amount of fines in two important ways: increased pressure resistance and impaired contact of the gaseous reductant and the solid burden. The latter will decrease the effective utilization of the reducing agent and the increased pressure will limit the maximum flow of the gas. The combined effect of these two will limit productivity and increase the reducing agent amount. In order to prevent those effects the grain size distribution has to be within a narrow range and very uniformly distributed. For the blast furnace process for lump ores, a minimum of size of 6 mm and a maximum of 10 % of material > 25 (or 30) mm is assumed to be the optimum for good burden permeability [10,47]. For the direct reduction in shaft furnaces the optimum grain size distribution is similar, within a range of a minimum of 90 % of material between > 6.3 and < 40 mm. Pellet size is even more important as excessively large pellets are more difficult to heat and reduce than lump ore [47]. Therefore the size range is distinctly smaller, from a minimum 85% (preferably 95 %) of 9 – 16 mm for MIDREX®-facilities and minimum 85 % of 10-16 mm for others. Also the fines amount is very restricted to a maximum 5 % of fines < 5 mm.

The term physical strength can be assumed as it determines its size and shape as it collides and abrades against other solids prior to the reduction process, hence the ability of keeping to the initial and required grain size. Starting from the ore deposit, the material has to withstand numerous dropping and falling processes. As a measure value for the material´s cold strength and therefore the ability to withstand all those mechanical stresses and strains, the tumbler strength and the compression strength are the values predominantly considered. The tumble index gives the portion of mass of material > 6.3 mm after the tumbling procedure as well as the portion of mass that is < 0.5 mm. For the generated fines, hence the portion -0.5 mm, a minimum requirement for direct reduction shaft furnace is given for pellets of 6 % [10] or 5 % [47] respectively. For lump ore 9 % of fines are named as sufficient and for sinter samples 70-80 % of material +6.3 mm after tumbling [10].

The cold compression strength, valid only for pellets, refers to a test where one single pellet is compressed between two even plates and the weight or force that is needed to crack the pellet is called cold compression strength and is given in either in N or kg. For direct reduction facilities the minimum value is 150 kg for MIDREX® but preferably above 250 kg. For BF pellets the average pellet should sustain 2500 N (= 256 kg) [10,47] whereas other literature deems 1780 N to be sufficient [51].

2.2.3 Metallurgical Properties

In order to improve plant operation results in terms of productivity and efficiency and, especially for direct reduction facilities, the ability to gain a sufficient metallization degree, the reducibility properties are one key factor for material characterization. The term metallurgical properties not only describes the material's ability to release oxygen, hence the reducibility index, but further includes other effects that occur during the reduction process. The tendency of degradation during the first stages of reduction in particular, the swelling behaviour of pellets or the sticking tendency belong to the category of metallurgical properties.

The lab scale tests for the reducibility index (RI) [52] as well as the reduction disintegration index (RDI) [53,54] are two broadly used tests when considering requirements for shaft furnaces. In order to do so, the tests are of static nature and are performed in a vertical reduction facility. Therefore a sample portion is heated up to a certain temperature (varies depending on the test) and at that point a reducing gas is purged through the sample for a certain time. During the testing procedure the weight loss is measured continuously and the value for RI can be calculated. Additionally, after a tumbling procedure, the RDI can be determined. It must be noted that these specially marked values are only one of several possible ways to describe the reducibility properties. Another common approach to describe the behaviour especially concerning the requirements of rotary kilns, is the so called “Linder-Test”. In this case the reduction vessel comprises of a rotating horizontal tube and hence the test is a dynamic one [55,56].

Generally, the reducibility (R) is described by the ratio of the mass of the initial oxygen within the sample potion ($m_{O,org}$) to the mass of the removed oxygen ($m_{O,rem}$) and is given in % according to

$$R[\%] = \frac{m_{O,org}\ [g]}{m_{O,rem}\ [g]} \times 100\ [\%]$$

The reducibility (R_{80} according to ISO 4695) itself is expressed by the time that is needed for the material to gain a reduction degree of 80 %. Another, even more common value for describing the reducibility properties is the reduction rate or reducibility index, $(dR/dt)_{40}$ given in [%/min] and calculated with

$$RI = \left(\frac{dR}{dt}\right)_{40} = \frac{33.6}{t_{60} - t_{30}}$$

whereby the t_{60} and t_{30} describe the time that is needed to gain a reduction degree of 60 % and 30 % respectively. What all reducibility indices have in common is the aim of reaching some distinct reduction degree (or metallization degree) within the shortest possible period of time. So, if there is any time value specified (e.g. R_{80} given in minutes), the best reducible material has the lowest value. For any given reduction rate (RI given in %/min) the value is preferably high, so a maximum change in reduction degree within a short period of time. For blast furnace burden, the reduction rate is to be within 1.4-1.6 %/min for sinter and at a minimum of 0.8 for pellets [57,47]. For DR processes these values are higher meaning that the material requirements for DR are distinctly higher. Another important parameter, in particular for direct reduction processes, is the metallization degree, which refers to the ratio of metallic iron to total iron after reduction for a certain time. This metallization degree is preferably at least 90 %, whereby depending on the test, the testing parameters vary.

The low temperature disintegration tendency (RDI) is a phenomenon occurring at the earlier stages of reduction due to the volumetric increase of the material during the transformation from hematite to magnetite. Therefore the test takes place at 500 and 550 °C respectively and after the tumbling procedures the material is sieved and the different values can be calculated. With the given equations, the disintegration tendency ($RDI_{+6.3}$) and the abrasion tendency

($RDI_{-0.5}$) can be calculated, whereby m_0 is the initial mass prior to tumbling; m_1, m_2, m_3 are the mass portions of the +6.3, +3.15 and +0.5 mm fractions, respectively. Hence, $RDI_{+6.3}$ refers to the percentage of mass, that remains larger than 6.3 mm and $RDI_{-0.5}$ refers to the percentage of mass of the sample portion that is smaller than 0.5 mm after tumbling.

$$RDI_{+6.3} = \frac{m_1}{m_0} \times 100\ [\%] \qquad RDI_{-0.5} = \frac{m_0 - (m_1 + m_2 + m_3)}{m_0}$$

The low temperature disintegration phenomenon is associated with sinter in particular but some pellet brands also tend to disintegrate. For direct reduction plants a disintegration tendency of > 88 % and an abrasion index of < 10 % are required. Although the range of different (standardized) testing procedures is broad, for the interpretation of most mechanical testing results and parameters the following guideline is valid. Whenever there is "+" in front of the numerical value (e.g. $RDI_{+6.3}$), it can be understood as the mass of the sample portion retained on the (in this case 6.3 mm) sieve in proportion to the initial sample mass. This value is preferably high, in contrast to a minus "-". This indicates that the higher the value, the more mass portion has disintegrated to the smaller grain size (and therefore more fines are created) and this value should be as low as possible. For testing under dynamic conditions (Linder-Test) the values are named LTD instead of RDI.

For the sake of completeness, it should be mentioned two more phenomena that possibly occur during reduction: swelling and sticking. Swelling is especially associated with pellets (although all other materials do swell to some extent) and describes a volumetric expansion upon heating. An increase in volume of < 10 % is favourable; values of > 20 % should be avoided [57,47]. This phenomenon is known to be promoted by alkalis [10]. Some pellets tend towards "catastrophic swelling" which is generally assumed from a volume increase of < 25 %, but can gain up to 732 % (especially associated with high sulphur contents) [58]. Sticking, in contrast to swelling, mainly occurs during the reduction of fine ores. Sticking describes the agglutination, or also agglomeration of reduced iron ore particles above 610 °C [13]. Within fluidized beds this can be harmful because of channelling effects or even the breakdown of the fluidized bed.

In Table 2-I the requirements for chemical, physical and metallurgical properties are summarized subdivided into the three different process routes.

Table 2-I: Guidelines for the requirements of different burden material for different process routes

				Blast Furnace	**DR-Grade** (MIXDREX®-specification)	**SR-Grade** (COREX®-specification)
Parameter	**Unit**			**Chemical Properties**		
Iron content	[%]			Ore > 60 [59], > 64 [50] Pellets > 60 [59], > 62 [50]	Ore/Pellets > 65 [59], 67 [10]	Ore/Pellets > 60 (min. 55), > 64 [60] Sinter > 50 (min. 45) [59]
Gangue/slag content	[%]			Ore and pellets 4 – 7 Sinter (FeO) < 6	Ore and Pellets < 5 [10]	Ore and Pellets 4 – 7, <5 [60]
S and P content	[%]			P < 0.030 and S < 0.008; S < 0.01 [10] Pellets < 0.026 (SO_4), Ore < 0.04 (SO_4) [50] Pellets < 0.06 (P_2O_5), Ore < 0.04 (P_2O_5) [50]		P < 0.05, S < 0.01 [59]
Alkalis	[%]			as low as possible; < 0.2 Na_2O+K_2O [59] < 0.25 [50]		
Moisture/LOI	[%]			as low as possible		
				Physical Properties		
Grain size distribution	[mm]	Ore Pellets Sinter		6-30[47], 6.3-31.5 (85%)[50] 6.3-30[47]; 8-12.5 (80%)[57]; 8-15 (85%) [50] 20-30[47]; 10-50 (80%) [57]; Fines < 2 %[61]	10 – 30 (70%)[47] 9 – 16 (85%) Fines < 5% < 5 -----	6 – 30 (70%) [47]; 10-25 [59] 6 – 30 (85%)[47]; 8-16 [59] 6 – 45 [47]; 10-32 (< 50%) [59]
Tumbling Index (ISO 3271)	[%]	Ore Pellets Sinter	+ 6.3 mm	> 80 [57] > 95 [57,61] 70-80 [57,61]	85 [10] 92 [10] ----	85 – 95 [47] 92 – 98 [47]; > 95 [60] ----
	[%]	Ore Pellets Sinter	- 0.5 mm [57]	< 10 < 5, < 5 [61] ---	< 10 < 6 ---	5 – 10 1 – 5 ---
Cold compression strength	[kg]		Only Pellets	> 256 [10,57]; > 200 [50]	> 150 [10,57]	> 250 [10,57]; >225 [60]
				Metallurgical Properties		
Reducibility Index (RI)	[%/min]	Ore Pellets Sinter:		ISO 4695 > 1.0 [10,57] > 0.8 – 1.2 [10,57], > 0.5 [61] > 1.4 – 1.6 [10,57], > 0.7 [61]		ISO 12258 Ore: > 0.40 [59] Pellets > 0.42 [59,60] ---
$RDI_{+6.3}$ (ISO 4696-2)	[%]	Ore Pellets Sinter	+6.3 mm	>70 [10] $LDT_{+6.3}$ > 60 [57], > 80 [61] ---	> 70 [10] > 88 [10] ---	> 80 > 90 [59,60] > 85
$RDI_{-0.5}$/$LDT_{-0.5}$ (ISO 4696-2 /LinderTest)	[%]	Ore Pellets Sinter	-0.5 mm	$LDT_{-0.5}$ < 15 [57] < 10 [61] ---	< 10 < 10 ---	--- < 4 [60] ---
$RDI_{-3.15}$ (ISO 4696-1)	[%]		-3.5 mm	Sinter < 33 [47], < 20 [61]		

Poveromo has noted that "*a good agglomerate for the blast furnace should have an iron content of 60 % or more, a minimum of undesirable constituents, a minimum of material less than 6 mm in size, and a minimum of material larger than 25 mm. The agglomerate should be strong enough to withstand degradation during stockpiling, handling and transportation to the furnace so as to arrive at the furnace skip containing a minimum 85-95 % of material with a size greater than 6 mm. In addition the agglomerate must be able to withstand high temperature and the degradation forces within the furnace without slumping or decrepitating. The agglomerate should be reasonably reducible so it can reduce at a satisfactory high rate in the blast furnace*" [47].

3 Fundamentals of Iron Oxides and Agglomeration Processes

Iron ore is the most important raw material required for iron and steel making in terms of tonnage and economical value. Due to the increasing demand worldwide for iron and steel products and therefore the rising demand on iron carrying raw materials, the depletion of natural raw materials and fuel is becoming an increasingly important concern that is even partly impeding the growth of metallurgy. The availability of lump iron carrying raw materials, whether of natural origin or artificially agglomerated, of sufficient quality is becoming an increasingly important aspect of ironmaking. Moreover, the fact that the process throughput is continuously increasing by means of constant improvement of the processes operation, further challenges a raw material's performance in every possible way.

Generally speaking, the term iron ore refers to that part of the total iron in the earth´s crust that is available to industry, both economically and spatially. Every iron ore deposit consists of a variety of different iron carrying materials as well as other oxidic, sulphidic or carbonatic compounds. In addition, the mineralogical and petrographic structure of the minerals can differ considerably.

Due in particular to the specific demands on the raw materials for the production of direct reduced iron, and also to the limited availability of naturally occurring high grade ores that can directly be used in a reduction facility, diverse beneficiation and pre-treatment steps have to be undertaken.

Nevertheless, all iron carriers used are comprised of the same few iron bearing minerals. Every natural ore is a compound of these iron minerals, but of different grain sizes, morphological appearance and portion, and of a variety of other gangue minerals. In order to characterize the different lump burden materials regarding a correlation between microstructure and reducibility behaviour, the different potentially appearing phases are summarized as well as the agglomeration step as a pre-treatment and origin of artificially generated slag phases.

3.1 Mining and Beneficiation of Iron Minerals

After the discovery of an iron ore deposit, the first step on a very long road towards the final product hot metal is the mining of the ore. The two possible methods of mining, open pit mining (which is distinctly lower in mining costs usually) and underground mining are described elsewhere [62,63]. Prior to the beneficiation process the natural ore can be graded by the producers to meet furnace demands for particular uniform chemical composition and structure. Recognition of the importance of uniformity has led to the use of elaborate ore blending facilities.

In the next step the iron containing ore is *beneficiated,* mainly at the iron ore deposit. "*The term beneficiation in regard to iron ores encompasses all of the methods used to process ore to improve its chemical, physical or metallurgical characteristics in ways that will make it more desirable feed for ironmaking furnaces*" [47].

Thereby the separation of the iron ore from the worthless gangue material or possibly detrimental elements or minerals (sulphurous for example) takes place by means of numerous mechanical methods including crushing, screening or jigging. Further methods using different physical properties of ore and gangue materials like magnetic separation, heavy media separation or spiral concentration may be used. The methods actually applied depend on the classification of the iron ore; altogether three different categories are compatible for most iron ores [47,62–64].

- *High grade or merchant ores*, for direct shipping. The iron content is high enough (> 60 % or 67 % respectively) to be charged directly to a blast furnace or another reduction facility and require only crushing screening and blending because of the required size range of 6-30 mm and a highly uniform product.
- Associated *low grade merchant ores* which appear mainly around the high grade ores and can be mined concurrently. Only minor upgrading by washing or gravity separation technique is necessary to increase the iron content. The natural ore forming process produces layers of relatively pure iron oxides interbedded with partially decomposed silica rich layers, also called banded iron formation (BIF). If the silica layers have been completely decomposed, the ore can easily be upgraded by processing techniques whereas ores in which the silica-rich layers have not been weathered as intensively, have to be broken by crushing and further upgraded by e.g. spiral concentrators.
- The *under-laying iron formations,* from which most of the deposits have been derived; a hard, dense, low grade material that requires extensive crushing, grinding and concentration to produce an acceptable concentrate. Those primary ores contain only 25-35 % recoverable iron, but nevertheless they provide almost unlimited iron unit reserves. To produce a final product that is uniform in chemical and physical properties blending of the crude ore is indispensable in producing an acceptable concentrate.

Depending on the actual situation of the deposit every ore has quite different processing requirements and the appropriate beneficiation steps have been considered with care.

3.2 Characterization of Naturally Occurring Iron Bearing Minerals

A large number of minerals contain iron; however only a few are used commercially as sources for ironmaking. All globally traded iron ore consists of various different petrographical structures. Depending on the geological and reduction history, every ore shows different structural characteristics (i.e. shape and size of crystals, specific surface, petrographic structures etc,). The mineralogy of most commonly traded and used iron ores is rather simple and can be divided into hematitic, magnetitic, limonitic or sideritic ores. Nevertheless, there is never only one single phase present, usually there is a mixture of the minerals named with possible accompaniments of i.e. kenomagnetite, maghemite, pyrite, ilmenite and gangue minerals intergrown with the iron mineral [63–65].

Table 3-I gives an overview of the most important and commercially used iron minerals including the countries with the largest deposits.

Table 3-I: Excerpt of the various occurring iron minerals [10,47,64–67]

Ore mineral	Chemistry	Acronym	Type	Max. Fe-content	Properties	Main deposits
Hematite	Fe_2O_3	h	Oxide	70 %	Low content of (acidic) gangue, low S and P	South Africa, Brazil, USA, Canada, Australia, Ukraine
Martite	Fe_2O_3	mr	Oxide		Pseudomorph of hematite after magnetite due to oxidation	as above
Magnetite	Fe_3O_4	m	Oxide	72.4 %	Often associated with other metals, lower reducibility	Sweden, Iran, China, Chile, Russia
Limonite	$Fe_2O_3{\cdot}3H_2O$	l	Hydroxide	62.6 %	Representative name for different minerals, containing crystal water	Australia
Siderite	$FeCO_3$		Carbonate	48.2 %	Often accompanied by Mn and Mg, low iron content	Russia, Austria

Hematite (h) has a chemical composition of Fe_2O_3, corresponding to 69.94 % iron and 30.06 % oxygen (in its pure form). It has a reddish appearance and is the most important iron mineral. It occurs associated with vein deposits in igneous, metamorphic, and sedimentary rocks and as an alteration product of magnetite.

The majority of hematite originated through recrystallization of a finely crystalline iron oxide and/or hydroxide mud, which was generated by chemical precipitation in the pre-cambrian sea. Depending on the overprinting conditions like temperature, pressure, fluids etc., smaller or larger crystals have been formed throughout the geological ages.

From a morphological point of view, three different forms of hematite crystals can be distinguished [62,63,67]:

- Idiomorphic crystals have defined crystal faces with an angular shape are dense and have hardly any pores
- Hypidiomorphic show crystal faces in some parts whereas
- Xenomorphic crystals have irregular surfaces only. The hematite is intergrown with neighbouring crystals and usually includes more pores, resulting in a higher specific surface area of the ore.

In Figure 3-1 microscopic pictures of typical hematitic structure is given; it can be seen that hematite crystals generally appear light grey. The left picture shows a hematite particle with an overall size of 10 mm, part of which is magnified in the picture on the right. The different crystal forms can be clearly differentiated, the idiomorphic crystals in the middle region (h_2 in picture b) surrounded by xenomorphic regions that make up the prevalent part of the grain (h_1).

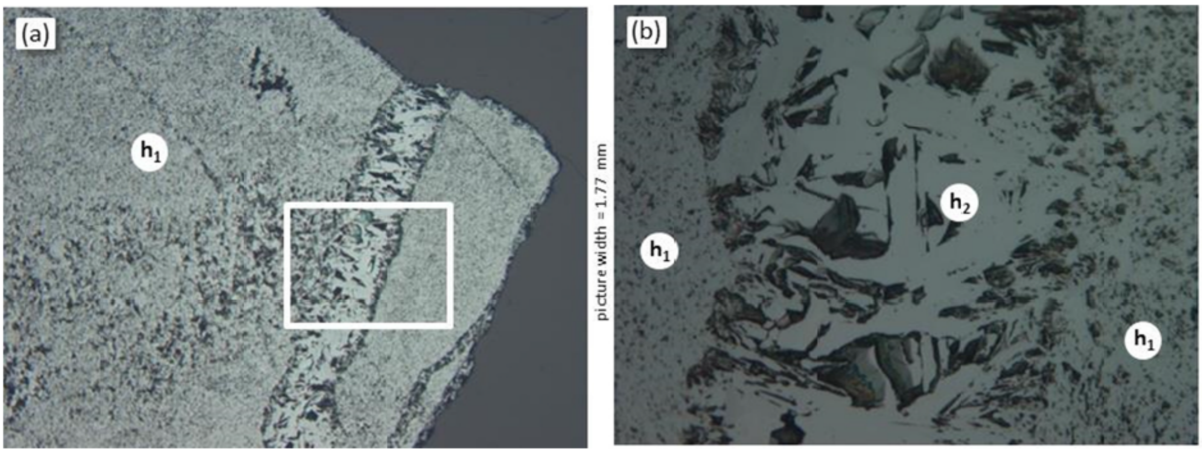

Figure 3-1: Light microscopic picture of a hematitic ore (a) and detail picture (b)

Magnetite (m), with the chemical formula Fe_3O_4, is a compound (spinel) of FeO and Fe_2O_3 with a content of 72.36 % iron and 27.64 % oxygen. It has a dark grey or black colour and is ferromagnetic. Magnetite occurs in igneous, metamorphic and sedimentary rocks. Magnetite is not stable under atmospheric conditions and most of it originated from recrystallization of a finely crystalline iron oxide and/or iron hydroxide which was generated by chemical precipitation (similar to hematite) [47,67,68].

Magnetite is rarely found in its pure form and is often associated with Ti, Mg, Al, Ni, Cr, V or Mn as these metals can replace Fe within the spinel structure. As a consequence of the improvement of magnetic concentration techniques, it has become increasingly important as a source of iron. The reducibility is generally known to be lower when compared to hematite, mostly due to the dense and coarse structure. Like hematite, the magnetite crystals can appear as idiomorphic, hypidiomorphic and xenomorphic crystals. Figure 3-2 shows the petrographical structure of a magneititic iron ore (visible as brownish grains in the picture). The dense structure of the ore and the distinctly coarser grain size compared to the hematitic ore can be seen.

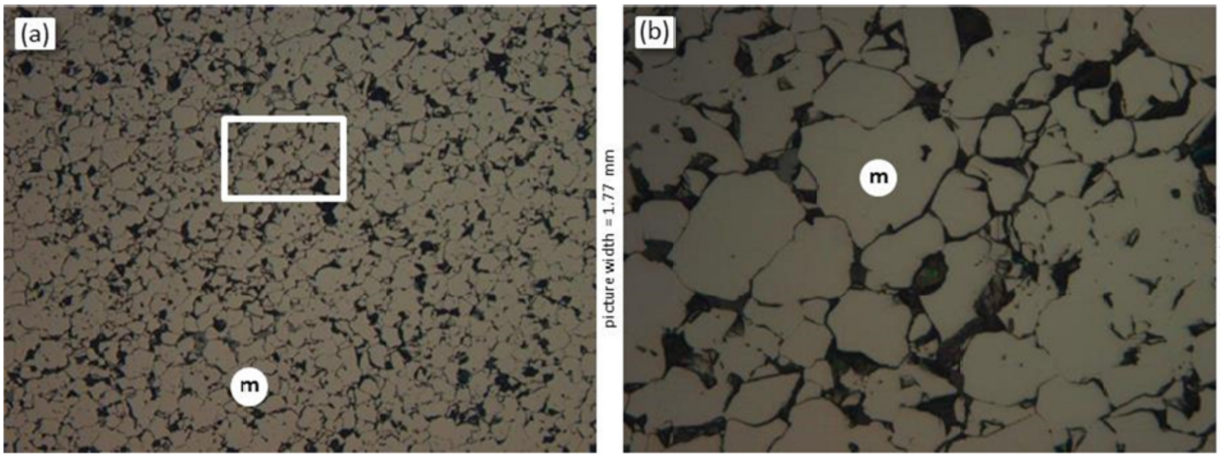

Figure 3-2: Light microscopic picture of magnetitic ore (a) and detail picture (b)

Since hematite is the stable phase at atmospheric conditions ***martite (mr)*** is an intermediate product due to the oxidation of magnetite. It is a pseudomorph of hematite after magnetite, which can contain different morphological types of hematite. The formation of martite occurs over the geological times. Further this effect can be artificially induced, during the sintering or pelletization process. A former hematite can be partly reduced to magnetite and might be reoxidised to hematite during e.g. the cooling process. Figure 3-3 depicts this phenomenon; the left side shows a partly martitized magnetite, while the right side shows hematite that has been fully transformed to martite. Especially within sinter structures this sort of hematite is called secondary hematite because it originates from an artificial solid state phase transformation (in contrast to primary hematite).

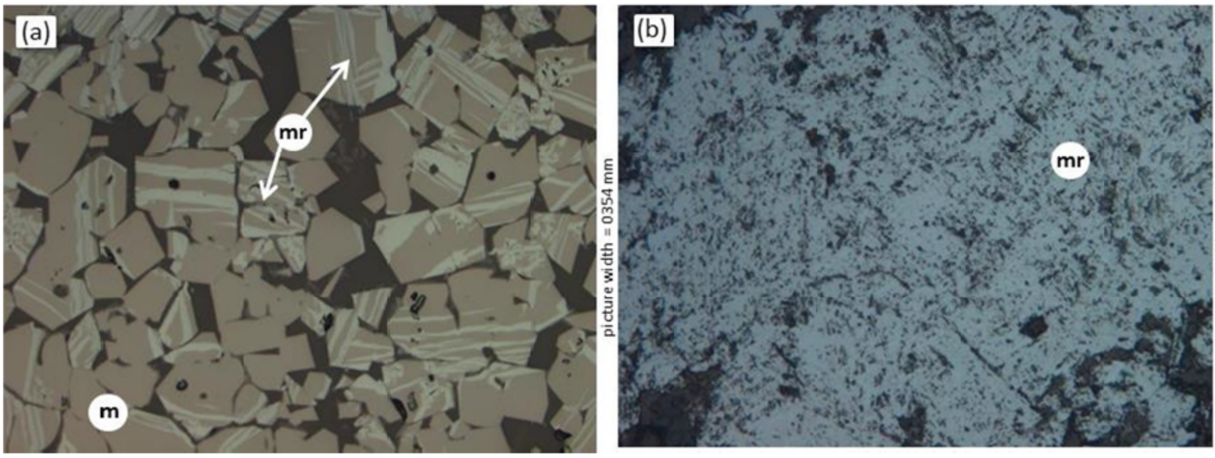

Figure 3-3: Picture of partly martitized magnetite (a) and fully transformed hematite (martite) (b)

Limonite (l) is the name commonly given to hydrous iron oxides that are mineralogically composed of various mixtures of the minerals goethite or lepidocrocite. Goethite contains 62.58 % iron, 27.01 % oxygen and 10.14 % water and the chemical formula is FeO(OH) whereas the water is incorporated in the crystal lattice. It is a secondary mineral, formed commonly by weathering and occurs in association with iron oxides and in sedimentary rocks. Limonite is mainly generated through weathering of the primary ore and can usually be found at the surfaces outcrops of every iron ore deposit [47,65,66,69]. Therefore, the amount of limonite usually decreases with the depth of the deposit. In most cases, limonite is intergrown with hematite and/or magnetite and/or siderite in a wide range of varying portions. Figure 3-4 shows pictures of typical limonite/hematite mixtures with different portions of limonite (dark grey colour in the pictures). There is also some martite visible in picture (b) plus xenomorphic hematite crystals (h_2). Above ~200-250 °C [70] the crystal water starts to be removed, this phenomenon is measurable by the weight loss and is denoted as dehydroxylation loss on ignition (LOI).

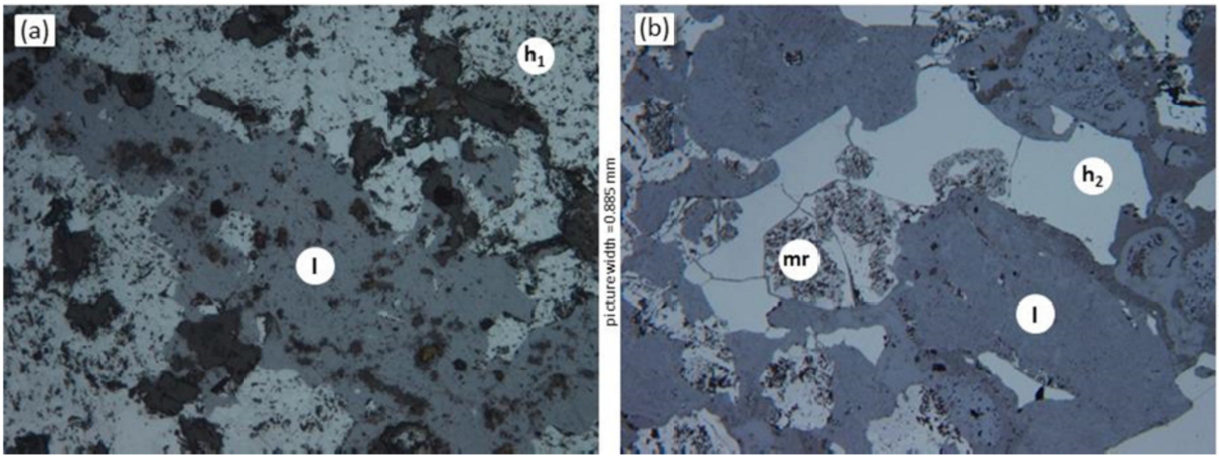

Figure 3-4: Mixture of limonite (grey) and hematite (light grey)

Siderite has the chemical formula of $FeCO_3$, corresponding to 48.20 % Fe, 27.99 % CO_2 and 13.81 % oxygen. Siderite commonly contains variable amounts of calcium, magnesium or manganese present as $(Mg,Fe)CO_3$ or $(Mn,Fe)CO_3$. Siderite varies from dense, fine grained and compact to crystalline, and is identified, in its calcined form, by its idiomorphic and angular shaped appearance. Depending on the composition, the calcination starts between 400-800 °C [70–73]. Carbonate ores are commonly calcined before charging into the blast furnace, mostly during the sintering or pelletizing process [47].

If the ore is too fine (see previous chapter) for a direct use in the reduction facility, it has to be artificially agglomerated. Depending on the agglomeration process, the ore used and the binding or fluxing material, the chemical and mineralogical composition is changed. In contrast to the described naturally occurring iron oxides additional phases and structures will become apparent.

3.3 Pelletization Processes and Microstructure of Pellets

Pelletization is understood as the agglomeration of very fine iron bearing material, usually with a grain size < 0.2 mm and a portion of ultra-fines < 40 µm of 70-80 %. Usually iron containing raw materials can consist of concentrates of limonite, hematite, magnetite or a mixture of hematite and magnetite as well as naturally occurring hematite or limonite fine ores or mixtures thereof [7,15,47,74,75]. The fine grained material is formed to a spherical shape by means of a rotating pelletizer plate, balling drums and disc pelletizers. Additionally a moistening fluid (H_2O within the range of 9-12 %) and additives (binders such as bentonite, clay or hydrated lime) are added to influence the ballability and strength of the green balls. Green pellets have minor mechanical stability, distinctly far too low for any use within a reduction aggregate, but sufficient for transport to the subsequent pellet induration facility. During the formation of green pellets, agglomeration is caused by capillary forces. The flame hardening process causes an increase in hardness by means of crystallization processes, glassy glue and restructuring of the materials components. Additional additives might be dolomite, lime, olivin etc.

The induration process at very high temperatures (depending on the aggregate between 1000-1350 °C) and the prevailing oxidizing conditions initiate changes in the mineralogical composition and structure of the original ore. On the one hand magnetitic ores are desired to fully oxidize to hematite, while on the other hand the hematite crystals will recrystallize; additionally the fluxes melt and hence glue the ore grains together. Figure 3-5 (a) shows a light microscopic picture of a typical pellet structure. It can be seen that the hematitic grains (h, grey) are well recrystallized, which is apparent in their spherical shape.

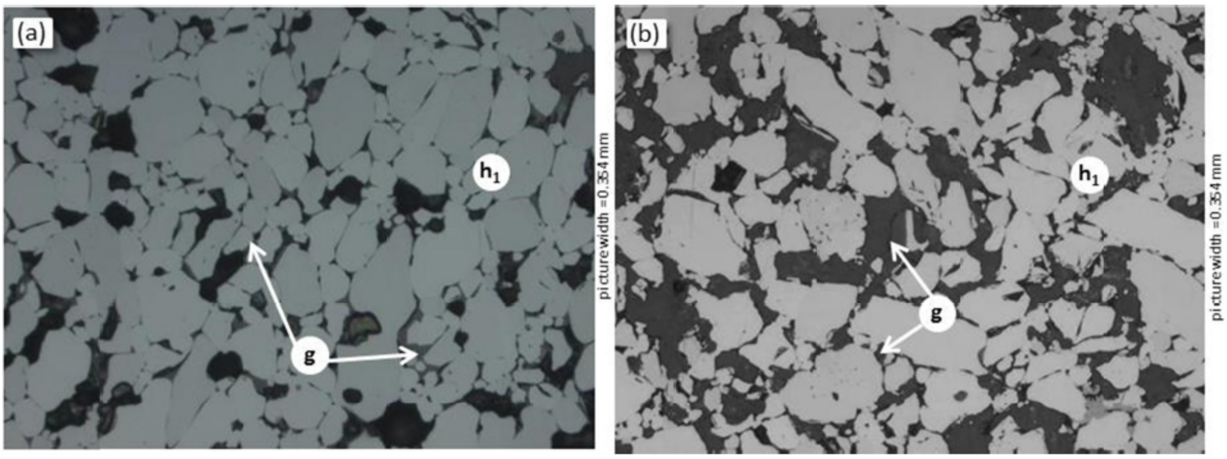

Figure 3-5: Light microscopic picture of a typical pellet structure, hematite grains with intercrystalline slag phase (glass) and pores

Intercrystalline slag/glass forming material can be seen as darker grey parts (g, black parts refer to pores that are filled with resin). The right picture (b) shows more or less the same components, hematite grains, slag and pores, but there is significantly more slag phase visible and the form and shape of the grains is different. This more angular shape of the grains is resulting from a partly incomplete burning process; the grains have not been fully recrystallized.

As the maximum content of slag and binding phases is very restricted due to the requirements of the subsequent reduction process (c.f. previous chapter) the microstructure of pellets can be compared to those of natural ores. Generally speaking the structure of a pellet consists of fine, mostly hematite grains and is quite porous.

3.4 The Sintering Process and different Sinter Phases

"Sintering has been referred to as the art of burning a fuel mixed with ore under controlled conditions" [47]. In contrast to pelletizing, where a green unbaked pellet or ball is formed and then hardened by heating, during the sintering process a porous clinker is formed and then crushed and sieved to the right size fraction needed for the blast furnace.

Sintering is a continuous process, carried out on a travelling grate that conveys a bed of ore fines or other finely divided iron bearing material, intimately mixed with approximately 5 % of a finely divided fuel such as coke breeze or anthracite. Due to the ignition at the first stages of the sintering process and the further combustion of the fuel, the materials temperature intermittently rises up to 1300-1480 °C. This heat is sufficient to cause a melting of the surface of the particles but no melting of the whole particle. The fine ore particles are sintered together into porous clinker. In contrast to that theoretical point of view, with regards to sinter produced on an industrial scale, observations of the microstructure show that distinctly more material is melted during the sintering process. Often up to 80 % of the material is melted and the formation of the mineral phases is happening via crystallization [7,47,73–75].

Before the sinter blend is fed to the sintering grate, the input materials have to be properly mixed to provide a uniform, homogeneous bed and prevent compacting of the bed. Therefore bedding and blending operations are used to premix different raw materials:

- The greater part of the sinter blend consists of ***fine iron*** ore with a grain size between of 0-10 mm Whereby the aim is to have 80 % bigger than 100 μm and with a mean diameter d_{50} of 0.7-0.8 mm. Too high a portion of fines would decrease the permeability of the bed whereas too coarse grains decrease the thermal transfer between solids and gas. Mostly hematitic and magnetitic ores are used. When magnetitic ores are used, due to oxidation the released heat can cause a decreased fuel rate [47].
- About 5 % ***recycling material*** (blast furnace dusts, steel plant dusts, mill scale,…) is used as an iron carrier. But its usage is restricted due to the high amount of Zn and Pb, and additionally the oily and fatty scale causes damage to the filtering devices.
- Depending on the desired basicity and the composition of the iron ore and the gangue material respectively, the portion of ***fluxes and additives*** ranges between 10-15 %. In most cases the gangue material is of an acidic nature and therefore dolomite, burnt lime or limestone or olivine are added as a basic flux with a grain size of < 3 mm. These fluxes cause an increase in sintering performance, better reducibility of the sinter, decrease in sintering temperature due to a decrease in the melting point and finally the configuration of the desired slag (in amount and basicity) for the blast furnace.
- Already sintered material with a size of < 6.3 mm, which is not sufficient for the use in the blast furnace, is mixed to the sinter blend as ***returned material*** with a portion of 25-30 %. The effects of adding sintered returned material can be enhanced nucleation for crystallization, decreasing melting point, enhanced reducibility, and increase of permeability and decreased fuel rate.
- As ***fuel*** providing the energy for the sintering processes, coke breeze or anthracite with a grain size of 0-3 mm are added to the blend. The content is desirably low at about 2-4 % and the content of volatile matter as well as sulphur and ash contents are also restricted.

- Finally 5-10 % **moisture** is added to the raw sinter blend for a better binding mechanism of the iron ore during the mixing and therefore increases the permeability of the sinter blend.

These components are mixed and fed to the grate upon a 30-40 mm thick bedding layer (consisting of returned material for protection of the grate) which leads to a total height of the sintering bed of 400-500 mm. After the ignition of the mixture, air is sucked through the bed and a thin burning zone moves from the top down to the grate across the sinter feed layer. After the sintering reaction the sinter is crushed and subsequently cooled by air flowing through the burden.

During the sintering process a wide range of reactions occur and different phases are created [47,73,76,77]:

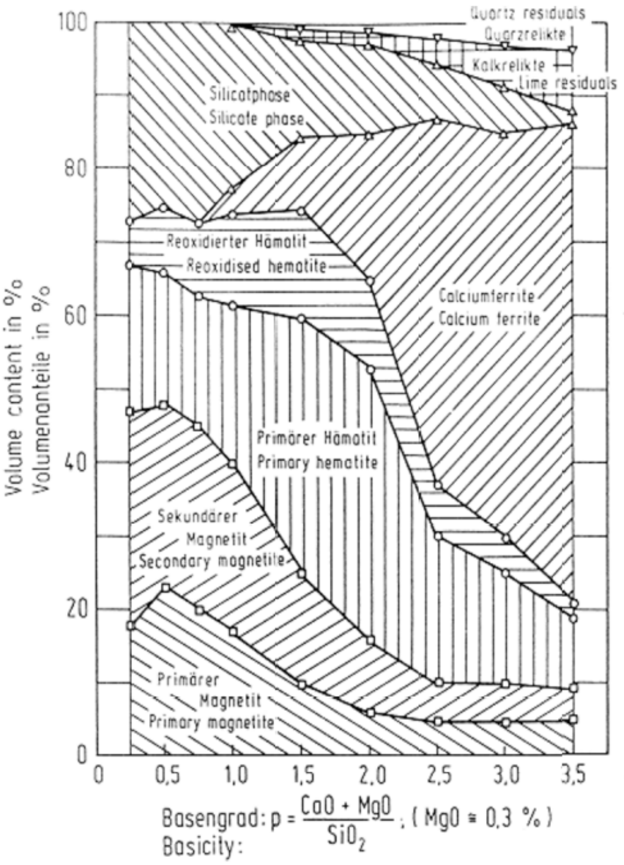

Figure 3-6: Different phases in sinter in dependence of the basicity [73,76]

- In the first stages an ***oxidation*** of magnetite iron ore happens if present.
- The separation of ***crystal water*** based on the reaction $Fe(OH)_2 \rightarrow FeO + H_2O$ and $Ca(OH)_2 \rightarrow CaO + H_2O$ occurs from 200 °C on. In the case of limonitic parts the residue consists of highly porous hematite. Owing to a low density there, pores are generated at these places preferentially during sintering.
- The ***calcination*** of carbonates starts at around 400 °C according to $FeCO_3 \rightarrow FeO + CO_2$ or $CaCO_3 \rightarrow CaO + CO_2$, all with an endothermic character.
- Development of the different ***sinter phases*** as the major sintering mechanism. Depending on the amount and nature of the additives and the ferrous burden material the composition of the final sinter is different. Figure 3-6 presents the different sinter phases which can occur depending on the basicity. It can be seen that with increasing basicity and hence an increasing amount of calcium, the portion of calcioferrites increases. Depending on the oxidizing or reducing conditions and the availability of magnesium variable amounts of spinel, hematite, Fe-Ca-oxides and SFCA (silico-ferrites of calcium and aluminum of different types) are generated. In sinter at the absence of carbonate ores calcioferrite (C_2F, CF) and SFCA will crystallize through solid body diffusion before melting on expense of decomposition of hematite. Afterwards the material starts to melt until the maximum temperature of some 1350 °C is reached, and depending on the quality of the feed a big portion of the material is melted. Other calcioferrites may crystallize before reaching the maximum temperature on the one hand, while on the other hand hematite and SFCA may form at expense of decomposition of calcioferrites. At the maximum temperature SFCA, calcioferrite, calciowustite, hematite, spinel and/or wustite can be the present mineral phases in contact with the melt. Due to rapid heating and cooling hardly, any equilibrium between mineral phases and melt is postulated.

  On cooling spinel (i.e. magnetite, magnesioferrite) growth is initiated. During further cooling the hematite-melt-stability field is passed. There the hematite crystallizes preferably in the shape of big skeleton-shaped crystals originated from the melt. At subsequent lower temperatures the stability field calcioferrite-hematite is passed. Calcioferrites of different chemical compositions are formed during the simultaneous dissolution of magnetite. On further cooling the generation of minerals like SFCA, Si-Fe-oxides and Ca-Si-oxides takes place. This crystallization of the minerals mentioned is stopped when the temperature is too low, and glass phase finally freezes. After the freezing of the melt, the only possible transformation is the oxidation of the magnetite to martite (hematite) if enough oxygen is available.

Accordingly it can be concluded that the structure of sinter is very complex and the variety of phases is great, whereby the quantitatively biggest portions refer to hematite, magnetite (hence spinel), calcioferrites and glass phases [47,73,74,78–80].

- ***Spinel (sp)*** generally refers to minerals with the chemical formula of $Me^{2+}O{\cdot}Me_2^{3+}O_3$ whereas the Me^{2+} position can be occupied by any bivalent metal like Fe, Mn, Mg, Ca… and the Me^{3+} position by Fe, Al, Ti, Cr, etc. Depending on the chemical composition of the ore, in most sinters the spinels consists of magnetite ($FeO{\cdot}Fe_2O_3$) and magnesioferrite ($MgO{\cdot}Fe_2O_3$) with varying portions of Mg.

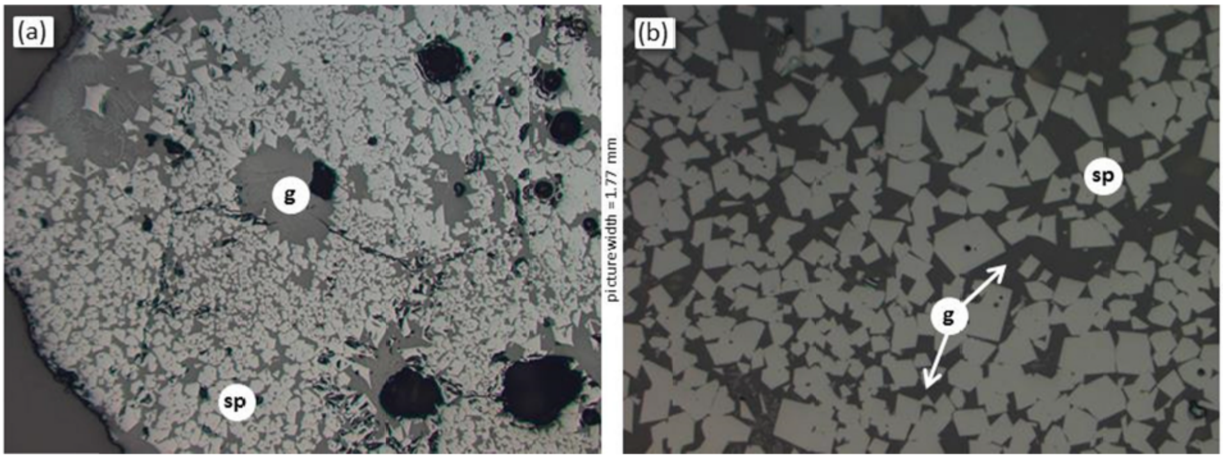

Figure 3-7: Typical appearance of spinel (brownish parts) within a sinter grain

Figure 3-7 gives a light microscopic picture of a sinter grain; the right hand side (b) shows a detailed picture. The spinel crystals (sp) are appearing as light brownish in the reflected light, the darker brown parts refer to the glass phase (g) and the black areas are holes and pores filled with resin. The coarse magnetite crystals have an idiomorphic shape with hardly any pores and are embedded in slag/glass phase.

- ***Hematite (h)*** of a different form and shape and hence different origins makes up a major portion of the sinter. First, it is most important to mention that hematite originates from hematitic ore relics (h_{pr}) with a crystal size of mostly < 0.3 mm. Smaller ore particles are fully assimilated by melt during the sintering process whereas larger particles are only infiltrated at the outer particle zones. Sometimes the hematitic crystals of ore relics can be recrystallized and identified by their spherical shaped crystals (comparable to pellet microstructures). Nevertheless, most of the hematite is created on cooling after having left the magnetite stability field. Preferably skeleton shaped crystals are created by simultaneous dissolution of the spinel. Because this hematite originates from the liquid melt it is understood as secondary hematite (h_{sec}). These two phenomena, an ore relic as a position where the growth of primary hematite is initiated and the growth of skeleton shaped primary hematite crystal, are shown in Figure 3-8. On the left hand side (a) at the top there is the big and dense ore relic (h_{pr}) and lower downw the h_{sec} grows at expense of the spinel. Also on the right side the hematite is growing at expense of the spinel, it has to be noted that all the visible hematitic parts (h_{sec}, light grey) refer to one big single hematite crystal. These hematitic ore relics are therefore not an undesirable component to some extent, too much can cause an insufficient sintering of the material and hence too lower mechanical stability.

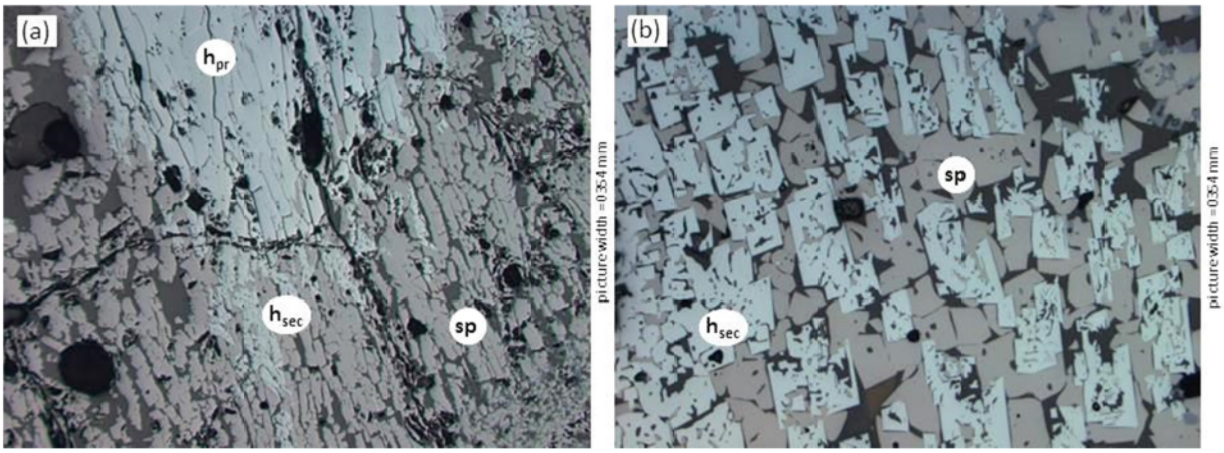

Figure 3-8: Different types of hematite of different origins

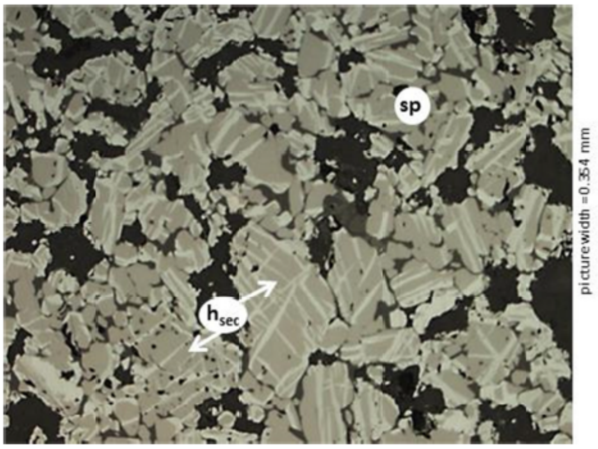

Figure 3-9: Secondary hematite due to oxidation on cooling

The third form to be mentioned here is secondary hematite (h_{sec}) presented in Figure 3-9. This kind of secondary hematite always refers to hematite originated during the cooling at temperatures where the material is already solid. If there is enough oxygen available the spinel crystals will oxidize to hematite and can also be understood as martite (c.f. chapter martite).

- From the literature at least 8 different forms of ***calcioferrites (cf)*** are known. Here only the two major forms are given; a detailed description of all calcioferrites is given elsewhere [73,74,76,81]. Primary calcioferrites can arise during crystallization directly out of the melt, preferentially at places where there is a lot of CaO within the melt (near limestone or burnt lime particles). In this case the structure of the CF crystals is acicular to columnar and has an intermeshing texture. On the other hand calcioferrites can arise during cooling through the dissolution of spinel crystals; calcioferrites then often surround the magnetite crystals and the mechanism can be assumed to be solid body diffusion. In Figure 3-10 both of the described calcioferrite shapes can be seen. On the left (a) the columnar crystals that have grown into the melt when it was still liquid; on the right side (b) the growth of CFs with simultaneous consumption of the spinel crystals

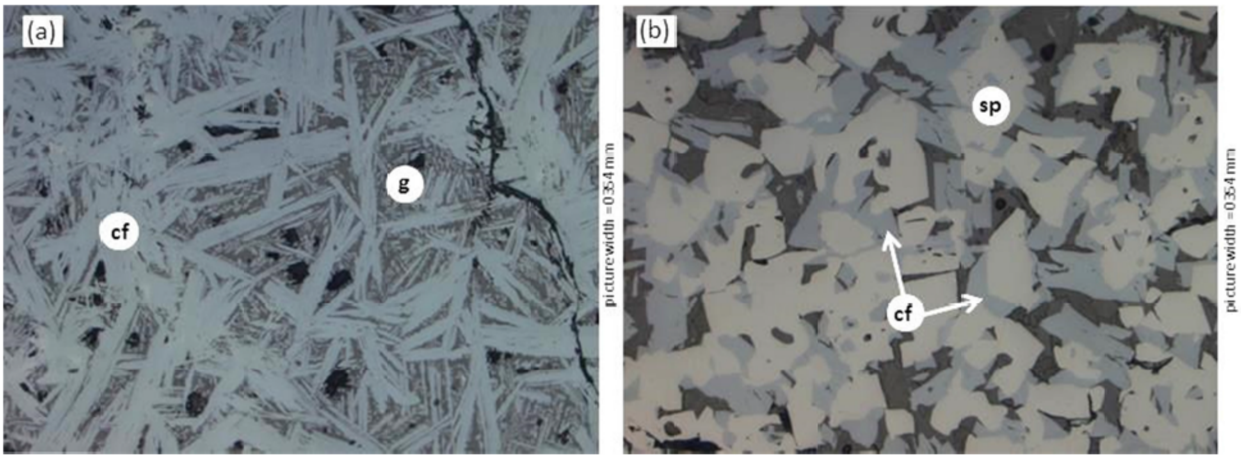
(a)
g
cf
picture width = 0.354 mm
(b)
sp
cf
picture width = 0.354 mm

Figure 3-10: Different types of calcioferrites, (a) directly grown from the meld, (b) as a result of dissolution of spinel

- Additionally an essential part of the sinter consists of ***glass phase (g)*****.** On the one hand it form intercrystalline masses, and on the other hand idiomorphic as well as skeleton crystals Ca-Fe phases; spinel or hematite can be embedded within the glass phase.

4 Fundamentals of Reduction and Metallic Iron Formation

Although the variety of industrial scale processes with the aim of producing either direct reduced iron or liquid hot metal is considerable, the fundamental mechanisms of reduction remain the same. All the different conceivable processes regarding different reduction facilities, different composition of burden material or different reducing agents have to comply with the same rules - the laws of nature - in order to make any oxygen release from the oxidic ferrous burden material possible.

First of all the thermodynamics of the reduction reaction have to be considered. By means of thermodynamic calculations, any changes of states can be described quantitively and equilibria of chemical reactions can be given. The thermodynamic calculations define the conditions that are inevitably needed for any reaction to occur regarding temperature, pressure and concentration; hence these give an idea whether or not the reduction reaction is at all possible at certain conditions.

Nevertheless, a thermodynamic point of view does not consider parameters like time, physical properties or contact of the reaction partners in any way. But for a description of the reaction as it happens beyond any equilibrium conditions, all the transportation mechanisms are of extraordinary importance and have to be taken into account. The kinetics can describe the reaction rate and hence the time that is needed to reach the desired conversion. An efficient production of metallic iron from iron ores by the step-by-step reduction of the bound oxygen with CO and H_2 as reducing agents, can only be accomplished by a combined consideration of thermodynamic and kinetic aspects of the reduction reaction.

In the special case of iron ore reduction, a distinction between two different possible reduction paths has to made; the direct and indirect reduction, distinguished from each other by the physical condition of the reducing agent (either solid or gaseous). Depending on the operational temperature, pressure and concentration, it is obvious that the reduction of an iron oxide to the final product metallic iron is only possible within a small operational slot. Within this window it is possible to produce iron but still the form and shape of the metallic iron formed and especially the time that the reaction takes differs widely. Within the subsequent sections, the basics of both thermodynamic and kinetic aspects will be outlined and by describing the different types of metallic iron formation, an example of the combined impact can be depicted.

4.1 Thermodynamic Aspects of Iron Oxide Reduction

The most important phase stability diagram for the reduction of iron oxides to metallic iron is the Fe-O system at atmospheric pressure as given in Figure 4-1 [82]. There the phase equilibria of the different oxides (in both solid and liquid states) and metallic iron respectively can be seen, depending on the oxygen content (in fact depending on the partial pressure p_{O2}). For industrial applications in different reduction facilities the equilibrium lines and the stability fields of magnetite and wustite are of the utmost importance [3,7,82–84].

Since the reaction between metal and oxide can be given as

$$Me + O_2 \leftrightarrow MeO_2 \qquad (4-1)$$

and the equilibrium constant (K_p) of this reaction can be written as

$$K_p = \frac{a_{MeO_2}}{a_{Me} \cdot p_{O_2}} \qquad (4-2)$$

it can be seen that K_p, as the driving force of the reaction, only depends on the partial pressure p_{O2}. It can be noted that from a thermodynamic point of view, the reducibility of oxides or oxide mixtures is defined by their oxygen partial pressure. Furthermore every oxide has its own oxygen partial pressure which is dependent on the temperature and the pressure of the external system. To gain a shift of the reaction (4-1) from the right to the left (hence the reduction of the oxide to the element with simultaneous generation of gaseous oxygen) either one component of the equation has to be removed by keeping K_p constant, or K_p must be influenced by changing the pressure or temperature of the system [15].

When thinking of the latter possibility, the change in temperature and pressure of the system, with a comparative look at the phase diagram in Figure 4-1 [82], the difficulties for an industrial scale application can be assumed. The decomposition temperature of an oxide at atmospheric pressure would be very high and hence would make a technical application uneconomical (the decomposition temperature of hematite is 1455 °C, at atmospheric conditions). On the other hand, due to the very low oxygen pressure of the iron oxides, decreasing the pressure of the system would require almost vacuum conditions for a reduction reaction [15,17,83].

At the chemical equilibrium, the oxygen partial pressures of gas (left side of equation 4-1) and the oxide are equal and therefore:

$$p_{O_{2\,(oxide)}} = p_{O_{2\,(gas)}} \qquad (4-3)$$

After transforming the equation 4-2, the dependence of the oxygen partial pressure can be expressed as the ratio of activities of metal, oxide and equilibrium constant. With the assumption that oxides and metals contained in the system in pure state have an activity value of one, the oxygen partial pressure only depends on the equilibrium constant in an indirectly proportional way:

$$p_{O_2} = \frac{1}{K_p} \cdot \frac{a_{MeO_2}}{a_{Me}} \quad \rightarrow \quad p_{O_2} = \frac{1}{K_p} \qquad (4-4)$$

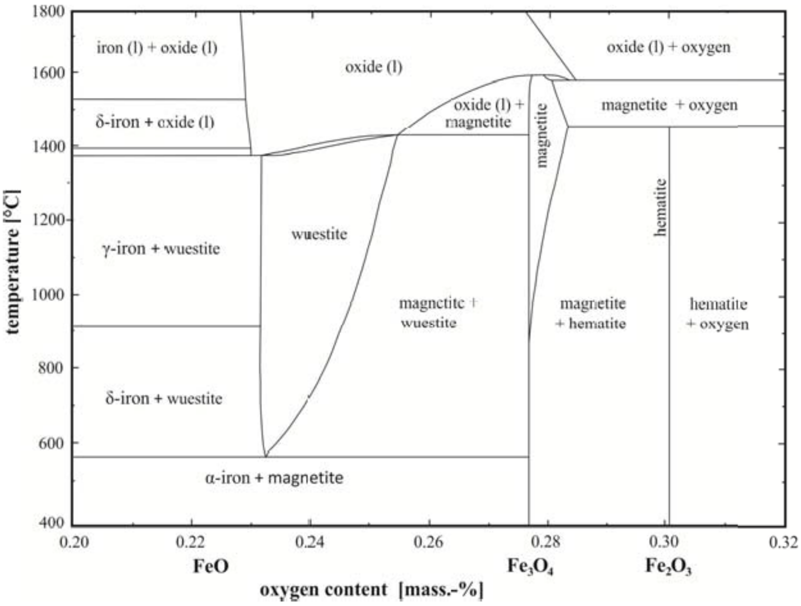

Figure 4-1: Phase diagram iron and oxygen [82]

In order to of predict the direction of a metal/oxide reaction possible, the equilibrium constant *Kp* is combined with the standard free energy (Gibbs energy) equation:

$$\Delta G^0 = -R \cdot T \cdot lnK_p \qquad (4-5)$$

The relationship can further be expressed as:

$$\Delta G^0 = -R \cdot T \cdot ln\frac{1}{p_{O_2}} \ = +R \cdot T \cdot ln\, p_{O_2} \qquad (4-6)$$

This Gibbs energy (or oxygen potential) characterizes the chemical affinity of an element to oxygen and is valid for every system of an element X and its oxide XO_2. If the ΔG^0 value is negative, the reaction can occur but only at certain conditions, whereas a positive value totally negates the reaction and the reverse reaction may take place.
After having depicted the fact that by changing the parameters of the external system (temperature and pressure) the reduction reaction is very difficult to achieve within industrial scale applications, attempts are made to bypass this fact. The reduction of an oxide to metal can be obtained by adding a solid or gaseous reducing agent (also called reductant) to the system. If the affinity of the reductant to oxygen is higher than those of the oxides and the Gibbs energy of the reductant and respectively the oxygen potential of the oxidized reducing agent is lower, any reduction reaction of oxide can happen according to:

$$Me_xO_y + R \leftrightarrow Me_xO_{y-1} + RO \qquad (4-7)$$

and hence the precondition for a reduction reaction to proceed is:

$$\Delta G^0{}_{(RO)} < \Delta G^0{}_{(Me_xO_y)} \quad or \quad p_{O_2(RO)} < p_{O_2(Me_xO_y)} \qquad (4-8)$$

Richardson and Jeffs summarized the oxygen potentials of different oxide systems for solid and liquid phases in the so called Richardson-Jeffs diagram (also known as Richardson-Ellingham diagram). This diagram is used to illustrate stability areas of metal oxides in dependence of the oxygen potential and temperature. From this diagram the following conclusions can be drawn. The oxygen potential increases with increasing temperature, except those in relation to carbon.

Hence carbon is able to reduce most of the oxides under blast furnace conditions. Furthermore carbon monoxide and hydrogen are the most important gaseous reductants, their oxygen potential rises with increasing temperature. Therefore the reduction with CO, H_2 and C are subsequently depicted.

4.1.1 Direct and Indirect Reduction of Iron Ores

As reducing agents applied on an industrial scale only carbon, hydrogen and carbon monoxide are used, though theoretically the reduction could be conducted with electrical energy or other more oxygen affine elements like aluminium but these are not used due to economic reasons [85].

In 1812 the French metallurgist *Jaques Assenfratz* suggested a classification of iron ore reduction based on the type of reducing agent. The reduction by carbon with formation of CO as a final product is called "direct reduction" (contact of ore with charcoal) whereas the term "indirect reduction" refers to the reduction by gaseous reducing agents (carbon monoxide and hydrogen with the formation of CO_2 and $H_2O_{(g)}$ as final products). The sum of direct and indirect reduction in a reduction process is 100 % [5,8,10,15].

In every case the oxygen that is chemically bound to iron is progressively released, starting from the most oxidized oxide hematite (Fe_2O_3) via magnetite (Fe_3O_4) and wustite ($Fe_{1-y}O$) to finally achieve metallic iron. As illustrated in Figure 4-2, below 570 °C wustite is not a stable phase and therefore there are two reduction pathways that have to be distinguished:

$$at\ T < 570°C \qquad Fe_2O_3 \rightarrow Fe_{3-\delta}O_4 \rightarrow Fe \tag{4-9}$$

$$at\ T > 570°C \qquad Fe_2O_3 \rightarrow Fe_{3-\delta}O_4 \rightarrow Fe_{1-y}O \rightarrow Fe \tag{4-10}$$

For industrial scale applications the latter mentioned pathway is of more importance, there are hardly any processes that operate at temperatures below 570 °C. The following chemical equations describe the development of the "indirect reduction" process steps, the reduction with the gaseous reductants CO and H_2. Additionally the qualitative heat tone, the plus/minus sign for the enthalpy of reaction is given (calculated according to FactSage). Subsequently, for the sake of simplification, the values for δ and y are assumed to be 0.

In the first step the hematite is reduced to magnetite:

$$Fe_2O_3 + CO \leftrightarrow 2\ Fe_3O_4 + CO_2 \qquad \Delta H = - \tag{4-11}$$

$$Fe_2O_3 + H_2 \leftrightarrow 2\ Fe_3O_4 + H_2O_{(g)} \qquad \Delta H = - \tag{4-12}$$

For the reduction path according to temperatures above 570°C (equation 3-10) the magnetite is reduced to wustite with a composition $Fe_{1-y}O$ whereas y has values ranging from 0.05-0.12 (but again the simplified form with y=0 is given):

$$Fe_3O_4 + CO \leftrightarrow FeO + CO_2 \qquad \Delta H = - \tag{4-13}$$

$$Fe_3O_4 + H_2 \leftrightarrow FeO + H_2O_{(g)} \qquad \Delta H = - \tag{4-14}$$

The final reduction to metallic iron refers to:

$$FeO + CO \leftrightarrow Fe + CO_2 \qquad \Delta H = - \tag{4-15}$$

$$FeO + H_2 \leftrightarrow Fe + H_2O_{(g)} \qquad \Delta H = + \tag{4-16}$$

Below temperatures of 570 °C the magnetite is directly reduced to metallic iron:

$$Fe_3O_4 + 4\,CO \leftrightarrow 3\,Fe + 4\,CO_2 \qquad \Delta H = - \qquad (4-17)$$

$$Fe_3O_4 + 4\,H_2 \leftrightarrow 3\,Fe + 4\,H_2O_{(g)} \qquad \Delta H = + \qquad (4-18)$$

From a thermodynamical point of view the process of indirect, hence gaseous reduction does not depend on the gas pressure because the gas volume does not change (the moles of gas components are the same on both sides of the equations). From the reactions 4-11 to 4-18 it can be summarized that the reduction of hematite to magnetite is exothermic and irreversible. Further, the reduction of magnetite to wustite and metallic iron is a reversible process and greatly depends on temperature [15]. According to the Hess Theorem the heat tone of the overall reaction can be calculated (calculated with FactSage):

$$Fe_2O_3 + 3\,CO \leftrightarrow 2\,Fe + 3\,CO_2 \qquad \Delta H = -\ 22.69\ kJ/mol \quad (4-19)$$

$$Fe_2O_3 + 3\,H_2 \leftrightarrow 2\,Fe + 3\,H_2O_{(g)} \qquad \Delta H = +100.72\ kJ/mol \quad (4-20)$$

From the plus/minus sign of the equations it can be drawn that the reduction with carbon monoxide is of an endothermic nature whereas the reduction reaction with hydrogen is exothermic. The chemical equilibria of the reduction reactions 4-11 to 4-16 as well as their temperature dependence can be described graphically by means of the *"Baur-Glaessner diagram"*.

4.1.2 Gas Oxidation Degree (GOD) and the Baur-Glaessner Diagram

As a deviation of the different phase diagrams of the systems Fe-C-O_2-H_2 the chemical equilibria of the different iron oxides at different temperatures and gas compositions can be shown. Depending on the gas composition and the temperature the different existence areas of the individual solid iron oxides and iron phases can be distinguished. Subsequently the single trinary systems Fe-C-O_2 and Fe-H_2-O_2 can be deduced.

By picking out an expanded part of the Fe-C-O_2 diagram, the Baur-Gleassner diagram results as given in Figure 4-2 [86], the stability fields of the iron oxides as a function of different mixtures of C and O_2 or CO/CO_2 respectively. The given Baur-Gleassner diagram shows the regions of stability of the different oxides and metallic iron as a function of temperature and the volumetric ratio of CO/CO_2 in the reducing gas. By this means, for a certain temperature the minimal required CO amount of the gas mixture for the full reduction to metallic iron can be allocated and vice versa. At the boundary line of stability fields the two phases (oxide or iron) are at equilibrium.

Additionally the Boudouard reaction according to the chemical formula

$$2\,CO \leftrightarrow C + CO_2 \qquad (4-21)$$

is given within the Baur-Glaessner diagram. This endothermic and, in contrast to the reduction reactions, pressure dependent reaction divides the diagram into two different regions. At gas compositions and temperatures above this curve, the reduction is supported due to CO-formation of carbon present; below the curve CO is decomposed to CO_2 and solid carbon; hence the reduction reaction is retarded. The intersection point of the Boudouard curve and the Fe/FeO equilibrium line determines the minimum required temperature for indirect reduction to occur.

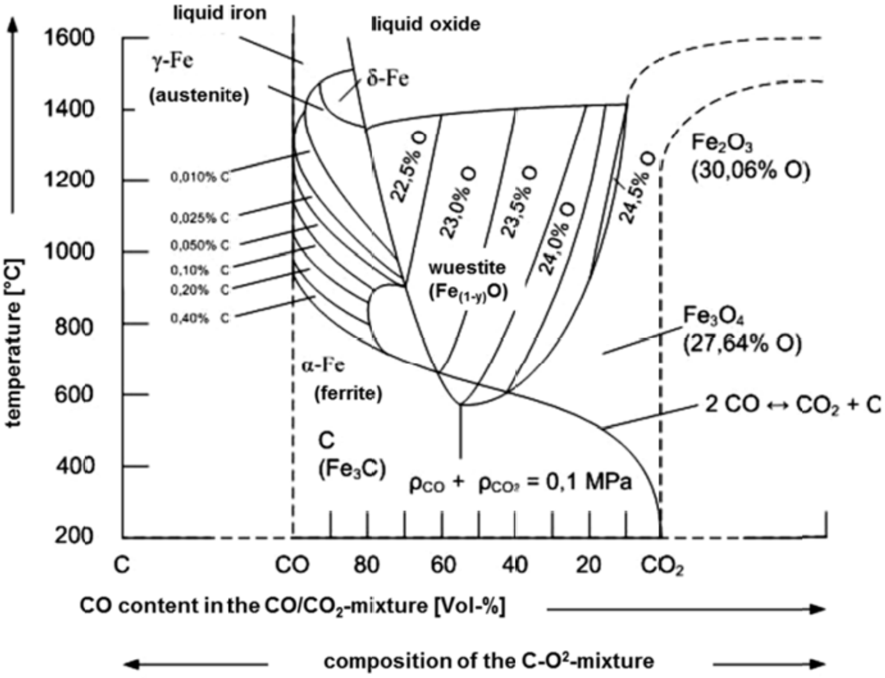

Figure 4-2: Baur-Glaessner diagram for the system Fe-O-C [86]

The same kind of diagram can be derived for the system Fe-H_2-O_2 and is given in Figure 4-3 together with the system Fe-O-C. On the x-axis of this diagram the reducing gas composition as a ratio of oxidized components to the overall reaction gas components is given, for the ratio CO/CO_2 as well as for H_2/H_2O and is summarized defined as GOD:

$$GOD = \left(\frac{x_{CO_2} + x_{H_2O}}{x_{CO_2} + x_{CO} + x_{H_2O} + x_{H_2}}\right) \qquad (4-22)$$

whereas the x_i is the molar ratio of component i.

Due to the low temperature dependence of the hematite reaction (equations 4-11 and 4-12) these equilibrium lines coincide with the vertical line at GOD = 1, hence very small amounts of CO and/or H_2 in the gas mixture are sufficient for the reduction to magnetite. As the minimum temperature for indirect reduction is defined as the intersection point of the Boudouard curve with the equilibrium line FeO/Fe it can be seen that at atmospheric conditions the indirect reduction is theoretically possible from 700 °C on. In addition the different reduction potentials depending on the temperature of CO and H_2 can be seen in Figure 4-3. At 810 °C there is an intersection of the equilibrium lines, therefore at this temperature they have the same reduction potential. At lower temperatures the efficiency of hydrogen is distinctly lower but the required H_2-amount within the gas decreases as the temperature rises, whereas those of CO decreases with increasing temperature. This concludes that at higher temperatures, above 810 °C, H_2 is the more efficient reducing agent.

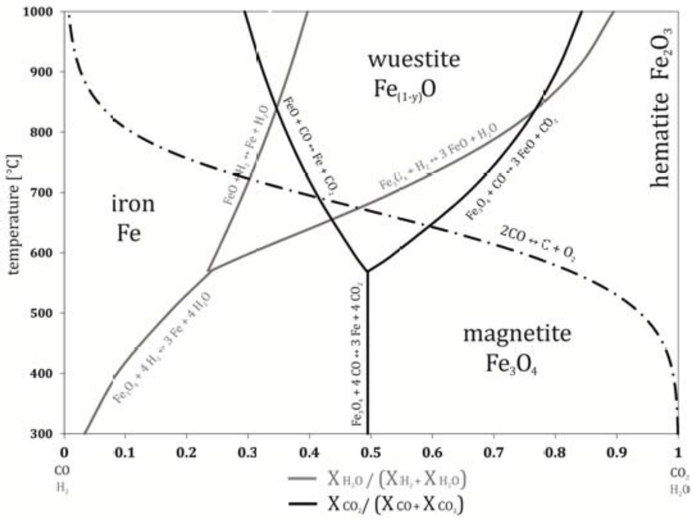

Figure 4-3: Baur-Glaessner diagram for gas mixtures of H_2/H_2O (grey) and CO/CO_2 (black)

4.1.3 Definition of Reduction Degree and Metallization Degree

Based on the chemical analyses the reduced material, both the reduction degree and the metallization degree can be calculated. Therefore for the calculation of the reduction degree (RD) the following formula is used:

$$RD = \left(1 - \frac{X}{1.5}\right) \cdot 100 \quad with \quad X = \frac{O}{Fe_{tot}} \quad (in\ \%) \qquad (4-23)$$

O refers to the oxygen content, Fe_{tot} to the total iron content and Fe_{met} to the metallic iron content which all have to be first converted into moles previously. Subsequently the metallization degree (MD) is calculated with

$$MD = \frac{Fe_{met}}{Fe_{tot}} \quad (in\ \%) \qquad (4-24)$$

According to this definition the reduction degrees of the different iron oxides are as follows:

Table 4-I: RD and MD of different iron oxide phases

Oxide phase	**Chemistry**	**RD**	**MD**
Hematite	Fe_2O_3	0 %	0 %
Magnetite	Fe_3O_4	11.1 %	0 %
Wustite	FeO	33.3 %	0 %
Metallic iron	Fe	100 %	100 %

As given in Table 4-I there is coherence between RD and MD. Up to a RD < 33 % the oxygen is gradually reduced from the lattice from one oxide to the next but no metallic iron is formed yet. In theory at a RD of 33 % the material is fully reduced to FeO and from there on the formation of metallic iron starts. This correlation of the metallization degree and reduction degree also can be calculated

$$MD = \frac{RD - 33.3\ \%}{66.6\ \%} \cdot 100 \qquad (RD\ in\ \%) \qquad (4-25)$$

This correlation is only valid for ideal conditions, when the formation of an oxide or iron starts after the full transformation of the prior step. In contrast to that, in reality there will always be a mixture of the different oxide for kinetic reasons. As a consequence, a reduced iron ore sample with a reduction degree of 33 % can exist on the one hand as pure FeO (MD= 0 %) or on the other hand as a mixture of Fe_2O_3, Fe_3O_4, FeO and Fe_{met} with a metallization degree > 0 %.

4.2 Kinetic Aspects of Iron Oxide Reduction

In contrast to the thermodynamic view of any reaction, the kinetics do not give evidence about the possibility that a reaction will occur, but rather give an idea about the rate and hence the time that is needed to reach a certain conversion. In the case of the reduction of iron oxides it describes as the rate at which iron ores and oxides are transformed to metallic iron by removal of oxygen from the solid oxide lattice.

For the description of the rather complex topic of the reduction reaction as a sequence of different reducing steps (Fe_2O_3 to finally metallic iron), different kinetic models and approaches have been developed [49,85,87–90]. What they all have in common is that there is always a simplification to some extent. In a very first approach the reduction reaction is described as a homogenous reaction, hence a reaction where it is assumed that all participating reactants are present in the same aggregate state or phase. On a closer look the description of the reaction is realized with different gas-solid reaction models (heterogeneous reaction models) and subsequently the gas-solid reaction is divided into different rate determining steps.

4.2.1 Simplification of the Reaction - Homogenous Reduction Reaction

In homogenous reactions all reacting partners are found within a single phase. For iron ore reduction for it is assumed for a first approach that all reaction partners are of a gaseous nature. For a description of the reduction rate it has to be considered that the reduction rate is influenced by the composition and the energy (besides temperature also light intensity or magnetic field could be considered); hence it is a function of both, temperature and concentration. Therefore the reduction rate is expressed by two terms, a temperature-dependent term and a concentration-dependent term, and can be described as [87]:

$$-r_A = f_1(temperature) \cdot f_2(concentration) = k\ C_A^a \qquad (4-26)$$

Here the reaction the rate (r_A) of the reaction of component A is described. According to this definition, if A were a reaction product, the rate would be positive and vice versa if A is a reactant which is being consumed, the rate is negative. Thus the term $-r_A$ describes the rate of disappearance of the reactant A. The concentration dependent part of this equation is represented by C_A^a and the temperature-dependent term with the rate constant k.

In depicting the concentration dependent part, in literature [3,49,87] the reaction is distinguished and assigned into different ***types of reaction.*** These types might be elementary reactions (either irreversible or to an equilibrium), series reactions or parallel reactions.

Concerning the reduction of iron oxides the reactions can be allocated as equilibrium and hence reversible reactions. The reaction comprises of both, the forward chemical reaction and the reverse reaction. At the moment when the reaction rate of both reactions is equal, the chemical equilibrium is reached.

Subsequently the ***order of the reaction*** (in equation 4-26 expressed as a) has to be determined. Whereas the reaction rate describes the number of molecules per time unit that are involved in a reaction, the order of the reaction is dependent on the concentration, the temperature and possible catalysts. The order of a reaction gives the probability of the collision of the reacting molecules. This consideration is concentration dependent because the more particles that prevail within a certain volume the more probable a collision is; the reaction rate increases with the increasing amount of educts (with the assumption of a constant temperature). Ditto, the probability of collision of educt molecules by forming a product increases.

Generally, when considering an elementary reaction A+B→C the reaction or disappearing rate of A can be given as

$$-r_A = k\ C_A C_B \qquad (4-27)$$

Furthermore the term molecularity has to be introduced and refers to the number of molecules involved in the reaction (only valid for elementary reactions) and can have values of one two and occasionally three. The reaction rate can now be written as:

$$-r_A = k\ {C_A}^a {C_B}^b \dots . {C_D}^d \qquad with\ a + b + \dots + d = n \qquad (4-28)$$

Where A,B,..,D refer to the acting materials and a,b,..,d, hence the powers to which the concentrations are raised, finally define the order of the reaction.

Practically reaction orders > 3 hardly occur, therefore the probability of a reaction order of 5, i.e. 5 molecules collide with sufficient energy for a reaction, is very low.

When the rate expression for a homogeneous reaction is written in the form of 4-28 the dimension of *rate constant k* depends of the reaction order, for a homogenous chemical reaction with nth order can generally be given as

$$(t)^{-1} \cdot (c)^{1-n} \qquad (4-29)$$

Finally the rate constant k as the temperature-dependent term of the rate equation can be described with the Law of Arrhenius:

$$k = k_0 \cdot e^{\left(-\frac{E_A}{R \cdot T}\right)} \qquad (4-30)$$

with k_0 as the frequency factor and E_A as the activation energy.

According to literature, several researchers have found that a first approach reasonably allows the description of iron ore reduction as an irreversible equilibrium reaction of the first order [49,88–92]. From equation 4-29 it can be seen that for a of reduction reaction assumed as a non-reversible reaction of first order, the reaction is only a function of concentration (by keeping the temperature constant).

4.2.2 Heterogeneous Reduction Reaction – Selection of a Model

For heterogeneous systems, hence a two phase system, there are more factors that must be accounted for beyond what is usually considered in homogeneous systems. For the description of the mechanisms that occur during the reaction by means of a mathematical model, it is always necessary to try to describe one single particle. For the first step one general consideration has to be made; the type of reduction progress. In Figure 4-4 two possible ways are depicted, either the reaction of a particle that does not change its initial size or the reaction of a shrinking particle that disappears at the end.

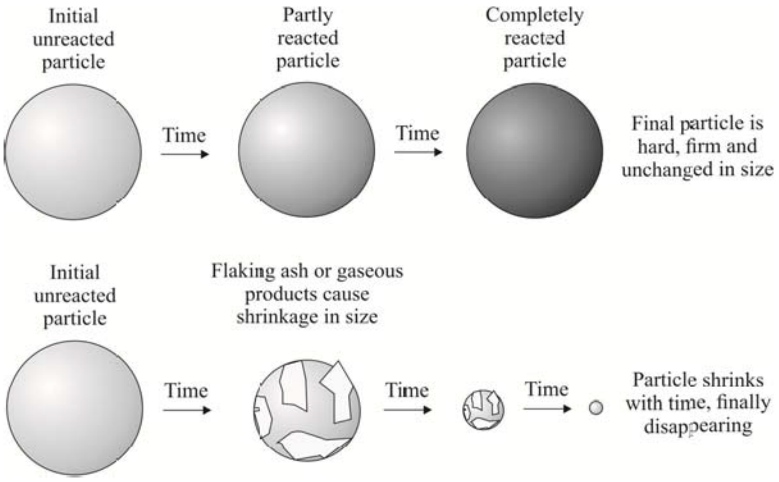
Initial unreacted particle
Time
Partly reacted particle
Time
Completely reacted particle
Final particle is hard, firm and unchanged in size
Initial unreacted particle
Time
Flaking ash or gaseous products cause shrinkage in size
Time
Time
Particle shrinks with time, finally disappearing

Figure 4-4: Different sorts of behaviour of reacting solid particles [87]

Fluid-solid reactions are numerous and of great industrial importance. The general valid form of the most important chemical reaction for the mechanism shown above might be either

$$a \cdot A_{(s)} + b \cdot B_{(g)} \leftrightarrow c \cdot C_{(s)} + d \cdot D_{(g)}$$

(here the indirect reduction reaction or any roasting reaction can be named as an example) or

$$a \cdot A_{(s)} \leftrightarrow c \cdot C_{(s)} + d \cdot D_{(g)}$$

which is valid for any calcination reaction. For a reaction according to the shrinking particle mechanism, one representative example is the Boudouard reaction beside any other dissolution reaction, the equation is written

$$a \cdot A_{(s)} + b \cdot B_{(g)} \leftrightarrow d \cdot D_{(g)}$$

Besides all the different reactions possible, the process of the iron ore reduction can generally be described as a fluid-particle reaction where a fluid (gaseous) material comes in contact with a solid particle and as a product forms a solid and fluid material. The actual change in size due to the volume differences of the different oxides are neglected for the mathematical modelling. Hence the reduction reacting is assumed as a reaction of unchanging size [49,88,89,93–95].

To describe a non-catalytic reaction of particles of unchanging size with a surrounding fluid, the literature considers are two simple idealized models, the progressive-conversion model and the shrinking-core model.

In case of the **progressive-conversion model** the reactant gas enters and reacts throughout the particle at all times, most likely at different rates at different locations within the particle. The solid reactant is converted continuously and progressively throughout the particle.

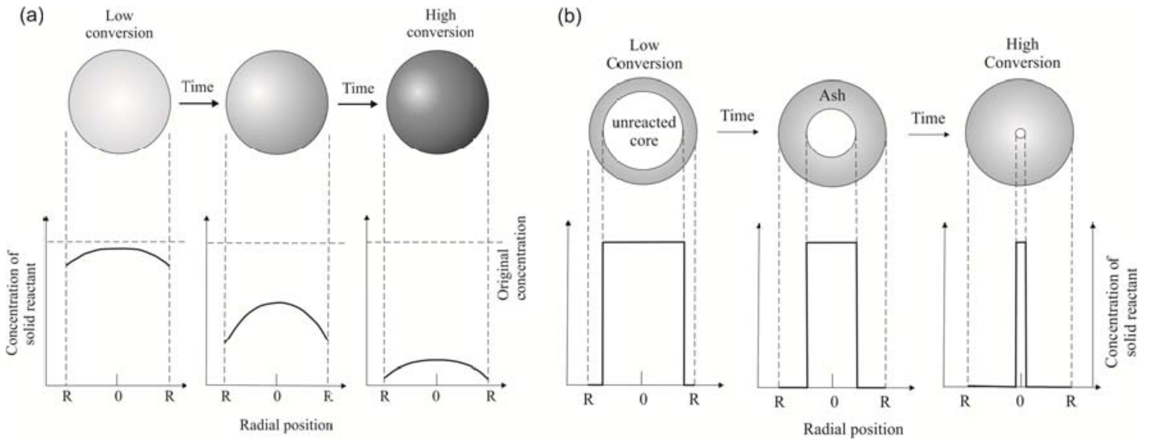

Figure 4-5: Concentration profiles of the solid reactant according to the progressive-conversion model (a) and the shrinking-core model (b) [87]

For the **shrinking-core model** the reaction is visualized as occurring first at the outer skin of the particle. The zone of reaction then moves into the solid in the form of a sharp reaction front, leaving behind a completely converted material and inert solid which is referred to as ash. At any time there exists an unreacted core of material which shrinks in size during reaction; this reaction model is typical of materials with a dense matrix and a high diffusion resistance for gas to enter the particle.

Figure 4-5 depicts the position-depending concentration profiles of the solid reactant at different stages of the reaction according to the different models. It can be seen that according to the shrinking core model (on the right) the reaction proceeds at a narrow front which moves into the solid particle. The solid reactant is completely converted as the front passes by, in contrast to the progressive-conversion model were the concentration decreases more uniformly.

When considering a reaction that proceeds according to the progressive-conversion model, it must be possible for the gas to enter the particle over the entire particle diameter at the same time. For iron oxide particles, these circumstances are highly unlikely and therefore the literature deems the shrinking-core model to better depict the reduction reaction. On further investigation a variety of different models have been developed which are aimed at introducing structural features into the reaction scheme. In the case of a particle of unchanging size, a widely used model is the “Grain-Model” where the solid body is considered to consist of uniformly sized spherical particles (and is subsequently described).

4.2.3 Sequence of Reactions and Possible Rate Determining Steps

The reduction reaction as a whole, hence the release of oxygen from the solid iron oxide lattice to the gaseous reducing gas, can be visualized as the following intermediate steps, according to *Bogdandy and Engell* [85].

The reacting ferrous burden can be visualized as a more or less porous lump of iron oxide; whereby this lump consists of individual grains. The macropores refer to the larger gaps between the grains and the micropores are the smaller gaps. The reduction reaction can be subdivided into different steps of reaction. Processes of this sort, made up of individual subsidiary processes taking place successively, are called reaction sequences. Every subsidiary process in a reaction sequence has its own sub-equilibrium. The overall reaction can be considered as the sum of the subsidiary processes in a way comparable to an electrical circuit; whereby every sub-reaction may be the rate determining step.

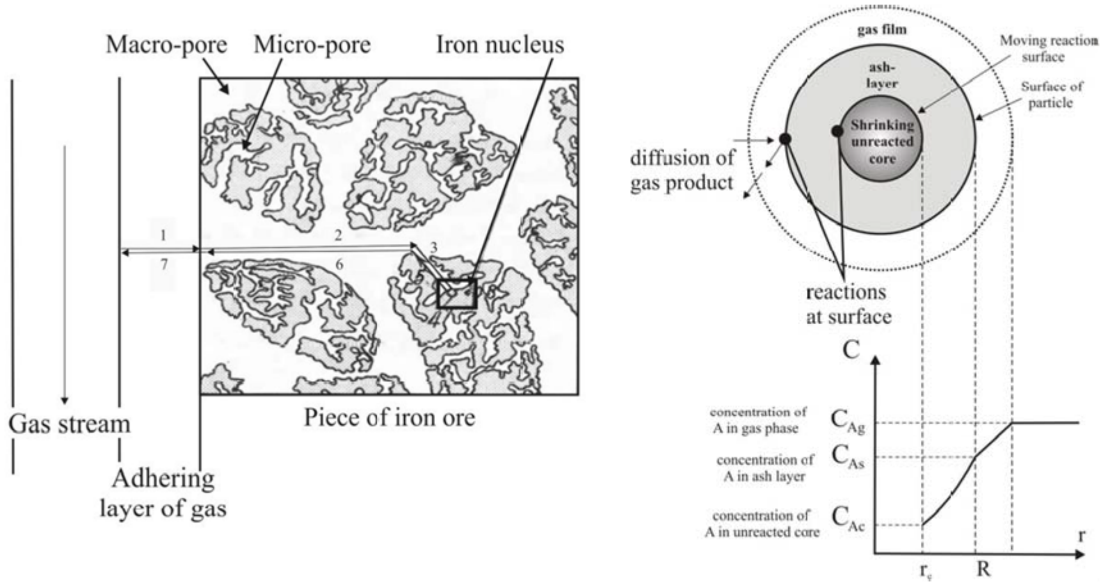
Macro-pore
Micro-pore
Iron nucleus
1
7
2
6
3
Gas stream
Adhering layer of gas
Piece of iron ore
gas film
ash-layer
Shrinking unreacted core
Moving reaction surface
Surface of particle
diffusion of gas product
reactions at surface
C
concentration of A in gas phase
C_{Ag}
concentration of A in ash layer
C_{As}
concentration of A in unreacted core
C_{Ac}
r
r_c
R

Figure 4-6: Different steps of the reduction reaction [85] (left) and gas concentration profiles for the reactions according to the shrinking-core model [87]

For the reduction reaction of iron oxide the different reaction stages and mechanisms are divided into seven individual steps according to *Bogdandy and Engell* [85] whereby the more commonly used descriptions are compacted into five steps. In Figure 4-6 the seven steps according to Bogdandy are graphically presented (left) and on the right side the concentrations profile of a cross-section of one single particle according to *Levenspiel* [87] is shown.

The reaction starts as the reducing gas enters the spaces between the lumps of ore and the boundary layer of gas which is formed around the individual lumps. At this stage the interchange of matter between the flowing gas-phase and the surface of the oxide takes place (c.f. step 1 in Figure 4-6 left) and consequently, if the mass transfer via gas diffusion in the boundary layer is the rate controlling mechanism, the reaction is assumed as mass-transfer controlled. As the reduction proceeds, the reducing gas diffuses through the macropores or microres of the lump of ore and the oxidized gas diffuses outwards along the same path. When this pore diffusion mechanism (shown as steps 2 and 3 for the diffusion inside the lump particle and as steps 5 and 6 for the back diffusion of the oxidized gas) is rate limiting, the reaction is called ash diffusion controlled. The actual chemical reaction finally takes place at the phase boundary between the oxide and the gas, step 4 in the Figure. This collectively named boundary layer reaction includes the adsorption of the reducing gas, the separation of oxygen from the oxide lattice, the formation and growth of nuclei of the reaction products and finally the desorption of the oxidized gas molecules from the surface of the solids. In parts of the literature steps 2 and 3 and 5 and 6 are summarized as one step of pore diffusion.

In some situations some of these steps do not exist. For example, if no gaseous products are formed, steps 5, 6 and 7 do not contribute directly to the resistance of the reaction. Also, it can occur or is even probable that the resistances of the different steps vary greatly from each other. For the determination of the rate controlling mechanism, the different steps are considered individually.

4.2.3.1 Mass Transport Controlled (Gas Diffusion)

In many gas-solid systems with a fast chemical reaction, the overall rate is found to be controlled by mass transport between the reaction surface and the bulk fluid. Moreover, the rate of mass transport is an important quantity in heterogeneous systems and the driving force for the mass transport via the diffusion in the boundary layer is the difference in concentration and can be described according to Fick's law of diffusion. With subsequent expending and transforming of Fick´s law, the assumption of the conversion as based on the available surface and the definition of the conversion X of the reaction as the ratio of reaction time t and the time for full conversion τ, the reaction can finally be written as [87]:

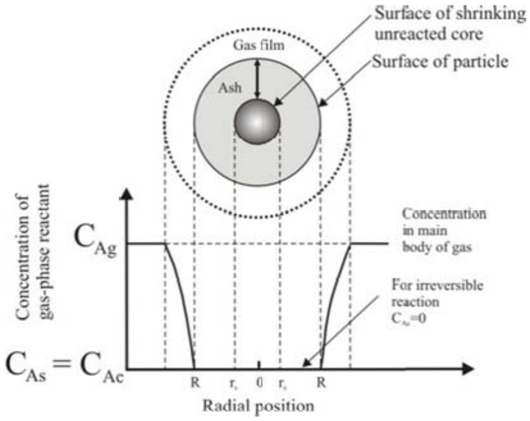
Surface of shrinking unreacted core
Surface of particle
Gas film
Ash
Concentration of gas-phase reactant
C_{Ag}
$C_{As} = C_{Ac}$
Concentration in main body of gas
For irreversible reaction $C_{Ac}=0$
R
r_c
0
r_c
R
Radial position

Figure 4-7: Gas concentration profile for mass transport control [87]

$$with\ \frac{t}{\tau} = X \quad is \quad \tau = \frac{\rho_S \cdot r_p}{b \cdot \beta_D \cdot F_P} \cdot \frac{\frac{K_E+1}{K_E}}{\frac{c_{A0}-c_{C0}}{K_E}} \qquad (4-31)$$

Without describing all the given parameters, it can be seen that the conversion clearly depends on the form and shape of the initial particle (via F_p as the shape factor), the equilibrium constant (K_E) and the initial concentration of the reactants A and C (C_{A0} and C_{C0}). In addition the temperature dependence of the reaction can be illustrated because of the mass transfer coefficient β_D (which is the quotient of the thickness of the boundary layer and the diffusion coefficient D which is in turn temperature dependent).

Whenever the reaction is controlled by mass transport only, the concentration profile of the gaseous reactant can be described as given in Figure 4-7. It can be seen that the driving force of the reaction is the difference in concentration of the gaseous reactant A between the gas phase (C_{Ag}) and at the surface of the solid particle (C_{As}). The concentration of gas at the surface of the particle (and within the unreacted core) is C_{As} everywhere and hence, this mechanism is totally independent from the form and shape of the newly formed product layer. There is no need to distinguish between porous or dense product layers and the reaction rate R is unchanging during the whole reduction reaction. The reduction rate $\dot{R}$ (= dX/dt) depending on the reduction progress can be qualitatively described as a constant value, which again illustrates that the reaction product formed does not influence the conversion:

$$\left(\frac{dX}{dt}\right) = \dot{R} \sim const. \qquad (4-32)$$

The temperature dependency of the mass transport control is described in literature [43,48] as only a slight correlation between β and T ($\beta \sim T^{1.2}$). For the other sub-processes the temperature influences the reaction to a far greater extent. For this reason it is only at high temperatures that the material transport can be expected to have an appreciable effect on the overall reaction rate and can further be disregarded, especially in the case of lump ores or pellets.

4.2.3.2 Ash Diffusion Controlled (Pore Diffusion)

When the reducing gas has passed the boundary layer and has reached the surface of the solid, it converts the ore into its reduction products at this surface. In the same way as for the gas diffusion, this equation can be derived from the Law of Fick and the assumption of the driving force as a result of a concentration difference. In the case of diffusion through the ash layer as the controlling resistance the concentration profile is given in Figure 4-8. The concentration of A in the gas phase is the same as at the surface of the solid ($C_{Ag} = C_{As}$) whereas in the core the concentration is C_{Ac} for an equilibrium reaction. Via integration the concentration profile between the outer surface of the product layer and the inner surface of the product layer (which is the same as the outer surface of the unreacted core) and the time dependent progress of the reaction can be given as:

$$\frac{t}{\tau} = 1 - 3(1-X)^{\frac{2}{3}} + 2(1-X) \quad and \quad \tau = \frac{\rho_s \cdot {r_p}^2}{2b \cdot D_E \cdot F_P} \cdot \frac{\frac{K_E + 1}{K_E}}{\frac{c_{A0} - c_{CO}}{K_E}} \qquad (4-33)$$

with D_e as the diffusion coefficient (a temperature dependent value). It can be seen that the reduction progress is not linear any more (c.f. 4-32) and the reduction rate dX/dt can qualitatively be described as (valid for spherical particles):

$$\left(\frac{dX}{dt}\right) = \dot{R} \sim \frac{(1-X)^{\frac{1}{3}}}{1-(1-X)^{\frac{2}{3}}} \qquad (4-34)$$

It is shown in Figure 4-8 that the reaction progress proceeds according to the shrinking core model (c.f. Figure 4-4). In this case the reaction product, the layer of formed metallic iron, is of a dense nature and diffusion through the dense iron layer is the rate determining mechanism, comparable to the diffusion within the micropores. With the expansion of the shrinking core model to the grain model, outlined on in the right side of Figure 4-8, the iron oxide particle consists of spherical grains of the same size which makes the oxide a porous solid. In literature it is assumed that primarily within large ore particles the diffusion through the macropores to the surface of the grain is rate determining. The grains at the outer surface are first reduced whereas the grains in the core part still consists of unreduced oxide and subsequently the overall reaction can in turn be described by the shrinking core model.

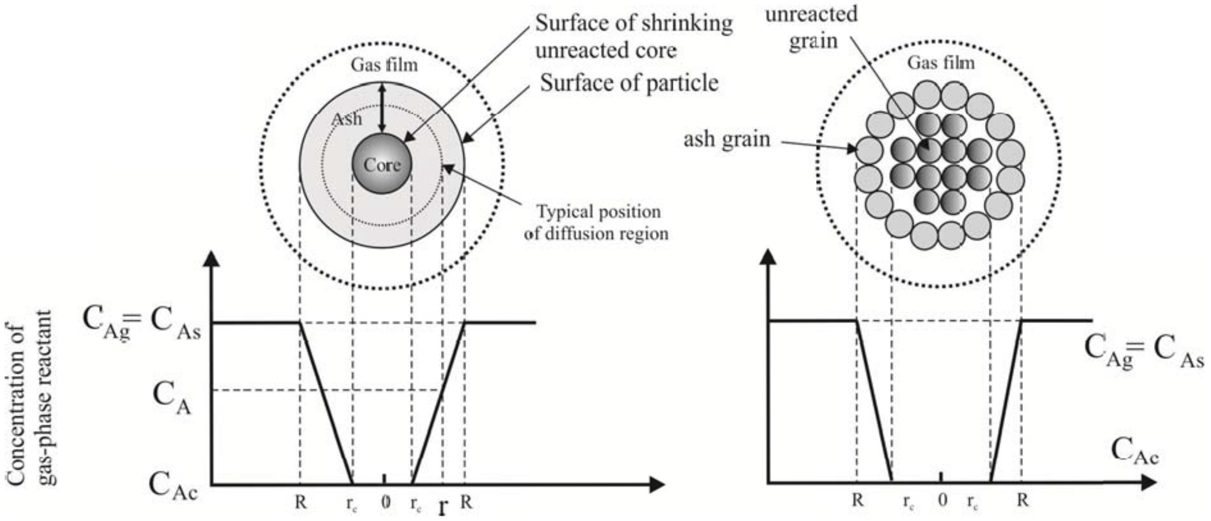

Figure 4-8: Gas concentration profiles with pore diffusion control of a non-porous solid (left) and a porous solid (right) [87]

In general, and particularly if the pieces are large (*Turktogan* [83] names a particle size of < 7 mm) and are only slightly porous, the following assumption is given as the most probable. The degree of the reduction at a given time decreases from the outer surface of the ore inwards. Therefore the end products of the reaction appear first on the outer surface of the pieces of ore; and, depending on the gas composition and temperature, these end products may be either metallic iron or lower oxides. The reduction appears in a layer like manner from the surface of the pieces towards the core. It has also been conjectured that the diffusion of the gas in the porous end-products of the reaction exerts an influence on the rate of reduction or may even be the sub-process which determines the rate of reduction. Another theory suggests that it is even possible that the metal migrates across the oxide layer to react with oxygen on the outer surface [40].

4.2.3.3 Chemical Reaction Controlled (Boundary Layer Reaction)

The rate of the phase boundary reaction in the reduction of iron ores, hence the separation of oxygen from the lattice, depends on the surface concentration at the reacting phase boundary. With the assumption of the reduction reaction as a reversible equilibrium reaction and the thermodynamic precondition for the proceeding of a reduction reaction expressed by the partial pressures of the gas phase (equation 4-8) the progress can be described as:

$$\frac{t}{\tau} = 1 - (1 - X)^{\frac{2}{3}} \quad and \quad \tau = \frac{\rho_s \cdot r_p}{b \cdot k} \cdot \frac{1}{\frac{c_{A0} - c_{C0}}{K_E}} \qquad (4-35)$$

The temperature dependence in this case is described by the rate constant k and the Arrhenius Law respectively. It is further dependent on the actual particle diameter. The reaction that is controlled only by the chemical reaction is not influenced by the form and shape of the resulting product layer (ash layer), but rather depends on the surface of the unreacted core. As before, we must distinguish between the reaction of a non-porous solid (Figure 4-9, left) and a porous solid (right). For a non-porous solid, the reaction proceeds in sharply defined layers according to the shrinking core model and is called a topochemical reaction.

The qualitative correlation of the reduction rate and the reduction progress can be given as [87]:

$$\left(\frac{dX}{dt}\right) = \dot{R} \sim (1 - X)^{\frac{2}{3}} \qquad (4-36)$$

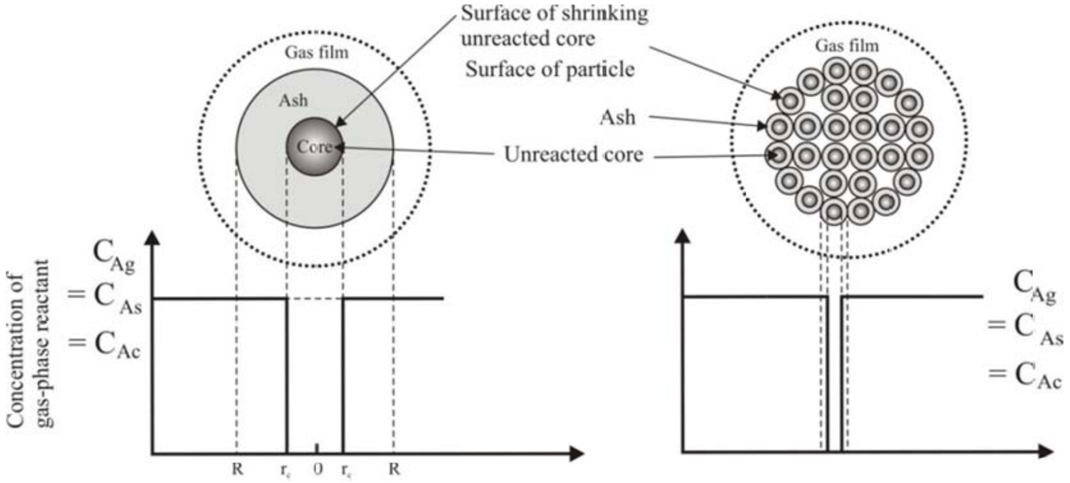

Figure 4-9: Gas concentration profiles and reaction progress with chemical reaction control of a non-porous solid (left) and a porous solid (right) [87]

If the reaction gas can enter the core of the particle unhindered, where the particle is of porous nature, the reduction starts at all regions within the particle at the same time. Every grain is reduced at the same time but in turn the reduction of the grains can be described by the shrinking core model with a sharp reaction interface. The main difference is that the reaction takes place at the inner parts of the particle as well as at the outer parts. The reaction does not depend on the initial particle size but however, this reaction mechanism has only been observed for small particles at lower temperatures.

4.2.3.4 Summary and Graphical Illustration

As the summary of the three described possible reaction mechanisms a graphical representation of the equations is given. In the left part of Figure 4-10 the equations 4-31, 4-33 and 4-35 are given, the progress of reduction X is plotted against the dimensionless time (given as the ratio $\frac{t}{\tau}$). On the right of Figure 4-10 the reduction rate in dependence of the conversion is plotted, according to equations 4-32, 4-34 and 4-36. It has to be noted that the right diagram only shows the qualitative progression during the whole reduction procedure and furthermore it is a time-independent depiction meaning that it does not give any information about the time that is needed to achieve full conversion.

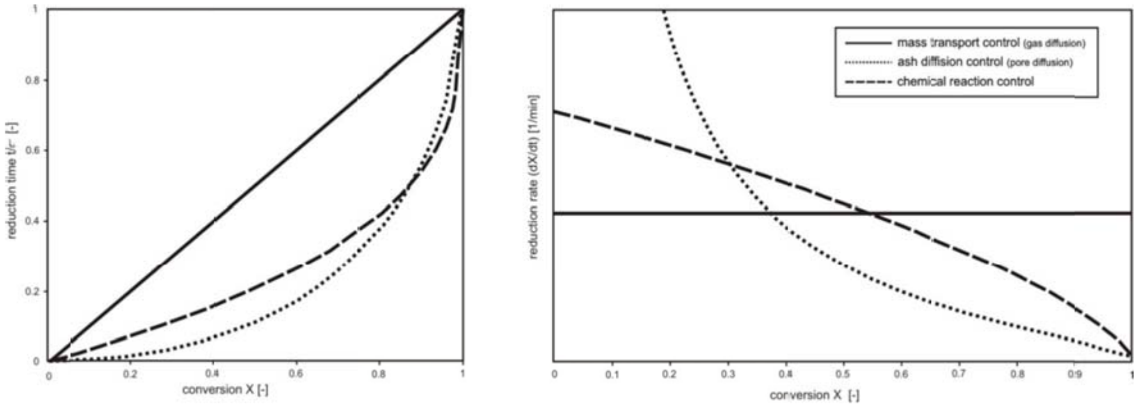

Figure 4-10: Time dependent conversion according to the different mechanisms (left) [49] and qualitative progress of reduction as a function of the reduction rate [85] (right)

The following conclusions can be drawn from that. If the mass transfer between the reaction surface and the bulk fluid is the controlling mechanism, the reaction is totally independent of the formed product and therefore the reduction rate remains constant for the entire period of time. The position of the curve within the diagram depends only on the temperature, the gas composition (equilibrium constants) and mass transfer parameters (initial particle shape and size, concentration differences as driving forces).

In the event that the controlling mechanism is only by pore diffusion, the curves are totally different. Besides the dependence on the same, and constant, parameters as for the mass transfer control the reaction is highly depending on the ash layer as a newly formed product. The ash layer in turn is dependent on the reduction progress in a complex way (layer thickness and surface of the spherical particles). At the initial stages the reduction rate is very high because the ash layer is very small and the conversion X proceeds very quickly, for example a conversion of 20 % is reached within only 1.5 % of the overall reduction time (dotted line in Figure 4-10).

The last described case, the control via the actual chemical reaction at the boundary between the unreacted core and the reduction product, is also given in Figure 4-10. Since the progress is dependent on the reaction surface, the reduction rate decreases during the further reduction progress because of the shrinking unreacted core.

Nevertheless it should be kept in mind that the mechanisms described are merely the extreme examples and will not occur separately. In the case of iron ore reduction, it is most probable that there will be a mixture of the different mechanisms or, more precisely, a reduction progress dependent shift of the rate controlling mechanism. At the early stages of the reduction the pore diffusion resistance hardly contributes because of the lack of an ash (product) layer and hence, the chemical reaction itself is the rate controlling step. From that point on, the reaction front moves inside the particle and the thickness of the ash layer increases more and more and the pore diffusion mechanism will become the rate controlling mechanism. Based on this description the reduction reaction is often divided into two different stages, earlier and final stages of reduction. This phenomenon has been described by [92,96].

For the reduction within a shaft furnace it can be assumed that the mass transport will hardly be the rate determining step. The gas velocity is sufficiently high and the ratio of particle surface to gas film thickness is small. This is in contrast to the reduction of fine ores within fluidized bed facilities where the mass transport indeed can be rate determining.

Different researchers have further pointed out that the reduction from hematite to magnetite and further to wustite proceeds considerably faster and therefore the rate determining chemical reaction is the final step in transforming wustite to metallic iron [40,43,68,86,89,94,97] and that for a first approach the assumption of a first order reaction is reasonable [49,89,91,92]. Most researchers describe the reduction proceeding according to the "shrinking core model" where the reduction proceeds in a topochemical way [49,88,89,95,94,97]. However, those observations could not be confirmed by [97] (in this case at temperatures lower than 1000 °C).

4.3 Combination of Thermodynamics and Kinetics - Different Types of Metallic Iron Formation

If hematite is reduced to iron then, in the course of the removal of oxygen, all the thermodynamically stable oxides of iron appear either successively or side by side. During the course of the reduction process, those phases which can co-exist with one another, i.e. Fe/FeO, FeO/Fe_3O_4 and Fe_3O_4/Fe_2O_3, are always in direct contact with each other. Which of the reduction products lie on the surface and are in direct contact with the gas phase depends not only on the corresponding phase equilibria (which refer to the thermodynamic point of view) but is also determined by the rates of removal of oxygen (chemical reaction control) on the one hand and by the diffusion process (pore diffusion control) on the other.

When considering the final reduction step, the formation of metallic iron as the rate determining step, this context of thermodynamics and kinetics can be described when considering the different types of metallic iron formed, visualized by light microscopic means. Altogether three different metallic iron formations have been described [7,13,68,98–101].

- ***Dense layer like, compact or topochemical iron formation*** occurs at lower temperatures but high reduction potential of the gas. The reduction starts at conditions of high nucleation densities at the grain surfaces by forming a thin metallic iron layer surrounding every wustite grain. Due to the lower diffusion rate the thin layer grows by moving inside with a sharp boundary interface (according to the shrinking core model) and subsequently forming a dense metallic iron layer. Because of the dense nature of the iron layers formed it is considered to be reduction hindering because of the high diffusion resistance and can even bring the reduction progress to halt.

- At higher temperatures and reduction potentials, the formed iron occurs in the shape of ***porous iron***. The high nucleation forming rates and good diffusion conditions lead to a sponge like appearance and subsequently, due to the porosity and therefore large specific surface, this form leads to a good reduction progress and is desirable.

- Furthermore a ***fibrous or acicular formation*** of the iron can be distinguished. When the reduction potential is quite low but not too low the temperatures, due to the low nucleation formation rates as well as good diffusivity, lead to a directional growth of metallic iron starting from the surface of a grain either towards the core (scraps and sparks) or growing perpendicular to the surface outwards as so called iron whiskers. It is these iron whisker formations that are known as the main mechanism for sticking of fine iron ores and are an undesired effect [102–105]. Further a fibrous iron formation lead to the phenomenon of swelling of pellets, which can in turn lead to catastrophic swelling (c.f. section 2.2.3) or disintegration of pellets.

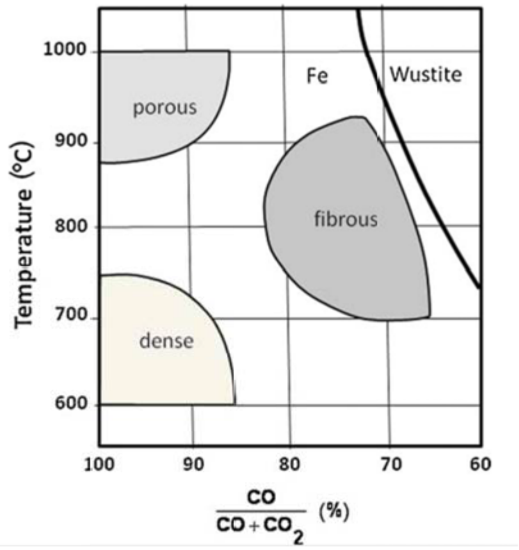

Figure 4-11: Regions of different metallic iron formation [7,98]

In Figure 4-11 the regions of occurrence of those three different forms of metallic iron are graphically shown in dependence of the gas reduction potential and the temperature. It has to be noted that this graph is only a very schematic depiction and the actual appearance is further influenced by a variety of parameters.

First of all the original structure of the ferrous material is of interest and furthermore the form and shape of the intermediate oxide products formed is assumed to influence the final iron formation. The first-mentioned ore structure and especially a large grain size and low porosity will have severe effects because of the lower nucleation density and longer diffusion pathways. Moreover, studies [40,66,68,106,107] have shown that especially dense wustite formation as a result of dense magnetite will enhance dense iron formation and therefore influence the reduction performance to a high degree when considering fine ore reduction. These circumstances have been depicted by means of the fluidized bed reduction with fluidized bed cascades where the earlier reduction step (formation of dense wustite and iron as a result of dense magnetite) could clearly be associated with the reduction performance of the latter steps.

As other influencing parameters, either the gas composition or the accompanying elements (of both ferrous burden and reducing gas) will change the metallic iron formation.

Investigations have shown [108–110] that lime and alkalis (potassium and sodium) definitely enhance the whisker formation and even small amounts of CaO can supress dense iron formation, whereas more CaO (> 4 %) will not further change the iron structure. In contrast to that, SiO_2 is responsible for an extension of the region for dense iron formation due to the formation of a fayalithic slag [98].

The influence of hydrogen is described opposed. On the one hand small amounts (1-2 %) of hydrogen are described [13] as changing the structure from porous to dense whereas other researchers [40,98] found that 100 % hydrogen atmosphere lead to porous iron formation exclusively and after the formation of a thin surface film (dense, layerlike) the material reduced from the inside towards the surface.

Additionally, it has to be taken into account that all the mechanisms described are only of unrestricted validity in ideal conditions. Due to the partial inhomogeneities within the reduction aggregates in an industrial scale process concerning temperature, gas compositions and material´s properties a mixture of the described metallic iron formation will always occur. In addition some of those observations that have been derived from the reduction of fine ores cannot always be adapted one-to-one for lump ores. The coarser particle structure enlarges diffusion ways and different agglomeration processes change the chemistry and morphological structure.

5 Literature Review – Influence on Reducibility and Mechanical Properties

Depicting a coherency between the reducibility and mechanical properties during the reduction process and process parameters like temperature and gas composition and furthermore with structural and chemical parameters of the ferrous burden material is a very complex and sophisticated aim. One the one hand a wide range of parameters influence the progress of oxygen release as well as mechanical stability but on the other hand it is the interaction between the single parameters that makes a prediction of the material's behaviour so difficult. These circumstances have led to comprehensive investigation work by many researchers concerning all the possible influencing factors, and additionally to a wide range of lab scale testing methods or even standardized testing procedures aimed at depicting and comparing materials behaviour. Following the description of the thermodynamic and kinetic fundamentals of the reduction of iron oxides in the previous chapter, within the subsequent sections the actual influence of different parameters on the reduction behaviour is listed. Since several of the factors that positively influence the reduction performance, high porosity and small grain size for example, adversely effect the mechanical properties, it is necessary to find a compromise solution in order to define the optimum material performance.

For the testing of the material's performance, a variety of different procedures have been developed in recent decades. Based on simple testing procedures, several standardized testing procedures have been derived, all with the aim of keeping the testing procedure as simple but yet expressive as possible. But since this simplicity struggles to meet the conditions present in an industrial scale process, it will be reasonable to further develop testing conditions to better meet different industrial scale process conditions.

5.1 Influencing Factors Concerning Reducibility

Since a depiction of parameters influencing the reducibility performance is very complex, different parameters are described separately but can never be seen separately within an industrial scale process. A distinct estimation of the change in reduction performance, expressible in numbers, by changing single or multiple parameters is almost impossible.

Additionally the variety of (lab scale) testing possibilities and facilities that have been used to gain results makes it difficult to give precise conclusions.

5.1.1 Temperature

As shown before, for different reasons, a higher temperature will always lead to a better reduction result. Although from the thermodynamic point of view the reduction of iron oxide to metallic iron is possible at quite low temperatures and the thermodynamic driving force for the reduction with CO/CO_2 even decreases as temperature increases (c.f. equilibrium line FeO-Fe in the Baur-Glaessner diagram in Figure 4-3). It is the kinetics that enhance the reduction velocity. Whereas the mass transport of the gaseous reducing agent is only slightly temperature dependent [85,94], the pore diffusion as well as the chemical reaction are distinctly more temperature dependent in a way that higher temperatures make both mechanisms easier.

Higher temperatures lead to a difference of metallic iron formation; due to the higher nucleation rate the metallic iron formed is of more porous nature and the pore diffusion is enhanced.

What has to be considered concerning the maximum temperature is that the appearance of molten and liquid phases can negatively interfere with the reduction performance. For a blast furnace process, the appearance of softening and sintering of the burden due to formation of liquid phases in the upper parts of the shaft can inhibit the gas flow and as a result an inhomogeneous gas distribution and channelling effects would occur. In the case of a direct reduction facility liquid phases are generally to be avoided because sintering and sticking effects would cause severe problems in terms of the discharge of the material.

In Figure 5-1 the temperature dependence of the reduction from hematite to wustite and of wustite to metallic iron is given, for both the reduction with H_2 as the reducing agent (black lines) and CO (grey lines), all for a hematitic ore. It can be seen that the gradual rise of temperature by 50 °C enhances the reduction velocity in every case, whereas the rise from 830 to 880 °C has more impact than from 780 to 830 °C, especially in the initial reduction step of hematite to wustite.

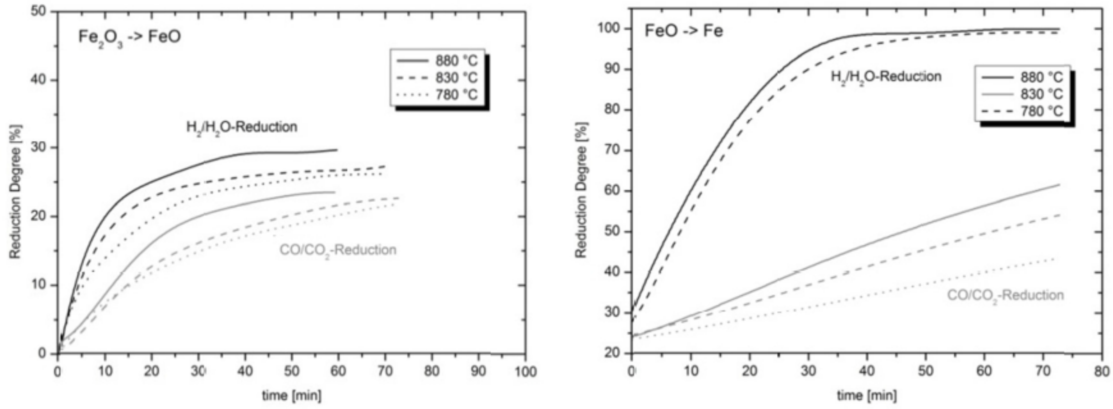

Figure 5-1: Temperature dependence of the initial reduction step of hematite to wustite (left) and the final reduction step of wustite to metallic iron (right) [92,119]

Other researchers [41,90,111–113] found similar results at similar testing conditions. For the transformation of hematite to magnetite *Kang et al.* [111,114] found a temperature dependence as given in Figure 5-2. Here the fractional reduction vs. time for the reduction of hematite pellets at the reduction temperatures 700, 800 and 900 °C is given. It can be seen that with a temperature rise from 700 to 800 °C the reduction progress is only slightly enhanced whereas a further temperature rise to 900 °C enhances the reduction results. As an example, the time needed to gain a reduction degree of 80 % (fractional reduction 0.8) decreases from ~70 min for 700 °C to

68 min and 55 minutes for 800 and 900 °C respectively which corresponds to a decrease of 3 % for the first 100 °C and 22 % for a rise up to 900 °C.

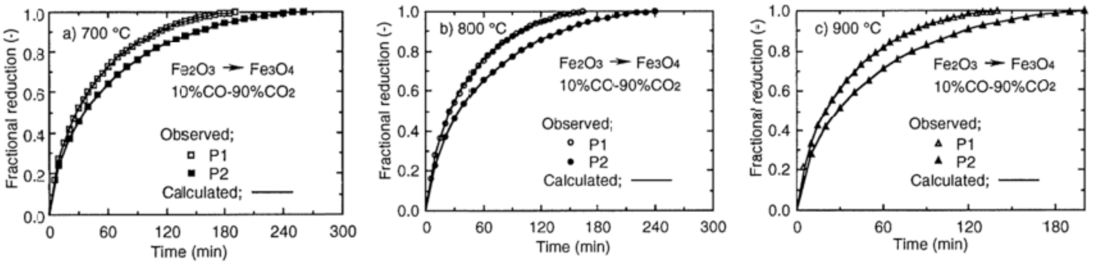

Figure 5-2: Temperature dependence of the reduction of hematite to magnetite [111]

Piotrowski et al. [41,42,90] showed the temperature dependence for a hematite powder by means of thermo gravimetric analysis as given in Figure 5-3. It can be seen that during the reduction with CO (left picture) as the reducing agent the gap between the reduction temperatures is greatest between 820 and 880 °C, the acceleration for reaching 80 % of reduction is 50 % (from 3 to 6 minutes). Generally it can be seen that the difference increases with the progress of reduction; until 60 % of reduction all the curves are within a narrow range compared to the later stages. When using H_2 as a reducing agent, the trend of accelerated reduction at higher temperatures is the same, whereby the gradual in the temperature led to a more or less uniform increase. *Edström* [40] also found similar results; in his work it is shown that a temperature decrease from 1000 to 900 °C did not significantly decrease the reduction rate for Fe_2O_3 (with CO gas), whereas a further decrease to 800 °C caused the reduction to be considerably retarded. The difference in the overall reduction time between the graphs given in Figure 5-1, Figure 5-2 and Figure 5-3 is a result of the significant difference in the particle size investigated and will be discussed later on.

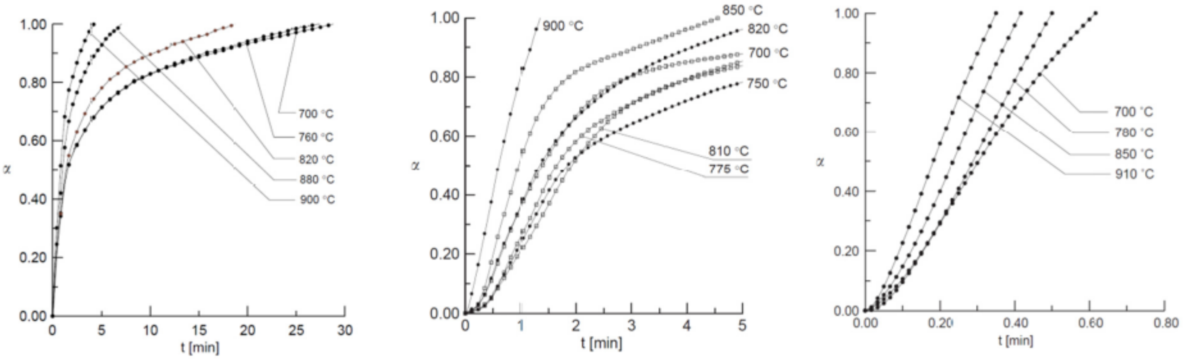

Figure 5-3: Temperature dependence of the reduction of hematite powder, reduction with CO (left), CO/H_2 mixture (middle) and H_2 (right) [41,42,90]

5.1.2 Gas Composition and Reducing Agent

As described before, the gas composition has a major influence on the thermodynamics of the reduction progress, as given in the Baur-Gleassner diagram Figure 4-2. A stronger reducing gas hence a gas mixture with a lower GOD will accelerate the reduction because of the greater thermodynamical driving force [115]. Another circumstance that clearly changes the reduction progress is the reducing agent used. Though from the thermodynamic point of few, at temperatures below 810 °C carbon monoxide is assumed to be the better reducing agent, the reduction with hydrogen is clearly enhanced, as depicted in Figure 5-1 and Figure 5-3. On the left side of Figure 5-1 (the reduction progress for the initial stages of reduction) the difference is distinctly less sidnificant than at the later stages. Comparing the highest temperature of 880 °C; after 40 minutes of reduction the reduction with hydrogen is almost finished, the maximum reduction degree of 33 % (theoretical value for the reduction of hematite to wustite, c.f. 4.1.3) is reached whereas for CO as reducing agent the RD has only gained ~22 %, in other words only reached two-thirds of the possible reduction degree.

This fact is even more obviously visible when the graph on the right, the reduction of the final step. After 40 minutes at 880 °C the reduction has completed for hydrogen but is around 47 % with CO.

The same facts can be pointed out in Figure 5-3. With the same testing procedure, even for the lower temperatures, full conversion to metallic iron could be reached within less than a minute. For the reduction of CO and at the highest temperature of 900 °C the time needed to gain 100 % RD is about 5 minutes. Some literature data give an acceleration of reduction between 75 and 400 % for pure H_2 compared to CO [40].

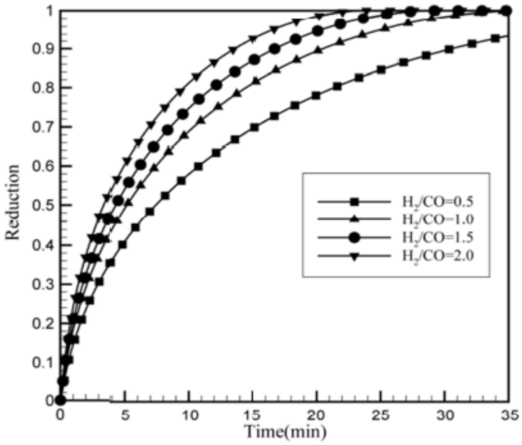

Figure 5-4: Influence of different H_2/CO rations on the reduction performance [89]

In Figure 5-4 the influence of different H_2/CO rations on the reduction performance is given, according to *Valipour et al.* [89]. The curves refer to a mathematical model for the reduction of pellets at a temperature of 900 °C, and the accelerated reduction with an increasing portion of hydrogen can be seen.

Despite the fact that at temperatures of 900 °C, hydrogen is the slightly better reducing agent, this significant increase of reduction velocity cannot be explained by thermodynamic reasons; at this temperature the difference between the equilibrium lines FeO-Fe and herewith the driving force for a chemical reaction in both cases is very small. The oxygen release from the crystal lattice and hence the mechanism of chemical reaction as the rate determining step is fairly similar for both reducing agents. It is more likely that due to the smaller hydrogen molecules, their diffusion to the reaction front (pore diffusion) is clearly facilitated. The less diffusion resistance for hydrogen also can be derived from the curves given in Figure 5-3. For the reduction of small particles (powder) the diffusion resistance is hardly present, and there is an almost linear reduction progress (right picture of Figure 5-3). By comparison to the CO reduction (left picture) it can be seen that at the final stages of reduction, even at higher temperatures, the progress slows down and this indicates that the reduction through the ash (product) layer is prevented.

5.1.3 Size of the Particles

Especially for kinetic reasons the grain size is of severe importance for the reducibility performance [43,111,116–118]. For the reduction of a hematite lump ore at 880 °C three different grain sizes have been investigated [92,119] and the graphs are given in Figure 5-5. For the reduction with hydrogen (black lines) it can be seen that in both cases (initial and final reduction steps) the difference between a grain size of 5.15 mm (mean diameter of 4 and 6.3 mm) and 11.25 mm, which is more than double the size, is not so great compared to the largest size with a mean diameter of 22.5, which is double the size again. When considering the grey lines (reduction with CO/CO_2) this trend is not that distinctive but yet there is a sharp decrease of the reduction performance by doubling the grain size at the initial stages of reduction. At the later stages the difference decreases further, the very slow reduction progress for the large grain size of 20-25 mm is additionally a result of the lower starting reduction degree which in turn is a result of the first reduction step. As an example it can be noted that after 30 minutes of reduction the RD gained 27.7, 24 and 13 % for H_2 and 20, 11.4 and 5.5 % for CO respectively.

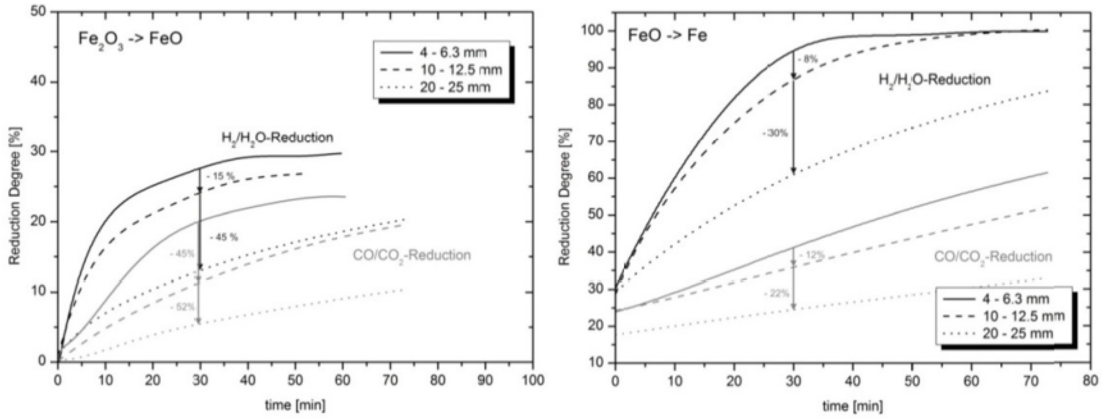

Figure 5-5: Grain Size dependence of the first steps of reduction of hematite to wustite (left) and final reduction step of wustite to metallic iron (right) [92,119]

This corresponds to a decrease of 15 % (H_2) and 45 % (CO) between the small and medium grain size and a further decrease of 45 % (H_2) and 52 % (CO). These values, as well as values derived the same way for the final stages of metallic iron reduction are graphically illustrated in Figure 5-5. From that it can be concluded that there is not a linear correlation between the grain size and the loss of reducibility; it is more likely there is a quadratic one. On considering the kinetics and hence the formulae for the reduction conversion progress given in 3-32 and 3-34, this fact is taken into account. The time calculated for full conversion τ increases with the square of the particle diameter, the assumption of the reduction of coarser particles as a pore diffusion controlled mechanism is substantiated.

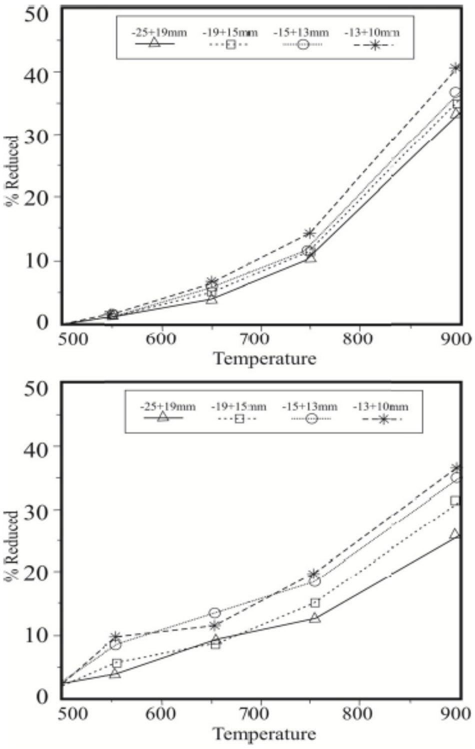

Figure 5-6: Reducibility of different grain sizes of lump ore (upper) and sinter samples (lower) [116,117]

For hematite pellets an attempt to depict the grain size dependence can be read from Figure 5-2. Pellets marked P1 correspond to a pellet diameter of 1.24 cm and P2 to 1.56 cm, which means an increase of 25 %. To achieve a reduction degree of 80 % the time increase at 700 °C is 33 %, whereas at 900 °C it is as high as 45 %, which indicates that due to the promoted reduction at higher temperatures, the effect of particle size increases.

Within their research work *Loo and Bristow* [116,117] compared different grain sizes of different materials, namely lump ore and sinter, at different temperatures, and some results are given in Figure 5-6. The size fraction between 10 and 25 mm is divided into four size fractions and reduced for 145 min at the different temperatures from 500 to 900 °C (not at standardized testing conditions) with the main result that it could be pointed out that particle size has a greater effect on lump ores than on sinter samples. This effect is assumed to be associated with the porosity of the material. It can also be seen that in both cases the decrease in reducibility and the increase in particle size is not linearly but quadratically.

5.1.4 Porosity and Pore Size Distribution

Generally, good reducibility is associated with materials having highly porous structure which provides passage for the reducing gas to penetrate and react with the iron oxide surface and for the gaseous product of the reduction reaction to escape. For kinetic reasons, over-fired iron ore pellets and hard, dense lump ores are not highly reducible because of their relatively low porosity [47,68,120–122].

Since the reduction reaction is definitely assumed to be majorly influenced by pore diffusion, the porosity of the material has severe impact on the reduction performance. But additionally, a more porous particle has a larger specific surface area and hence provides more surface for the chemical reaction; consequently the chemical reaction will be advanced with increasing porosity. Last but not least, when considering larger pores, the mass transport via gas diffusion might be enhanced. Generally speaking the porosity of lump ore is much higher than for pellets and sinters due to the lack of heating and pre-treatment steps. During sintering and burning the pellets are heated up to temperatures where (partly) the melting of binding phases occurs and therefore the pores are either filled with melt or have coarsened due to coalescence. Studies have shown [43,68,93,120,122,123] that for fine ores and partly lump ores the reducibility can directly be related to the microstructure and further to the porosity. In particular, ores with portions of limonite, goethite or siderite will have favoured reduction properties because of the cracks and pores formed during the release of crystal water upon heating [68,118,124].

Due to the fact that porosity influences all possible controlling mechanisms, a further distinction between fine and coarser pores is reasonable, since coarser pores will have more influence on gas diffusion whereas finer pores will enhance pore diffusion and chemical reaction. A problem when considering the different literature studies is the fact that a clear distinction between small and coarse pores can rarely be found, and there is also a general lack of a precise way to determine the specific surface area.

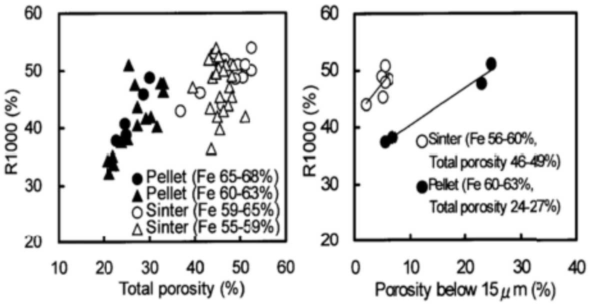

Figure 5-7: Effect of total porosity (left) and small pores (right) on the reducibility at 1000 °C [79]

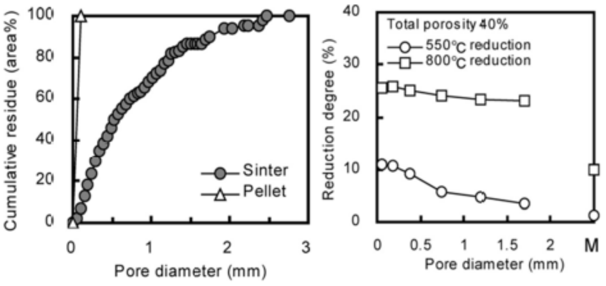

Figure 5-8: Pore size distribution (left) and reducibility at different pore diameters [125]

Higuchi, K., et al. [78,79,125] therefore compared the reduction performance of pellets and sinter samples in terms of their overall porosity (Figure 5-7 left) and small pores (right) at reduction conditions of 1000 °C. It can be seen that all the sinter samples have greater overall porosity compared to pellets, in fact up to twice as much. Assessing the micropores which refer in this case to pores below 15 µm in size, the sinter samples have distinctly lower porosity. Nevertheless, concerning reduction behaviour R1000 (reducibility at 1000 °C) the sinter samples are significantly favourable and this indicates that macropores have a greater influence. This circumstance is confirmed by [126–128], they succeeded in pointing out that sinter samples with increasing pore volume of pores of < 10 µm in size the reducibility is increasing.

Another study by *Higuchi and Heermara* [125] also showed the distinctly higher values concerning pore diameter of sinter samples compared to pellets (Figure 5-8, left) and additionally the inhomogeneous pore size distribution can be derived. The mean pore diameter has been determined at 0.05 mm for pellets and 0.53 mm for sinter, both industrial scale produced products. The reducibility of the different pore diameters at constant porosity is given in the diagram on the right. In this case the materials have been artificially produced and it can be seen that for both initial reduction steps, hematite to magnetite and magnetite to wustite, with an increase in pore size the reduction performance lowers, especially the transformation of hematite to magnetite declines more steeply. Contrary to that *Maeda and Ono* [129] found especially macropores to be the more reducibility influencing factor, the stated reason for this is that macropores supply reducing gas to each mineral grain and therefore play an important role in determining the overall reducibility of sinter. Nevertheless, the term macro- and micropore is very diverse within the different literature, mostly pores < 10 µm are deemed micropores whereas pores of a size > 20 µm are described as macropores.

5.1.5 Mineralogy

Since it has been described that that the increased reduction performance of limonite, goethite or siderite is more or less a result of increased porosity, *Edström* [40] described the difference in reduction performance of single and pure hematite and magnetite crystals, given in Figure 5-9. A prior oxidation of the magnetite samples to different extents (C and D in the figure) also enhances the reducibility to almost the same level as initial hematite. The influence of the origin of wustite on reducibility was also compared (right diagram) and it could be revealed that wustite from former hematite is far more reducible than wustite from magnetite. This could be confirmed by [68,106,130].

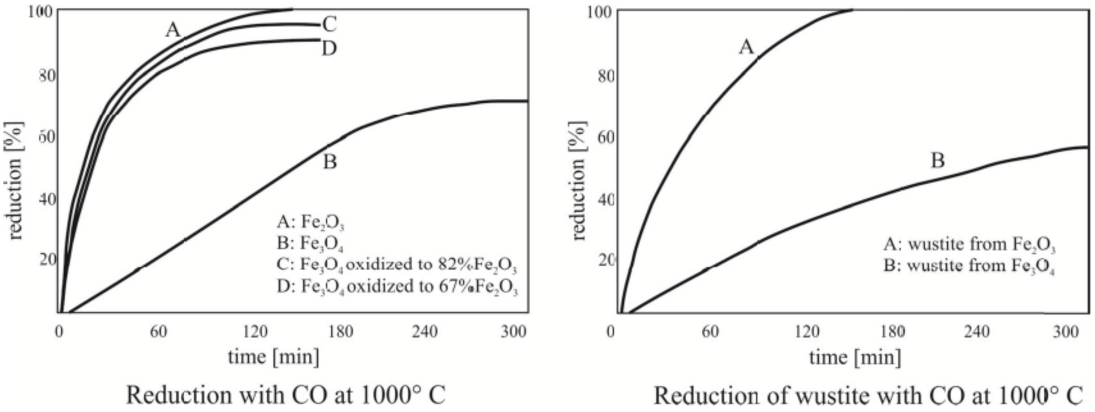

Figure 5-9: Reducibility properties of different iron oxides [40]

Based on this, it could be noted for sinter, that the transition of hematite grains to magnetite during induration, followed by re-oxidation to hematite upon cooling (secondary hematite), results in an increasingly irregular grain shape and increasing size. Consequently, due to cracks caused by stresses, the microstructure is more open structured. The result is a weak, open structure amenable to rapid reduction and breakdown [131–133]. Furthermore the better reducibility of hematite rich region compared to magnetite and spinel containing regions is described by [129] for sinter samples.

In general hematite phases are favourable for a good reducibility performance either naturally occurring in iron ores or within artificially produced agglomerates, in contrast to magnetite or spinel phases, which have a lower reducibility. Studies [134,135] showed that concerning pellets there is a dependence between pellet size and FeO and magnetite respectively, because of the insufficient oxidation during pelletizing.

5.1.6 Chemistry

Owing to the impossibility of changing the chemical composition of pure ore the influence of chemical composition concerning the different oxidic compounds is primarily investigated for sinter, partly for pellet brands. Therefore the amount and ratio of the different oxidic phases Al_2O_3, CaO, SiO_2, MgO and FeO are of major interest.

Increasing MgO contents reduces the reduction performance of sinter [133,136,137] as given in Figure 5-10. The decrease of hematite and calcioferrites and an increase in magnetite and spinel phases (which are known as having a lower reducibility) are given as reason for this [137].

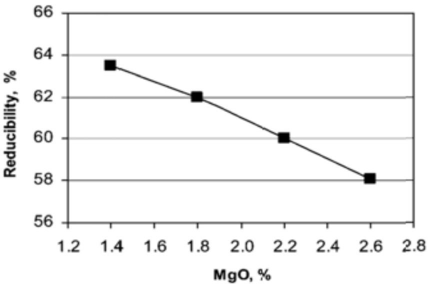

Figure 5-10: Influence of MgO on sinter reducibility [136]

Matsumura et al. [138] describe in their work that not only the presence of MgO but the origin of MgO is of importance. Sinter using dolomite actually increases reducibility whereas serpentinite as MgO source causes lower reducibility. One more circumstance is described by [137], there it is indicated that due to higher amounts of MgO the slag amount is decreasing by increased slag viscosity during the sintering process. The lower amount of fluid with a higher viscosity will have a limited flowability into the spaces between particles and hence the porosity might be increased.

The considerably high content of CaO as a flux within the sinter mixture of up to 15 % changes the reducibility properties distinctly because of the great variety of formed phases during sintering. Table 5-I gives an overview of different oxides containing Ca, Fe, Si and their reducibility properties. Though this list is only a selection of possible oxides a broad range of reducibility can be seen. What can be derived is that whenever there is silica included in the phases the reducibility is rather poor compared to those where only Ca, Fe and O prevail. It can be assumed that higher alumina contents promote the formation of fayalitic phases and the reducibility is impeded. When detecting ferrites of SFCA type (silicoferrites of calcium and aluminium) the strength as well as the reducibility is improved [85,133,139–141].

Table 5-I: Reducibility properties of different mineral phases [85,139]

Oxide	Mineral	Reducibility
Fe_2O_3	Hematite F	49.4
Fe_3O_4	Magnetite WF	25.5
$Fe_{3-x}Ca_xO_4$ (x>0.04)	Calcioferroferrite $W_{Ca}F$	30.0
$Fe_{3-x}Ca_xO_4$ (x>0.12)	Calcioferroferrite $W_{Ca}F$	37.6
$Fe_{1-x-y}Ca_xO$	Calciowustite W_{Ca}	27.0
$CaFe_2O_4$	Calcioferrite CF	49.2
$Ca_2Fe_2O_5$	Calcioferrite C_2F	25.5
$CaFe_4O_7$	Calcioferrite CW_2F	58.4
$Ca_3Fe_{15}O_{25}$	Calcioferrite C_3WF_7	59.6
$CaFe_3O_5$	Calcioferrite CWF	51.4
Fe_2SiO_4	Fayalite W_2S	5.0
$CaFeSiO_4$	Kirschsteinite CWS	12.8
$Ca_2FeSi_2O_7$	Ferroåkermanite C_2WS_2	6.8

Al_2O_3 is assumed to lower the reducibility performance for sinters as well as for iron ores [133].

Concerning the basicity as a summary of the previously described influence of the single oxide phases it can be noted that a higher basicity leads to a better reducibility because higher basicity leads to higher ferrite content [132,133]. In Figure 5-11 three different approaches for giving a correlation of sinter basicity and different reducibility parameters are given. As shown on the left side of the figure [139] the reducibility increases as the ration of CaO/SiO_2 exceeds 1.6. This is in good accordance to [129], the reduction rate increases constantly up to a basicity value of 2. In another research work plotted on the right side of Figure 5-11 [140] it is shown that on further increasing the basicity the reducibility decreases further. In this case this phenomenon is associated with a higher Al_2O_3 content at the very high basicities and subsequently the enhanced formation of hard reducible compounds oxides containing aluminum and silicon (low-iron alumosilicoferrites).

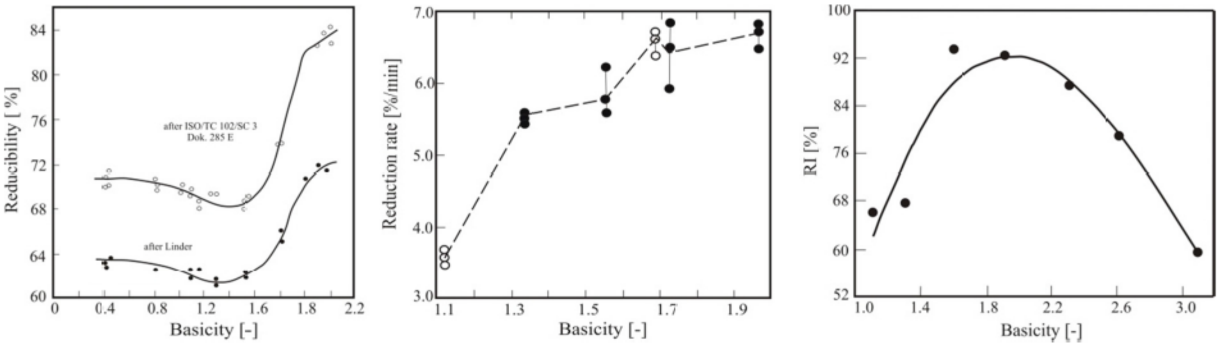

Figure 5-11: Influence of CaO/SiO$_2$ ratio on reduction degree [139] (left), reduction rate on basicity [129] (middle) and reduction degree on basicity [140] (right)

5.2 Influencing Factors Concerning Mechanical Properties

It is generally assumed that the strength after reduction is influenced by the strength before reduction and the strength of the different single components [125,132]. Porous ores for example will have bad mechanical properties at room temperature; the diverse dropping and falling processes will lead to a generation of fines. This behaviour will not improve during the temperature region of low temperature disintegration or on further decent of any reduction aggregate.

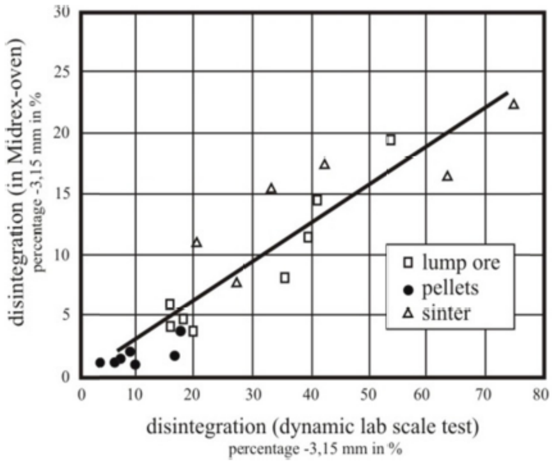

Figure 5-12: RDI tendencies of different raw materials [142]

The tendency of disintegration of different raw material groups is given in Figure 5-12 according to *Grebe et al.* [73,76,142]. The diagram also gives the comparison of industrial scale observations (the y axis plots the disintegration tendency -3.15 mm in a direct reduction facility) and lab scale test results (disintegration in a lab scale aggregate). This diagram reveals that pellets also barely tend to any disintegration. Some ore types will hardly disintegrate, whereas the majority of the sinter samples tend to fall apart to a very high extent. This figure also indicates that a lab scale test within a rotary tube (hence a dynamical testing method) leads to distinctly higher values than the static consideration for the industrial scale shaft furnace.

5.2.1 Reduction Rate

In their research work [125] a summary of the mechanical stability concerning artificially created compacts is given and it is pointed out that increasing porosity resulted in low strength after reduction due to their low initial strength as well as the high reduction rate.

Generally, on considering the described parameters that enhance reducibility, it is a logical consequence that this is at least partly in contrast to good mechanical properties. As pointed out, that the porosity is one key factor for good reducibility and furthermore it is obvious that a porous structure has weaker resistance to any mechanical stress. Therefor a negative empirical correlation between reduction performance and mechanical stability can be noted.

The described correlation between mineralogy and reducibility also leads to a direct correlation between mineralogy and mechanical stability during reduction. Together with the better reducibility of hematite, the induced cracks due to the volumetric change by transformation lead to a higher reducibility because of increased porosity. At the same time this increased porosity decreases stability, and the additional stresses due to rapid reduction weakens the structure [143]. So whenever one parameter increases the hematite content, it can automatically be assumed that the mechanical performance decreases to some extent. In literature it is recorded that in sinter with an oxidation degree lower than 90% (and hence high magnetite contents), disintegration is not as high a risk [76].

5.2.2 Temperature and Gas Composition

Wu et al. [143] described in their work the influence of parameters such as temperature and gas composition on the disintegration tendency of different raw material as shown in Figure 5-13. The diagrams are in good accordance with Figure 5-12, in every case sinter showed the worst resistance, followed by pellets and finally lump ores with the lowest disintegration tendency. Compared to lump ores, as for the sinter with high porosity, the reducing gas easily entered the sinter during the reduction process. As a result, the stress was highly centralized and led to more degradation. Besides, the strength of its bonding matrix is weaker, as is the ability of bearing the volume expansion, so the crack and degradation of sinter is more serious.

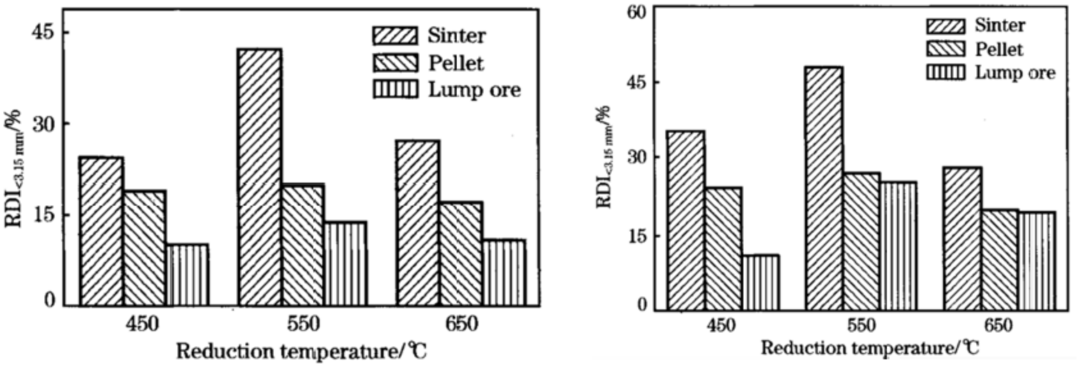

Figure 5-13: Comparison of $RDI_{-3.15}$ of different materials at different temperatures for gas composition A (without H_2, left) and B (25 % H_2, right) [143]

Concerning the temperature influence of the three kinds of iron oxide material all showed the tendency of inverted V-shape in the temperature range from 450 to 650 °C, and the RDI reached the maximum value at 550 °C. The influence of reduction temperature is that due to the certain increase in reduction rate with the rising temperature, the inner expansion stresses increase, and the materials tend to crack. On the other hand, with the rising temperature, the plasticity increases, and the ability to bear the volume expansion stresses increases beyond the critical point at 550 °C. On considering the gas composition, the reduction degradation is extended when mixing the gas with hydrogen, but the extents of influence are discrepant for the different materials. The influence of the reducing gas on lump ore is the greatest; the influence on sinter is second, and the sensitivity of pellets on the reducing gas properties change is relatively small [143].

5.2.3 Porosity

The mechanical strength of a sinter sample depending on the total porosity and in relation to the reduction degree is shown in Figure 5-14 [125]. Low-temperature reduction at 550 °C results in transformation of hematite to magnetite and at 800 °C further to wustite. The strength after reduction decreases sharply as a function of porosity, much more steeply than the strength of the unreduced samples. The highest strength occurred with fine, homogenously distributed pores (-0.125 mm), and with large pores in a dense hematite matrix.

A relationship between the specific surface area and the cold strength of sinter samples could be revealed by *Kasai et al.* [144–146]. An increase in specific surface area of ~ 30 % led to a decrease of the tumbling index of 20 %, from 62 to 50 %.

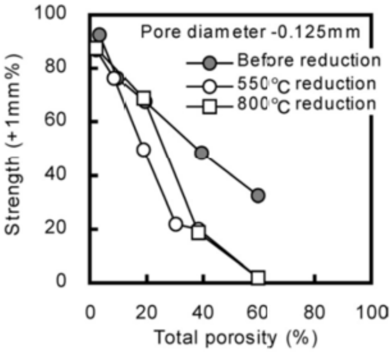

Figure 5-14: Strength vs. porosity [125]

5.2.4 Chemical Composition and Mineralogy

FeO increases RDI (lowers resistance against disintegration) because of increased magnetite content and therefore more hematite related volumetric increase due to transformation [73,76,124,131,132]. Concerning pellets a correlation between the prevailing magnetite content and the cold crushing strength could be revealed. Due to the insufficient firing process and the subsequently remaining FeO content, the FeO content is a function of pellet size and cold crushing strength of the pellet [134,135]. A study [132] of the fracture strength of the single components has shown the following sequence of mechanical stability: primary (or residual) hematite -> secondary (or precipitated) hematite -> magnetite -> SFCA (silico-ferrites of calcium and aluminium).
Al_2O_3 decreases RDI as a result of low temperature melting phases [133]. Alkalis and chlorine are both associated with lowering the disintegration performance [109,147,148].

MgO within the sinter is known to improve resistance against low temperature disintegration [77,135,137] as shown in Figure 5-15 according to two different research works but decreases the room temperature stability. As a reason for the first mentioned increase in RDI the magnetite (spinel) stabilization is named. For the drop of the tumbling index TI the formation of vitreous glassy matrix and dicalcium silicates, which are harmful to sinter strength, are given (because these structures exhibit a high degree of stress).

The diagrams in Figure 5-16 outline the cold compression strength of different apparent phases as well as the dependence of stability parameters on the basicity of different investigations concerning sinter. An increasing binder content results in higher CaO as well as higher basicity. In accordance with the diagram in the middle of the figure it can be seen that there is a loss on strength within the range of 1.2-1.5 which corresponds to a total binder content of 30.0–35.0 %. If the phase composition of the binder is considered, it is obvious that at this basicity, the binder consists mainly of ferrocalcium olivines and fayalite, which are phases of low strength. With increasing basicity the increasing formation of calcium ferrites of higher strength increases the strength [77,80,139,140,149]. Also the low temperature disintegration tendency (right diagram) has minimum values at the range of basicity of some 1-1.2.

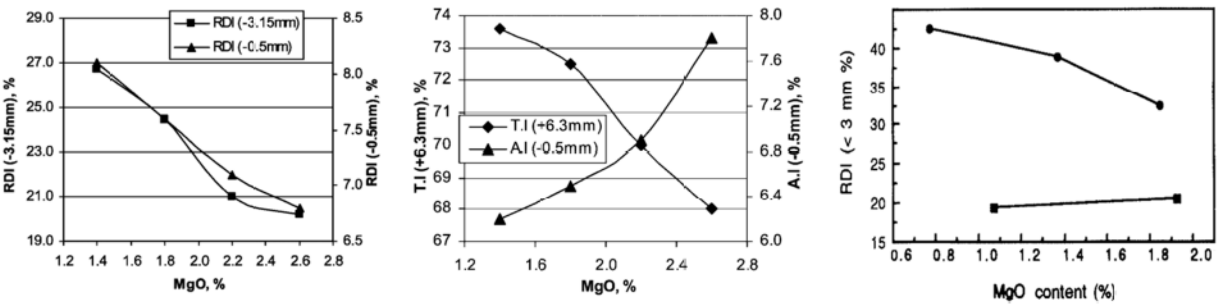

Figure 5-15: Influence of MgO on the stability at room temperature (left) [135] and TI values (middle) [135] and RDI values (right) [77]

Material	Compressive strength, kN/cm^2
Fe_2O_3	26.7
Magnetite Fe_3O_4	36.9
Olivine $CaO \cdot FeO \cdot SiO_2$	23.3
Olivine $CaO \cdot FeO \cdot SiO_2$ (glass)	4.0
Calcium ferrite $2CaO \cdot Fe_2O_3$	37.0
Fayalite $2FeO \cdot SiO_2$	20.3
Dicalcium silicate $2CaO \cdot SiO_2$	15.0

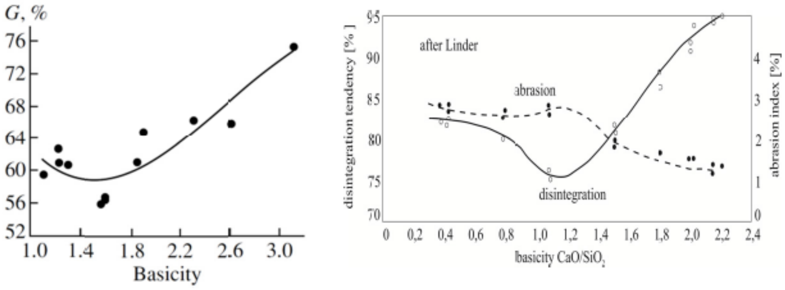

Figure 5-16: Influence of phases [80] and basicity on cold strength [140] and on the mechanical performance during reduction at weak reduction potentials (RDI) [139]

The following Table 5-II summarizes the described parameters. It can be seen that more often than not the influence on reducibility and mechanical performance is inverted. Only an increased CaO content and accompanying an increase in basicity will lead to a better overall performance.

Table 5-II: Summary of influencing parameters of reducibility and mechanical properties

Parameter	Influence on reducibility	Influence on mechanical performance	Explanation
Increasing temperature	↑	↑↓	Higher temperature promote the reduction kinetics, pore diffusion is facilitated even if thermodynamically lower temperatures would be favourable, for RDI above the critical value higher temperatures are favourable
Hydrogen content of gas mixture	↑	↓	Promotion of the reduction kinetics because of better pore diffusion (smaller molecules) and slightly better thermodynamics above 810 °C, more stresses because faster reduction
Particle size	↓		Inhibited kinetics due to less specific surface
Porosity	↑	↓	Provides larger surface for reduction, enhanced gas and pore diffusion, decreases strength
Hematite	↑	↓	Better reducible than magnetite, also wustite originated from hematite is better reducible than that originated from magnetite. Cracks during transformation decrease RDI stability, lower cold strength
FeO	↓	↑	Higher FeO indicates higher magnetite content, hence lower reducibility but higher mechanical performance
CaO	↑	↑	Results in greater portion of different calcioferrite phases which are better reducible, CaO stabilizes spinel (better strength) and creates more stable CaO phases
SiO_2	↓	↓	Formation of hardy reducible silicate and fayalitic phases, increases overall slag amount, formation of low strength phases (fayalithe, olivine)
Al_2O_3	↓	↓	Decreases RDI because of low melting phases, decreases reducibility by forming low reducible oxide phases (fayalithes,..)
MgO	↓	↑(↓)	Improves stability against disintegration (but decreases low temperature stability) because stabilizes magnetite but reduces reducibility
Basicity	↑	↑	By increasing the basicity (higher than 1.6) the CaO amount increases, therefore better reducibility and higher overall slag content makes it more stable due to more stable CaO containing phases

5.3 State of the Art – Lab Scale Testing

All those different parameters that will influence the reducibility performance as well as the material's strength combined with the wide range of material requirements as described in section 2.2, mean the possibilities of testing are numerous. Since the reducibility describes the oxygen release from the crystal lattice by a gaseous reducing agent, every testing procedure suitable for testing gas solid reactions can generally be considered as an option. Every testing procedure, starting from thermo gravimetric analysis to calorimetric analysis or fluidized bed reactor testing to name but a few, has its own testing conditions. In order to choose a lab scale testing facility and procedure that best meets the requirements for industrial scale applications, a comparison of for the current standards in lab scale testing has been performed. In choosing the best suitable testing conditions for depicting reducibility properties combined with the possibilities and restrictions of the lab scale testing facility, the following considerations have been taken into account.

- The pressure during testing needs to be atmospheric
- Temperature range should be within the region of indirect reduction
- Sample amount and size should be as close as possible to the industrial scale application
- At least some comparability to literature and industrial data should be granted
- Simultaneous testing of the mechanical properties for the sake of simplicity

A variety of different standardized testing procedures are available and considered suitable

Since the foundation of "International Organization for Standardization (ISO)" in 1946 [150] and covers all possible research fields except electrics and electronic the number of ISO standards for testing iron bearing raw materials is huge. The following

provide a summary of the most commonly used standardized testing procedure concerning reducibility and mechanical properties of lump burden material. For the sake of a cost and time saving lab scale test with a maximum of information output, it can be seen that some of the testing procedures cover both, the reducibility and mechanical testing procedures and are therefore listed in both tables.

, every reducibility test listed has a different operational mode, although the basic steps of testing are more or less the same. Within every test the sample portion (in most cases between 500 and 2000 g) is heated up at nitrogen inert gas atmosphere until reaching the desired final testing temperature. After some homogenization time the gas is switched to a reducing gas of variable compositions of the components CO, CO_2, H_2, CH_4 and N_2, which makes the reduction potential and the GOD of each test unique. Also the construction type of the reaction vessel is different. The simplest possibility of testing is a static testing within a small reduction tube. Also there are test with an application of a load on the burden material within a bigger reduction tube (125 mm), but still the test is a static one. Only the last mentioned is actually a dynamic test within a so called "Linder-Testing facility" which is a rotating horizontal tube. Finally the test results itself, are not straightforwardly comparable to each other. Some test give a time needed to gain a certain reduction degree as the result whereas other tests compare the reduction rate at different stages or the metallization degree after a distinct reduction time.

To test the mechanical or metallurgical properties concerning the mechanical stability, the variety of possible testing procedures becomes even more complex. Again only the most commercially used testing procedures are given in the table. From the testing procedures listed all mechanical testing procedures, which almost always comprise of some rotating tumbling procedure, refer to the mechanical stability after some reduction treatment, with the exception of the determination of the tumble strength (ISO 3271). These tumbling and abrasion indices temperature but always of a static nature. The subsequent tumbling procedure is executed in different kinds of drums. The Linder Test is once again an exception, due to the dynamic reducibility testing the mechanical stress is applied during the reduction procedure, not afterwards. The calculation always comprises a ratio of initial sample mass and the mass portion of some certain size fraction, determined by a sieving procedure.

Table 5-III: Standardized testing procedures for determining reducibility parameters

Standard	Name	Testing facility for reduction	T_{Red}	Gas component					Load	Aim/Output
			[°C]	CO	CO_2	CH_4	H_2	N_2	[kPA]	
ISO 4695	Iron ores - Determination of reducibility [52]	Vertical reduction facility, 75mm retort diameter	950	x				x		Determination of the reducibility index $(dR/dt)_{40}$
ISO 7215	Iron ores - Determination of relative Reducibility [151]		900	x				x		Determination of the RD after 180 minutes
ISO 11258	Iron ores for shaft direct-reduction feedstocks — Determination of the reducibility index, final degree of reduction and degree of metallization [152]		800	x	x		x	x		Determination of RD90 and metallization degree, reducibility index $(dR/dt)_{40}$ and $(dR/dt)_{90}$
ISO 7992	Iron ores - Determination of reduction properties under load [153]	Vertical reduction facility, 125mm retort diameter	1050	x			x	x	50	Determination of differential pressure and change of height of the bed at RD=80%
ISO 11256	Iron ore pellets – Determination of clustering of feedstock for direct reduction by gas reforming [154]		850	x	x		x	x	147	Determination of time needed for RD = 95% (in addition to Clustering Index)
ISO 11257	Iron ores – Determination of disintegration and metallization of feedstock for direct reduction by gas reforming process [55]	Horizontal rotating reduction tube (Linder-Test)	760	x	x	x	x			Determination of Metallization degree after 300 minutes of reduction (in addition to disintegration tendency)

Table 5-IV: Standardized testing procedures for different mechanical parameters

Standard	Name	Testing facility for mechanical stress	Comment	Aim/Output
ISO 8371	Iron ores for blast furnace feedstocks — Determination of the decrepitation index [155]	---	Heating up to 700°C at atmospheric conditions	Determination of $DI_{-6.3}$ (percentage of material < 6.3 mm)
ISO 4696-1	Iron ores for blast furnace feedstocks Determination of low-temperature reduction-disintegration indices by static method — Part 1 [53]	Rotating tumbling drum, inner diameter 130 mm	Reduction at 500°C with CO, CO_2, H_2,N_2 gas mixture	After reduction tumbling procedure with 300 revolutions and determination of RDI-1$_{+6,3}$, RDI−1$_{-3,15}$, RDI−1$_{-0,5}$;
ISO 4696-2	Iron ores for blast furnace feedstocks Determination of low-temperature reduction-disintegration indices by static method — Part 2 [54]		Reduction at 550°C with CO ,N_2 gas mixture	After reduction tumbling procedure with 900 revolutions and determination of RDI-2$_{-2.8}$,
ISO 4698	Iron ore pellets for blast furnace feedstocks — Determination of the free-swelling index [156]	---	Reduction at 900°C with CO ,N_2 gas mixture	Determination of the free-swelling index (indicates the volume change of the pellets during reduction)
ISO 11256	Iron ore pellets – Determination of clustering of feedstock for direct reduction by gas reforming [154]	Rotating tumbling drum, inner diameter 1000 mm	35 revolutions ins total	After reduction testing, determination of clustering index CI (percentage of mass that have clustered)
ISO 15967	Direct reduced iron — Determination of the tumble and abrasion indices of hot briquetted iron (HBI) [157]		25 r/min for 200 revolutions	Determination of tumbling index TI (mass portion > 6.3mm) and abrasion index AI (mass portion < 0.5mm)
ISO 3271	Iron ores – Determination of tumble strenght [158]		Raw material, 200 revolutions	Determination of tumbling index TI (mass portion > 6.3mm) and abrasion index AI (mass portion < 0.5mm)
ISO 11257	Iron ores – Determination of disintegration and metallization of feedstock for direct reduction by gas reforming process [55]	Horizontal rotating reduction tube (Linder-Test)	Reduction at 760°C with CO, CO_2, CH_4, H_2,N_2 gas mixture	After reduction testing, determination of RDI$_{-3.15}$ (percentage of material < 3.15mm)
ISO 13930	Iron ores for blast furnace feedstocks – Determination of low-temperature reduction-disintegration indices by dynamic method [56]		Reduction at 500°C with CO, CO_2, H_2,N_2 gas mixture	Calculation of the low-temperature disintegration indices (LTD$_{+6.3}$, LTD$_{-3.15}$ and LTD$_{-0.5}$)

6 Experimental Setup and Testing Facilities

In the following sections the different testing facilities and investigation methods used for this research work (as a consequence of the previously described demands for a suitable lab scale test) are briefly described. Since the vertical reduction aggregate is the most complex lab testing facility it is described more comprehensively, whereas for other facilities external sources of further information are provided. However, a variety of testing and investigation have been performed with other testing facilities, not all of them located at the Chair of Ferrous Metallurgy. This description is intended to give a short overview of the experimental setup and the methodology of testing: a detailed description of the operation mode of the facilities can be found within the aforementioned literature references.

6.1 Reducibility Testing - Vertical Reduction Aggregate

The main lab facility for exploring the reducibility behaviour of different raw materials is the vertical reduction aggregate. The facility for performing the reduction tests as well as reactivity tests was designed and constituted by *Siemens VAI Metals Technologies* in 2011. Besides the need to conduct various standardized testing procedures (see Table 5-III and Table 5-IV) it was necessary to perform more sophisticated testing procedures. To perform different modifications of the standardized testing procedures or even the approach of depicting any industrial scale process, different adaptations and modifications have been considered. Whereas any standardized testing procedure runs in a more or less steady state mode in any industrial scale process, parameters like temperature and gas composition change dependent on time. Therefore the process control unit in particular can be computed to that; hence it is possible to linearly change the gas composition within a given period of time through simultaneous heating or cooling. Tests can be run fully automatically or manually if desired.

A schematic drawing of the reducibility testing apparatus is given in Figure 6-1; additionally Figure 6-2 shows pictures of the facility as set in the laboratory. Table 6-I summarizes all the technical data. Besides the reduction retort where the reduction reactions actually occur, the facility consists of a process control unit, a gas supply unit, a gas mixing unit (including humidification and preheating components), an electrically heated furnace with three heating sections, a weighing device and finally an offgas system.

The whole testing procedure can be summarized as follows. In the first step the material for testing is set inside the high temperature stainless steel reduction retort which is 75 mm in inner diameter. In order to guarantee that the sample material is placed in the hot zone of the furnace and hence an even temperature distribution, a metal grid is set inside the retort. A double-layer of alumina balls is filled on top of this, both for preheating the gas flow and to ensure a uniform gas flow through the overlaying burden material. The sample portion of 500±1 g, which refers to a height of about 10 mm, is finally covered by another two layers of alumina balls, according to the standard.

After filling, the retort has to be closed properly (reasonably gas-tight), hung onto the weighing device, connected to the thermocouple (which is set inside the sample portion) and positioned into the furnace. It must be ensured that there is no contact between any of the retort parts and the furnace so there is no failure in measuring the weight loss. The process parameters as temperature, gas composition, heating rate, etc. for the entire testing procedure have to be entered to the process control unit. After switching on the off-gas system, which ventilates the off-gas above roof level without any post combustion, a short purging with nitrogen is inevitable to start the test. At the very moment the test is started, the process control unit starts recording the entire process data at a 5-second interval. During the heating up period the retort is purged by nitrogen, the heating performance of each of the three single heating elements is controlled separately by the thermocouples within each heating element as well as the thermocouple set inside the sample. On reaching the determined sample temperature, the purging gas is switched to the defined reducing gas composition. Each single gas component is provided from gas bottles and the flow rate is controlled by flow meters of different ranges. If desired, the nitrogen gas flow can be humidified; two different gas evaporators and gas-preheating units are available for this purpose. The gas, either dry or humidified, is mixed at a certain point within the gas mixing unit. Via metal pipes and finally a hose the gas enters the retort at the upper point, flows downwards along the outside of the retort, where it is first preheated and then enters the reaction vessel at the lowest point. During the up flow through the alumina balls, the gas is finally heated up when it comes in contact with the sample material. The reduction reaction proceeds within the sample and the oxidized reduction gas leaves the retort at the upper point into the offgas system. The weight loss caused by the oxygen release is measured and contemporaneously the reduction degree is calculated. The test is finished automatically when the previously defined testing time has run out, or manually if the time needs to be shortened or exceeded. The gas is again switched to nitrogen purging gas until the sample temperature is below 80 °C and hence the retort can be disassembled.

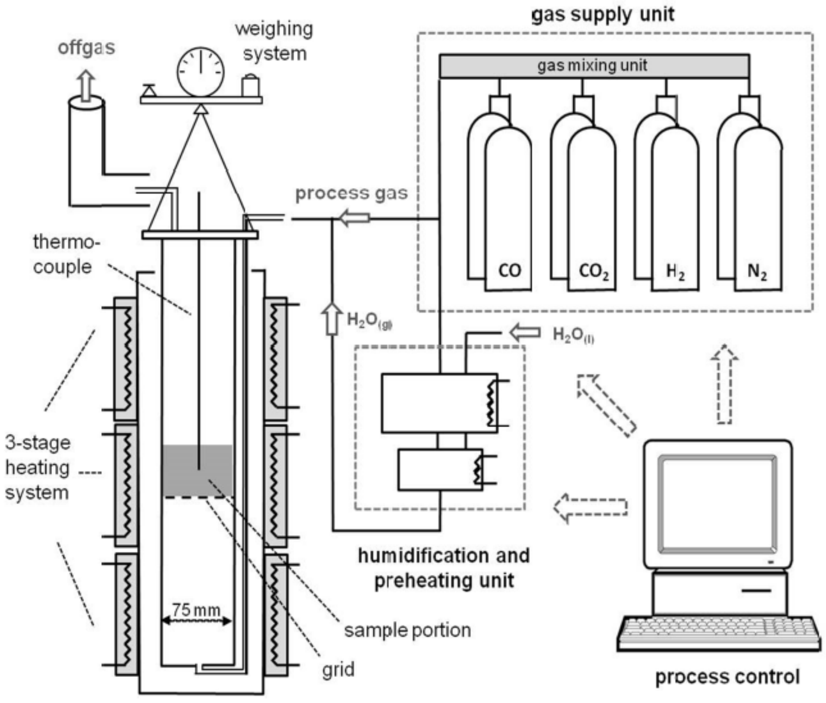

Figure 6-1: Constitutional plan of the vertical reduction aggregate as set in the laboratory

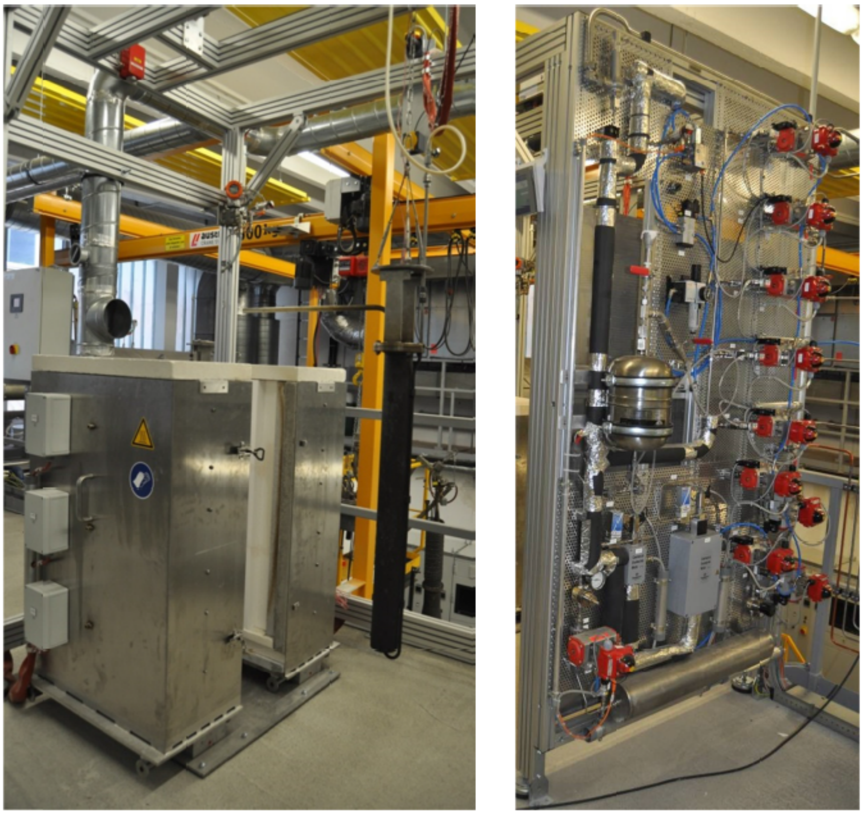

Figure 6-2: Photo of the furnace and the reduction tube (left) and the gas mixing unit (right)

Table 6-I: Technical data of the vertical reduction aggregate

Furnace details	Range	Unit
Number of heating elements	3	[---]
Power	3 x 2.4	[kW]
Temperature range	RT - 1100	[°C]
Heating rate	30	[K/min]
Gas supply system		
Gas flow N_2	2-100	[Nl/min]
Gas flow H_2	0.5-25	
Gas flow CO	0.7-35	
Gas flow CO_2	0.5-25	
Gas flow H_2O	0.60-500	[g H_2O/h]
Additional facts		
Recording of data	5	[sec]
Weighing device	0-64 000	[g]

6.2 Other Lab Testing Equipment and Methods

Since the characterization of the different burden materials is not finished just by depicting the reduction properties but rather by merging all the single pieces of materials characteristics to get a full picture of the material´s behaviour, far more testing methods with different facilities were applied.

6.2.1 Rotating Tumbling Drum

In order to test the mechanical behaviour a rotating tumbling drum according to the standard [53,54] has been used. A picture and a schematic drawing of this facility are given in Figure 6-3. The equipment consists of a metal vessel with an inner diameter of 130 mm which is connected to the motor unit by elastic tensioning clamps. With the process control unit the number of revolutions are adjusted and monitored.

The material is set inside the proper closed drum; the rotation starts with a rotation speed of 30 rpm for a total of 900 revolutions. Afterwards the masses of the grain size fractions are determined by carefully sieving the sample portion with both standardized sieves and a standardized sieving procedure according to [53,54]. With the grain size distribution, different values for describing the mechanical behaviour can be calculated.

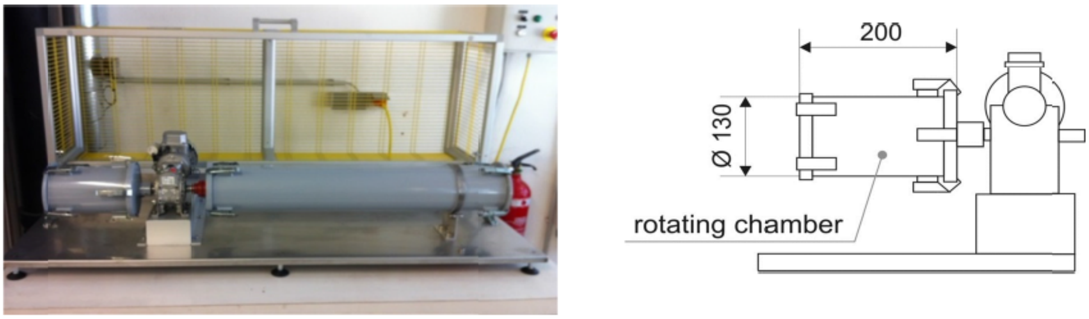

Figure 6-3: Picture and sketch of the rotating tumbling drum

6.2.2 Light Microscopic Analysis and Scanning Electron Microscopy

In order to make a morphological characterization for both, the raw as well as the reduced material, every sample is investigated with the light microscope. With a reflected light microscope of the type *Olympus BX60* from the manufacturer *Zeiss* as used for this work, the surface of polished samples can be investigated. Therefore the samples have to be prepared in order to obtain polished sections with a suitable surface, and the preparation procedure can be summarized as follows.

For the investigation with microscopic means only a part of the sample portion is considered, nevertheless it has to be ensured that the number of pieces is sufficient to give a representative picture of the materials morphology.

Of each material, raw or reduced, some pieces with the size of 10-12.5 mm (the same size as for the reducibility tests) were taken randomly. Due to the restricted size of the lab facilities the pieces have to be cut into halves or even quarters. These smaller pieces are imbedded in resin.

After the hardening of the resin the polished sections pass through a number of grinding and polishing steps.

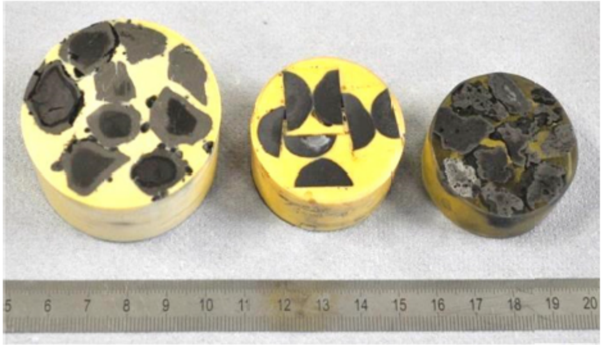

Figure 6-4: Polished sections of a lump ore (left), pellet particles (middle) and sinter pieces (right)

During the whole preparation procedure it is important to avoid any modification of the material due to mechanical (breakout, smearing), chemical (dissolution, transformation, reaction) or thermal (disintegration) influences. The phases must be retained regarding their characteristics and additionally the polished sections should be free from cracks, open pores and scratches. It has further been taken into account that especially sinter samples have to be handled with care regarding water. Due to an incomplete and insufficient sintering process, still some water soluble components, such as calico-silicate phases, might still prevail. These can react with water; even small portions of water (for example within the alcohol that is used for cleaning the polished sections) can lead to a partial dissolution of silicates.

Figure 6-4 shows exemplary finished polished sections, ready for light microscopic investigation. On the left, some pieces of a (reduced) lump ore, in the middle some pellet particles that are cut into quarters and on the right pieces of a (reduced) sinter sample. Two different resins have been used, in most cases a mixture of the resin Araldit F and the hardener Araldur HY 905 at a ratio of 1:1 was decided as best for the further requirements (transparent appearance, visible in Figure 6-4 right side).

6.2.3 B.ET. – Specific Surface Area Measurement

The B.E.T.-technique is named after the inventors *Stephen Brunauer, Paul Hugh Emmet and Edward Teller* and describes an analysing method of sizing surfaces by means of gas adsorption. This method is broadly used, especially for porous but solid materials, and can be carried out according to the standard DIN ISO 9277:2014-01 [159].

During the measurement of the specific surface area, an equivalent amount of adsorptiongas (widely used gases are nitrogen or carbon dioxide) is passed over the sample. At the surface an equivalent amount of the gas is adsorbed, depending on the pressure and temperature. By performing the tests at a certain and constant temperature the adsorbed gas amount now only depends on the pressure. When increasing the pressure within the apparatus, the gas is partly adsorbed at the material's surface and desorbed on pressure release. Subsequently the adsorption-desorption-Isotherms can be determined and based on those curves the specific surface can be calculated and given as surface area per unit mass, mainly given as m^2/g. For a detailed description of the testing and calculation methods and models see elsewhere [159–162].

For the determination within this investigation work the following testing parameters can be summarized. The lab facility at the Chair of Non-Ferrous Metallurgy which was used is of the type *Quantachrome NOVA 2000e*. To meet the circumstance of testing lump burden material in terms of reducibility properties of those coarser particles, it was aimed to use a particle diameter within the same grain size as is subsequently used for the reducibility tests. Since the grain size of 10-12.5 mm particle diameter is not suitable for the testing facility, the particles were within the size range of > 6.3 and < 10 mm. In every test some particles (between 5 and 10 with a sample weight of 7-12 g) are set inside the glass sample container at the testing facility and in the first step a preheating for degassing for at least three hours at 350 °C was performed.

The gas used for adsorption was nitrogen and the measuring temperature was 77K. For every raw material at least three tests with a positive result were performed and the resulting mean value is subsequently used to describe the specific surface of the material.

6.2.4 Chemical Analysis

For the determination of the chemical analysis both for the raw materials and the reduced samples, the samples were sent to be examined at the laboratory of the *voestalpine Stahl Linz*. Therefore a series of chemical and physical methods can applied whereas the most important ones used are titration for determining the metallic iron, Fe^{2+} and further Fe^{3+} and X-ray fluorescence analyses for the total iron content and the elementary analysis [163–166].

6.2.5 Definition and Determination of the Loss on Ignition (LOI)

The loss on ignition, hence the release of crystallization water or the release of carbon dioxide on heating under inert-gas atmosphere has been determined prior to the reducibility testing as part of the raw material characterization. Unlike some other methods used in this case the loss on ignition only refers to the release of crystallization water within limonitic parts and/or calcination of siderite parts within the ore according to the decomposition reactions

$$FeO(OH) \rightarrow FeO + H_2O_{(g)} \quad and/or \quad FeCO_3 \rightarrow FeO + CO_{2\,(g)}$$

Therefore the sample portion of 500 g (the same sample portion that is subsequent used for reducibility testing) is set inside the vertical reduction aggregate (cf. 0). Before starting the reduction, test the material is heated up at nitrogen purging until reaching 950 °C and the weight loss is recorded. From the weight loss of these 500 g sample portion the LOI given in wt.-% can be recalculated.

7 Methodology of Testing

The first approach to the behaviour of the different materials after the characterization of the raw material by chemical and morphological characterization was the testing at standardized testing conditions. Since the standardized testing procedure ISO 4695 is the most commonly used and known standardized test, all the standard tests were executed according to that standard. This enables a comparison of the materials morphology and reduction behaviour. Additionally, by means of interrupting some tests, the morphological evolution of the different phases can be seen. Combining these results with the testing of the mechanical behaviour, a first picture of the different ferrous burden material can be given.

For the next testing series, different considerations have been taken into account. On the one hand an attempt to depict the distinct influence of single process parameter variations, whereas on the other hand it was hoped to describe the performance at conditions as they exist in industrial scale processes. In order to do so, testing procedures as an approach to blast furnace and direct reduction facilities have been developed. According to literature and industry data, time dependent temperature and gas composition profiles are determined which are assumed to best depict the conditions during the material's descent of the shaft part. Additionally the material testing included a mechanical testing procedure, before (for raw material characterization) and after each and every testing procedure to describe the evolution of the material's stability behaviour after the different reducibility treatments.

Subsequent to the ISO testing and some modification of the standard, in total five different industrial scale testing conditions have been repeated for three iron ores, three pellet brands and two sinter samples. The following sections describe the methodology of testing and ideas behind it.

7.1 Calculation of the actual Reduction Degree (RD)

According to the definition of the reduction degree given in 4.1.3, the RD can be calculated by

$$RD = \left(1 - \frac{X}{1.5}\right) \cdot 100 \qquad with \qquad X = \frac{O}{Fe_{tot}} \qquad (in\ \%) \qquad (7-1)$$

whereby O are the moles oxygen bound to iron and Fe_{tot} are the moles of iron within the sample. The reduction degree of 0 % refers to pure hematite and 100 % to pure metallic iron. During the test the reduction degree is calculated online as a result of the continuous weight loss of the sample. Therefore the oxygen content bound to iron (given in g) of the sample has to be calculated. For this purpose the reduction degree of the raw material (i.e. magnetite content) has to be taken into account by calculating a pre-reduction degree.

- Calculation of the O-content and the pre-reduction degree

The theoretical oxygen content O_{theor} of the sample portion considers the sample portion as only consisting of hematite, hence fully oxidized with a reduction degree of 0.

$$O_{theor}\,[g] = SamplePortion\,[g]\cdot\frac{Fe_{tot}}{100}\cdot\frac{3}{2}\cdot\frac{16\left[\frac{g}{mol}O_2\right]}{56\left[\frac{g}{mol}Fe\right]} \qquad (7-2)$$

The sample portion is known from the sample preparation and is defined with 500 ±1 g and the wt.-% of total iron (Fe_{tot}) is known from the chemical analysis. Since known from the chemical analysis that not all raw materials are fully oxidized to Fe_2O_3, the actual oxygen content O_{act} takes possible magnetite parts into account:

$$O_{act}\,[g] = SamplePortion\,[g]\cdot(FeO\ \cdot 0.22 + Fe_2O_3\ \cdot 0.30) \qquad (7-3)$$

where the wt.-% of FeO and Fe_2O_3 refer to those from the chemical analysis. The difference of those to O-contents is referred to the pre-reduction degree RD_{pr} of the raw material.

$$RD_{pr}\,[\%] = \frac{O_{theor} - O_{act}}{O_{theor}} \qquad (7-4)$$

- Online calculation of the reduction degree

The reduction degree can generally be described as the ratio of oxygen that has been removed from the crystal lattice of the iron oxide and the overall oxygen content prevailing in the raw material, the change of reduction degree during the process (depending on the time t) can be calculated by:

$$\Delta RD(t) = \left(\frac{O_{rem} = weight\ loss\ (t)}{O_{theor}}\right)\cdot 100 \qquad given\ in\ [\%] \qquad (7-5)$$

whereby both oxygen contents are given in gram. The overall reduction degree at every stage of the reduction process can furthermore be given as:

$$RD(t) = RD_{pr} + \Delta RD(t) \qquad (7-6)$$

It is this reduction degree RD that is subsequently used in describing the reduction progress at every stage for every test result.

From the reduction curves, as a result of the weight loss recorded, the reduction rate dR/dt is subsequently calculated and described. Therefor the weight loss curves are smoothed by implementing a spline followed by the calculation of the first derivative. This first derivative describes the reduction rate at any point during the reduction process and gives a good indication of the progress of reduction.

7.2 Reducibility Tests – Standardized Testing Procedure

The standardized testing procedure according to ISO 4695 [52] is a commonly executed and quite simple test but at the same time the results are very expressive. The exact ways and means of the testing procedure is given elsewhere [52] but nevertheless the important parameters are summarized and the way of evaluating the results is given.

A sample portion of 500±1 g is set inside the vertical reduction facility and heated up under constant nitrogen purging gas flow of 50 l/min. On reaching 950 °C and an additional temperature homogenization time of 10 minutes, the gas composition is switched to a mixture of 30 l/min N_2 and 20 l/min CO, which corresponds to a GOD of 0. The weight loss beside any other process data is measured at 5 seconds intervals and additionally the reduction degree at every stage is calculated and plotted.

7.2.1 Description of the Evaluation – ISO 4695

As an example of the evaluation of the results, test data of a limonitic iron ore is given in Figure 7-1. The temperature of the sample (thin grey line), the gas flow (dashed lines), the weight loss (grey) and the calculated reduction degree (black) versus time are compiled. From plots like these the following results and conclusions can be derived.

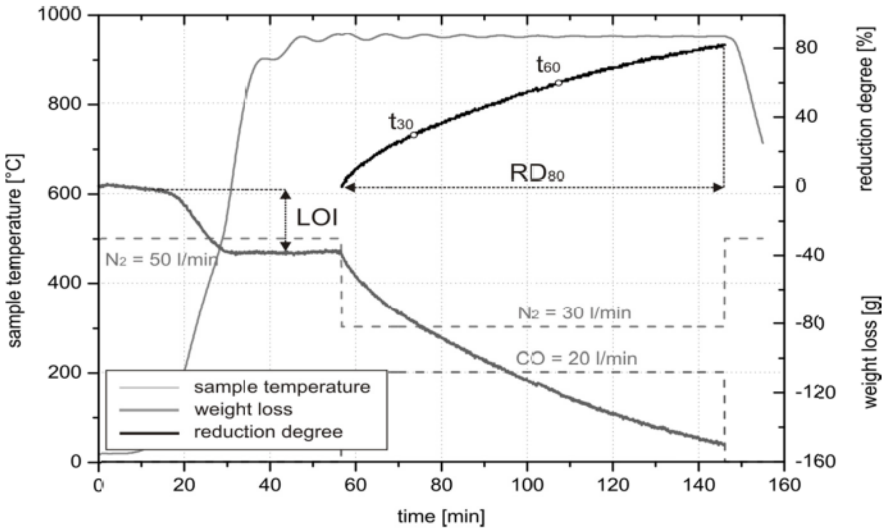

Figure 7-1: Example of the recorded data and interpretation of characteristic values

The weight loss during the heating period is related to the release of crystal water and is designated as LOI (c.f. 6.2.5). From the reduction curves two important standardized parameters can be determined. First it is important to mention the value for RD_{80}; this is subsequently given for every test result and is assumed to describe a materials performance well. RD_{80} is defined as the time needed to gain 80 % removal of oxygen. The value $(dR/dt)_{40}$ gives the reduction rate. It is calculated from the time needed to reach a RD of 30 and 60 % respectively.

$$RD_{80} = RD_{pr} + \left(\frac{O_{rem}}{O_{tot}}\right) \cdot 100 = 80\,\% \qquad given\ in\ [min] \qquad (7-7)$$

$$\left(\frac{dR}{dt}\right)_{40} = \left(\frac{33.3}{t_{60} - t_{30}}\right) \cdot 100 \quad given\ in\ [\%/min] \qquad (7-8)$$

7.2.2 Modification of ISO 4695

The first approach to more industrial scale related testing conditions led to a modification of the ISO 4695 standardized test. Whereas the original testing conditions prescribe a GOD = 0 (gas consists only of CO and N_2) the same test was executed with a GOD of 0.10 (by substitution of CO by 10 % CO_2 in the gas mixture). For a further depiction of the hydrogen effect the test was further modified by adding 3 and 6 % H_2 (substitution of CO respectively), the testing conditions are either graphically given in the Baur-Glaessner diagram in Figure 7-2 or in tabular form in Table 7-I. Additionally, the shift of the stability fields of the Baur-Glaessner diagram caused by the portion of hydrogen within the gas can be seen in this figure. The solid grey line refers to a mixture only composed of CO/CO_2 whereas the dashed line refers to 3 % H_2 and the dotted line to 6 % H_2 respectively. However, from a thermodynamical point of view, this small portion of hydrogen addition does not cause any great changes.

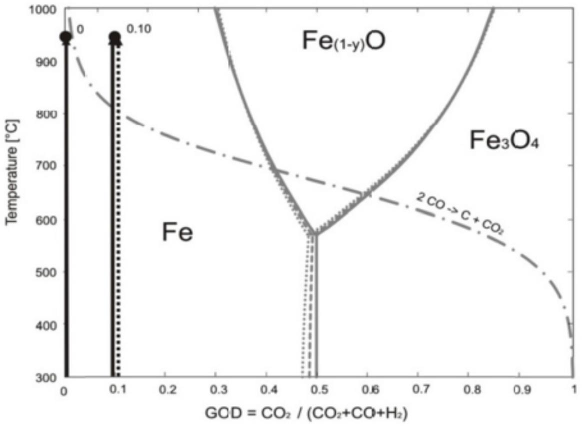

Figure 7-2: Gas composition of different modified ISO 4695 conditions

Table 7-I: Gas composition of modified ISO 4695 testing procedures

	ISO 4695	GOD 0.1	GOD 0.1 3 % H_2	GOD 0.1 6 % H_2
		[vol.-%]		
CO	40	36	33	30
CO_2	-	4	4	4
H_2	-	-	3	6
N_2	60	60	60	60

7.3 Reducibility Tests – Industrial Scale Process Conditions

For a testing procedure that approximates reality by means of temperature dependent gas profiles, some considerations have been taken into account when defining the parameters. On the one hand the tests cannot exceed a temperature of 1000 °C because of the facility's restriction. On the other hand there is the need to still be somewhat comparable to both the standardized testing procedure and the different testing procedures for BF and direct reduction facilities. With the start-up, by considering different literature data, whether attained via calculation or experiment, the parameters for the blast furnace testing procedure could be fixed. For a further description of the materials behaviour within an industrial scale process with respect to the different positions within a shaft furnace are considered by means of changing the gas composition at the initial stages of reduction as well as at the final stages. As a further approach to the modern blast furnace ironmaking by adding hydrocarbons as an additional fuel, attention is paid to the effect of small hydrogen amounts. The same considerations have been adapted to the direct reduction route of ironmaking and the shaft part of a smelting reduction facility, respectively.

7.3.1 Approach to the BF-Profile

From a theoretical point of view, the decent of the materials and the ascent of the gas through the shaft part of the blast furnace can be envisioned as follows. When the material is charged at the upper part of the furnace, the top gas that the material gets in contact with first is not particularly hot and has a low reduction potential. While the iron bearing material is descending the shaft the temperature continuously rises due to the countercurrent flow of the gas. Concomitantly, the gas composition changes during the upflow due to different oxidation reactions.

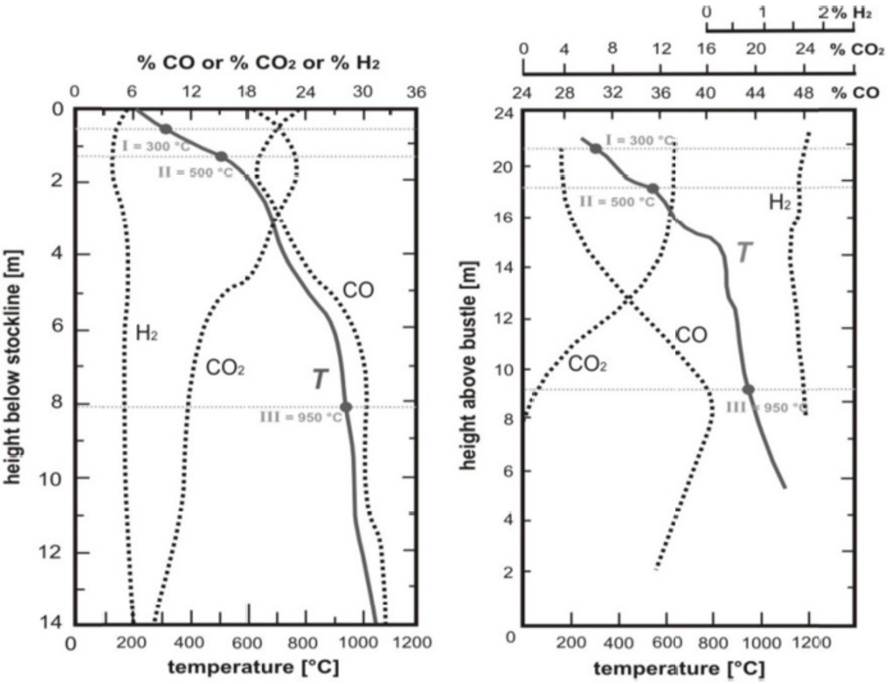

Figure 7-3: Blast Furnace temperature and gas concentration profiles according to *Biswas* [8] (left) and *Gudenau* [7] (right)

For the determination of the temperatures and gas composition profiles for the initial stages of reduction as well as the final stages a variety of literature and operational data has been considered [7,8,10,13,19,84,167]. As an example of these, two different temperature and gas concentration profiles are given in Figure 7-3. The change of temperature and each individual gas component H_2, CO_2 and CO along the height (and correspondingly the residence time of the material) of the blast furnace is shown. It can be seen that the H_2 content is almost constant along the shaft (at a percentage of 5 % (left) and 2 % (right) respectively), whereas the amount of CO increases and CO_2 decreases as the material moves downwards. The CO and CO_2 change is at its greatest within a temperature range of 500 and 950 °C and roughly stays constant upon reaching 950 °C. Also at the upper parts of the shaft the gas composition hardly changes. The materials and gas temperature respectively, is increasing in an almost linear pattern until reaching 950 °C at which point they only slightly increase further.

These circumstances have now been applied in defining a testing procedure in the following way. To eliminate the effect of LOI, the reduction procedure starts at reaching 300 °C sample temperature (marked as Point I in the subsequent figures and tables) with a reducing gas of a distinct, but weak reduction potential (comparable to top gas composition). Upon further heating from 500 °C (Point II) until the maximum testing temperature (Point III) has been reached, the gas composition linearly changes to the final composition with a stronger reduction potential. This temperature and gas composition is kept constant for a maximum of 300 minutes, which corresponds to the time the materials need to descend the indirect (gaseous) reduction zone of a blast furnace. In Figure 7-4 one example of the derived testing procedure is given. The temperature (black line) is linearly rising from 300 °C to 950 °C within 90 minutes which corresponds to a heating rate of 7.2 K/min. For the first 30 minutes until reaching 500 °C the gas composition stays constant. During the next 60 minutes (and simultaneous heating from 500 to 950 °C) the gas composition approaches the final GOD and is kept constant until the sample has reached a RD of 80 % (or for a maximum of 210 minutes).

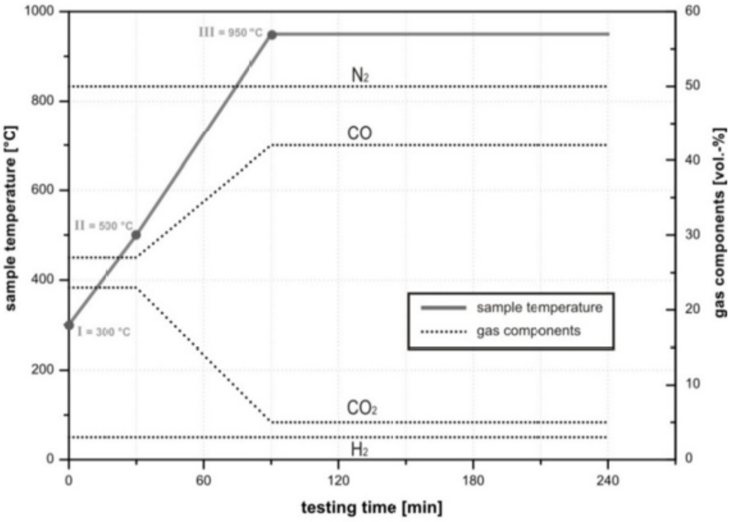

Figure 7-4: Example for the developed temperature and gas concentration profiles

Since it is known from literature [43,68,94,130] (at least for the reduction of iron ore fines in fluidized bed reactors) that the first reduction significantly influences the overall outcome, it is assumed that a continuous change of gas composition and temperature will change the reduction performance. Additionally due to the great differences between the centre and outer part in a shaft furnace, the influence of different reduction potentials needs to be demonstrated.

7.3.2 BF-Profile – Effect of Initial and Final GOD

The next approach of depicting the distinct influence of single process parameter is variation of the initial and final GOD for different blast furnace operation modes. For the different testing procedures the same hematitic ore (c.f. Chapter raw material description) has always been used as iron carrier.

According to different data two different initial and two different final GOD have been determined as shown in the Baur-Glaessner diagram in Figure 7-5 whereby the time dependent temperature profile stays the same for all the four different testing conditions. The initial GODs have been chosen at 0.46 and 0.54; it is assumed that due to the different reduction potentials the formation of metallic iron (or intermediate oxides) will differ and subsequently influence the overall performance. Because of the even more severe difference at the final stages of reduction the GODs for these stages have been chosen at 0.10 and 0.28. The lower reduction potential is quite narrow to the equilibrium line of Fe-FeO and therefore the thermodynamical driving force is rather small. It is assumed that the decrease of GOD to 0.10 will noticeably enhance the reduction performance. The exact gas compositions at every stage of the resulting four different testing procedures are summarized in Table 7-II.

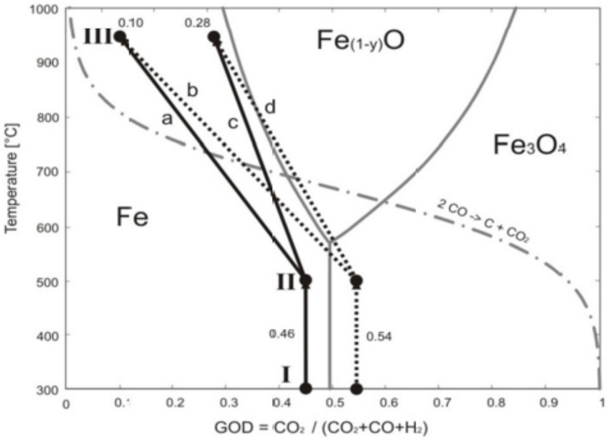

Figure 7-5: Testing conditions for BF profiles with different GODs

Table 7-II: Gas compositions at every stage of the different BF testing conditions

		BFa =BF1	BFc	BFb	BFd
			[vol.-%]		
I (300 °C) **II** (500 °C)	CO	27.0	27.0	23.0	23.0
	CO_2	23.0	23.0	27.0	27.0
	N_2	50.0	50.0	50.0	50.0
	GOD	**0.46**	**0.46**	**0.54**	**0.54**
III (950 °C)	CO	45.0	36.0	45.0	36.0
	CO_2	5.0	14.0	5.0	14.0
	N_2	50.0	50.0	50.0	50.0
	GOD	**0.10**	**0.28**	**0.10**	**0.28**

Within the subsequent investigation the blast furnace profile BFa with the GODs of 0.46 to 0.10 is refered as the so called base case and is named BF1.

7.3.3 BF-Profile – Effect of Hydrogen

In order to meet the requirement of being similar to industrial scale processes small amounts of H_2 – generated by injection of H_2-containing reducing agents like pulverized coal or heavy oil to the tuyères – are taken into account. Also the rising trend of injecting waste plastics as a reducing agent increases the amount of hydrogen since waste plastics consist of a variety of hydrocarbons which decompose within the blast furnace after injection.

In order to depict these circumstances 3 and partly 6 % H_2 have been added to the reduction gas by substituting the same amount of CO whereby the other parameters (namely GOD and temperature and time steps) stayed constant. Hence the position of the stages I, II and III within the Baur-Glaessner diagram stays the same (c.f. Figure 7-3) and the testing procedures a´ to d´ for adding 3 % H_2 and a´´ and b´´ for 6 % H_2 are summarized in the Table 7-III.

Table 7-III: Gas compositions at every stage of the different BF testing conditions (including H_2)

		BFa´ =BF2	BFa´´ =BF3	BFb´	BFb´´	BFc´	BFd´
				[vol.-%]			
I (300 °C) **II** (500 °C)	CO	24.0	21.0	20.0	17.0	24.0	23.0
	CO_2	23.0	23.0	27.0	27.0	23.0	27.0
	H_2	3.0	6.0	3.0	6.0	3.0	3.0
	N_2	50.0	50.0	50.0	50.0	50.0	50.0
	GOD	**0.46**	**0.46**	**0.54**	**0.54**	**0.46**	**0.54**
III (950 °C)	CO	42.0	39.0	45.0	41.0	36.0	36.0
	CO_2	5.0	5.0	5.0	5.0	14.0	14.0
	H_2	3.0	6.0	3.0	6.0	3.0	3.0
	N_2	50.0	50.0	50.0	50.0	50.0	50.0
	GOD	**0.10**	**0.10**	**0.10**	**0.10**	**0.28**	**0.28**

7.3.4 Approach to Direct and Smelting Reduction

To develop testing conditions such as those which can be found in shafts parts of different direct and smelting reduction facilities, the same considerations have been taken into account as for the BF conditions. In order to keep the most possible comparability, some parameters are still kept constant while others have been adapted for the different processes. In the end two different testing procedures, one for depicting a direct reduction facility and one as a representative for the shaft part of a smelting reduction process, have been developed and are graphically described within the Baur-Glaessner diagram in Figure 7-6 and the exact gas compositions at every stage are summarized in Table 7-IV.

Based on the blast furnace testing conditions BF1 – BF3 the initial and final GODs remain the same at 0.46 and 0.10 respectivly. The heating pattern differs in that due to the shorter time the material takes to descend the shaft compared to a blast furnace, the heating rate is increased and hence the time for heating up from 300 °C to the final testing temperature is shortened from 90 to 60 minutes. The concept of a constant gas composition from 300-500 °C remains the same, and also the linear change in gas composition from 500 °C to the final temperature and gas composition. According to literature [10,23,24] and internal sources, [59] the gas compositions of the two testing profiles DR1 and DR2 have been chosen as follows. For the DR1 (dark grey in Figure 7-6) test the final temperature is restricted to 800 °C which is distinctly lower than for BF. At the moment of reaching 800 °C the gas composition has a rather high hydrogen amount of 25 % which is assumed to compensate for the lower kinetics due to the lower temperature. For the dipiction of another direct reduction facility the DR2 testing profile (light grey in Figure 7-6) the final temperature is specified at 850 °C and additionally the hydrogen is further increased to 54 % altough the gas is enriched with water vapour to an extent of 27.6 % for the initial stages and 6 % at the final stages.

In the figure the modification and the shift of the equlibrium conditions of the Baur-Glaessner diagram are also shown. For the conditions DR2, especially at the initial stages the reduction is assumed to be very retarded due to the chemical equllibrium in addition to the inhibited kinetics. With these five different testing conditions, the behaviour of the different materials at most industrial scale processes is assumed to have been described and an estimation of a material's behaviour can be given.

Table 7-IV: Gas compositions and GODs at different stages for all process related testing conditions.

		BF1 0 % H_2	BF2 3 % H_2	BF3 6 % H_2 [vol.%]	DR1	DR2
I (300 °C) **II** (500 °C)	CO	27.0	24.0	21.0	39.0	21.6
	CO_2	23.0	23.0	23.0	46.0	18.4
	H_2	-	3.0	6.0	15.0	32.4
	H_2O	-	-	-	-	27.6
	N_2	50.0	50.0	50.0	-	-
	GOD			**0.46**		
III (950 °C)	CO	45.0	42.0	39.0	65.0	36.0
	CO_2	5.0	5.0	5.0	10.0	4.0
	H_2	-	3.0	6.0	25.0	54.0
	H_2O	-	-		-	6.0
	N_2	50.0	50	50.0	-	-
	GOD			**0.10**		

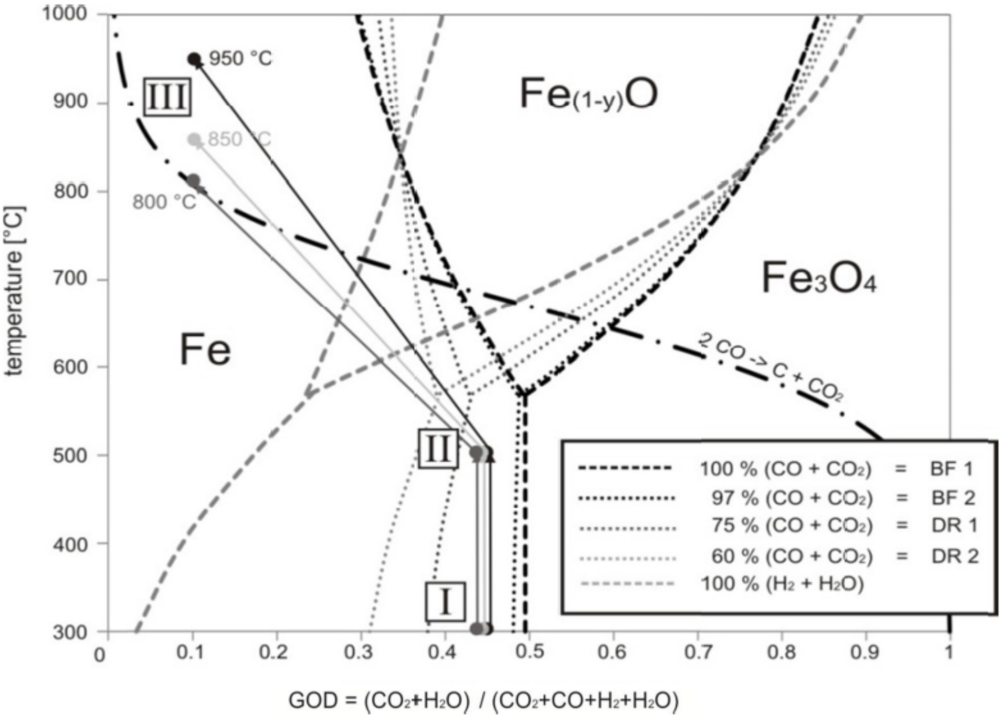

Figure 7-6: Baur-Glaessner diagram for gas mixtures of H_2, H_2O, CO, CO_2 with Boudouard equilibrium and reduction testing paths of BF conditions (black), DR1 (dark grey) and DR2 (light grey)

7.4 Mechanical Testing Procedure

In order to correlate the mechanical properties and the reduction behaviour and further show the evolution of mechanical strength at the different reduction procedures, the feed materials were tested after each reducibility test and additionally prior to reduction to depict the evolution of the materials stability.

In terms of describing the mechanical strength in a distinctive but not overly complicated way, two values have been chosen as significant for a description. In order to do so, the determination procedures of the abrasion and disintegration tendency, conditions related to standardized testing procedures (ISO 4696 1+2 [53,54] for tumbling procedure and ISO 3271 [158] for calculation) were chosen.

After the 900 revolutions during tumbling the material´s grain size distribution is measured and the results are used to calculate the two indication values *DT* and *AT*. With equation (7-9) the disintegration tendency (*DT*); and with equation (7-10) the abrasion tendency (*AT*) can be calculated whereby m_0 is the initial mass prior to tumbling; m_1, m_2, m_3 are the mass portions of the +6.3, +3.15 and +0.5 mm grain size fractions respectively. Hence, DT refers to the percentage of mass that remains larger than 6.3 mm and AT refers to the percentage of mass of the sample portion that is smaller than 0.5 mm after tumbling.

$$DT = \frac{m_1}{m_0} \cdot 100 \qquad (7\text{-}9) \qquad\qquad AT = \frac{m_0 - (m_1 + m_2 + m_3)}{m_0} \cdot 100 \qquad (7\text{-}10)$$

These two values have been determined to describe the mechanical properties in the best possible way by keeping it simple. If the material tends to disintegrate, as a raw material as well as after the different reduction procedures, the DT value will increase. On the other hand the values for AT are desirably low for material with good mechanical stability. More often than not, both of these values for describing the mechanical performance tend to follow the same trend. If the raw material´s properties are weaker and even at room temperature without any reduction progress the tumbling procedure leads to distinct increase of crumbling and abrasion, most likely the material's performance will not improve during the reduction progress. The volume changes during reduction, release of the crystallisation water or other volatile components and finally the oxygen release via gas phase will additionally weaken the structure.

It has to be noted that the values for DT and AT cannot directly be correlated to the standardized RDI values. All those subsequently described DT and ATs are related to the RDI values but are not exactly the same. They are a result of the different reduction testing procedures (both standardized and industrial scale related), a standardized tumbling procedure (ISO 4696) and a standardized sieving and calculation procedure. Nevertheless these artificial and newly created parameters can give a comparison of the different testing procedures and materials and are assumed to be perfectly suitable to describing a material's performance in terms of mechanical stability.

8 Raw Material Characterization

As part of this work the different raw materials have been investigated, since grain size, mineralogical composition of grains, crystal size, habitus, intergrowth conditions, porosity and specific surface of grains, as well as those of crystals are known as main reducibility controlling parameters for burden material. It can be pointed out that whenever a materials performance needs to be depicted, the majority of the subsequent reduction performance can be explained by taking into account the raw material's structure, chemistry and morphology.

Having listed the whole spectrum of influencing parameters on reducibility and mechanical behaviour within the prior chapter, this knowledge combined with the raw material's characterization by means of chemical analysis, specific surface area measurement and finally light microscopic means will contribute to a better comprehension of the interaction of material structure and the reduction performance.

In total eight different raw materials were investigated. In a first approach, for a comprehension of the behaviour of different mineralogical and structural types, three representative globally treated iron ores were selected. To further depict the effect of an addition of binding phases as well as the burning step as a kind of pre-treatment, three different pellet brands (also globally traded and used for industrial scale applications), were studied in the same way. At the last step, due to the most complex mineralogical and morphological structure, two sinter samples from the production line of two different sinter plants as well as three lab scale produced sinter samples were investigated.

8.1 Chemical Analysis, LOI and B.E.T.

- Calculation of the Fe_2O_3 and Fe_3O_4 portions

The chemical analysis was performed by the laboratory of *voestalpine Stahl GmbH* in Linz according to wet chemical analysis and XRF-analysis with the methods as described above. With the information about the total iron content Fe_{tot}, the portion of metallic iron Fe_{met} and the FeO content (as a result of the Fe^{2+} value) from these analyses and the assumption that within the raw material Fe^{2+} only prevails as magnetite ($Fe_2O_3 \cdot FeO$ c.f. Chapter 3) the following statements can be derived.

With the assumption that the total iron content Fe_{tot} comprises the sum of metallic iron parts Fe_{met} and the oxides FeO and Fe_2O_3 (given in wt.-%) it can be calculated as:

$$Fe_{tot}[\%] = Fe_{met}[\%] + FeO[\%] \cdot \frac{56\frac{g}{mol} \cdot Fe}{72\frac{g}{mol} \cdot FeO} + Fe_2O_3[\%] \cdot \frac{2 \cdot 56\frac{g}{mol} \cdot Fe}{160\frac{g}{mol} \cdot Fe_2O_3} \qquad (8-1)$$

After rearranging the equation the hematitic portion can be given as:

$$Fe_2O_3[\%] = [(Fe_{tot}[\%] - Fe_{met}[\%] - FeO[\%] \cdot 0.733) \cdot 1.429] \cdot 100\% \qquad (8-2)$$

The chemical analysis of the investigated materials is summarized in Table 8-I and reveals the differences in the raw material. Out of three iron ores it can be seen that Iron Ore 2 consists of more or less pure magnetite whereas the other ores contain hardly any magnetite as derived due to the absence of FeO. Due to the quite low amount of FeO within the pellet samples, it can be assumed that the induration process was successfully executed, and all the (possibly) prevailing magnetitic parts of the raw ore prior to pelletization have been fully oxidized to hematite during the burning process.

Within the sinter samples some FeO parts still prevail. This can indicate two different phenomena, first the insufficient oxidation during the sintering. If magnetitic ore or recycling material is mixed to the raw sinter burden it may be that due to locally insufficient sintering conditions (not enough temperature or hot air stream) the sinter mixture is not fully oxidized during sintering. Rapid cooling can also cause magnetite residues because of a suppressed oxidization in the solid state (martitization). Another possible source of Fe^{2+} might be because of already reduced parts of hematite. Because of locally appearing reducing conditions due to the insufficient combustion of fuel some hematite parts can be reduced during sintering. However, this effect is assumed to disappear on cooling (and reoxidizing) for the most part and therefore at least wustite is not likely to be present within the cooled sinter. The investigated sinter samples show moderate and comparable values for FeO which indicates a proper sintering process with uniform conditions within the considered sample amount.

- Gangue Content and Basicity Values

From the chemical analysis and the calculated portions of the elements oxides respectively, the characteristic value for the gangue content (as a percentage of mass) can be given just as the basicity values B_2 and B_4 can be calculated according to

$$B_2 = \frac{CaO}{SiO_2} \qquad (8-3) \qquad and \qquad B_4 = \frac{CaO + MgO}{SiO_2 + Al_2O_3} \qquad (8-4)$$

whereby the gangue content refers to the sum of those four oxides. The lower the basicity value, the more acidic the designation of a raw material. It has to be noted that all mentions of basicity, if not noted otherwise, refer to the B_4 value.

From the chemical analysis it can be derived that only the magnetitic ore has a considerably high amounts of gangue material combined with an unusual high value for B_4 for iron ores; since most of the gangue material of iron ores is of an acidic nature. It can be assumed that this ore was sourced directly from the mine without any beneficiation, which explains the high level of silicate and apatite still present. The other two ores contain hardly any other oxides besides silicates and therefore the B_4 is very low, and the overall amount of gangue is also quite low.

The Pellet Brands 1 and 3 have a rather similar chemistry with around 5.5 % slag forming and binding material and a basicity value of around 1. In contrast to that, Pellet Brand 2 has a larger slag phase portion and very low basicity, which is a result of a very high portion of silica (almost triple the silica portion).

The Sinter Samples consist of up to almost one quarter of gangue, slag or binding phases. It has to be noted that the origin of the sinter samples is different between Samples 1 and 2 and Samples 3-5 respectively. Samples 1 and 2 originate from industrial scale sinter plants, whereas the others derive from lab scale tests by means of a sinter pot sintering procedure. Whereas Sinter Sample 4 consists of 100 % sinter feed, hence comparable to the industrially produced samples, Samples 3 and 5 consist of special mixtures. Sinter 5 consists of a mixture of sinterfeed, pelletfeed and micropellets and Sample 3 consists of a large portion of iron oxide containing concentrate.

Sinter Sample 1 has quite a low basicity (which is not too usual for sinters) whereas Sample 2 has a higher B_4 value. Samples 4 and 5 have the highest B_4 values at almost 2, which is quite high. The overall slag content is within the same range for the industrial sinters 1 and 2, as is the FeO content. The main difference between these two Sinter Samples is the increased CaO content with a difference of 4 %. The sinter pot sinter samples differ in a wider range. Sinter 3 consists of almost 10 % SiO_2 and 15% CaO, which make the basicity lower but the overall slag amount is high at 28 %. The Samples 4 and 5 have quite a similar chemical analysis with a low silica content and a low slag amount.

Table 8-I: Chemical composition, specific surface and basicity of the raw materials investigated

material	B.E.T	Fe_{tot}	Fe_2O_3	FeO	Al_2O_3	CaO	K_2O	MgO	P_2O_5	SiO_2	TiO_2	**gangue content**	B_2	B_4
	[m²/g]					[wt.-%]						[%]		
Hemtitic ore	0.42	67.0	94.4	1.30	0.71	0.02	0.12	0.01	0.09	2.60	0.05	**3.34**	0.01	**0.01**
Magneitic ore	0.08	65.2	63.9	26.4	0.41	2.24	0.02	0.05	0.04	3.76	0.03	**8.23**	0.68	**0.82**
Limonitic ore	3.74	65.1	92.8	0.25	1.03	0.09	0.02	0.01	0.10	1.68	0.07	**2.80**	0.01	**0.01**
Pellet Brand 1	0.40	65.4	93.1	0.33	1.28	2.26	0.02	0.01	0.65	2.10	0.07	**5.56**	1.08	**0.67**
Pellet Brand 2	0.23	64.6	90.0	1.77	0.38	0.17	0.08	0.33	0.05	6.24	0.04	**7.12**	0.03	**0.08**
Pellet Brand 3	0.66	65.8	93.4	0.65	0.44	2.42	0.01	0.01		2.47	0.07	**5.34**	0.98	**0.84**
Sinter 1	0.57	52.41	67.2	6.98	2.25	9.72	0.54	2.99		7.90	0.08	**22.86**	1.23	**1.25**
Sinter 2	0.68	51.6	65.7	7.23	1.64	13.5	0.27	2.88		7.14		**25.16**	1.89	**1.87**
Sinter 3		50.4	62.5	8.62	0.95	15.2	0.13	1.86		9.70	0.04	**27.71**	1.57	**1.60**
Sinter 4		55.0	71.2	6.65	1.19	10.6	0.10	3.06		5.83	0.07	**20.68**	1.82	**1.95**
Sinter 5		54.5	68.5	8.46	1.15	11.3	0.14	3.07		6.14	0.07	**21.66**	1.84	**1.97**

- Loss on ignition (LOI)

From the investigation concerning the loss on ignition and therefore describing the portion of limonite and/or siderite only the third ore showed any loss on ignition to an extent of only 2.1 %. This indicates that this ore consists of some limonitic parts, but to a quite small extent. Nevertheless this ore is subsequently identified by the name Limonitic ore.

The other two ores do not show any loss on ignition; considering artificially produced burden material like pellets and sinters, it is highly unlikely to determine any loss on ignition because of the previous burning or sintering procedure.

- Specific Surface area (B.E.T)

The determination of the specific surface area was afflicted with some uncertainties. On the one hand the investigated materials grain size is not straightforwardly comparable to both the literature data and the reducibility testing result. Due to the restriction of the lab facility concerning particle size, the particle had to be smaller than 10 mm but still desirably lumpy with a minimum size of 6.3 mm. In contrast to that, data for specific surface area given in the literature refer almost always to the investigation of powders or at least crushed material. Another factor concerning the precision of the results is the range of the surface area of the samples. Due to the coarse particles the specific surface area is rather small compared to powders (where the results indicate surface areas of at least ten times larger) and meets the minimum limit of analytical determination of the lab facility. Therefore the results should be seen more as an indicator than as precise results.

Nevertheless, the investigation could reveal the differences and tendencies of the various materials. The densest material with the smallest specific surface the magnetitic ore followed by the hematitic ore with a surface five times higher. In addition, the Limonitic ore has a comparably high value, which is a result of the limonitic parts. Because of the preheating step within the lab facility the crystallization water is released and subsequent cracks and pores are formed. This newly created surface contributes to the high specific surface area.

Pellets generally have lower specific surface areas, comparable to (most) ores, which is a result of the burning process. During heating up to 1300 °C the binding phases are melted for the sake of agglomeration and hardening and the melt infiltrates the interstices between the ore grains and lowers porosity. However, the results of the Pellet Brands are noticeably different, lowest for Brand 2 followed by 1 and 3. The Sinter Samples are within the same range, although Sinter 1 has a higher specific surface area than Sample 2.

8.2 Morphological Characterization

In the next step of raw material characterization, the polished sections of the raw materials were investigated by light microscopic means. It has to be noted that this characterization is only of qualitative nature. The different phases are shown but there has not been any attempt at a quantitative characterization in terms of giving a distribution of the appearing phases as a percentage.

The possible appearing phases and structural types thereof might be of different iron oxidic nature (with the accompanying elements), slag phases, gangue material or resin filled pores. Concerning sinter samples further calcioferrites and water soluble silicates will be distinguishable within the light microscopic pictures. Additionally the different kinds of hematite will be described, distinguished first by their phenotype (coarse and fine hematite crystals) and secondly by their origin (primary, secondary or tertiary hematite). The possibly occurring phases and the acronyms noted in the subsequent pictures are summarized in Table 8-II (c.f. Chapter 3)

8.2.1 Iron Ores

Each traded iron ore is composed of a mixture of different structural types; exemplary pictures of the structures of the different ores are given in Figure 8-1 to Figure 8-3. The pictures only show a small but hence representative detail of the morphological structure. Due to the inhomogeneities of every iron ore deposit, a wide range of other phases, oxides and structural types prevail though in very small portions.

Table 8-II: Different appearing phases within the structure of the different raw materials

Acronym	Chemistry	Colour	Description/origin
h_1	Fe_2O_3	Light grey	Fine hematite crystals, highly porous, naturally occurring within iron ore
h_2			Coarsely crystalline, dense hematite, naturally occurring within iron ore
h_{pr}			Primary hematite within sinter samples only refers to hematite originating from iron ore (relics)
h_{sec}			Hematite phase of different origins, either as grown during the melting within the liquid phase, grains are always surrounded by (a thin film) of glass phase, idiomorphic to hyp-idiomorphic appearance or hematite which is originating on cooling as a result of reoxidation of magnetite, recognizable due to the absence of glass/melt phase between the boundary hematite/magnetite
h_{ter}			Hematite from a returned grain, evolves of h_{sec} within a second sintering period, looks similar to h_{sec} but in turn there is a thin slag film between the boundary hematite/magnetite
mr			Martite, naturally reoxidized magnetite, comparable to h_{sec}
l	$Fe_2O_3 \cdot H_2O$	Grey	Limonite
m	Fe_3O_4	Brownish	Magnetite, originating from magnetite ore
sp	$MeO \cdot Fe_2O_3$	Brownish	Spinel refers to phases that are similar to magnetite but with a certain but variable amount of accompanying elements which replace Fe-atoms within the oxide lattice.
cf	$(FeO)_x(CaO)_x$	Grey	Calcioferrites of different composition form during the sintering process, different apparent forms might be acicular or blocky
g	variable	Dark grey	Gangue/slag
p		Black	Pores filled with resin

Figure 8-1 shows two exemplary microscopic pictures of the Hematitic ore. The Hematitic ore is mainly composed of xenomorphic to hypidiomorphic, finely (h_1 - as shown on the right side of the left picture (a)), to more coarsely (h_2) crystalline hematite. The crystal sizes of hematite vary from a few microns up to 200 µm. Some grains have large specific surfaces, but then again many others are rather dense. In some regions even larger hematite crystals prevail (not given in the picture) but the major part of the ore sample consists of the structural type shown. In the picture on the right (b) another prevailing structural type is shown, the banded iron formation. The alternate layers of hematite rich parts (light grey) and silica rich parts (darker) can easily be distinguished, but on considering the chemical analysis, this structural type is also not present in higher concentrations.

The Limonitic ore as given in Figure 8-3 (a) is mainly composed of finely crystalline trellis martite (mr) in addition to some limonite masses and patches. Xenomorphic, small sized hematite is situated interstitially to the martite. The average hematite crystal size is smaller, the overall porosity and permeability is significantly higher than that of Hematitic ore. Due to incomplete oxidation of magnetite, trace amounts of xenomorphic magnetite intergrown with various structural types of martite are present. Limonite contents of ore grains are variable depending on the topographic position of the different ore bodies mined. In general ores close to the surface are richer in limonite due to weathering. As well as the Hematitic ore, the limonite bearing ore derive from banded iron formations (BIF, picture b).

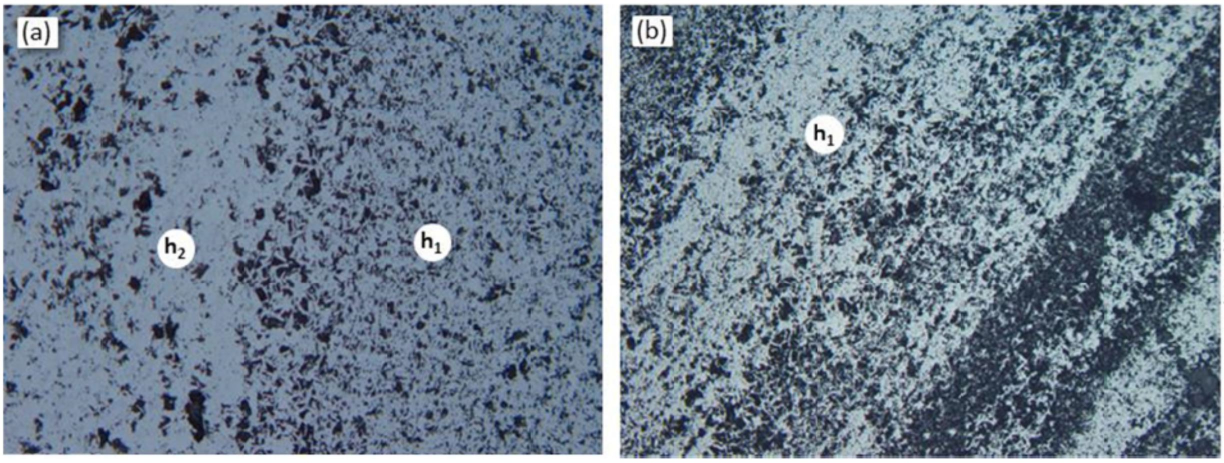
(a)
h_2
h_1
(b)
h_1
picturewidth = 1.77 mm

Figure 8-1: Light microscopic pictures of different regions of the Hematite ore

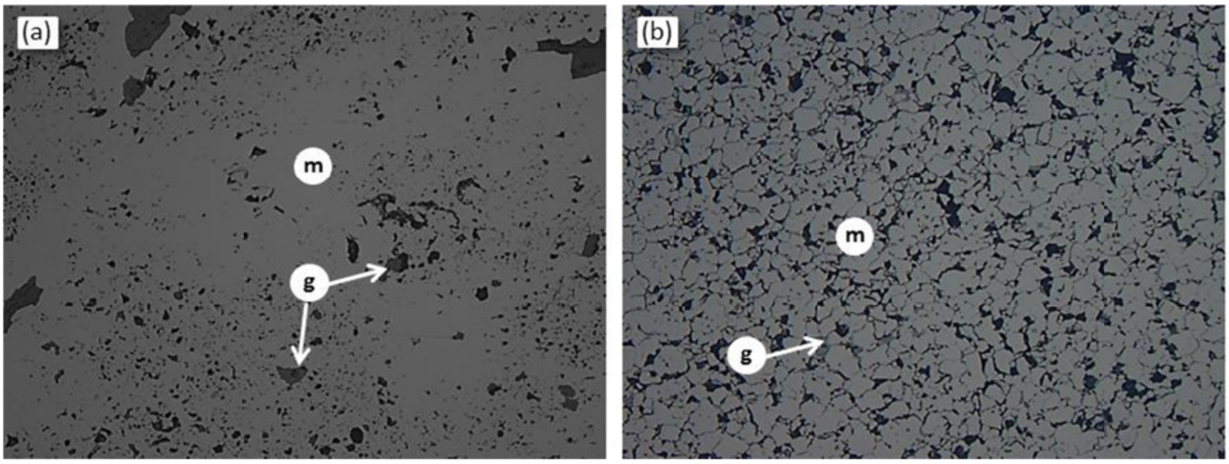
(a)
m
g
(b)
m
g
picturewidth = 1.77 mm

Figure 8-2: Light microscopic pictures of the Magnetite ore

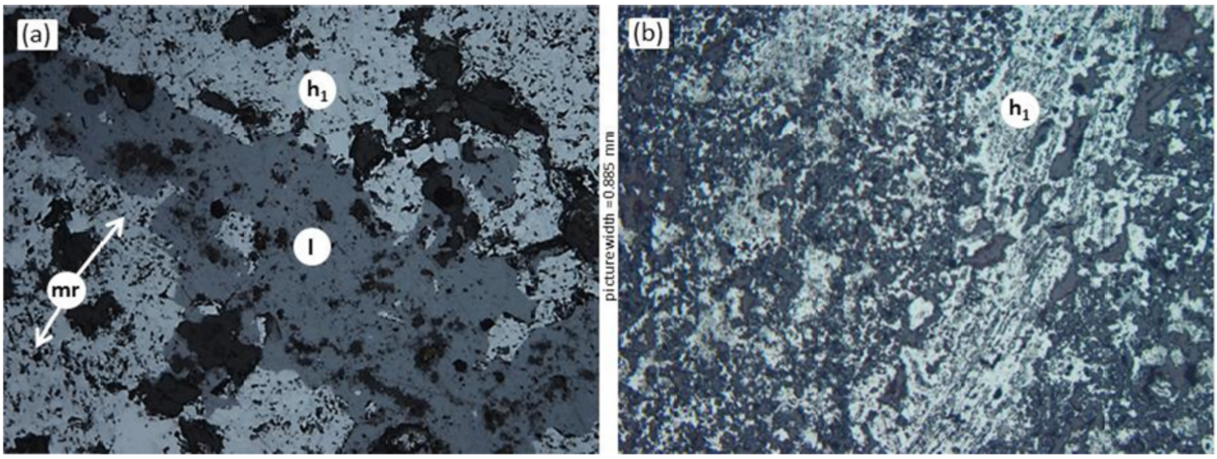
(a)
h_1
mr
l
picturewidth =0.885 mm
(b)
h_1
picturewidth =1.77 mm

Figure 8-3: Light microscopic pictures of the Limonitic ore

In terms of genesis, the magnetite ore (Figure 8-2) is of a different type. It stems from a liquid-magmatic type ore deposit and contains a lot of coarsely crystalline magnetite with crystal sizes of up to 300 µm, visible in the right picture. No intra-crystalline pores were observed; limonite is absent. The hematite content is well below 0.1 %. The ore was sourced directly from the mine without beneficiation. Therefore a lot of gangue minerals like iron containing silicates and apatite are present. Compared to the hematitic ore, the specific surface area is almost one power of ten smaller; the left picture shows an area that is extremely dense with coarse crystals.

8.2.2 Pellet Brands

The main constituents of pellets are hematite, partly magnetite and glass. Glass is the least reducible iron containing component of every pellet. Thus the amount and distribution of glass will have significant influence on the reduction properties of pellets but the action of glass on the reduction is still not well understood. Generally for all pellet brands investigated, the following statements are valid. Most of the prevailing hematite crystals show rounded edges due to recrystallization and surficial dissolution into the glass phase and nearly all hematite is coated by a thin glass layer as shown in Figure 8-4 left (picture of Brand 1). On the right hand side of the figure larger crystals with small glass inclusions can be observed.

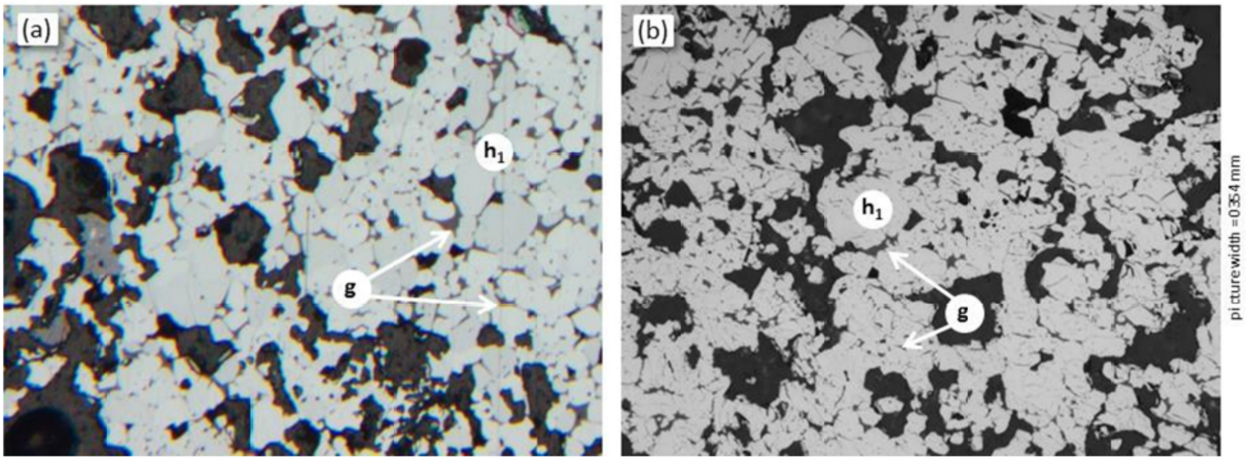

Figure 8-4: Hematite grains surrounded by glass and glass inclusions within larger crystals from Pellet Brands 1 (a) and Brand 3 (b)

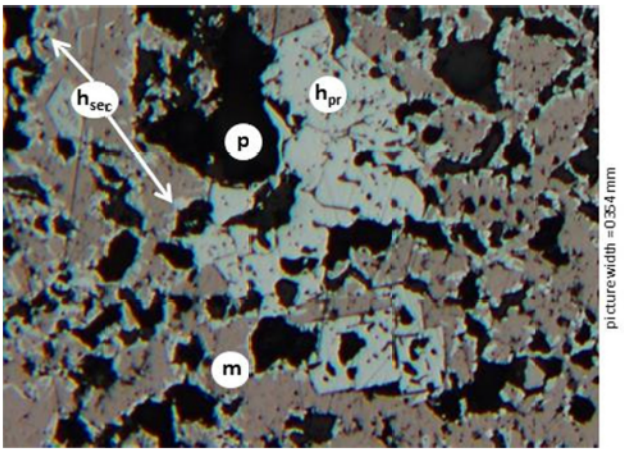

Figure 8-5: Microstructure of a single pellet, residue of magnetite

The structures of well burned pellets are to a certain extent comparable with those of fine grained sinters of very low basicity. Most of the material is melted by sintering. Figure 8-4 shows well burned (strongly recrystallized) pellets, most of the hematite crystallizes in a liquid melt, evident both by the hypidiomorphic to idiomorphic habitus of the crystals and by the glass coatings. As an example of an incomplete burning process, a picture of the same pellet as given on the left in Figure 8-4 (Pellet Brand 1) is shown in Figure 8-5. It can be seen that at the inner core part of the pellet the recrystallization process was not finished; the crystals appear as recrystallized hematite grains only at some parts, whereas the majority consists of sharply edged magnetite grains. The distinction between primary and secondary hematite is also clearly visible and marked on the right of Figure 8-5.

For a comparison of the investigated pellet brands a representative microstructural picture of each brand is given in Figure 8-6. It can be seen that compared to Brand 1, the grains of Brand 2 are a little smaller but noticeably more sharply edged. Though it seems that both Brands 1 and 2 have a small crystal size and a high microporosity, the B.E.T specific surface area measurement indicated that the overall porosity is higher within sample 3. However, the crystal size is considerably larger. Although the glass phase amount and composition of Brands 1 and 3 are comparable, their distribution differs. Whereas in the structure of Brand 1 the glass phase is finely distributed and surrounds almost every single grain, in Brand 3 the glass phase is accumulated rather than distributed. Based on the chemical analysis, it is assumed that those accumulated glass parts are some sort of calico ferrites (darker grey parts) and hence well reducible in contrast to the silicate glass phases of Brand 2. In the detail picture of Brand 2 (b) the high amount of silica (as known from chemical analysis) is apparent as rather large quartz parts (marked as q in the figure). These phases are assumed to be the least reducible parts.

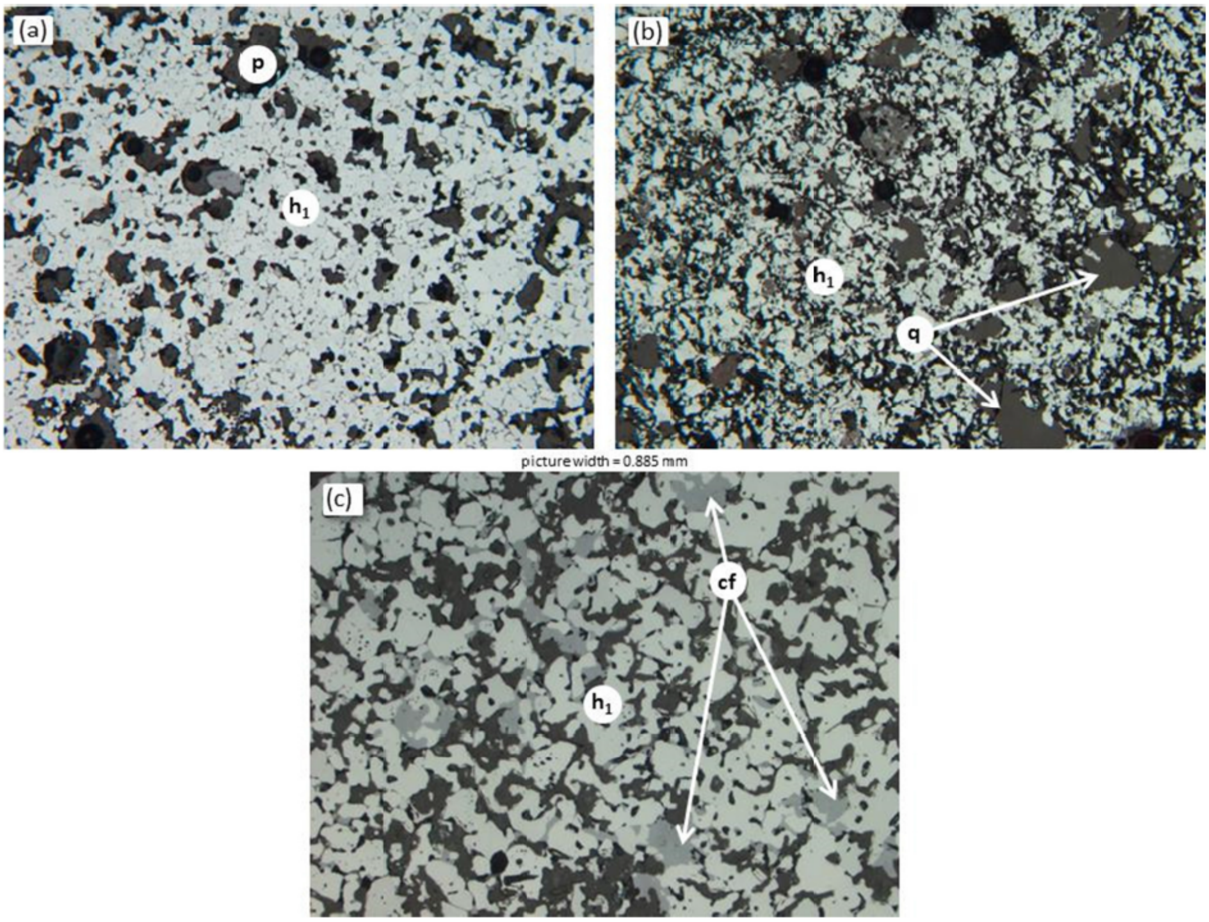

Figure 8-6: Light microscopic pictures of the Pellet Brand 1 (a), Pellets Brand 2 (b) and Pellet Brand 3 (c)

8.2.3 Sinter Samples

On closer comparison of the two Sinter Samples investigated (Samples 1 and 2), they showed quite diversive but yet similar microstructure. Generally speaking the appearing structural phases are of the same nature, at least because of the higher CaO content based on the chemical analysis, the portion of calcioferrites is assumed to be higher within Sinter Sample 2.
On taking a closer look at the microstructure of the sinter samples, a distinct description of the overall microstructure is very difficult to achieve. Since the mixture of the raw materials is multifaceted and inhomogeneous, the appearance under the microscope changes every millimetre within the polished section. In Figure 8-7 some typically appearing phases and structures are shown (c.f. Section 3.4) and a further exceptionally structural phase is given in (e). The top left picture (a) shows the effect of enhanced growth of hematite into the melt starting at ore relics. Ore relics refer to iron ore grains that have not been fully assimilated during heating,

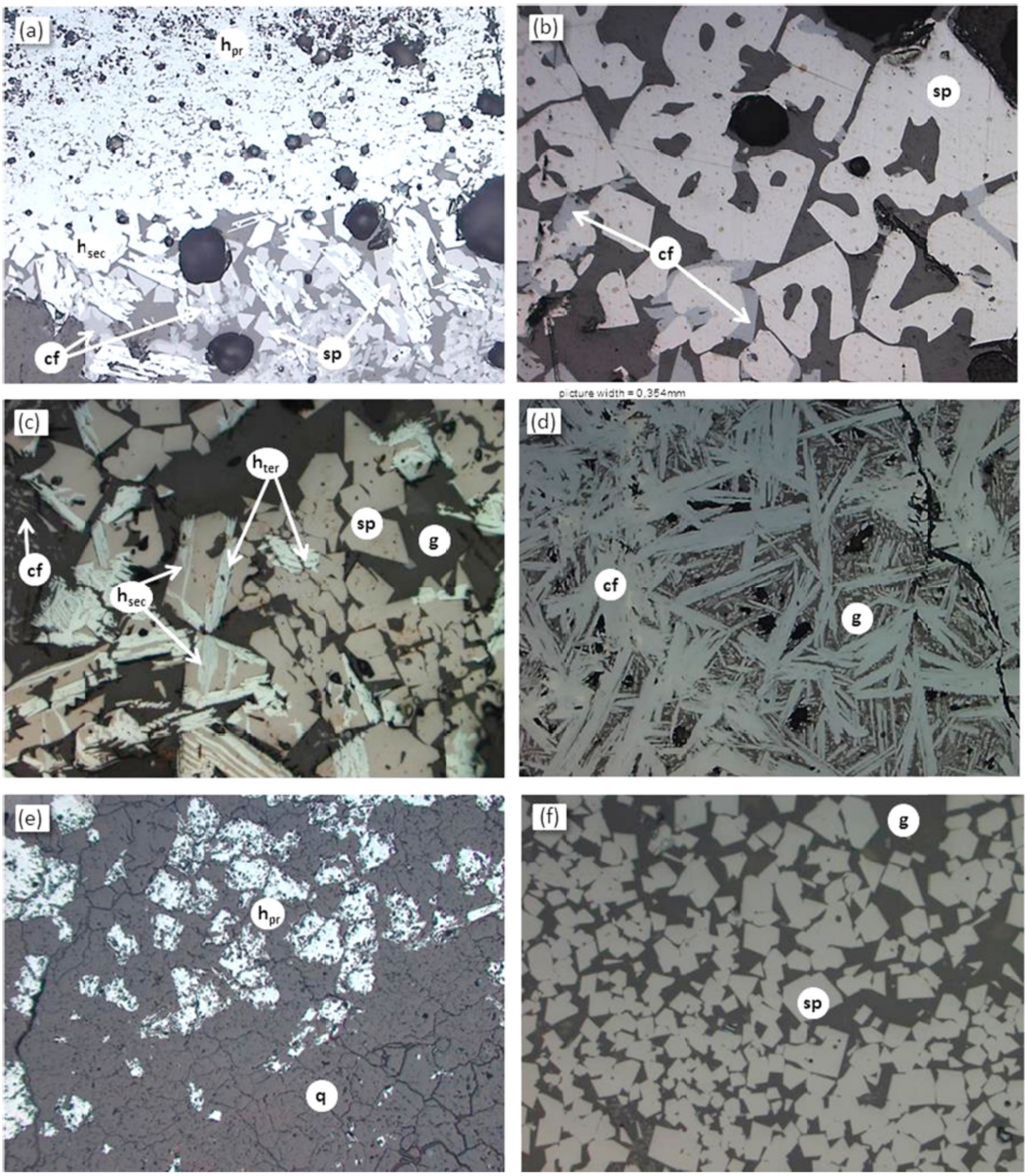

Figure 8-7: Exemplary pictures of different phases appearing in Sinter Sample 1 and 2

these (primary) hematite grains survive the entire sintering procedure. On subsequently cooling, originating from the ore relic, hematite grows further at the expense of spinel. On the lower part of (a) a structure of spinel and calcioferrites is apparent. In the middle left picture (c) an example of the further oxidation of the magnetite/spinel crystals to secondary hematite is visible. The interstices are filled with glass phase (darkest parts) and on the far left some small calcioferrites surrounded by glass are visible. The difference between secondary and tertiary hematite can also be seen It can be concluded that this sinter piece has been sintered at least twice. On the left two hematite-poor sections are given with very different occurrences of calcioferrites. In the upper picture (b) both the spinel and the calcioferrites have a very coarse, blocky and dense structure. During the sintering process or the subsequent cooling process, the calcioferrite grows at the expense of the spinel and retains a very blocky form within the structure. Picture (d) shows the acicular form of the calcioferrites which originated due to the growth of calcioferrites in the liquid melt, and in picture (f) a very calcioferrite poor region appears. Finally, picture (e) shows a less frequent structure, an iron ore relic with a lot of gangue material (most probably formed from different silicates and quartz, q). This part is assumed to be of a very acidic nature.

Interestingly, compared to lump ores and pellets, sinter samples are considerably coarser and have a denser microstructure. During the sintering process and the liquification and subsequent solidification, a coarsening of the grains occurs. The microporosity is also very low; in the two figures hardly any pores are visible. In contrast, the measurement of the specific surface are indicates that the porosity is within the same range as those of pellets.

In summary, the raw materials can be characterized as follows. The three different iron ores represent the most commonly traded structural types, a more or less pure hematitic ore, almost pure magnetitic ore and finally a mixture of hematite and limonite. Combined with the chemical analysis and the microstructure it is assumed that the Limonitic ore is most reducible, after the Hematitic and Magnetitic. The pellet brands as raw material indicate that due to the fine structure and high porosity Brand 1 is well reducible, whereas Brand 2 with the low porosity (B.E.T) and high amount of silica phases will reduce more slowly. All sinter samples comprise of a comparably dense structure with large crystals, nevertheless the good reducibility of calcioferrites will enhance the overall reduction performance. It is assumed that due to the higher CaO content Sinter Sample 2 is even more reducible.

9 Experimental Results

Within the first section the behaviour of the material at standardized testing conditions was described and gives an initial picture of the ability of oxygen release and mechanical performance. Based upon that, the performance at all industrial scale conditions is given, whereby the single parameter variation of the testing procedures for one single material is described. For this special investigation hematitic ore has been chosen because of its simple structural composition (more or less only consisting of hematite crystals) and yet representative chemical analysis (medium, acidic slag amount, no artificial binding phases).

What is of major additional interest is the morphological evolution during the reduction progress and subsequently the change in the metallic iron formation by changing the reduction conditions. Every microstructural phase within the raw material acts in a different way depending on the initial microstructure and the reducing conditions. With knowledge of the actual way iron oxide is converted to metallic iron and the influence of gas composition and temperature, a more precise prediction of a raw material´s behaviour is possible.

Finally the results are implemented in a simple kinetic approach to depict the progress of reduction. Altogether the elaborated matrix of testing conditions and raw materials is expected to further illuminate the complex topic of iron oxide reduction.

9.1 Comparison of Different Raw Materials according to ISO 4695

The three iron ores, three pellet brands and five sinter samples as they were characterized in Chapter 8 were tested according to the standardized testing condition ISO 4695 and evaluated as described in Section 7.2.1. Subsequently the mechanical properties were tested and results for disintegration and abrasion tendencies calculated according to Section 7.4. In order to compare the evolution of the mechanical properties during the reduction procedure, as a special feature the mechanical stability of the raw materials was additionally tested.

The reduction degree, calculated as a result of the weight loss (full lines) and the derivated reduction rates (dash dotted lines) at any point during the reduction progress are given separately for ores, pellets and sinters in Figure 9-1 to Figure 9-3. The numerical results of the testing procedures are summarized in Table 9-I. On considering the ore samples, the following statements can be made. The limonite containing ore (light blue) is distinctly the best reducible compared to the Hematitic and the Magnetitic ore. Especially the Magnetitic ore (grey) reduces rather slowly even though the reduction starts at an initial RD of 11 % (due to the inherent RD of the magnetite lattice). The time needed to reach R_{80} can be estimated at about 165 minutes for Magnetite and 142 min for Hematite. This corresponds to a retardation of 65 % (Hematite) and almost 100 % (Magnetite) compared to the Limonitic ore.

From the progress of the reduction rate a difference in the path of reduction can be seen. Whereas the limonitic ore starts at high reduction rate for the initial stage of reduction (up to some RD= 20 %) and slows down at the final stages to a more or less linear decrease, the other two ores have a linear decrease in reduction rate from the beginning. This indicates a different pattern of reduction mechanism as a result of the raw material properties. It is assumed that resulting from the crystallization water release pores and cracks are initiated and therefore at the initial stages the reducing gas is able to ingress into the interior regions of an ore particle. In contrast to that the dense, non-porous structure especially of the Magnetitic ore, prevents any gas diffusion to the inner parts of the ore particle.

The evolution of the mechanical stability of the ores shows results compatible with the raw material. The raw Hematitic and Magnetitic ore have a slightly higher raw material strength compared to the Limonitic, nevertheless all ores have values for DT > 90 % and are therefore deemed to have good raw material strength. Despite the high temperatures of 950 °C and the phase transformations during the reduction process there is hardly any loss in mechanical strength. A decrease of only 7 to13 percentage points was determined. It is assumed that the high reduction degree of > 80 % (and hence the large portion of metallic iron that has already formed) is accountable for keeping the former ore grains together and prevent disintegration.

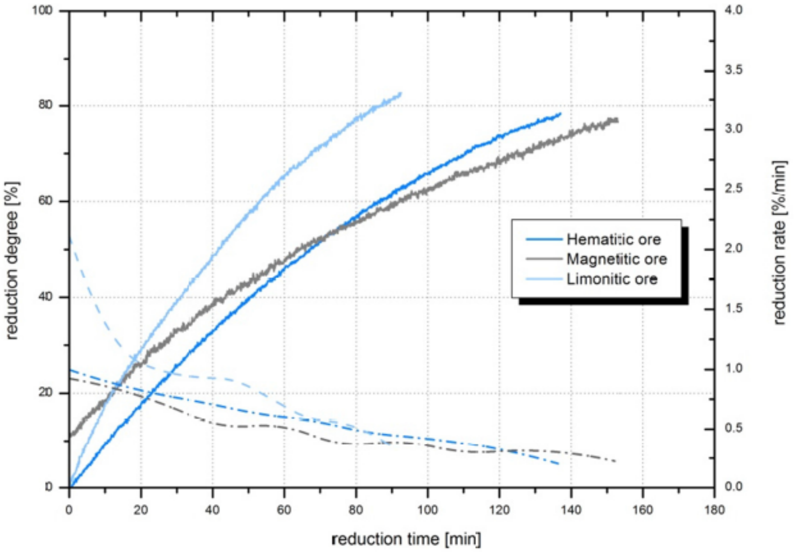

Figure 9-1: Reduction progress of different iron ores according to ISO 4695

In Figure 9-2 the reduction progress and rate are given for the pellet brands. Pellet Brand 1 is clearly the most easily reducible pellet brand in contrast to Brand 2, which reduces quite slowly. On comparing the reduction rates of these two samples a strong correlation of the reduction pattern is obvious. Both samples start at high rates until attaining a reduction degree of 30 %, before slowing down and continuing at a lower but more linear reduction rate. The gap between the two curves for the reduction rate stays constant until the very final stage. Pellet Brand 2 is somewhat contrary to that; its final reduction result of R_{80} lies somewhere in between the two others. The reduction rate at the very initial stage is very high, even higher than that of Brand 1 but during the reduction progress it slows down more dramatically and by the end the rate is the lowest of all pellets. A numerical comparison of the pellets shows some contradiction. Considering R_{80}, based on Brand 1 at 78 minutes, a deceleration of reduction performance of 50 % for Brand 2 and 80 % for Brand 3 respectively can be seen, whereas the reduction rate $(dR/dt)_{40}$ indicates a very contrary sequence of characterization of reducibility which indicates that Brand 2 is significantly more reducible than Brand 3. The requirements for mechanical stability of pellets are generally high and the pellet samples investigated all show good performance as raw materials. Additionally there is hardly any loss in DT after the reduction process. Once again, the trend, although inconspicuous, towards lower DT after reduction corresponds to higher reducibility parameters.

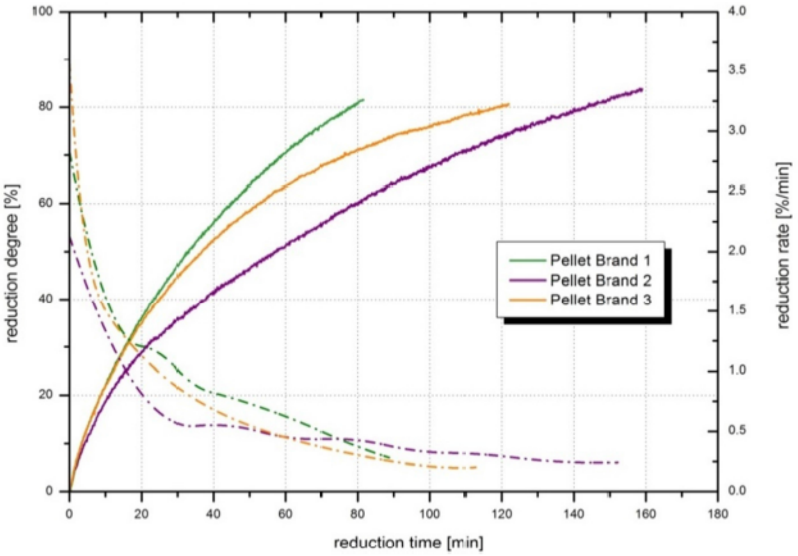

Figure 9-2: Reduction progress of different pellet brands according to ISO 4695

For the last group of material investigated, the Sinter Samples, the results are given in Figure 9-3. As is known from the chemical analysis, some magnetite prevails within the samples and therefore the pre-reduction degree has been calculated. The range of the pre-reduction is 3.4 to 4 % RD and is considered in the diagram. Two facts are immediately apparent. On the one hand, all Sinter Samples are within a small range for both reduction progress and reduction rate, although the chemical analysis distinctly differs (c.f. Table 8-I). Given in percentages, the increase in time for R_{80} from the slowest reducing Sample 3 is 30 % compared to the fastest reducible Sinter 1 and 5. First the samples show very high reduction rate with a starting value of some 3 %/min. After a sharp decrease within the very first stage after a few minutes the decrease becomes less steep and further flattens until the end of the test. The reducibility performance of all sinter samples is good and within a small range but especially the difference of the basicity and therefore the CaO content was presumed to lead to a more diverse reduction performance in terms of an enhanced reduction because of the higher CaO amount in Sinter Sample 2 compared to Sample 1.

On the other hand, compared to pellets and ore samples, the reduction proceeds rather rapidly. Within 75 minutes every sinter gained a reduction degree of 80 % which makes every sinter better reducible than all the other materials even though the morphology of the Sinter Samples indicates a very dense and coarse structure, especially considering the micro porosity.

One more surprising fact is the mechanical stability of the samples after the reduction treatment. Since it is known that sinter samples tend to disintegrate during the early stages of reduction to a great extent, the non-existent loss of strength was not expected. This confirms the assumption that because of the nitrogen purging during the heating up and at the high reduction temperature the critical temperature for disintegration is skipped. At 950 °C and a GOD of 0 the metallic iron formation proceeds fast enough and secondly the glass phase has softened to some extent to keep the grains together by some sort of sintering effect.

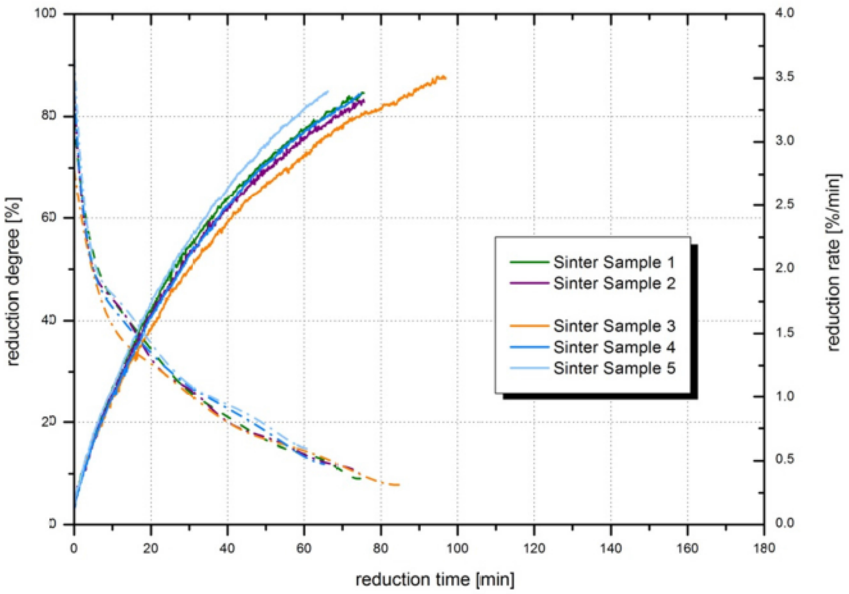

Figure 9-3: Reduction progress of different sinter samples according to ISO 4695

Table 9-I: Reducibility and mechanical characteristics according to ISO 4695

material	*DT*	*AT*	R_{80}	$(dR/dt)_{40}$	*DT*	*AT*
	[%]	[%]	[min]	[%/min]	[%]	[%]
	raw material				after reduction	
Hematitic ore	99.0	0.8	**142***	**0.67**	89.0	2.5
Magnetitic ore	96.6	1.7	**165***	**0.51**	89.2	3.3
Limonitic ore	94.5	4.8	**85**	**1.05**	81.1	5.0
Pellet Brand 1	98.0	1.9	**78**	**1.14**	96.1	1.7
Pellet Brand 2	98.8	1.2	**140**	**0.60**	99.3	0.3
Pellet Brand 3	n.a.	n.a.	**119**	**0.90**	94.5	3.5
Sinter 1	90.2	1.5	**65**	**1.42**	92.0	1.6
Sinter 2	97.0	1.4	**68**	**1.34**	95.1	1.5
Sinter 3	n.a.	n.a.	**75**	**1.21**	96.6	0.4
Sinter 4	n.a.	n.a.	**65**	**1.37**	97.8	0.2
Sinter 5	n.a.	n.a.	**58**	**1.51**	99.8	0.0

n.a… data not available

In summary, it can be said that the materials showed different behaviour concerning different stages of reduction and as a result different values for the reducibility parameters R_{80} and $(dR/dt)_{40}$. The different ore types within the same raw material group showed the biggest range. Due to their very diverse morphological structure and the lack of any artificial homogenization process, such as pellets and sinter samples receive during the mixing process, the difference in their behaviour could be illustrated. The pellet brands also differed markedly from each other, whereas the sinter samples behaved almost the same way. Nevertheless, with the exception of Hematitic and Magnetitic ore, every material showed a steep decrease of the reduction rate after the initial stages of reduction and a flattening of the reduction rate at some RD= 30 %. Concerning the mechanical stability during the reduction process, hardly any loss of stability could be found, which indicates that at 950 °C the critical temperature range for low temperature disintegration has already been exceeded.

9.2 Effect of Parameter Variation – Hematitic Ore

With the standardized testing procedure as the starting point, different parameters have been varied to depict the consequence of each parameter variation separately. For the sake of simplicity all these tests were performed with the same raw material: the medium coarse structured, medium reducible hematitic ore with a low content of slag and gangue material. This circumstance will allow a good comparability of the results by mostly avoiding distortion due to material inhomogeneities.

9.2.1 Variation of the ISO 4695 – Hydrogen and GOD Influence

As described above, the GOD as well as the gas composition was changed, the interpretation of the results, the calculation of the weight loss curves as well as the reduction rate and further the mechanical testing procedure remains the same. The continuously measured reduction curves (solid lines), the calculated reduction rate (dashed lines) and the numerical output are given in Figure 9-4.

Regarding the reduction curve of the standardized testing procedure (orange line) as the base line, it can be seen that at an increase of the GOD of 10 % (dark blue line), the reduction is considerably slower; 20 % more time is needed to reach R_{80}.

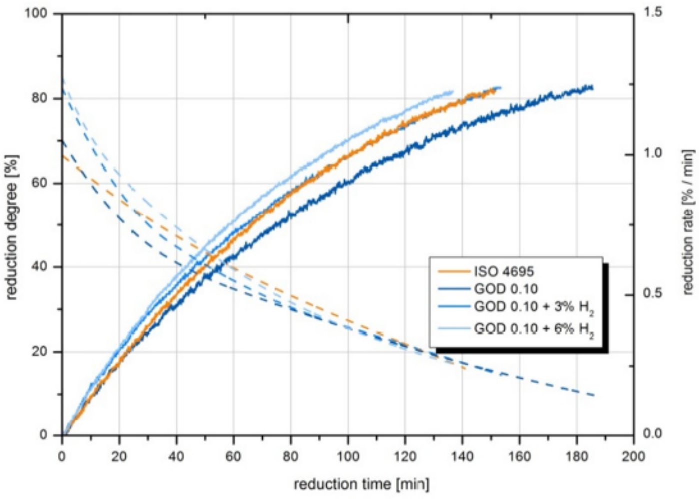

Condition	R_{80} [min]	$(dR/dt)_{40}$ [%/min]	$DT_{+6.3}$ [%]	$AT_{-0,5}$ [%]
ISO 4695	142	0.67	89.0	2.5
GOD 0.10	170	0.55	87.7	2.4
GOD 0.10 + 3 % H_2	140	0.63	91.2	1.4
GOD 0.10 + 6 % H_2	129	0.73	82.5	2.2

Figure 9-4: Graphical (left) and numerical (right) effect of variation of ISO 4695

With the subsequent substitution of CO by small amounts of hydrogen the reduction performance increases again. 3 % of hydrogen within the gas mixture (by keeping the GOD at 0.10) undoes the reduction retardation of the GOD increase; the result for R_{80} is almost the same. With a further increase of hydrogen up to 6 % this tendency continues with a decrease in reduction time of 9 %. From the reduction rate curves it can be derived that the addition of hydrogen especially influences the initial phase of the reduction. The reduction rate at the beginning is considerably higher (1.25 %/min for 3 and 6 % H_2 compared to ~ 1 %/min without H_2) whereas at the later stages the reduction rate of all testing procedures approach approximately the same value. Concerning the mechanical stability no significant trend could be observed. The disintegration and abrasion values indicate quite a good stability for all samples; only at 6 % H_2 the DT value is lower at 82.5 %

9.2.2 BF-Profile – Effect of Initial and Final GOD

As a kind of base case for any parameter variation concerning the blast furnace testing procedure the testing procedure *BFa* (= BF1, c.f. 0, dark blue lines in Figure 9-5) is understood and has subsequently been adopted. Considering the reduction progress of this base case it can be seen that at the initial stages, here the temperature is still low and the GOD is high, the reduction proceeds very slowly. The reduction rate (dashed dark blue line) is also low but yet increasing. On gaining temperature and lowering the GOD the reduction rate reaches a maximum value of about 0.65 %/min and subsequently decreases until the test is finished, when a reduction degree of > 80 % has been reached (which refers to some 250 minutes of reduction time).

Based on that the final and initial GODs have been changed, the reduction curves in comparison to the base case are given in Figure 9-5 and first of all it can be seen that there is a dramatic difference in the reduction performance by changing the GOD of the later stages (comparison of blue and green curves) but hardly any difference when changing the GOD in the first step (comparing light to dark curves). With the decrease in the initial GOD of 15 % from 0.54 to 0.48, the performance scarcely differs in any case, all four reduction curves are overlapping. This indicates that due to the very low temperature and the slow kinetics the thermodynamical driving force because of the higher CO-content is neglectable and that in this case the pre-reduction does not influence the overall performance. Due to the higher reduction potential of the lower GOD it could be presumed that the reduction has further progressed when reaching the final conditions and subsequently the final RD is reached faster, but this is not the case. By depicting the green curves, the results actually indicate the opposite.

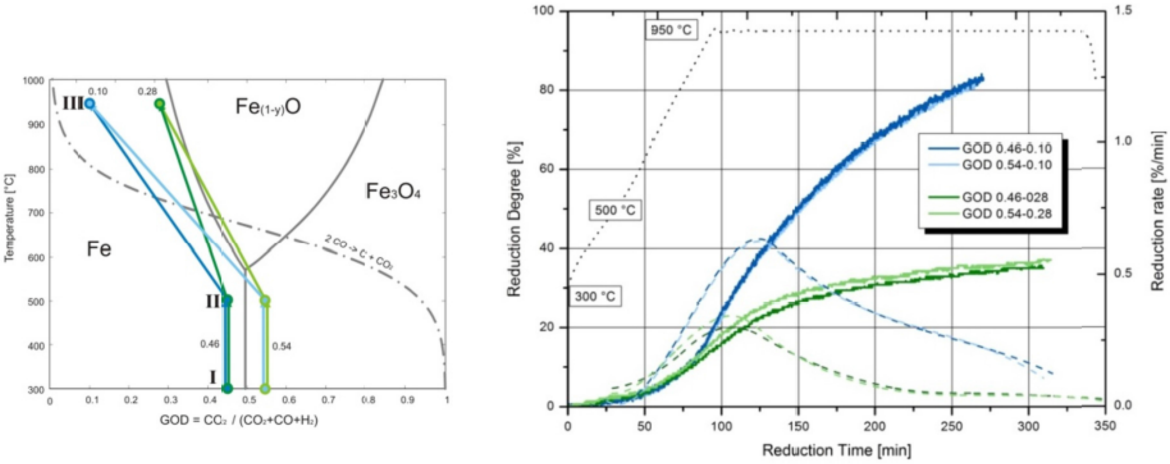

Figure 9-5: Testing conditions within the Baur-Glaessner diagram (left) and results on reducibility as a result of different initial and final GODs (right)

In contrast to that, a decrease of the final GOD of 65 % from 0.28 to 0.10 significantly enhances the reduction progress. At a GOD of 0.10 (blue lines) a reduction degree of 80 % is reached within some 250 min whereas at 0.28 (green lines) within the defined 300 min of overall reduction time a reduction degree exceeding 37 % cannot be gained. Nevertheless the course of reduction is comparable; the reduction rate reaches a maximum value (although at a distinctly lower level of about 0.3 %/min) at the point of reaching 950 °C and the final GOD. On further progress the reduction rate decreases and at the later stages the reduction rate is at a very low level. Reaching a reduction degree of 80 % would, if at all, take very long time.

These results indicate that, on envisioning an industrial scale blast furnace, there are considerable differences in the extent of reduction when the material reaches the lower levels of the furnace in dependence of the location of the burden material. At positions where the reducing gas with a low GOD has good access to the ferrous burden the material is definitely reduced earlier to a higher extent and some softening, dripping and melting will occur earlier compared to positions with a well oxidized gas and hence lower reduction potential. These differences in gas compositions will result in different behaviour at different furnace locations and subsequent inhomogeneities during the descent of the burden material.

9.2.3 Influence of Pre-reduction Step

To examine the influence of pre-reduction, the hematitic ore is tested at different conditions with the following scheme. In the first step, as given above in section 0 as the dark blue and dark green line respectively, the testing procedure was similar to the standard test, heating up at nitrogen atmosphere and switching the gas to a CO/CO_2 mixture with a GOD of 0.10, hence there is no pre-reduction (directly reducing at Point III within the small Baur-Gleassner diagram in Figure 9-5). This curve is given in both diagrams in Figure 9-6; due to the lack of pre-reduction it is valid for both diagrams. The second condition was a pre-reduction step at a GOD of either 0.46 (medium blue curve, left diagram) or 0.54 (medium green curve, right diagram) at a temperature between 300 and 500 °C, referring to steps I to II with the Baur-Glaessner diagram. Upon reaching Point II the gas is switched to nitrogen again and after the further heating up to Point III the reduction proceeds at GOD 0.10. The last test refers to the industrial scale process conditions as described in 0, BFa (light blue) and BFc (light green) testing conditions. That means an expanded continuous pre-reduction from 300 to 950 °C. The results are given in Figure 9-6; the very moment when at all testing procedures the conditions are the same (950 °C and GOD 0.10) is marked within the diagrams.

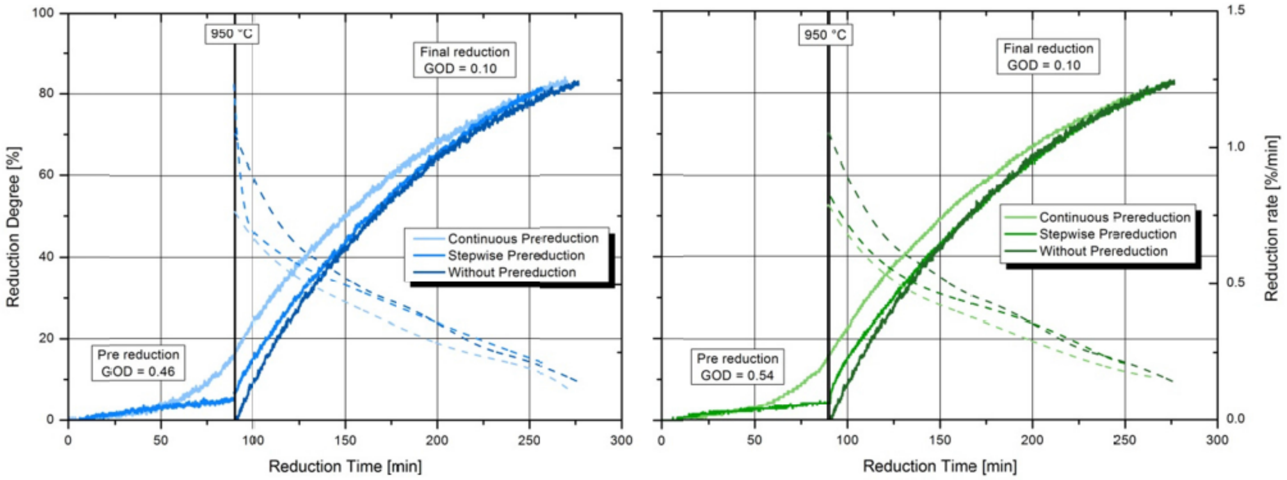

Figure 9-6: Effect of pre-reduction step at GOD 0.46-0.10 (left) and GOD 0.54-0.10 (right)

The results of these testing conditions are to some extent unexpected. Since the absence of influence of the initial stages of reduction for the small GOD variation of 0.46 and 0.54, as shown in Figure 9-5, is assumed as a result of the small range of variation, a total lack of any influence of a pre-reduction step is surprising. Even a 90-minute period of pre-reduction and a resulting RD of about 17 % at the moment of reaching 950 °C (in both cases) could not result in an enhanced reduction performance on considering R_{80}. Although the reduction rates without pre-reduction are enhanced at first, the decrease is steeper and at the later stages the reduction rate is almost at the same level for all curves.

These results are contrary to observations in literature that have been performed for the reduction of fine ore [68,96]. For the reduction of iron ore fines these circumstances are explained by the difference in morphology. A lower reduction potential of the gas is assumed to lead to dense wustite during reduction which subsequently leads to the formation of dense metallic iron shells surrounding the grains and hence a retardation of the further reduction. Furthermore higher reduction potential at the initial stages is assumed to form porous wustite and further fine metallic iron scraps and warts, which do not hinder the further reduction.

9.2.4 Effect of Hydrogen Addition on Reduction

To depict the influence of the addition of small amounts of hydrogen another variation of the blast furnace testing procedure was perfumed. All the tests with the hydrogen enriched gas composition to an extent of 3 and partly 6 % of H_2 are given in Figure 9-7, the left for an initial GOD of 0.46 and 0.54 at the right, always compared to the testing profile without H_2 (c.f. testing conditions as given within the Baur-Glaessner diagram in Figure 9-5). It can clearly be seen that the presence of hydrogen enhances the reduction performance in every case. Compared to the reduction only with CO at an initial GOD of 0.46 (dark blue curve) the enhancement for gaining R_{80} was around 11 % for 3 % H_2 and subsequently another 10 % for another increase from 3 to 6 % H_2. Altogether 6 % of hydrogen enhances the reduction performance for R_{80} from 250 minutes to 199 minutes for an initial GOD of 0.46 and from 258 to 198 minutes for 0.54 initial GOD, which corresponds to 23 %.

Considering the lower final GODs, the addition of hydrogen also enhances the reduction performance, just not to the same extent. At 300 minutes of reduction without H_2 the RD has reached some 36 % in both cases, whereas the addition of 3 % hydrogen leads to some 40 % of reduction. This indicates an increase in the reduction degree of about 8 % after 300 minutes of reduction time.

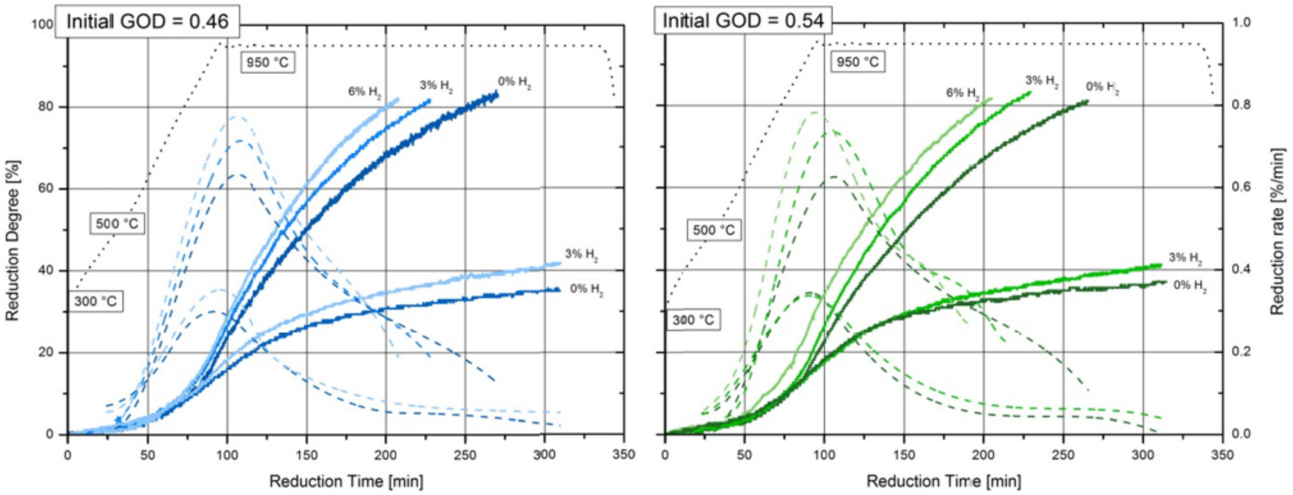

Figure 9-7: Effect of hydrogen addition on the reduction performance

When considering the curves for the reduction rate (dashed lines) another circumstance, corresponding to section 0 can be seen, the accelerating effect of hydrogen is only predominant at the initial and intermediate stages of the reduction, not at the final stages. During the first reduction period within this test, the heating from 300 °C to the final temperature, the reduction rate progressively increased until it reached a maximum value. This maximum emerges at almost the same time but the level of the maximum reduction rate is different. As an example, for the BFa-a´´ (BF1-3 respectively) profile (GOD 0.46-0.10, left picture), the maximum reduction rate (peak level) is increased by 19 %. On further reduction, the reduction rate is only slightly enhanced at the higher final GODs, not at the GOD of 0.10.

9.3 Comparison of Different Raw Materials at Industrial Scale Process Conditions

Having described all the different materials concerning their raw material characteristics and subsequently their reduction behaviour at the standardized testing procedure, their behaviour at the industrial scale process conditions has therefore been depicted. Is a is a question of real interest whether the sequence of reduction performance that was pointed out by means of test ISO 4695 test will remain the same. Due to their very similar behaviour at the standard test, only two of the five sinter samples, the industrial scale produced sinter samples Sinter 1 and Sinter 2 were tested at industrial scale process conditions.

9.3.1 Different Iron Ores

The reduction curves for all five testing conditions are given in Figure 9-8, as is the modified Baur-Glaessner diagram depicting the different process conditions. Within the reducibility diagrams the sample temperature during the testing procedure is also given as dotted lines. It has to be noted that the pre-reduction stages, starting from 300 °C in each case, of the BF conditions take longer than those of DR because of the slower heating rate and therefore the reduction degrees in dependence of testing time are not easily comparable to each other. The starting point, the base case, of consideration remains the hematitic ore (a). The acceleration as a result of hydrogen addition has already been described. The impact of lowering the temperature with simultaneous increase of hydrogen content is generally known as opposed, for this raw material the observations can be described as follows. Although the final testing temperature for DR1 (orange line) compared to BF is 150 °C lower, the addition of hydrogen led to an explicit enhancement of the overall reduction performance, however the pattern of reduction remains comparable. The reduction rate reaches a maximum value upon reaching the final temperature, even though the level is almost twice the height for DR1, and sharply decreases until the end of the test. At the testing time RD > 80 %, the reduction rate is still twice the value of the BF test. On further testing at 850 °C (DR2, green line) which is 50 °C more than for DR1, it can be seen that at the initial stages the curves overlap. On reaching the moment of maximum temperature the reduction rate is at its maximum value and then sharply decreases until the end. The numerical results for R_{80} and for the reduction rate $(dR/dt)_{40}$ are summarized in Table 9-II, the gradual increase of $(dR/dt)_{40}$ from BF1-3 to DR1 and DR2 in terms of the hematitic ore can be seen.

For the Limonitic ore, shown in (c) the trend is similar to that of the Hematitic ore. As already shown with the standardized testing procedure, the reduction performance is better than that of the Hematitic ore, for the base case, BF1 profile, the enhancement for R_{80} is 30 %. There is also a trend towards better reduction performance when adding small amounts of hydrogen whereas the effect of adding 3 % is more pronounced as the further increase of 3 % up to 6 %. With the addition of further hydrogen (DR1) the reduction is even faster despite of the lower temperature and the best possible conditions for Limonitic ore is DR2. There is also a continuous increase of the reduction rate in the same way as for Hematitic ore. Different to the Hematitic ore is the first peak of the reduction rate curves appearing at the initial stages (at some 5-8 % reduction degree). Although this is not a direct result of the crystallization water release (because the weight loss of the LOI has been corrected prior to the reducibility testing), it is assumed to indirectly influence the reduction performance at the initial stages. Due to the LOI the water vapour induces cracks within the entire ore particle and therefore the reducing gas has better access to the internal parts of the piece. After the first time the reduction slows down again because of the formation of first reduction product layers, and the temperature is still too low to further precede the reduction (inhibited kinetics). Only upon gaining temperature does the reduction progress accelerate again, up to levels distinctly higher than for hematite.

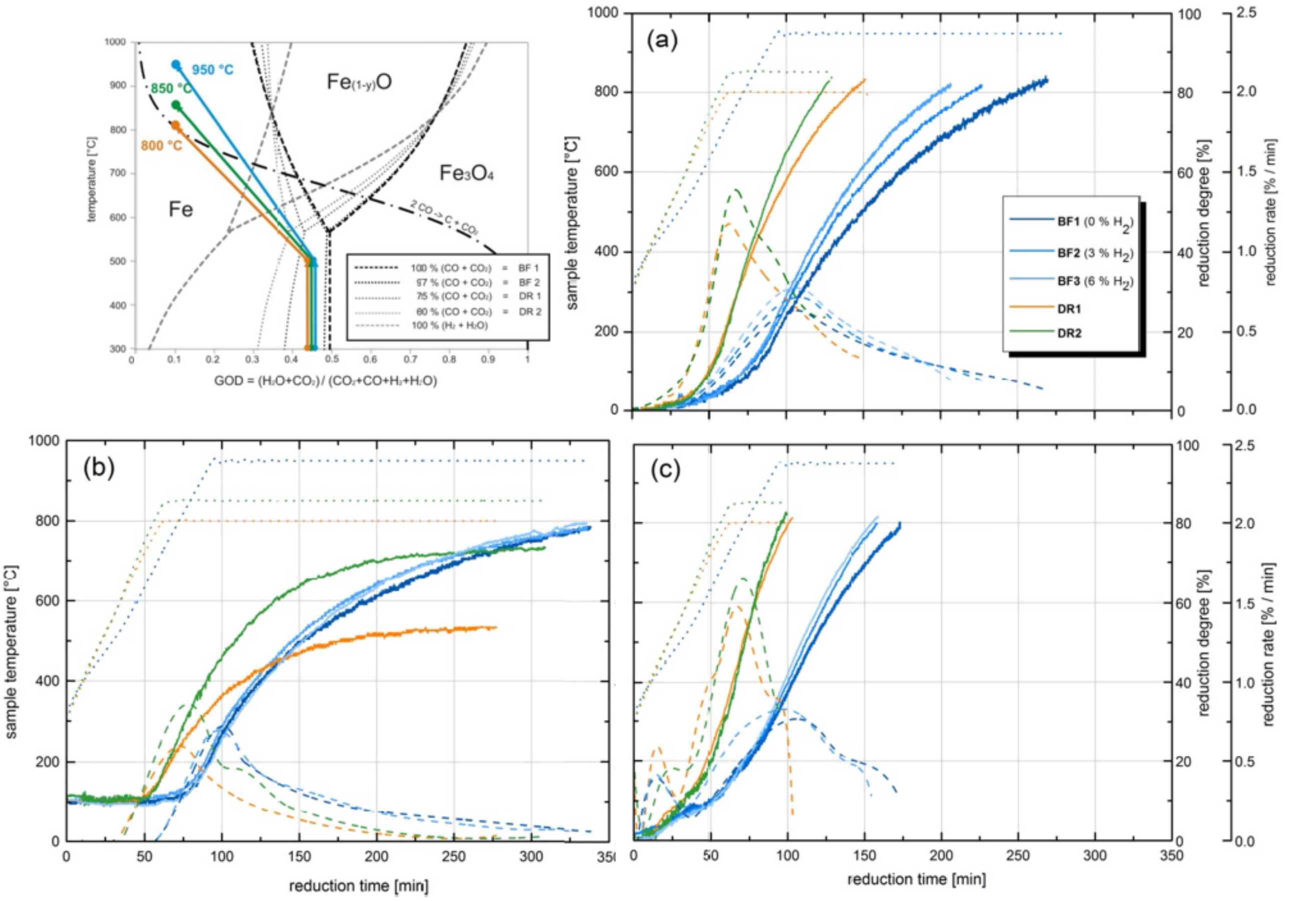

Figure 9-8: Reduction progress of the investigated iron ores at all different process conditions Hematitic ore (a), Magnetitic ore (b) and Limonitic ore (c)

The results of the Magnetitic ore finally give quite a different result especially concerning DR tests. Again all the reduction curves start at a reduction degree of 11 %, yet a reduction degree of > 80 % cannot be reached within the maximum testing time of 300 minutes in any case. This slow reduction performance at 950 °C corresponds to the observation from the ISO standard; a very slow reduction during the whole process (no peaks at the start). Nevertheless there is a maximum peak at the same time as for every other material tested and the value, at 0.75 %/min, is only slightly lower than for the other ores. But the decrease in reduction speed sharply sinks after that peak and is at very low levels in the final stages of reduction.

At the lowest reduction temperature, the appearing peak at initial stages is lower for DR1 than for BF1 (in contrast to the other ores) and finally the reduction progress has almost stopped only upon reaching a RD of 50 %. It is assumed that due to the very coarse and dense structure, the formed metallic iron appears as extremely dense layers and the retarded kinetics at 800 °C makes a diffusion of the gaseous reducing agents to some extent impossible. The temperature increase of 50 °C up to 850 °C leads to the very same effect although shifted to later stages. In this case, the reduction proceeds to some 70 % until no more oxygen release is possible. Nevertheless, in any case the pattern of the reduction rate is comparable to the other ores, a peak upon reaching maximum temperature and a subsequent loss of reduction velocity.

Table 9-II: Reducibility characteristics of different iron ores at industrial scale process conditions

	BF1 0 % H_2		BF2 3 % H_2		BF3 6 % H_2		DR1		DR2	
Ore type	R_{80} [min]	$(dR/dt)_{40}$ [%/min]	R_{80} [min]	$(dR/dt)_{40}$ [%/min]	R_{80} [min]	$(dR/dt)_{40}$ [%/min]	R_{80} [min]	$(dR/dt)_{40}$ [%/min]	R_{80} [min]	$(dR/dt)_{40}$ [%/min]
Hematitic	250	0.53	222	0.65	199	0.72	140	0.98	123	1.40
Limonitic	175	0.84	159	0.92	155	0.97	100	1.49	95.7	1.70
Magnetitic	350*	0.38	350*	0.43	345	0.44	---	0.25*	---	0.58

* extrapolated

9.3.2 Pellet Brands

The next series of material testing has been executed with the different Pellet Brands, the results are summarized in Figure 9-9. Based on the results from the performance of the different iron ores and the standardized test, there will be a comparison of their behaviour.

Pellet Brand 1 (a) indicates good reducibility properties at every testing condition. For the BF1 test R_{80} is about 147 minutes which corresponds somewhat to the value of the Limonitic ore. Also the evolution upon the hydrogen increase is similar to the Limonitic ore: an increase of 3 % H_2 enhances the reduction whereas another 3 % hardly has any impact, and finally the difference between DR1 and DR2 is small but yet present. The very same behaviour can be seen in the lower left picture (b) of Pellet Brand 2, but what makes these results a little surprising is the overall reduction performance when comparing Brand 1 and Brand 2. Whereas at the standardized procedure the increase of time gaining R_{80} between Brand 1 and Brand 2 has been 84 % (78 to 140 minutes), it is only 23 % on comparing BF1 condition and furthermore on comparing the DR2 condition the difference becomes even smaller to only 9 % of increased time. In both of the cases there is the step-by-step increase of $(dR/dt)_{40}$ from BF to DR1 and DR2 (given in Table 9-III), which indicates that for both of the pellet brands the accelerating effect of the hydrogen presence is more dominant than the inhibited kinetics due to the lower temperature.

On further integration of the last pellet sample, Pellet Brand 3 (c), some general trends can be confirmed. The effect of the small amounts of hydrogen corresponds to the observation of all materials so far tested, including the enhanced reduction performance for DR2 compared to BF conditions. A comparison of Brands 1 and 3 and the performance concerning R_{80} from the ISO test leads to an increase in time of 52 %. By comparison of the BF1 results, it takes 17 % longer (c.f. Table 9-III, 147 to 172 minutes) and finally the DR2 condition leads to an acceleration gain of R_{80} of 15 %. A non-conventional behaviour of Pellet Brand 3 can be seen in the figure, as the reduction progress is slows down considerably at the DR1 condition. This behaviour is to some extent comparable with the standardized testing results where a deceleration at the later stages was also noticeable, but it is not comparable to the other testing procedures where no such effect occurs at the later stages.

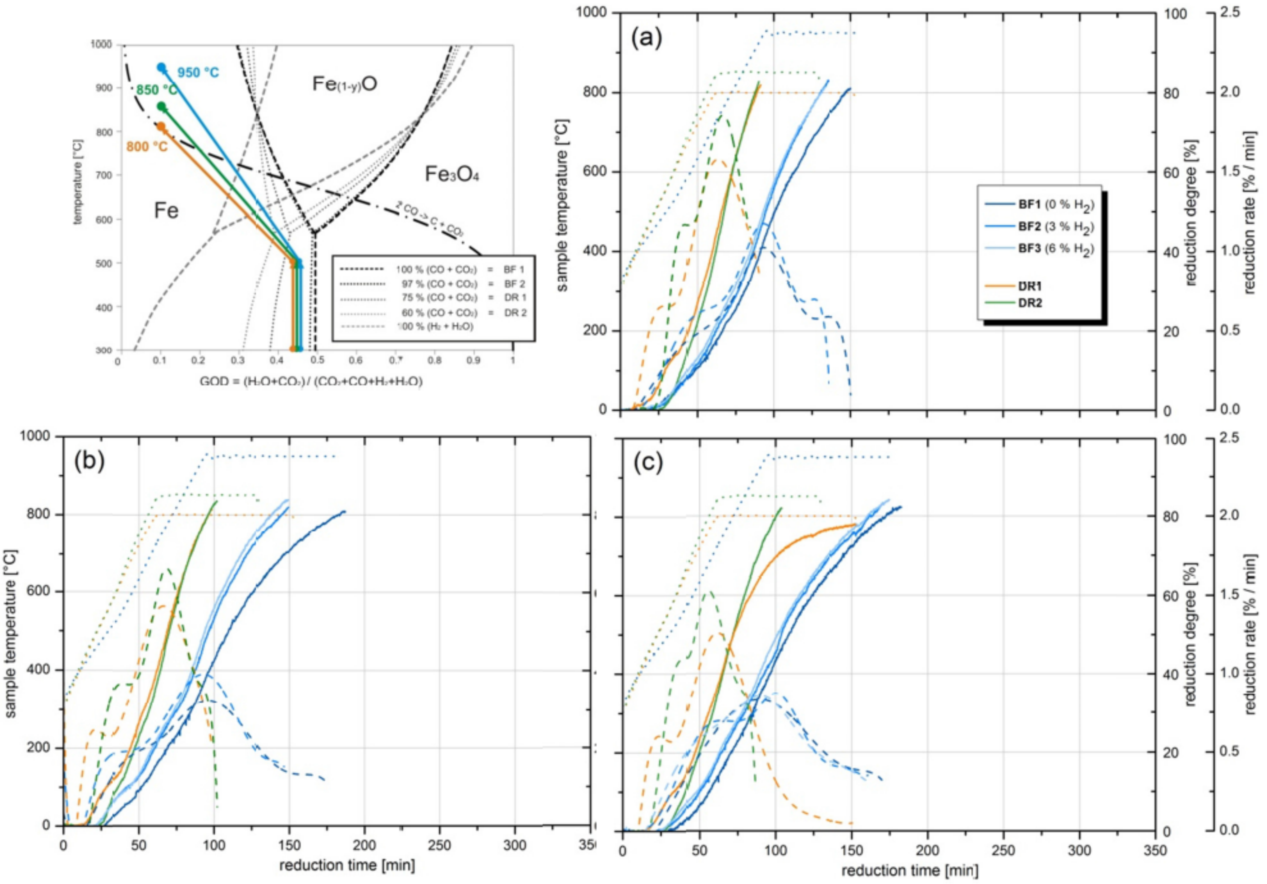

Figure 9-9: Reduction progress of the investigated pellet brands at all different process conditions Brand 1 (a), Brand 2 (b) and Brand 3 (c)

Table 9-III: Reducibility characteristics of different pellet brands at industrial scale process conditions

Pellet brand	BF1 0 % H_2		BF2 3 % H_2		BF3 6 % H_2		DR1		DR2	
	R_{80} [min]	$(dR/dt)_{40}$ [%/min]	R_{80} [min]	$(dR/dt)_{40}$ [%/min]	R_{80} [min]	$(dR/dt)_{40}$ [%/min]	R_{80} [min]	$(dR/dt)_{40}$ [%/min]	R_{80} [min]	$(dR/dt)_{40}$ [%/min]
Pellet Brand 1	147	1.02	130*	1.21	130	1.14	88.5	1.66	87	1.98
Pellet Brand 2	181	0.84	145	0.95	138	1.10	96	1.51	95	1.71
Pellet Brand 3	172	0.85	163	0.90	160	0.91	---	1.23	100	1.61

* extrapolated

By comparing the reduction curves of all pellet samples, some commonalities can be derived from the Figure. What all curves for the reduction rate (even the ore samples) have in common is again the peak of maximum reduction rate at the time when the sample temperature approaches the maximum value. In any case this peak gets higher with the increasing hydrogen amount, the maximum value can be observed for DR2 conditions ranging from 1.5 to 1.8 %/min. For the BF1 the values are lowest at 0.8 to 1.0 %/min. What all the curves for the pellet samples alone have in common is another peak at the early stages of reduction, and this is definitely not an effect of any LOI or carburization reaction due to the prior burning process of pellets during production. On comparing the ore samples, either hematitic or limonitic ore show a slow but not infinitely small increase during the first stages. The pellets show some retardation at the very beginning, followed by a short accelerated period and again a slowing down, which subsequently leads to this peak on considering the first derivation. For all three Brands the level of the first peak is more or less the same for the different testing conditions. At the DR2 conditions the retardation at the initial stages can best be seen, no weight loss is measurable until 500 °C and more has been reached, but once started the reduction proceeds very rapidly. This fact indicates that the presence of the binding and glass phases within the microstructure (c.f. 8.2.2 morphology of pellet samples) inhibit the access of the gaseous reducing agent into the internal parts of the pellet in the early stages due to the low temperature. Whereas for iron ores the gas reduces the iron oxide grains at least to some small extent, the glass phase that surrounds every single small hematitic grain within the pellet prevents any reduction. Only upon reaching a certain temperature, which is proved to be distinctly dependent on the gas composition (because of the difference between DR1 and DR2) can the reduction start. This fact compared to the standard test results (where the reduction does not start until the material is heated up to 950 °C but starts with a very high reduction rate at the beginning for all pellet brands), indicates that due to the high temperature, the structure of the binding phase changes in some way. It might be that the glass and binding phase already starts to melt to some extent or at least becomes of lower viscosity so that the gas has better access to the reaction surface. The diffusion resistance might also change at higher temperatures so that the gaseous agents can diffuse more easily through the glass film surrounding the grains.

What can be concluded about the reduction performance of the investigated Pellet Brands is that their behaviour is different depending on the reduction parameters. Although there was a great difference at the standardized testing conditions, the range between well and badly reducible brands is no longer that obvious: even a reversal of the prior sequence could be illustrated.

9.3.3 Sinter Samples

The final and most complex raw materials to be investigated were the two industrial scale produced sinter samples, and the results of the reduction progress are given in Figure 9-10. In good accordance with the standardized test, both sinters are very reducible and showed a comparable reduction performance to each other. Once more the tendency towards better reducibility by adding 3 % hydrogen can be seen whereas 6 %H_2 does not further enhance the reduction performance. For Sinter Sample 2 (b) even the DR2 test was performed, though it is not of particular industrial interest because of the lack of usage of sinter within any direct reduction facility. It is, however, of scientific interest.

The progress of the reduction rate indicates a retarded start of the reduction progress similar to that of the pellet brands. But then on reaching some 600 °C the process starts at very high velocities and the maximum peak values are definitely the highest at 1.25 for BF1 and >1.5 %/min for DR1, when compared to Pellet Brand 1. No first peak is visible at the early stages of reduction. After reaching the maximum reduction rate, it decreases again very sharply. For both sinter samples the conditions of DR1 showed an even higher decrease, whereas the DR2 condition did not show this deceleration at the end. In this case the behaviour is comparable to Pellet Brand 2.

On evaluating the different times needed to gain R_{80} (Table 9-IV) and the different testing procedures compared to the Hematitic ore the reduction performance is better for sinter throughout all the conditions but the distance reduces from ISO (difference in time is 55 %) through BF1 (difference of 40 %) and finally to DR1 (15 %). Again it is obvious that despite the different chemical analysis of the Sinter Samples, their reduction performance is very similar.

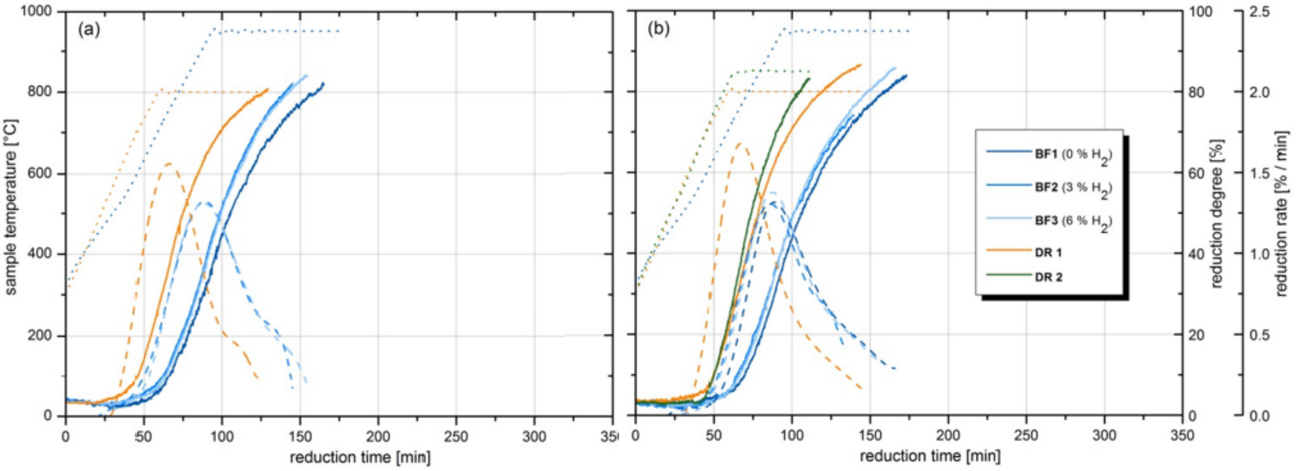

Figure 9-10: Reduction progress of the investigated sinter samples at all different process conditions for Sinter 1 (a) and Sinter 2 (b)

Table 9-IV: Reducibility characteristics of different sinter samples at industrial scale process conditions

	BF1 0 % H_2		BF2 3 % H_2		BF3 6 % H_2		DR1		DR2	
Sample	R_{80} [min]	$(dR/dt)_{40}$ [%/min]	R_{80} [min]	$(dR/dt)_{40}$ [%/min]	R_{80} [min]	$(dR/dt)_{40}$ [%/min]	R_{80} [min]	$(dR/dt)_{40}$ [%/min]	R_{80} [min]	$(dR/dt)_{40}$ [%/min]
Sinter 1	151	1.14	134*	1.40	137	1.40	115	1.58	n.a	n.a
Sinter 2	150	1.14	144	1.24	142	1.35	112	1.65	105	1.83

* extrapolated n.a….data not available

When considering all the materials and testing procedures together, the results indicated different reduction performance for the same material depending on the reduction conditions. For hematitic and limonitic ore the behaviour at industrial scale process conditions was best comparable to the standardized testing procedure. In this case the reduction performance was to some extent predictable from the raw material characterization and the ISO test results. Especially the very poor reducibility of the magnetitic ore at lower temperatures was not expected based on the prior investigation.
The behaviour of the pellet brands at industrial scale conditions was also unexpected, when considering the ISO standard tests. The least reducible pellet brands at standardized testing conditions proved to be very suitable for industrial scale applications, whereas the medium reducible pellets at ISO 4695 proved to have very poor reducibility properties at lower temperatures (and therefore DR1 conditions). The sinter samples kept their good reducibility behaviour at all conditions though the difference between less reducible materials and sinters got smaller from ISO to BF to DR conditions.

In general, however, it can be pointed out that the better reducible a material behaves at conditions without any hydrogen (ISO, BF) the less impact in terms of accelerated reduction velocity can be observed at conditions with higher hydrogen content.

9.4 Mechanical Stability at Industrial Scale Conditions

For each material at any testing condition the material's strength in terms of disintegration and abrasion tendency was determined by means of a tumbling procedure as described in section 7.4. In this case the mechanical stability is related to the reduction degree after the reduction procedure, which means a reduction degree of more than 80 %. A summary of the results is given in Table 9-V and as a conclusion, the following statements can be made.

Iron ores showed very good raw material strength as well as stability after the reduction procedure according to ISO standardized testing conditions (c.f. Table 9-I); only a loss of DT of about 10 % occurred due to the reduction procedure at 950 °C. The other materials also showed the same tendency of proper raw material strength and an insignificant loss of strength after ISO reduction but in contrast to that, the different industrial scale process conditions exerted a stronger influence on the mechanical properties.

One general tendency can be derived by considering the table; at direct reduction conditions the materials tended to disintegrate more compared to BF conditions (valid for most of the test results, though not all). Hematitic ore shows comparable values for DT as well as AT for ISO and BF conditions and a further loss of DT of about 10 % at DR conditions. What is interesting is that the extent of abrasion stays constant at a very low level (< 2 %); hardly any formation of fines occurs. The Limonitic ore´s stability decreased on testing at BF conditions and further decreased at DR conditions; but in this case the abrasion tendency increased as the disintegration tendency increased, which is according to literature data. Mostly a bad mechanical stability affects both the tendency to disintegrate and the formation of fines due to abrasion. In contrast to the Hematitic and Limonitic ore, here the mechanical stability decreased consistently combined with the higher reduction velocity due to the higher hydrogen content, the Magnetitic ore showed two different phenomena. At ISO as well as BF conditions, where there is a temperature of 950 °C and the material gained a reduction degree of at least 70 %, the DT is quite high and the AT values are at some 5-6 %. In turn, after the DR testing procedures, the DT values are lower than 50 % and more than one third of the material has a grain size smaller than 0.5 mm, the material is almost crumbled.

Pellet Brands 1 and 3 show similar behaviour, it can be noted that after every reduction procedure the material has hardly lost its initial mechanical stability. Only the direct reduction procedures led to a slightly increase in abrasion. Brand 2 gives a somewhat different picture; at the tests BF1 and DR2 the strength is still very high whereas at BF2, BF3 and DR1, the pellets disintegrated to a great extent by keeping the abrasion index very low.

As was presumed to some extent, the Sinter Samples showed the least resistance to the tumbling procedure after the reduction tests; Sinter Sample 1 even moreso than Sample 2. This, in relation to the reducibility results, stands in good accordance with the literature review (c.f. Section 5.2) where it is noted that higher CaO amounts will lead to higher mechanical stability. Though the values for DT and AT have been quite good, after the ISO standard test the material disintegrated to a very high extent. Again by retaining the small portions of fine fraction; sinters obviously tend more to disintegrate than to form fines by abrasion.

As en explanation for the good mechanical stability after the ISO test compared to the BF test, although the final testing temperature and the material's reduction degree are comparable, the following considerations have been taken into account. It is assumed that the slow increase in temperature and the concomitantly low reduction potential of the gas at the initial stages of reduction enhance the low-temperature disintegration. This low temperature disintegration occurs preferably in a temperature range of 500-550 °C and is caused by a volumetric increase of the grains during the transformation from hematite to magnetite. The difference between the ISO and the BF testing profile is the temperature at which the transformation of hematite to magnetite takes place. At ISO conditions, the material is already heated up to 950 °C before the first reduction can occur and due to the very strong reduction potential of the gas, it is assumed that some metallic iron appears at least at the outer shells of the grains and therefore the disintegration is prevented (by some kind of sintering effect). In addition, the prevailing glass phases might already be softened at temperatures of 950 °C and this can further increase the mechanical stability by keeping the grains together.

Table 9-V: Mechanical properties after industrial scale process conditions

	Raw material		BF1 0 % H_2		BF2 3 % H_2		BF3 6 % H_2		DR1		DR2	
Material	$DT_{+6.3}$ [%]	$AT_{-0,5}$ [%]	$DT_{+6.3}$ [%]	AT [%	$DT_{+6.3}$ [%]	$AT_{-0,5}$ [%]	$DT_{+6.3}$ [%]	$AT_{-0,5}$ [%]	$DT_{+6.3}$ [%]	$AT_{-0,5}$ [%]	$DT_{+6.3}$ [%]	$AT_{-0,5}$ [%]
Hematitic ore	99.0	0.8	87.8	1.8	88.0	0.9	87.8	1.8	77.3	1.6	73.4	1.4
Limonitic ore	96.6	1.7	67.9	6.3	62.1	6.0	73.6	4.8	60.9	9.7	59.0	11.3
Magnetitic ore	94.5	4.8	87.7	5.2	86.8	6.4	88.5	5.3	48.6	32.6	48.1	34.6
Pellet Brand 1	98.0	1.9	98.9	0.5	93.5	1.2	93.9	1.2	87.7	4.8	87.8	6.3
Pellet Brand 2	98.8	1.2	97.8	0.4	69.5	1.3	65.7	1.2	63.6	2.2	93.4	0.9
Pellet Brand 3	n.a.	n.a.	98.4	0.8	96.3	0.9	n.a.	n.a.	93.1	3.5	97.8	1.2
Sinter 1	90.2	1.5	45.8	3.3	39.7	3.7	44.4	3.0	37.6	4.3	n.a	n.a
Sinter 2	97.0	1.4	61.6	4.9	65.1	3.9	69.4	3.5	53.6	3.5	57.5	3.0

n.a.…data not available

9.5 Morphological Evolution during Reduction

As described before, the reduction of iron oxide to metallic iron is simplified formulated as the gradual release of oxygen from the oxide crystal lattice but in fact it is a highly sophisticated and complex topic. In order to depict the morphological evaluation during the reduction process the materials were investigated by light microscopic means, the same as for the raw materials. In some cases the tests have been interrupted at a certain reduction degree to facilitate the visualization of the intermediate reduction products Fe_3O_4 and FeO before almost everything had turned to metallic iron with it´s different kinds of metallic iron formation. Table 9-VI gives an overview of the different prevailing phases and their appearance within the microscopic pictures.

In order to substantiate the assumption of the kinetic model, which describes the reduction as proceeding according to a shrinking core model with a sharp phase boundary, Figure 9-11 gives a cross section of a lump ore piece of the Hematitic ore (left) and an exemplary pellet from Pellet Brand 1 (right). In both cases the reduction degree is at some 30 % and both of the materials initially consisted of a more or less porous hematite matrix. What can be seen is that the reduction begins at the surface of the ore particle and, in the course of reduction; the hematite (h) is first reduced to magnetite (m), then to wustite (w) and later to metallic iron (I) in a layer- or shell-like structure. At this time and hence reduction degree, all possible different (intermediate) reduction products prevail simultaneously and three different reaction fronts exist. These reaction fronts further move into the inside of the grain on further reduction. On taking a closer look at the boundaries of these different reaction fronts, it can be seen that the boundary line between the hematite and magnetite as well as magnetite to wustite is a very sharply defined line. In contrast to that, the boundary between the wustite and the metallic iron is definitely not a clear line but a small region where both phases exist parallel to each other.

These differences in the reaction fronts are an indication of the velocity of the different reactions. The transformation of hematite to magnetite and further to wustite takes place more easily and rapidly, whereas the transformation of wustite to metallic iron takes more time. It is the final step of iron formation from wustite that is the rate determining reaction within the reduction of iron ore. This is in good accordance to observations that have been derived from literature data [40,43,68,89,94,96,97].

Table 9-VI: Description of different phases in reduced samples

acronym	chemistry	colour	description/origin
h_1, h_2	Fe_2O_3	light grey	fine (h_1) or coarsely (h_2) hematite
m	Fe_3O_4	brownish	magnetite
w	FeO	grey	wustite
I_s			scraps of metallic iron
I_l	Fe_{met}	white	metallic iron layers and skins
I_p			highly porous metallic iron
g	variable	dark grey	gangue/slag
p		black	pores filled with resin

Another circumstance can be further interpreted from these pictures. On considering the thickness of the different oxide layers, a clear difference especially for the thickness of the magnetite layer is obvious, and the hematite core of the lump ore is still distinctly greater in volume. The reason for this might be seen in the different porosities and therefore the possibility for the gaseous reduction products to enter and leave the inner parts of the material. Pellets are artificially produced agglomerates and although the microporosity might be less than those of ore (see 0 raw material characterization) it is possible that a coherent network of larger pores enhances the gas diffusion and the reduction performance to a greater extent. Thereafter the reaction products will be more porous and it might be the chemical reaction that controls the overall rate to a greater extent within pellets than it does in ore.

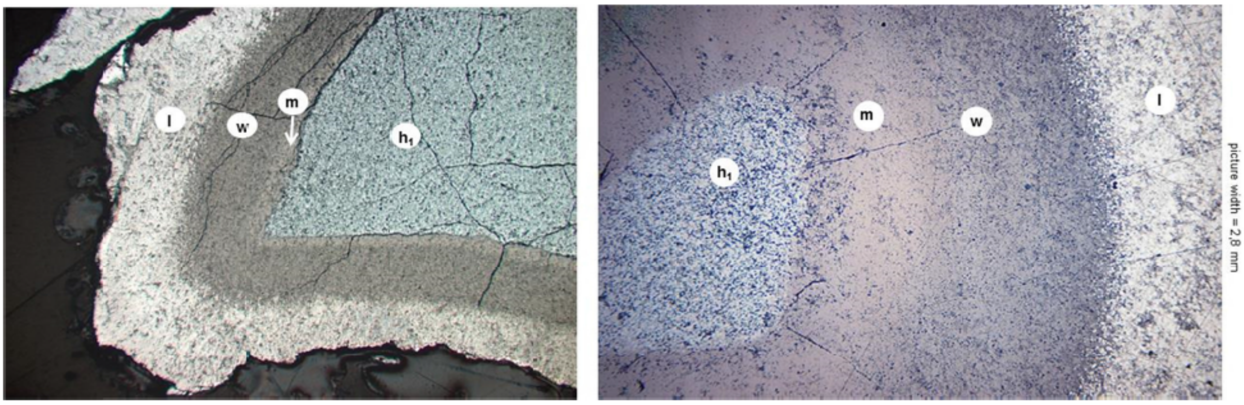

Figure 9-11: Different reaction fronts at intermediate stages of reduction of a (hematitic) lump ore piece (left) and a pellet (right)

Another visualization of the reduction procedure is given in Figure 9-12. This figure shows different mineralogical structures at different stages during the reduction procedure at more or less the same position within the ore particle. In the first picture (a) the reduction is at the very initial stages, from the outer edge of the hematitic ore particle (top right of the picture) two rather small layers of both, magnetite and wustite can be seen. On further progress, the intermediate magnetite layer moves inwards simultaneously with the thickening of the wustite layer all at the expense of the initial hematite core. When a thickness of 0.3 to ~2 mm of the wustite layer is reached, small scraps and warts (I_s in picture b) start to grow at random places on the surface of a grain and the surface of the pores; a few tenths of millimetres below the grain boundary. Further reduction generates thin skins of Fe_{met} (I_l in c). In addition to the thickening of the metallic layer one possible step is the formation of highly porous Fe_{met} (I_p). In picture (d) the whole microstructure has been transformed to metallic iron.

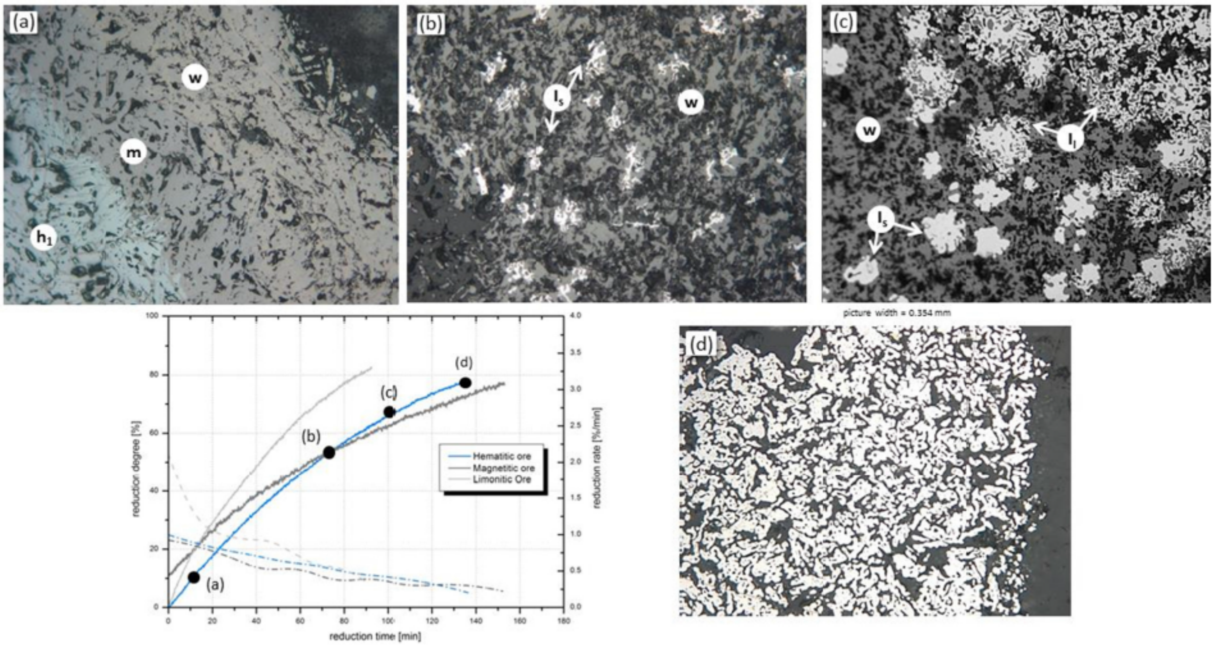
(a)
w
m
h1
(b)
Is
w
(c)
w
Il
Is
picture width = 0.354 mm
(d)
reduction degree [%]
reduction rate [%/min]
reduction time [min]
0
20
40
60
80
100
0.0
0.5
1.0
1.5
2.0
2.5
3.0
3.5
4.0
0
20
40
60
80
100
120
140
160
180
Hematitic ore
Magnetitic ore
Limonitic Ore
(a)
(b)
(c)
(d)

Figure 9-12: Morphological evolution of a hematitic ore particle during the testing procedure ISO 4695

What can be seen within Figure 9-13 is that the progress of the final metallic iron formation is a discontinuous one. At some random time and place below the region of already transformed metallic iron, single scraps and warts appear at a single point. On further movement of the reaction front, originating from those warts, the formation of a metallic iron layers starts. These iron layers are very small at the initial stages but yet surrounde every single grain. On further progress the layers thicken and again the iron moves inwards the grain on expand of the wustite in the form of a shrinking core model.

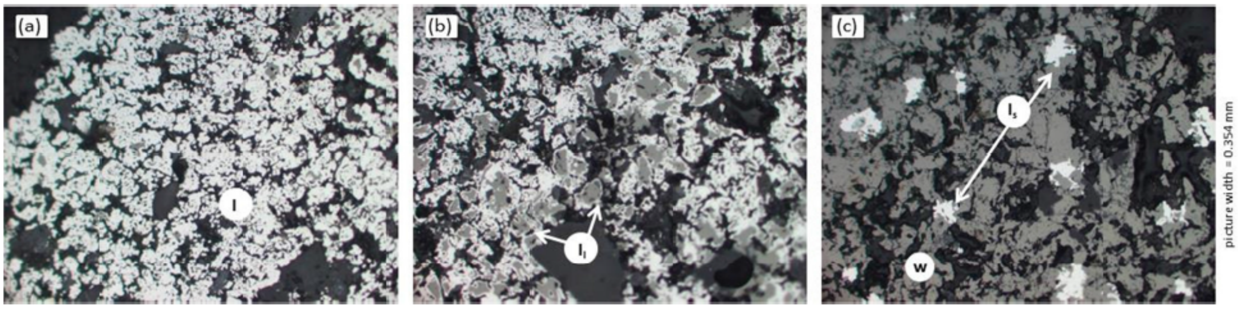
(a)
I
(b)
Il
(c)
Is
w
picture width = 0.354 mm

Figure 9-13: Different stages of metallic iron formation depending on the distance to the surface, outer edge (a) to core part (c), Hematitic ore, RD = ±80 %

Depending on the different microstructural phases and structures of the raw material, the reduction and the metallic iron formation will occur in different ways. It is the phase composition (the amount and distributions of slag phases and the porosity) that severely change the final outcome. In Figure 9-14 the described forms of metallic iron are shown in detail (light microscopic) pictures of the different iron ores investigated. Simultaneously the coherency of the different initial structures of the ore and the preferred metallic iron formation can be derived.

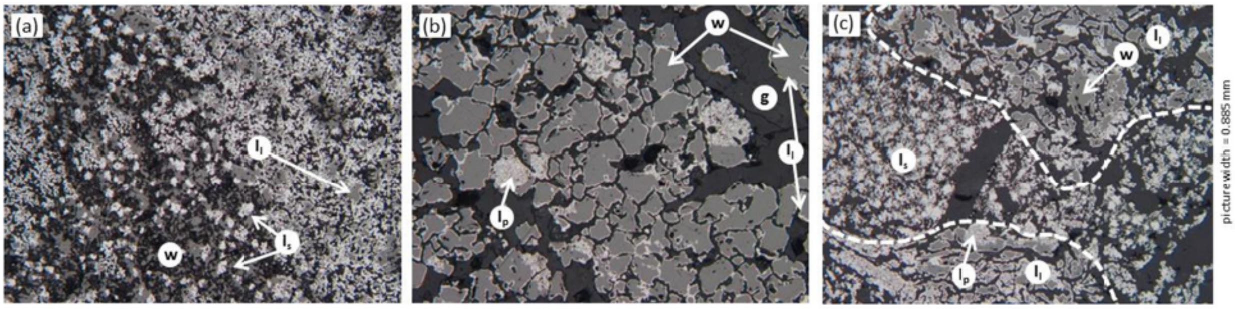

Figure 9-14: Different kinds of iron formation depending on the morphology of the raw ores RD = ±80 %

The materials have been reduced to some RD ±80 % at ISO conditions. It can be seen that within these finely detailed pictures, the variety of phenomena appearing is rather high. The picture on the left (a) gives the microstructure of the hematitic ore. As the reduction front moves further inside the particle, the former hematite and now wustite first forms iron scraps and subsequently metallic layers surrounding the grains are formed. These layers thicken until the whole structure has been transformed to metallic iron, comparable to Figure 9-13. The detailed picture (b) shows the microstructure of the magnetite ore and gives a very different picture. The coarse and dense former magnetite microstructure is intermediately reduced to dense wustite which is very hard to reduce; the nucleation of iron scraps is hardly apparent. The coarse grains are surrounded by thin but rather dense iron layers which hinder the diffusion of the gas. But at some random point the dense wustite is transformed to a very porous iron sponge (I_p), some grains within the picture are fully reduced to porous iron whereas others are only rimmed by a small layer. The difference in reducibility of limonitic and hematitic parts can be seen in picture (c). At the upper and lower positions, the boundaries between the former hematite and limonite parts are marked and the picture reveals that within the former hematite grains wustite is still present whereas the former limonitic part has been fully reduced to metallic iron. At some coarser grains even porous iron has formed; due to the finer grained and more porous microstructure of the limonite, these parts can form iron scraps more easily and hence are more rapidly reduced compared to the hematite structure.

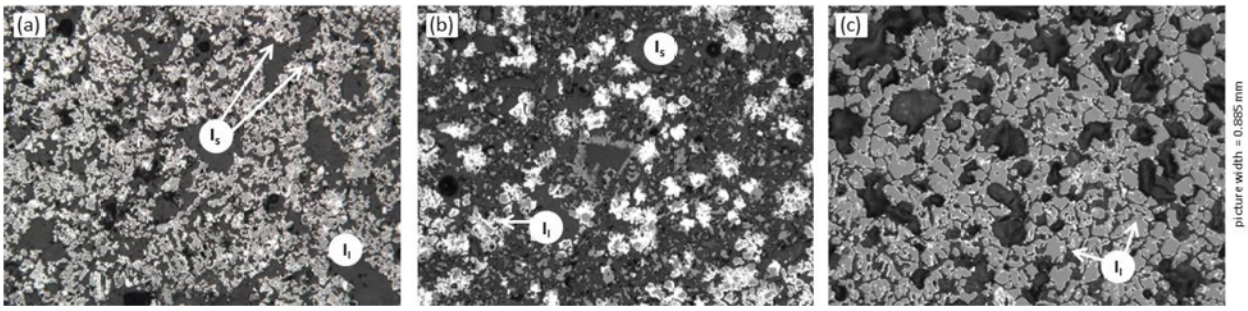

Figure 9-15: Different kinds of iron formation depending on the morphology of the raw pellets RD = ±80 %

The microscopic investigation of the reduced pellet samples showed a similar picture of the dependence of the metallic iron formation and the initial microstructure. The left picture (9-15a) shows Pellet Brand 1; the initially finer grained structure led to a finer distribution of iron scraps and subsequently smaller iron layers. The detailed picture of Brand 2 (b) shows a region with high gangue content, the scarcely existing wustite grains form coarser iron scraps. On the right side (c) the distinctly coarser hematite grains of Pellet Brand 3 led to the same effect as observed for the magnetitic ore: a slow reduction progress as a result of the dense wustite and iron layers and only scarcely occurring scraps.

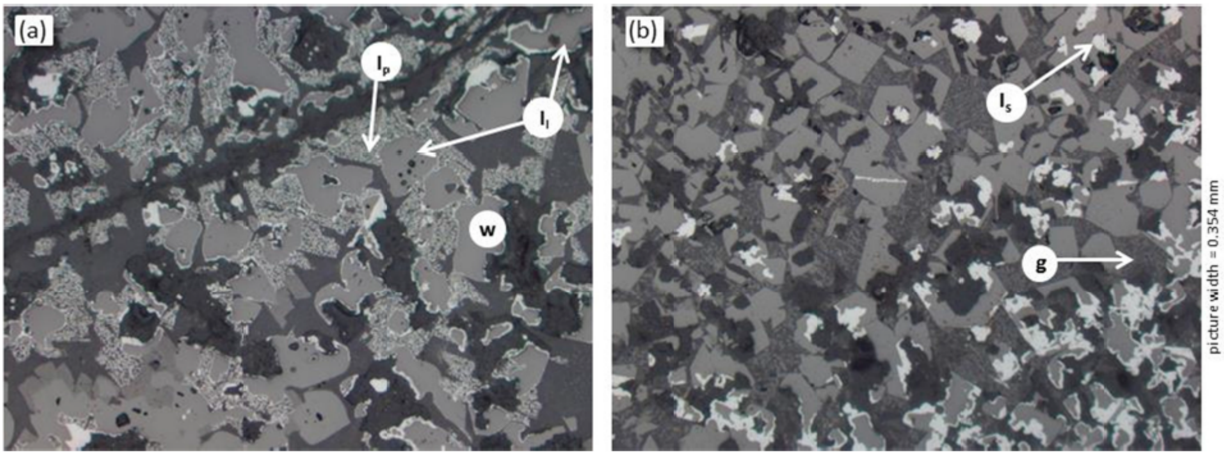

Figure 9-16: Different kinds of metallic iron formation depending on the initial phases within sinter

Finally, when looking at the numerous different phases within sinter structure, the different reducibility performance can easily be illustrated as given in Figure 9-16. In both pictures one of the main prevailing phases prior to reduction was spinel. This spinel has not been fully reduced to metallic iron yet, only small rims surrounding the wustite grains are apparent. At some parts at the right side of picture (b) iron scraps already exist and are coarsening. In the right picture another circumstance can be seen: the distinctly better reducibility of hematite as compared to magnetite.. In the very center of the picture there is a grain where there has been a secondary hematite lamella (partly oxidized magnetite lamella during the cooling phase). In contrast to the former magnetite grain, now wustite, this small lamella has already been fully transformed to metallic iron. The difference in reducibility between (former) spinel and calcioferrites is also apparent in these pictures. In the left picture the coarse wustite grains are about to start the formation of metallic iron, small layers of metallic iron prevail, whereas nearly all the former calcioferrites have already formed a very highly porous iron sponge. This indicates that calcioferrites enhance the overall reduction performance and therefore the presence of calcioferrites is definitely desirable.

9.6 Changes of Metallic Iron Formation – Effect of GOD and Hydrogen

Since the reducibility performance describes the ability of an iron oxide to release oxygen, it is directly interconnected with the formation of metallic iron within a microscopic scale. This means that the differences in reduction behaviour are associated with differences of the microstructural evolution during the reduction process. Within the different reducibility testing procedures the behavior of the iron oxides at different prevailing reducibility conditions could be shown. Thereby a strong correlation between reduction performance and the gas reduction potential as well as the hydrogen content of the gas could be shown.

One reason for the correlation of the decidedly weaker reduction performance at the higher GOD which is closer to the thermo dynamical equilibrium of wustite and metallic iron, is the difference in the kind of metallic iron formed. Figure 9-17 shows this special modification of metallic iron. At the inner parts of the Hematitic ore piece (a) metallic iron scraps and warts can be seen, appearing in the earlier stages of metallic iron formation as shown in the previous pictures. The difference is that unlike conditions at final GODs of 0-0.10, there is no start of the layerous iron formation visible even at the edges of the ore piece. The detailed picture (b) shows these special forms of iron, the fibrous iron formation. Thereby a diffusion of the iron molecules towards the peripheral zone occurs. There the iron forms thin and elongated structures, so called iron whiskers, which grow at the surface of the grains and pieces and further grow outwards by solid body diffusion. This is in contrast to the growth of metallic iron inwards to the core on the expanse of wustite as observed thus far. Nevertheless, this in good accordance with the literature (c.f. 4.3) and this growth due to the diffusion of single iron atoms explain the extremely retarded reduction progress at the lower gas reduction potential.

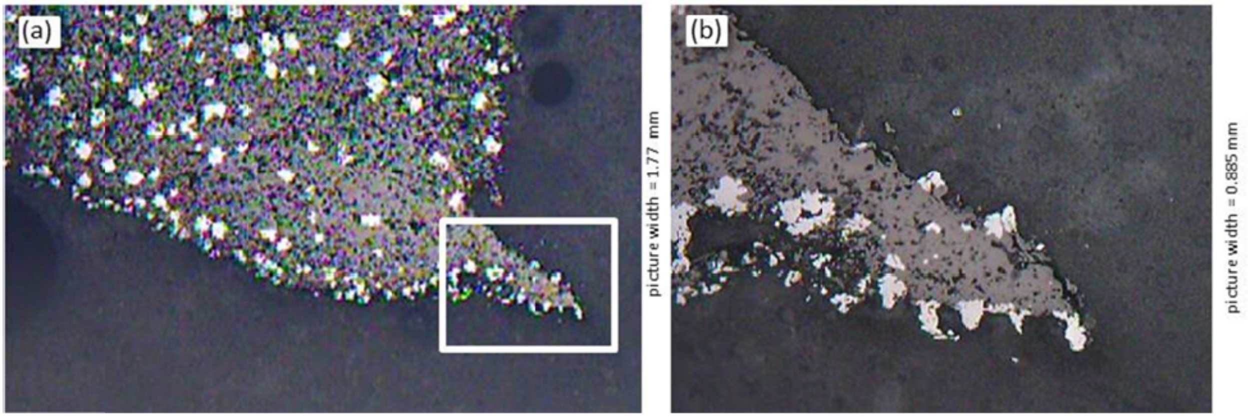

Figure 9-17: Formation of metallic iron whiskers at lower final GOD of 0.28, hematitic ore, RD = ± 37 %

As shown within all the different reducibility testing procedures, the presence of hydrogen enhances the progress of reduction in every case. This effect is also more comprehensible by taking a look at the microstructure and the difference in metallic iron formation. Figure 9-18 shows three reduction stages of a pellet at three different distances from the pellet surface. The upper row (a-c) refers to the reduction conditions BF1 (without any hydrogen) whereas the lower row (d-f) refers to the DR1 condition (25 % H_2 within the gas mixture). It can be seen that the types of metallic iron formed are exactly the same. Starting from iron scraps at the early stages, changing to metallic layers until finally all wustite has been transformed to iron.

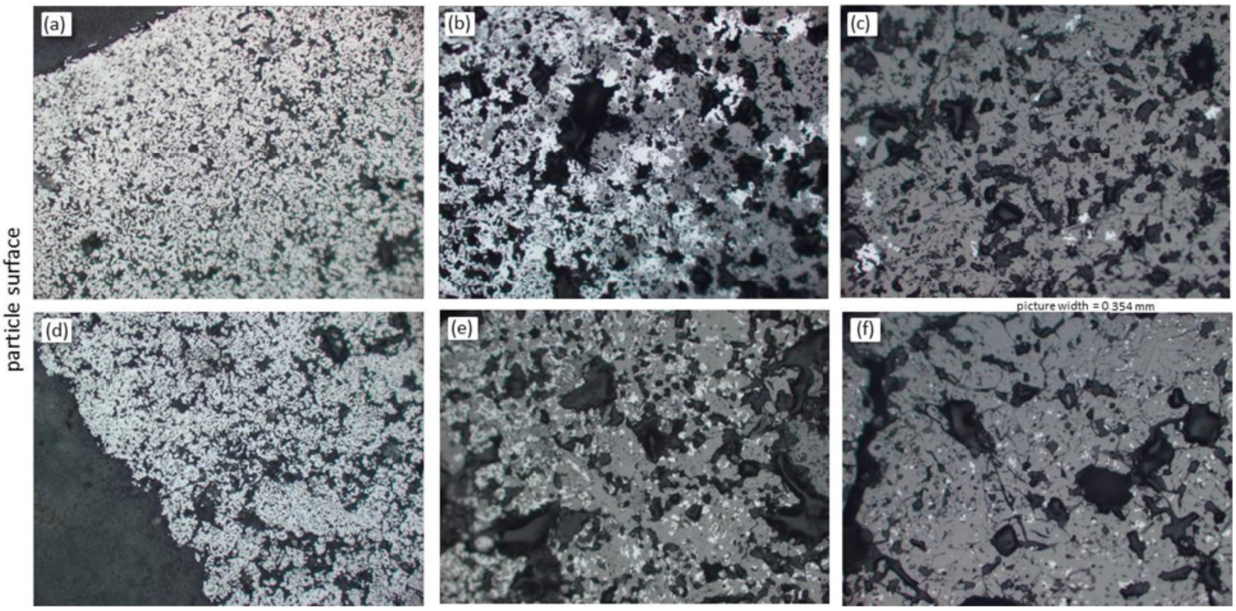

Figure 9-18: Different types of metallic iron formation depending on the surface distance, comparison between BF1 (a-c) and DR1 (d-f) testing conditions, Pellet Brand 1

However, the difference is the size and amount of iron scraps formed. On comparing pictures (c) and (f), the amount of already formed metallic iron is more or less the same but while in picture (c) there are only a few and coarse iron spots at random places, in picture (f) the iron scraps are small in size but are distributed more widely. This indicates that due to hydrogen the nucleation is forwarded.

As a result of the increased number of small iron scraps, each as a nucleus for the formation of iron layers on further reduction, the subsequently formed reduction products are finer and more finely distributed and due to diffusion kinetics, the overall reduction progress is enhanced.

Even though the magnetitic ore did not gain a reduction degree greater than 50 % during the DR1 testing condition there is a significant change in the metallic iron formation. On the left side (a) of Figure 9-19 iron layers surrounding almost every wustite grain can be seen. At some random point the formation of the porous iron starts and proceeds throughout the grain. In the right picture (b) the same initial structure of coarse and dense magnetite grains prevail, the iron layers appear as very thin ones. But on the left side of the picture two grains have fully transformed to porous iron and a third grain is about to be transformed. This shows that even at lower temperatures and despite the fact of inhibited kinetics the nucleation is enhanced by the presence of hydrogen.

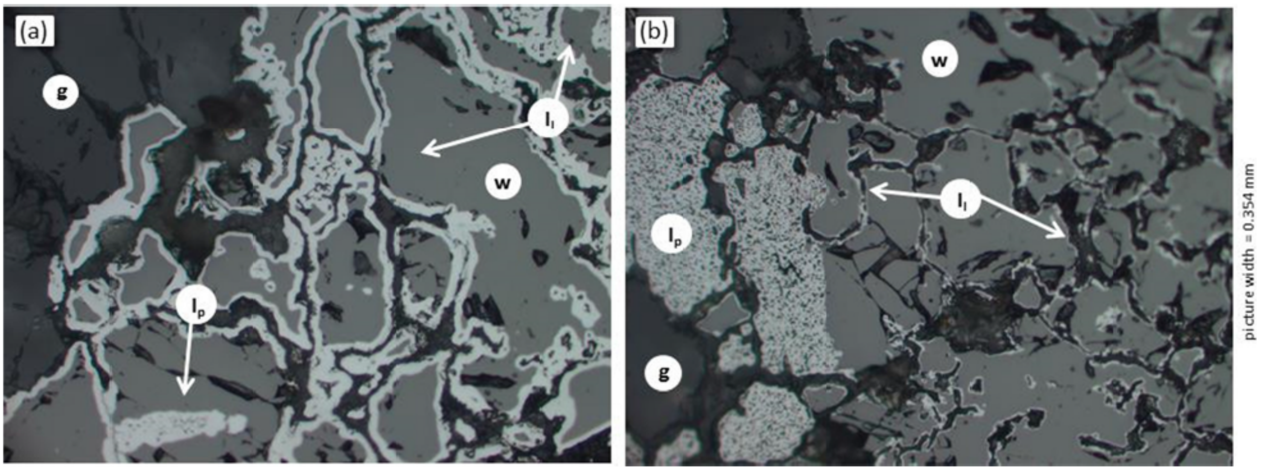

Figure 9-19: Magnetitic ore reduced at the absence of H_2 (left) and at DR1 conditions (25 % H_2, right)

9.7 Kinetic Interpretation of the Results

Although the different raw materials have been investigated with a variety of testing and investigation methods, the reduction performance as a whole is not yet fully understandable. As pointed out within the previous sections, it is the kinetics of the oxygen release from the crystal lattice that significantly influences the reduction performance of the materials. As an approach to getting a combined view of reduction behaviour and the raw material characteristics, the kinetic approach based on the assumption that the reduction proceeding according to the shrinking core model (c.f. 4.2.2) is adapted. In order to do so the reduction progress from the standardized testing procedure has been considered and (combined with the raw material characteristics (chemical analysis, B.E.T,…)) an attempt is made to define the rate determining step of the reduction process.

The three mechanisms that might be rate determining according to the different prescriptions in literature are the mass transport (gas diffusion), ash diffusion (pore diffusion) or chemical reaction (boundary layer reaction). In the case that one mechanism is so inhibited and the overall reaction is exclusively controlled by only one of these three mechanisms, the qualitative progression for each mechanism is given in Figure 9-20. This figure plots the reduction rate depending (dR/dt) versus the reduction progress (given as fractional reduction) during the whole process. This type of plotting gives an idea of the reduction rate at certain stages of the reduction but does not give any idea about the time that is needed to gain this certain stage of reduction. It is a time independent way of picturing the reduction progress.

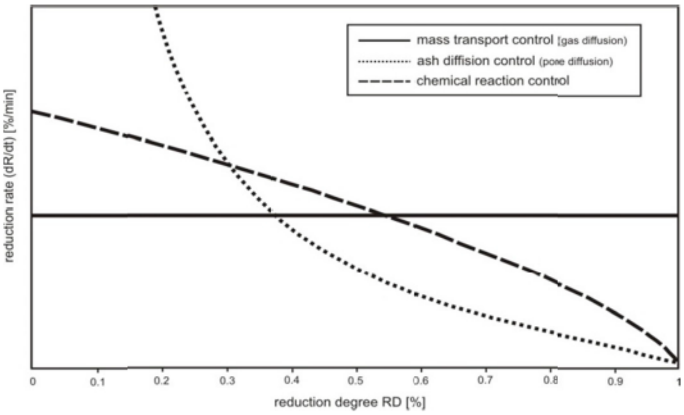

Figure 9-20: Qualitative progress of reduction rate for different rate determining steps [85]

This way of plotting the reduction progress has been adapted to the curves based on the ISO testing procedure. In order to do so the data for the reduction degree RD (corresponding to the reduction progress) and the reduction rate (dR/dt) (as a result of the first derivation of the reduction progress RD) are plotted against each other. The behaviour of the three different kinds of raw materials is broadly described separately but it will be shown that there are commonalities.

For the three iron ores investigated, diagrams given in the top row of Figure 9-21, it can be said that Hematitic and Magnetitic ore behave in a similar manner whereas the Limonitic ore shows a different progression. On considering the dark blue and grey curve in the right diagram it can be seen that the curves have an almost vertical linear shape; there is no peak at the early stages of reduction but only a flat decrease in reduction rate during the whole reduction procedure. This indicates that over the entire period of reduction there might be no change in the mechanism and the reduction progress is hardly influenced by either the reduction product formed (pore diffusion control) or the decrease in the reaction surface (chemical reaction control), or at least the influence is smaller than in the case of any other material.

In contrast to that, for the Limonitic ore (as well as all the other materials given) the curve can be divided into two stages of reduction (as marked as a black dotted line in the left column), the early stage up to some 30 % and the later stages until the end of reduction at > 80 %. For the shape of the curves of the pellet brands a distinction between early and later stages can also be seen, although a difference between the three brands is visible. The curves for Brands 1 and 3 have a very similar shape, only their levels are different (an almost constant higher value of about 0.6 %/min for Brand 1 during the whole process). At the first stages there is a more sharp decrease than at the final stages; however the kink of the curves is shifted to a slightly later stage of reduction compared to the Limonitic ore and the sinter samples. Especially Brand 3 has an almost constant level at the end, comparable to the Hematitic and Magnetitic ore. For Pellet Brand 2 there is an even more sharp decrease at the initial stages and after the dividing line at 30 % the decrease flattens but remains steeper.

All five sinter samples show very similar behaviour. The two stages of reduction can clearly be distinguished, a very steep decrease at the early stages and an absence of the total flattening at the later stages prevail.

On comparing the shape of the curves with the three curves from the extreme cases of rate determining steps, some trends can be derived but two circumstances have to be kept in mind. First, the diagrams in Figure 9-21 derive from lab testing of particles of a size range between 10-12.5 mm and not only single grains or ideal conditions. There are definitely some concentration profiles and inhomogeneities within every ore particle and furthermore the conditions within the reaction vessel are not perfectly homogeneous and therefore there will always be a mixture of the different mechanisms. Secondly, within the following descriptions only the final step of reduction, the transformation of wustite to metallic iron, is considered. Although, by means of morphological investigation of the materials behaviour during reduction (Figure 9-11) and different literature data [40,43,68] it can reasonably be assumed that it is this final step that is rate determining, the overall reaction from hematite to metallic iron may interfere in some way. It can be assumed that the transformation of hematite to magnetite and wustite at the initial stages (according to the definition up to 33 % RD) will at least contribute to the height of the reduction rate at the initial stages.

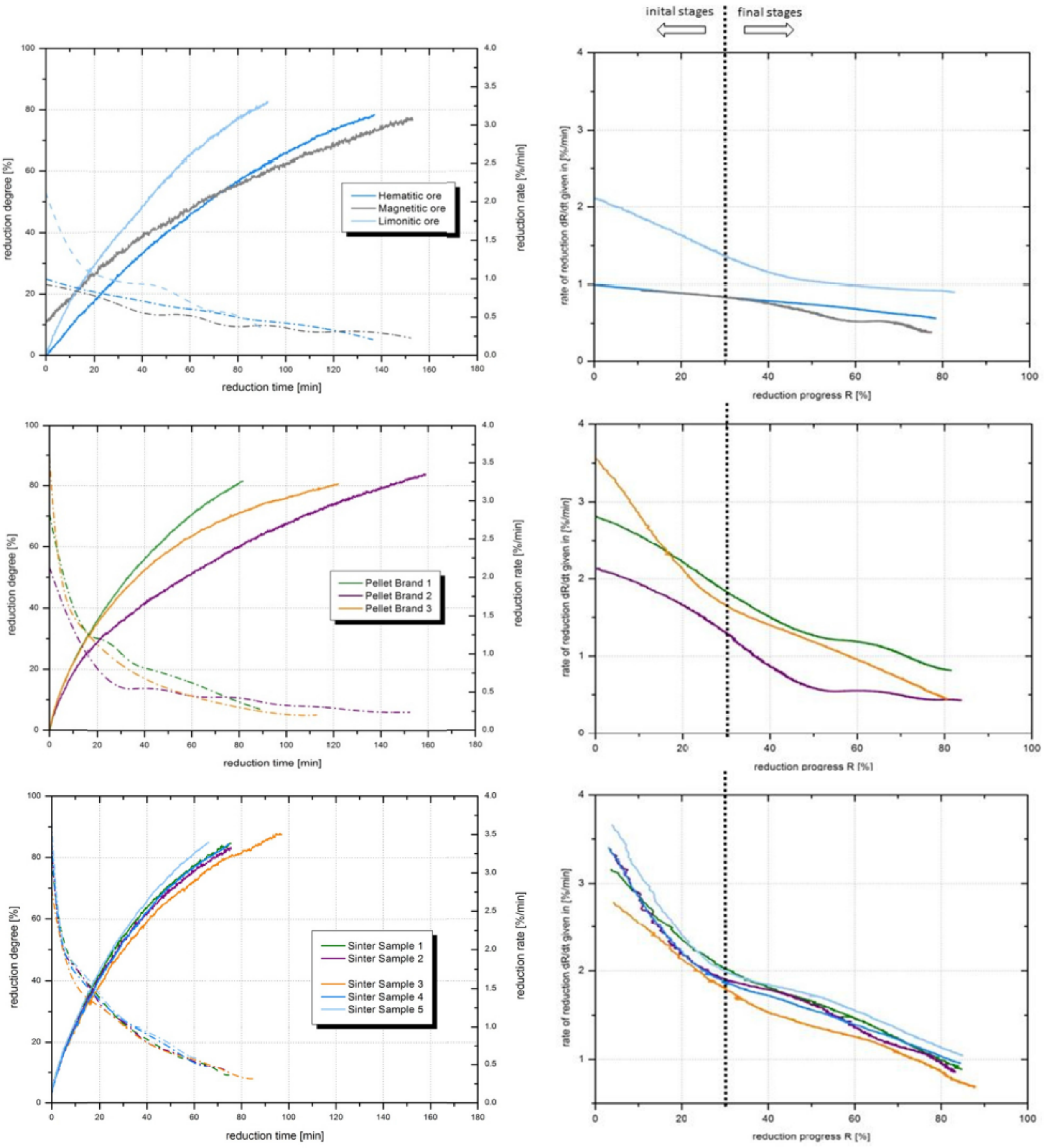

Figure 9-21: Reduction curves as a result of the standardized testing procedure (left column) and derived qualitative progress of reduction rate (right column) for iron ores (top row), pellet brands (intermediate) and sinter samples (bottom)

For those materials with a clear distinction between the two stages, the progress of reduction might proceed as follows. The slope of the initial stages lies somewhere between the dotted and dashed line in Figure 9-20 and hence is comparable with a mixture of reaction control and pore diffusion, but the shape is more associated with the reaction control curve. At this stage all the prevailing (wustite) grains are unreacted and the surface where the chemical reaction takes place is not covered with any product layer so that the rate determining step is the removal of the oxygen. Due to the coarse size of the particles, some resistance for pore diffusion will always exist, also at the very initial stages, but the main rate determining step is the boundary reaction. At the later stages, where the product layer of metallic iron gets increasingly thicker, the shape of the curves tends to approximate the gas diffusion mechanism. Although at chemical reaction control the reduction rate gets lower during the ongoing reduction procedure due to the smaller prevailing reaction surface, it is the ash layer that obviously has a greater effect as can be seen in the flattening of the curves at the final stages in Figure 9-21.

To some extent the Hematitic and Magnetitic ores act differently and the course of reduction can therefore be interpreted in a different way. The curves seem to lean towards the mass transport control regime, especially at the early stages. This stands in contrast to the common opinion that indicates that only on considering fluidized bed reactors is the mass transport one major controlling step.

On combining these results with the (macroscopic view of) porosity of the materials, the following statements can be derived. All the investigated pellet brands and sinter samples show a high porosity concerning macropores. Every piece of sinter and every single pellet consists of large and mostly connected pores that can be seen with the naked eye (hence without any microscopic magnification). For the Limonitic ore it can be assumed that due to the release of the crystal water on heating the cracks initiated also form a connected network of pores and cracks. In contrast, the Hematitic and Magnetitic ore do not have any larger pores; the Hematitic consists of numerous but very small pores and the Magnetitic ore has hardly any porosity at all. This might be one reason for the different reduction behaviour or path of reduction. Via the larger, connected pores the reducing gas can more easily enter the inner parts of the raw material particles and the length of the (pore) diffusion way is distinctly shorter. In that case the gas diffusion resistance is negligible and the subsequent reduction is controlled by a mixture of pore diffusion control and boundary reaction control. For the dense ores (or at least ores with no connected porosity), the mass transport of the gas might have more influence and at least affects the rate controlling regime. It can definitely be noted that there are two different stages and furthermore on describing the reduction reaction, it is reasonable to differentiate between the early and the later stages of reduction at least for porous materials.

10 Conclusion and Outlook

Within this research work, a variety of iron bearing raw materials was investigated by diverse ways and means. For the sake of characterizing the overall performance of a raw material at industrial scale conditions, not only the reduction behaviour but also the mechanical performance were tested. As a starting point and in order to gain an idea about material's behaviour, tests were performed according to a standardized testing procedure. From that testing procedure, different modifications concerning gas composition and hydrogen content were derived and finally reducibility tests at near industrial scale conditions were performed. These conditions, related to blast furnace and direct reduction facilities, included testing by means of time dependent gas and temperature profiles at different final temperatures and gas compositions. Contemporaneously, the development of the mechanical stability was investigated by means of a tumbling test. All these tests revealed a picture of the material's behaviour at the different conditions and led to a recommendation of their use within the different industrial scale iron making process routes. At least to some extent, these results stand in contradiction to the industries´ state of the art lab scale testing procedures, which are comprised of only very simple testing procedures.

What is of additional major interest concerning the usage of various raw materials is the possibility to predict the material´s behaviour by characterizing only their raw material morphology and mineralogy. Different attempts have been made in the past but nevertheless an overall analogy of the reducibility performance and the mechanical stability to the mineralogy (hence the chemical analysis) and the morphology (form and shape of the different prevailing phases) is not easy to depict. A multitude of effecting parameters has to be collectively considered. It could be revealed that, whereas for naturally occurring phases and structures a prediction can be made more easily and precisely, the numerous artificially created phases, especially during sintering, made a prediction difficult.

10.1 Applicability of the materials in industrial scale processes

It total 11 different materials were investigated. The following sections give a summary and interpretation of the three different categories of raw material; ores, pellets and sinters.

- Iron ores

The three different ores are comprised of one representative of Hematitic, Magnetitic and Limonite-containing (mixture of hematite and limonite) ore. It has to be noted that Magnetitic ore in the form of lumps has only minor importance in industrial scale applications but nevertheless it gives a good outline of the behaviour of a pure magnetite microstructure.

All the iron ores investigated meet the requirements concerning chemical analysis for blast furnace applicability at least to some extent. Every ore has a sufficient iron content of > 60 %, only the gangue content of the Magnetitic ore is comparable high. The requirement of a minimum iron content of 67 % for DR facilities could not be fulfilled, and the restricted gangue amount means that not all the ores are suitable. The mechanical testing of the raw ores gave good values, although the values for tumbling and abrasion index cannot be directly compared (due to a different tumbling procedure). All ores showed a disintegration tendency (DT) value of > 90 % with only a small portion of fines, which is also sufficient for DR grade requirements.

The metallurgical properties of the ores, mainly the reducibility performance, differed in a wide range depending on the testing procedure. At the testing according to the ISO standard, the results indicate that the Limonitic ore is the most reducible, the Hematitic is medium and the Magnetitic is least reducible. The difference between the ores is quite high and, with a reduction rate of 0.67 %/min for Hematite and 0.51 for Magnetite, only the Limonitic ore barely fulfils the criterion for ores for BF which is > 1.0 %/min. The even higher values for DR facilities are definitely not fulfilled. All these facts indicate that according to most operational industry data the ores investigated are not very preferable.

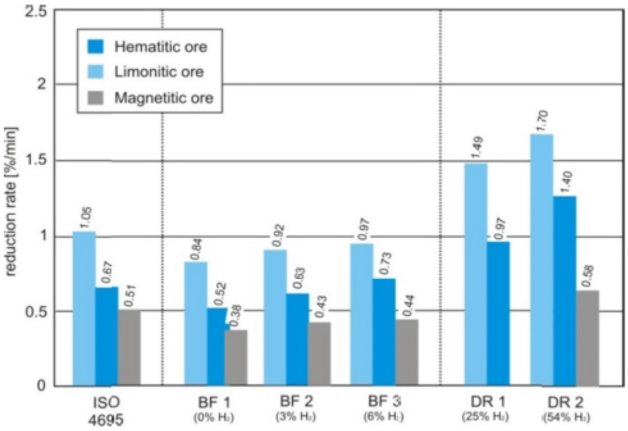

Figure 10-1: Comparison of the reduction performance $(dR/dt)_{40}$ of the investigated iron ores

The testing according to the industrial scale process conditions revealed different facts. For a comparison of all testing results, a graphical comparison of the results for $(dR/dt)_{40}$ is plotted separately in Figure 10-1 for every different testing condition. The testing conditions are in turn ranked by the hydrogen content of the gas mixture, and additionally the values of the standard tests are given (left side). It can be seen that in every test the Limonitic ore is best reducible, to some extent the enhancement of the reduction rate for all ores increases linearly with increasing hydrogen amount. Also the difference in height between the ores stays more or less the same. This indicates that whenever an ore is characterized as better reducible compared to another, this sequence will remain the same for every different testing procedure.

Concerning Hematite and Limonite, the material strength after reduction (although not comparable to the standardized RDI values) indicated a proper mechanical behaviour for all reduction conditions with a final temperature of 950 °C. The DR conditions with the lower temperature and associated higher reduction rates led to a decrease of stability, especially the limonitic ore´s disintegration resistance decreased. The Magnetitic ore showed a decrease at BF conditions comparable to the Hematitic ore to some 87 % DT but at DR conditions the ore almost totally crumbled with a fines formation of > 30 %, which again makes ore not very preferable.

In summary, it can be said that not all ores investigated are particularly suitable for industrial scale processes. The Limonitic ore shows good reduction properties, but is weak concerning mechanical stability whereas the Hematitic ore reduces rather slowly with good mechanical properties. The Magnetitic ore is not suitable for industrial scale in any way. These observations stand in good accordance to the literature data, ores are generally not known as to be very susceptible to disintegration compared to sinter [76,73,142] and hematite is better reducible than magnetite [40].

- Pellet Brands

The investigation of three different pellet brands produced and used on an industrial scale partly revealed contradictory results.

Strictly speaking, on comparing the chemical requirements, none of the pellet brands can be used at DR facilities due to the insufficient iron content combined with too high a level of slag amount. The resistance to abrasion and disintegration during the tumbling procedure for the raw pellets is very high (< 95 %), which might be a result of both a sufficient burning process and the higher amount of binding phases.

As shown in Figure 10-2 the metallurgical properties indicate a different reduction performance for either ISO standard conditions or industrial scale conditions. In particular Pellet Brand 2 showed minor reduction performance at the standard test with only a $(dR/dt)_{40}$ of 0.60 %/min. Brands 1 and 3 have higher rates and a level of 0.90 (Brand 3) and 1.14 (Brand 1), on the basis of this result those pellets would definitely be described as suitable for BF use. As a reason for the retarded reduction progress of Brand 2 the distinctly higher silica content (almost three times higher than the other brands) can be assumed since it is known that silica containing glass phases are least reducible [85,139]. On further considering the industrial scale process conditions, the sequence of the evaluation of the brands has to be corrected. Almost every testing condition led to a higher level of the reduction rate for Brand 2 compared to Brand 3. Only Brand 1 is best reducible at every testing condition. In this case it could be shown that the assessment according to the ISO standard test does not always give the right assessment of the material´s behaviour at industrial scale applications. On considering the morphological structure of the Pellet Brands, the results of the industrial scale conditions are rather easily explicable. Brand 1 has a porous structure of fine grained hematite crystals with not too high an amount of gangue material and can be assumed as good reducible. Brand 2 consists of almost the same fine hematite grains but nevertheless the higher silica and gangue amount (and hence its very low basicity of 0.08) makes the reducibility lower. Finally Brand 3 has the same low amount of silica and binding phases and associated higher basicity, but on considering the distinctly coarser hematite crystal size, the retarded reduction progress is traceable, especially the retarded reduction reaction at the lower temperatures as for DR1 conditions.

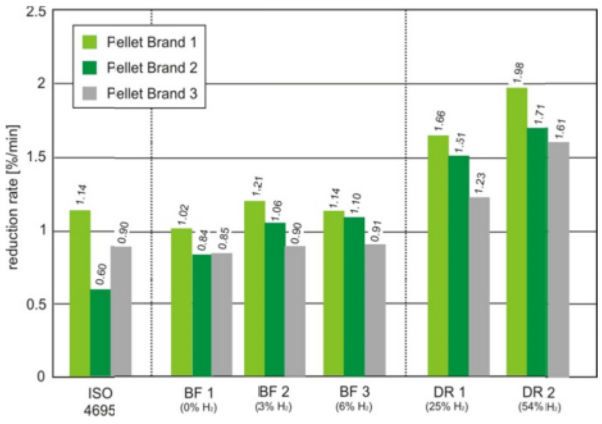

Figure 10-2: Reduction performance $(dR/dt)_{40}$ of the investigated pellet brands

The mechanical testing of the pellets after the different reduction procedures showed that Pellet Brands 1 and 3 could withstand every reducing condition; hence gas composition, temperature and reduction rate. Although there is a little decrease in stability for Brand 1 after the direct reduction testing procedures (fast reduction rate and lower temperatures), nevertheless these two brands can be described as more than sufficient. Brand 2 showed partly minor stability, at some testing conditions the disintegration tendency values became < 70 % with hardly any fines formation (less than 2 %). On considering the testing results in literature especially the high mechanical resistance to disintegration is known [142] whereas pellets are assumed to have a higher amount of smaller pores but a lower overall porosity at the time compared to sinter [79,125,126]. The morphology of the investigated Pellet Brands showed concerning porosity differences compared to ores in terms of a higher overall porosity but especially in terms of larger pores. This might be one of the key factors why all Brands are more rapidly reducible than the Hematitic ore.

- Sinter Samples

Concerning the description of the behavior of sinter samples at industrial scale testing conditions, only the two industrial scale produced samples were investigated further. Nevertheless, the reduction testing at the standard for all sinter samples could reveal tendencies of the reduction performance depending on the basicity and the overall slag amount as given in Figure 10-3. It can be seen that within the range of sinter basicity tested, there is a minimum of reduction performance at a basicity of around 1.6. This is in good accordance with the literature review (c.f. 5.1.6 and Figure 5-11) where a minimum reducibility of 1.6 is also given [139]. And a further increase in reducibility from 1.6 has also been reported [129]. Between the overall amount of slag forming oxides and the reduction performance, the correlation is almost linear as shown in the left diagram; the more slag forming oxides the lower the reduction rate. It can be assumed that with the increase of slag amount, the portion of phases having low reducibility will increase and the overall reduction performance will decrease.

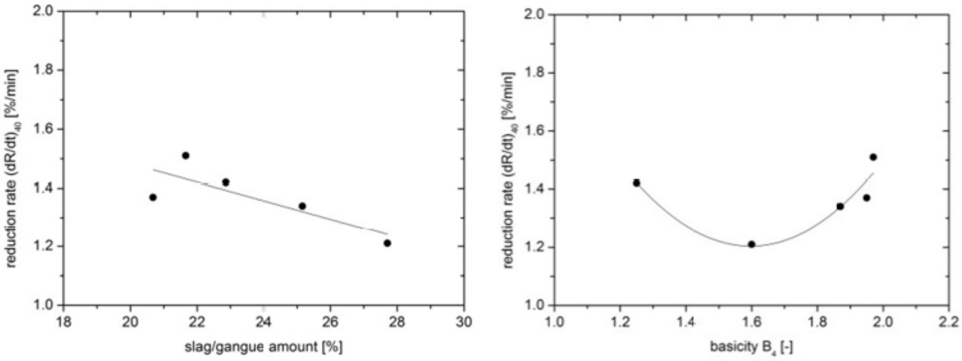

Figure 10-3: Correlation between slag amount (left) and basicity (right) and the reduction rate of the investigated Sinter Samples

All the sinter samples investigated showed a superior reduction performance at every testing procedure compared to the other materials. Notwithstanding this, the ISO standardized testing conditions revealed values for $(dR/dt)_{40}$ at levels (1.42 for Sample 1 and 1.34 for Sample 2) that means that these two samples are not sufficiently suitable for industrial blast furnace use; desirable values for $(dR/dt)_{40}$ are described from 1.4 – 1.8 %/min [10,57].

Since sinter is generally neither designed nor intended for use in any direct reduction facility, the testing at DR testing conditions was not of industrial scale interest, but it did succeed in giving an idea of how hydrogen containing conditions and lower temperatures influence the reduction behavior. The different reduction procedures enhanced the reduction rate; a continuous increase from BF1 to DR2 can be seen especially for Sinter 2.

Again it can be seen from the different testing procedures that the reduction proceeds more rapidly at direct reduction conditions compared to BF conditions. It is the distinctly higher hydrogen amount in the gas phase that enhances the release of oxygen more than the lower temperatures can impede it (the same as for the other materials with the exception of the Magnetitic ore). Nevertheless, small amounts of hydrogen (in this investigation 3 %) can also enhance the overall performance to a not negligible extent. The interesting thing is that a further increase up to 6 % H_2 does not lead to a further increase.

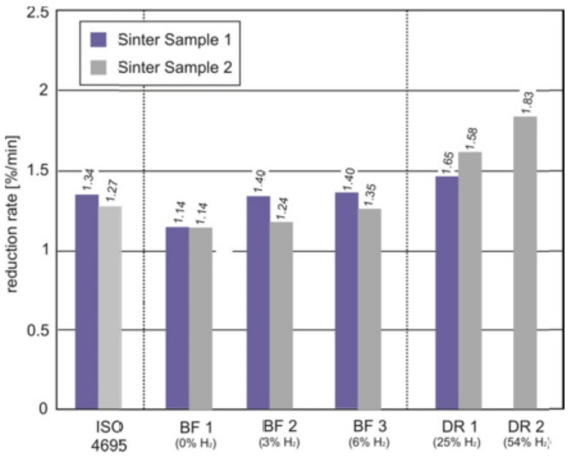

Figure 10-4: Reduction performance $(dR/dt)_{40}$ of Sinter Sample 1 and 2

On considering the mechanical properties, sinter has by far the most adverse properties. Every industrial scale testing condition (due to the temperature within the critical temperature range of 500-600 °C) led to a severe tendency of disintegration; Sinter Sample 1 (range for $DT_{+6.3}$ between 38-45 %) even more than Sample 2 ($DT_{+6.3}$ 54 – 65 %). On comparing these results with the diagram given on the right of Figure 5-15 in section 5.2.4, this can be perfectly explained with the basicity of the two samples. Sinter 1 with a basicity of 1.25 is located at the shown minimum of mechanical performance, whereas at the basicity values of Sample 2 (B_4 of 1.87) the disintegration tendency increases again. As a reason for that, the better mechanical stability of the calico-ferrite and spinel phases is given [80,139–141].

As a summary of all the investigation, two different statements can be derived from the comparison between ISO tests and industrial scale testing conditions. First, with the exception of one pellet brand, some correlation in the sequence of the different materials concerning reducibility performance can be given. Good and rapidly reducible materials at ISO conditions will show a good performance at industrial scale conditions and vice versa. Although the correlation is not particularly linear, there is a correlation between the different results. Nevertheless, a more precise prediction of the behavior at the different conditions cannot be given. From the knowledge of $(dR/dt)_{40}$ at ISO conditions, no value can be derived for DR1 condition from that. Only its tendency could be shown.

On the other hand some general valid statements concerning the conditions related to the industrial scale process can be given. There is a distinct enhancing effect of hydrogen within the gas mixture but again not in a linear way. Every test result of the blast furnace conditions showed an accelerated effect by adding 3 % hydrogen but in turn a further increase up to 6 % did not have the same noticeable effect: only a very small further enhancement was measured. On comparing the DR testing conditions, the lower temperature additionally has to be taken into account but there is again an increased reduction performance.

In general, however, it could be revealed that the more reducible a material behaves at conditions without any hydrogen (ISO, BF), the less impact in terms of accelerated reduction velocity can be observed at conditions with higher hydrogen content.

These facts make it obvious that despite the multitude of reduction tests, it is still only possible ti give a qualitative tendency, not a quantitative prediction of a material's behavior at different conditions.

10.2 Outlook

All these investigation results; the literature review, the testing of the raw material properties, the reducibility performance at standardized conditions as well as at conditions related to industrial scale, the testing of the mechanical properties and finally the morphological evolution during reduction revealed the different behaviour of various materials and structures and ultimately led to a characterization of their applicability for different reduction routes.

Building on this, the upcoming research activities are dedicated towards a prediction of the behaviour of a raw material without doing costly and time-consuming lab scale reducibility testing. Therefore, in order to assess the tendency of the reduction behaviour, it will only be necessary to characterize the microstructure by means of light microscopic investigation of fabricated polished sections and/or by means of chemical analysis combined with specific surface area measurement. Although within this investigation various aspects of the correlation between microstructure, chemistry and mineralogy could be illuminated, there are still issues that are not yet fully understood. However, the investigation within this research work, combined with literature data, provided a basis for further research activities concerning:

- The influence of the initial *structural type*. It could be shown that limonite, due to its fine crystalline structure, is the best reducible material, hematite the second best and finally magnetite the third best (due to its dense and coarse structure). Hence, the behaviour of naturally occurring iron minerals with only a low amount of gangue material can already be sufficiently predicted. The reducibility behaviour of pellets, which more or less consist of hematite grains and are assumed to reduce in a similar way, is most likely influenced by slag phases and their distribution and hence more difficult to predict. Sinter samples consist of a broad range of different phases and structures, which are all reducible to a different extent. Even the same structural type (magnetite or calcioferrites for example) acts differently depending on the exact chemical composition. These facts have to be taken into account in a more sophisticated way.
- Since it is known from the kinetic point of view that increased *porosity* provides more surface area for the chemical reaction and *larger pores* enhance mass transport both via gas diffusion and pore diffusion, porosity is a major factor influencing reducibility. However, the exact measurement of porosity still represents a problem. Within this work an attempt was made to measure the specific surface area by means of B.E.T and it could be shown that this is affected by uncertainties. No distinction between micro and macro pores or between closed pores and a coherent pore network was possible and therefore a suitable testing procedure is necessary to gain significant and comparable results.
- G*angue* and *slag amount and distribution* also need to be characterized in a better way. Slag phases comprising of silicates are very hard to reduce (mostly originating from acidic and silica rich nature of the gangue within the ores) and aluminium rich phases are also assumed to influence the reduction behaviour in a negative way.
- Since the *mechanical performance* of the raw material is of extreme importance – especially concerning the low temperature disintegration behaviour of sinter samples – the influence of the chemical and mineralogical composition on the mechanical stability needs to be investigated further.
- As a limiting factor for the testing and investigation procedures, all series of trials were performed at temperatures below 1000 °C in order to avoid liquid phases and also due to the restrictions of the lab scale testing equipment. This temperature range represents the region where gaseous reduction occurs, but no melting or dripping is supposed to take place. Nevertheless, this represents a temperature range where *sticking and/or swelling* might occur.
- There are still factors that influence the overall performance of the materials that cannot be avoided and eliminated. As an example *the presence of alkalis* is assumed to greatly influence the reduction behaviour as well as the mechanical performance, therefore this influence needs to be investigated and depicted.

Nevertheless, this investigation of the materials' behaviour concerning reducibility and mechanical stability, combined with the morphological and structural characterization gave an impression of the different aspects of the raw materials. The lab scale testing of selected representatives of ores, pellets and sinters in accordance with industrial scale process conditions could further reveal the evolution of the reduction progress. The test results achieved indicate that a generally valid correlation between the raw material structure, the standardized testing results and the industrial scale testing procedures is not easy to determine.

Based on the results of this research work, further research activities have been planned or have already been executed. At the Chair of Geology, an automated characterization tool for iron ores (fine ore as well as lumpy) has been developed and is about to be further improved for characterizing pellets and sinters. Therefore special algorithms and programming steps for implementing the materials' porosity and pore size distribution and subsequently the different structural phases and quantitative phase distribution are in the final phase.

Furthermore, at the Chair of Ferrous Metallurgy, the topic of the influence of alkalis is being examined. Tests modelled on the testing procedures developed, as described within this thesis, could show the weakening of the mechanical performance at the presence of alkalis with simultaneous increase in reducibility.

11 References

[1] worldsteel Association: World Steel in Figures 2013, http://www.worldsteel.org/, downloaded: 13th Nov. 2013.

[2] MIDREX - World Direct Reduction Statistics (2012).

[3] Schenk, J.L.: Vorlesungsskriptum zu Eisen- & Stahlmetallurgie I, Montanuniversität Leoben, Chair of Metallurgy (2009).

[4] Lüngen, H.B., M. Peters and P. Schmöle: Eisenerzeugung, Stahl und Eisen 130 (2010), 4, 36–64.

[5] Schenk, J.: Reduktionstechnologie, in: Eisen- und Stahlmetallurgie I (2011), 5/35.

[6] Schenk, J.: Hochofentechnologie, in: Eisen- und Stahlmetallurgie I (2011), 5/77.

[7] Gudenau, H.W.: Eisenhüttenmännische Verfahrenstechnik - Vom Erz zum Stahl, Druck- & Verlagshaus Mainz GmbH, Aachen, Germany (1989).

[8] Biswas, A.K.: Principles of blast furnace ironmaking: Theory and practice, Cootha, Brisbane, Australia (1981).

[9] Feinman, J. and D. Mac Rae (Eds.): Direct Reduced Iron: Technology and Economics of Production and Use, The Iron & Steel Society (1999).

[10] Feinman, J.: Direct Reduction and Smelting Processes, in: D.H. Wakelin (Ed.), The making, shaping and treating of steel, 11th ed. (1999), 741–780.

[11] Schenk, J.L.: Recent status of fluidized bed technologies for producing iron input material for steelmaking, Particuology 9 (2011), 14–23.

[12] Kommission der Europäischen Gemeinschaften (Ed.): Direktreduktion von Eisenerz: Eine bibliographische Studie, Verlag Stahleisen, Düsseldorf (1976).

[13] Gudenau, H.W.: Direktreduktion, Institut für Eisenhüttenkunde, Metallurgie von Eisen und Stahl der Rheinisch-Westfälischen Technischen Hochschule Aachen, Aachen (1997).

[14] Gudenau, H.W., K. Mavrommatis and A. Babich: Blastfurnaceprocess, Aachen, Germany (2002).

[15] Babich, A., D. Senk, H.W. Gudenau and K. Mavrommatis: Ironmaking, Wissenschaftsverlag Mainz, Aachen (2008).

[16] Wallace, J.P. *et al.*: The Blast Furnace Facility and Equipment, in: D.H. Wakelin (Ed.), The making, shaping and treating of steel, 11th ed. (1999), 643–698.

[17] Verein Deutscher Eisenhüttenleute: Grundlagen des Hochofenverfahrens, Physikalisch-chemische und physikalische Zusammenhänge, Verlag Stahleisen M.B.H, Düsseldorf (1973).

[18] Cheeley, R.: Gasification and the MIDREX Direct Reduction Process, Direct from Midrex 2nd Quarter (2009), 8–11.

[19] Steffen, R.: Direct reduction and smelting reduction - an overview, Steel Res. 60 (1989) 3-4, 96–103.

[20] Elliott, A. and J. Kopfle: New Development in the MIDREX Direct Reduction Process.

[21] Garza, C.: HYL Direct Reduction, Millenium Steel - Raw Materials and Ironmaking (2006), 43–45.

[22] Schenk, J.L. *et al.*: Development and Future Potential of the FINEX-Process, 2nd International Congress on Science and Technology of Ironmaking and 57th Ironmaking Conference, Toronto, Canada (1997), 1549-1557.

[23] Lüngen, H.B., K. Knop and R. Steffen: State of the art of the direct reduction and smelting reduction processes, Stahl und Eisen 126 (2006), 7, 25–40.

[24] Steinmetz, E., R. Steffen and R. Thielmann: Stand und Entwicklung der Verfahren zur Direktreduktion und Schmelzreduktion von Eisenerzen, Stahl und Eisen 106 (1986), 9, 421–429.

[25] Kepplinger, W.L.: Actual state of smelting-reduction processes in ironmaking, Stahl und Eisen 129 (2009), 7, 43–51.

[26] Tanaka, H. *et al.*: FASTMET - Waste Recycling at Kakogawa and Hirohata, Direct from Midrex 4th Quarter (2000), 9–10.

[27] Tanaka, H., K. Miyagawa and T. Harada: FASTMET, FASTMELT and ITmk3: Development of New Coal-based Ironmaking Processes, Direct from Midrex (2008), 8–13.

[28] Tanaka, H., T. Harada and H. Sugitatsu: FASTMELT - Process for a Sustainable Steel Industry in Asia, SEAISI, Bangkok, Thailand (2003).

[29] Prattes, W.U.: Die technologische Entwicklung des COREX-Verfahrens, Masterarbeit, Institut für Verfahrenstechnik des industriellen Umweltschutzes, Montanuniversität Leoben (2002).

[30] Grill, W., C. Böhm, K. Wieder and U. Schmidt: COREX/FINEX - Prepared for present and future ironmaking challenges, Siemens VAI Metals Symposium (2009).

[31] Thaler, C.: Entwicklung eines Massen- und Energiebilanzierungsmodells für den FINEX®-Prozess, Masterarbeit, Lehrstuhl für Metallurgie, Montanuniversität Leoben (2011).

[32] Joo, S. *et al.*: FINEX: a new process for production of hot metal from fine ore and coal, Scandinavian Journal of Metallurgy 28 (1999), 4, 178–183.

[33] Rio Tinto: HIsmelt Sustainable Development, Report (2007).

[34] Goldsworthy, T. and S. Gull: HIsmelt - The new Technology for Iron Production, SEAISI, Improvement of Product Quality and Environmental Control by the Utilization of Advanced Technologies in the Iron and Steel Industry (2002).

[35] Cavaliere, P. and A. Perrone: Optimization of Blast Furnace Productivity Coupled with CO_2 Emissions Reduction, Steel Research International 84 (2013).

[36] Carpenter, A.M.: Use of PCI in the blast furnace, IEA Coal Research, Clean Coal Centre, London (2006).

[37] Gostenin, V.A. *et al.*: Improving Blast-Furnace Operation by Optimizing the Natural-Gas and Oxygen Consumption, Steel in Translation 42 (2012), 2, 131–135.

[38] Anishchenko, S.A., D.Y. Fedorenko and V.P. Kravchenko: Influence of Technological Parameters on Blast-Furnace Productivity, Steel in Translation 41 (2011), 12, 999–1005.

[39] Wagner, D., O. Devisme, F. Patisson and D. Ablitzer (Eds.): A laboratory study of the reduction of iron oxides by hydrogen, Proceedings of the Sohn International Symposium, San Diego, (2006), 111-120.

[40] Edström, J.O.: The Mechanism of Reduction of Iron Oxides, Journal of the Iron and Steel Institute (1953), 289–304.

[41] Piotrowski, K. *et al.*: Simultaneous influence of gas mixture composition and process temperature on Fe_2O_3-FeO reduction kinetics: neural network modeling, Brazilian Journal of Chemical Engineering 22 (2005), 3, 419–432.

[42] Piotrowski, K. *et al.*: Effect of gas composition on the kinetics of iron oxide reduction in a hydrogen production process, International Journal of Hydrogen Energy 30 (2005), 15, 1543–1554.

[43] Hofbauer, H. *et al.:* Grundsatzuntersuchung zur Wirbelschichtreduktion von Feinerzen, Final Report, Technische Universität Wien, Institut für Verfahrens-, Brennstoff- und Umwelttechnik (2001).

[44] Harste, K. and H.B. Lüngen: Steel production under economic extremes, Stahl und Eisen 130 (2010), 8, 45–54.

[45] Siemens VAI Metals Technologies: Oral Communication, Franz Hauzenberger (2013).

[46] Stahlinstitut VDEh: Jahrbuch Stahl 2012 (2012).

[47] Poveromo, J.J.: Iron Ores, in: D.H. Wakelin (Ed.), The making, shaping and treating of steel, 11th ed. (1999), 547–642.

[48] Bogdandy, L. von and H.-J. Engell: The reduction of iron ores, Stahleisen, Düsseldorf (1971).

[49] Szekely, J., J.W. Evans and H.Y. Sohn: Gas-Solid Reactions, Academic Press, New York (1976).

[50] voestalpine Donawitz: Interne Betriebsdaten.

[51] Srivastava, U., S.K. Kawatra and T.C. Eisele: Study of Organic and Inorganic Binders on Strength of Iron Oxide Pellets, Metall and Materi Trans B 44 (2013), 4, 1000–1009.

[52] International Organization for Standardization: ISO 4695 - Iron ores - Determination of reducibility (1995).

[53] International Organization for Standardization: ISO 4696-1 - Iron ores for Blast Furnace Feedstocks - Determination of low-temperature reduction-disintegration indices by static method (2007).

[54] International Organization for Standardization: ISO 4696-2 - Iron ores for Blast Furnace Feedstocks - Determination of low-temperature reduction-disintegration indices by static method (2007).

[55] International Organization for Standardization: ISO 11257 - Iron ores – Determination of disintegration and metallization of feedstock for direct reduction by gas reforming process (1998).

[56] International Organization for Standardization: ISO 13930 - Iron ores for blast furnace feedstocks – Determination of low-temperature reduction-disintegration indices by dynamic method (2007).

[57] Studiengesellschaft für Erzaufbereitung (SGA): Anforderungen an Einsatzmaterial (1997).

[58] Hayashi, S. and Y. Iguchi: Abnormal swelling during reduction of binder bonded iron ore pellets with CO-CO_2 gas mixtures, ISIJ International 43 (2003), 9, 1370–1375.

[59] Siemens VAI Metals Technologies: Interne Betriebsdaten: Rohstoffkennwerte.

[60] Kumar, M. and S.K. Patel: Assessment of reduction behaviour of hematite iron ore pellets in coal fines for application in sponge ironmaking, Mineral Processing and Extractive Metallurgy Review 30 (2009), 3, 240–259.

[61] Geerdes, M., H. Toxopeus and Vliet,C. van der: Modern blast furnace ironmaking: an introduction, Second Edition, IOS Press, Amsterdam (2009).

[62] Pohl, W.L.: Economic Geology Principles and Practice: Metals, Minerals, Coal and Hydrocarbons - Introduction to Formation and Sustainable Exploitation of Mineral Deposits, Wiley-Blackwell, Oxford, UK (2011).

[63] Evans, A.M.: Ore geology and industrial minerals - An introduction, 3rd ed, Blackwell Scientific Publications, Oxford, Boston (1993).

[64] Morris, R.C.: Genesis of iron ore in banded iron-formation by supergene and supergene-metamrophic processes- a conceptual model, in: K.H. Wolf (Ed.), Genesis of iron ore in banded iron-formation by supergene and supergene-metamorphic processes - a conceptual model. In: Handbook of strata-bound and stratiform ore deposits, Amsterdam, Oxford, New York, Tokyo (1985), 73–235.

[65] Morrison, A.L. and J.K. Wright: Evaluation of Raw Materials by simulation of Direct Reduction in the Shaft Furnace, Transactions ISIJ 26 (1986), 10, 858–864.

[66] Mali, H.: Evolution of minerals and structures in the Fior, Finmet and Finex processes, Internal Report, Department of Geosciences and Geophysics, Montanuniversität Leoben.

[67] Guilbert, J.M. and C.F. Park: The Geology of Ore Deposits, W.H. Freeman and Company, New York (1986).

[68] Skorianz, M.: Classification of iron ores regarding their reduction behavior in fluidized bed technologies, Dissertation, Lehrstuhl für Eisen- und Stahlmetallurgie, Montanuniversität Leoben (2012).

[69] Boswell, P.F. and R. Blanchard: Cellular structure in limonite, Economic Geology 24 (1929), 8, 791–796.

[70] Jang, K.-O. *et al.*: Chemical and mineral transformation of a low grade goethite ore by dehydroxylation, reduction roasting and magnetic separation, Minerals Engineering 60 (2014), 14–22.

[71] Loo, C.E. *et al.*: Sintering reactions between a complex Chinese iron ore concentrate and Australian ores, Trans. Inst. Min. Metall. C (England) 104 (1995), C51-116.

[72] Alkac, D. and Ü. Atalay: Kinetics of thermal decomposition of Hekimhan–Deveci siderite ore samples, International Journal of Mineral Processing 87 (2008), 3-4, 120–128.

[73] Grebe, K., H. Keddeinis and K.P. Stricker: Possibilities of Controlling Sinter Disintegration, Stahl und Eisen 104 (1984), 20, 1031–1037.

[74] Majercák, S. and T. Karwan: Theory of Sintering Fine Materials, Kosice (1998).

[75] Engel, K. *et al.*: Blast Furnace Behaviour of Various Burden Materials, Stahl und Eisen 99 (1979), 17, 891–896.

[76] Grebe, K., H. Keddienis and K.P. Stricker: Untersuchungen über den Niedertemperaturzerfall von Sinter, Stahl und Eisen 100 (1980), 17, 973–982.

[77] Hsieh, L.-H.: Effect of Raw Material Composition on the Sintering Properties, ISIJ International 45 (2005), 4, 551–559.

[78] Higuchi, K., M. Naito, M. Nakano and Y. Takamoto: Optimization of Chemical Composition and Microstructure of Iron Ore Sinter for Low-temperature Drip of Molten Iron with High Permeability, ISIJ International 44 (2004), 12, 2057–2066.

[79] Higuchi, K. *et al.*: Quality Improvement of Sintered Ore in Relation to Blast Furnace Operation, Nippon Steel Technical Report (2006), 94.

[80] Bersenev, I.S., V.I. Klein, V.I. Matyukhin and Y.G. Yaroshenko: Assessing the quality of iron-ore sinter on the basis of its chemical composition, Steel in Translation 39 (2009), 10, 843–846.

[81] Patrick, Tim R. C. and M.I. Pownceby: Stability of Silico-Ferrite of Calcium and Aluminum (SFCA) in Air–Solid Solution Limits between 1240 °C and 1390 °C and Phase Relationships within the Fe_2O_3-CaO-Al_2O_3-SiO_2 (FCAS) System, Metallurgical and Materials Transactions B 33 (2002), 79–89.

[82] Fröber, J., *et al.*: Eisen und Stahl, 4th ed., Carl Hanser Verlag, München, Wien (1986).

[83] Turkdogan, E.T. and R.J. Fruehan: Fundamentals of Iron and Steelmaking, in: D.H. Wakelin (Ed.), The making, shaping and treating of steel, 11th ed. (1999), 37–160.

[84] Gudenau, H.W.: Materialsammlung zum Praktikum Metallurgie, RWTH Aachen, Institut für Eisenhüttenkunde (2002).

[85] Bogdandy, L.v. and H.-J. Engell: Die Reduktion der Eisenerze: wissenschaftliche Grundlagen und technische Durchführung, Verl. Stahleisen, Düsseldorf (1967).

[86] Oeters, F.: Metallurgie Teil 1: Eisenerzeugung, Stahleisen, Düsseldorf, Germany (1982).

[87] Levenspiel, O.: Chemical Reaction Engineering - Third Edition, John Wiley & Sons (1999).

[88] Szekely, J. and J.W. Evans: A structural model for gas-solid reactions with a moving boundary, Chemical Engineering Science 25 (1970), 1091–1107.

[89] Valipour, M.S., Hashemi,M. Y. M. and Y. Saboohi: Mathematical modeling of the reaction in an iron ore pellet using a mixture of hydrogen, water vapor, carbon monoxide and carbon dioxide: an isothermal study, Advanced Powder Technology 17 (2006), 3, 277–295.

[90] Piotrowski, K. *et al.*: Topochemical approach of kinetics of the reduction of hematite to wüstite, Chemical Engineering Journal 131 (2007), 1-3, 73–82.

[91] Mondal, K. *et al.*: Reduction of iron oxide in carbon monoxide atmosphere reaction controlled kinetics, Fuel Processing Technology 86 (2004), 1, 33–47.

[92] Mairhofer, S. and C. Brunnbauer: Kinetik der Reduktion von Wüstit zu Eisen am Beispiel eines stückigen Hämatiterzes, Bachelorarbeit, Lehrstuhl für Eisen- und Stahlmetallurgie, Montanuniversität Leoben (2013).

[93] Weiss, B.: Kinetics of iron fines reduction under fluidized bed conditions at elevated pressures, Dissertation, Technische Universität Wien, Institut für Verfahrenstechnik, Umwelttechnik und Technische Biowissenschaften, Wien (2008).

[94] Habermann, A.: Kinetik der Eisenerzreduktion in der Wirbelschicht, Dissertation, Technische Universität Wien Institut für Verfahrenstechnik, Umwelttechnik und Technische Biowissenschaften, Wien (2001).

[95] Krammer, G.: Gas-Feststoffreaktionen am Einzelteilchen (AK), Vorlesungsunterlagen, Technische Universität Graz, Austria (1998).

[96] Habermann, A. *et al.*: An experimental study on the kinetics of fluidized bed iron ore reduction, ISIJ International 40 (2000), 10, 935–942.

[97] Noguchi, D. *et al.*: Kinetics of Reduction Step of Wustite to Iron of Hematite and Quaternary Calcium Ferrite Mixtures, ISIJ International 53 (2013), 8, 1350–1357.

[98] Gebel, U.J.: Einfluss von Fremdphasen auf das Ausscheidungsverhalten von Eisen während der Reduktion von Eisenoxid, Fakultät für Bergbau, Hüttenwesen und Geowissenschaften der Rheinisch-Westfälischen Technischen Hochschule Aachen (1989).

[99] Gudenau, H.W., H.-P. Eisen, Y. Qi and G. Steinbeck: Sticking von Feinerz in der Wirbelschicht zur Schmelzreduktion, Stahl und Eisen 111 (1991), 9, 47–52.

[100] Schuster, S.H.: Reaktionskinetik von Hämatit mit H2-reichen Gasgemischen in der Wirbelschicht bei hohem Druck, Dissertation, Technische Universität Wien, Fakultät für Technische Chemie, Wien (2007).

[101] Weiss, B., *et al.:* Comparisation of the Reduction Kinetics of Hematite with CO-rich and H2-rich Gases at Elevated Pressures, Conference Proceedings of STEELSIM Graz/Seggau, Austria (2007), 19-24.

[102] Fang, J.: Stickingprobleme im Fluidatbett zur Schmelzreduktion, Dissertation, Fakultät für Bergbau, Hüttenwesen und Geowissenschaften der Rheinisch-Westfälischen Technischen Hochschule Aachen (1988).

[103] Degel, R.: Eisenerzreduktion in der Wirbelschicht mit wasserstoffreichen Gasen - Sticking und Ansatzbildung, Dissertation, Technische Hochschule Aachen (1996).

[104] Gudenau, H.W., J. Hochhaus and R. Degel: Stickingerscheinungen während der Reduktion von Eisenerzen in der Wirbelschicht, 9. Aachener Stahlkolloquium (ASK) (1994), 115-124.

[105] Wezel, W. and H.W. Gudenau: Das Sticking bei der Fluidatbettreduktion von Eisenerzen - Der Einfluß der Ausscheidungsart des Eisens, Aufbereitungstechnik (1972), 9, 568–572.

[106] Pawlik, C. *et al.*: Reduction of Iron Ore Fines with CO-rich Gases under Pressurized Fluidized Bed Conditions, ISIJ International 47 (2007), 2, 217–225.

[107] Ananth, V., S.C. Sircar and S.K. Bose: Reduction Kinetics of Dense Wustite at 1073K in CO-CO_2 Gas Mixtures Under Impressed D.C. Current and Under Short-Circuiting, Transactions of the Japan Institute of Metals 26 (1985), 2, 134–143.

[108] vom Ende, H. and K. Grebe: Das Verhalten von Hochofeneinsatzstoffen bei der Reduktion, Stahl und Eisen 92 (1972), 7, 303–314.

[109] Bahgat, M., K.S. Abdel Halim, H.A. El-Kelesh and M.I. Nasr: Metallic iron whisker formation and growth during iron oxide reduction: K_2O effect, Ironmaking & Steelmaking 36 (2009), 5, 379–387.

[110] Pan, W. and Z.J. Ma et al.: Effect of Na_2O on the Reduction of Fe_2O_3 Compacts with CO/CO_2, Metallurgical and Materials Transactions B 43 (2012), 6, 1326–1337.

[111] Kang, H.W., W.S. Chung and T. Murayama: Effect of iron ore size on kinetics of gaseous reduction, ISIJ International 38 (1998), 2, 109–115.

[112] Bradshaw, A.V. and A.G. Matyas: Structural Changes and Kinetics in the Gaseous Reduction of Hematite, Metallurgical Transaction B 7 (1976), 81–87.

[113] Ünal, A. and A.V. Bradshaw: Rate Processes and Structural Changes in Gaseous Reduction of Hematite Particles to Magnetite, Metallurgical Transaction B 14 (1983), 743–752.

[114] Kang, H.W., W.S. Chung, T. Murayama and Y. Ono: Effect of iron ore shape on gaseous reduction rate, ISIJ International 38 (1998), 11, 1194–1200.

[115] Bernasowski, M.: Theoretical Study of the Hydrogen Influence on Iron Oxides Reduction at the Blast Furnace Process, steel research int. 84 (2013).

[116] Loo, C.E. and N.J. Bristow: Properties of iron bearing materials under simulated blast furnace indirect reduction conditions. Part I: Review and experimental procedure, Ironmaking and Steelmaking 25 (1998), 3, 222–232.

[117] Loo, C.E. and N.J. Bristow: Properties of iron bearing materials under simulated blast furnace indirect reduction conditions Part II: Reduction degradation, Ironmaking and Steelmaking 25 (1998), 4, 287–295.

[118] Loo, C.E. and N.J. Bristow: Properties of iron bearing materials under simulated blast furnace indirect reduction conditions Part III: Reducibility, Ironmaking and Steelmaking 25 (1998), 5, 366–373.

[119] voestalpine Stahl Linz: Interner Forschungsbericht (1998).

[120] Hanel, M.B. *et al:* Characterization of burden material for ironmaking by means of reduction tests with morphological characterization, Proceedings of the 4th ISIJ-VDEh Seminarand the 8th Japan-Nordic Countries Joint Symposium on Science and Technology, Osaka, Japan (2013).

[121] Hanel, M.B. *et al:* Characterization of Different Lump Ore Brands According to Industrial Scale Process Conditions by Means of Reducibility Testing and Morphological Investigation, Proceedings of the AISTech, May 6th-10th, Pittsburgh, USA (2013).

[122] Skorianz, M. *et al.:* Classification of fine ores regarding their reducibility with tests in a lab scale fluidized bed reactor and petrographical analysis, Proceedings of the AISTech, May 7th-10th, Atlanta, USA, (2012).

[123] Kain-Bückner, B., H. Mali and B. Spuida: Valuation and Optimization of Metallurgical Raw Materials, Internal Report, Montanuniversität Leoben (2012).

[124] Loo, C.E.: A Perspective of Goethitic Ore Sintering Fundamentals, ISIJ International 45 (2005), 4, 436–448.

[125] Higuchi, K. and R.H. Heerema: Influence of Artificially Induced Porosity on Strength and Reduction Behavior of Hematite Compacts, ISIJ International 45 (2005), 4, 574–581.

[126] Ono, H., Y. Dohi, Y. Arikata and T. Usui: Effect of mineral composition and pore structure on reducibility of composite iron ore sinter, ISIJ International 49 (2009), 5, 722–728.

[127] Ono-Nakazato, H., Y. Tsubone and T. Usui: Gaseous reduction behavior of powdered iron ore sinter and analysis on the basis of Rist model for fixed bed, ISIJ International 42 (2002), 5, 482–488.

[128] Bhagat, R.P., U.S. Chattoraj and S.K. Sil: Porosity of Sinter and Its Relation with the Sintering Indices, ISIJ International 46 (2006), 11, 1728–1730.

[129] Maeda, T. and Y. Ono: Experimental Study on the Relation Between Microstructures of Constituent Minerals and Pores and Reducibility of Sinter, Tetsu-to-Hagane 72 (1986), 7, 775–782.

[130] Skorianz, M. *et al.:* Mineralogical and structural evolution of iron ore fines reduced in a lab scale fluidized bed reactor, 6th International Congress on the Science and Technology of Ironmaking, Oct. 18th, Rio de Janeiro, Brazil (2012).

[131] Higuchi, K. and R.H. Heerema: Influence of sintering conditions on the reduction behaviour of pure hematite compacts, Minerals Engineering 16 (2003), 5, 463–477.

[132] Cores, A. *et al.*: Relationship between sinter properties and iron ore granulation index, Ironmaking & Steelmaking 39 (2012), 2, 85–94.

[133] Cores, A. *et al.*: The Influence of Different Iron Ores Mixtures Composition on the Quality of Sinter, ISIJ International 50 (2010), 8, 1089–1098.

[134] Umadevi, T. *et al.*: Optimization of Firing Temperature for Hematite Pellets, ISIJ International 53 (2013), 9, 1673–1682.

[135] Umadevi, T. *et al.*: Effect of Iron Ore Pellet Size in its Properties and Microstructure, Steel research international 80 (2009), 10, 709–716.

[136] Umadevi, T., P.C. Nelson, M. Prabhu and M. Ranjan: Influence of magnesia on iron ore sinter properties and productivity, Ironmaking & Steelmaking 36 (2009), 7, 515–520.

[137] Yadav, U.S., B.D. Pandey, B.K. Das and D.N. Jena: Influence of magnesia on sintering characteristics of iron ore, Ironmaking & Steelmaking 29 (2002), 2, 91–95.

[138] Matsumura, M., M. Hoshi and T. Kawaguchi: Improvement of Sinter Softening Property and Reducibility by Controlling Chemical Compositions, ISIJ International 45 (2005), 4, 594–602.

[139] Wyderko, M. and E. Mazanek: Zur Optimierung der Eigenschaften von Eisenerzsintern Arch. Eisenhüttenwesen 47 (1976), 8, 457–463.

[140] Malysheva, T.Y. and Y.S. Yusfin *et al.*: Mechanism of mineral formation and metallurgical properties of sinter of basicity 1.1-3.1 at OAO MMK, Steel in Translation 37 (2007), 2, 126–130.

[141] Hsieh, L.-H. and J.A. Whiteman: Sintering Conditions for Simulating the Formation of Mineral Phases in Industrial Iron Ore Sinter, ISIJ International 29 (1989), 1, 24–32.

[142] Grebe, K. and H. de Haas: Untersuchungen über das Ausmaß des Sinterzerfalls im Hochofen, Stahl und Eisen 102 (1982), 6, 253–260.

[143] Wu, S.-L. *et al.*: Low Temperature Reduction Degradation Characteristics of Sinter, Pellet and Lump Ore, Journal of Iron and Steel Research International 18 (2011), 8, 20–24.

[144] Murakami, T., Y. Kamiya, T. Kodaira and E. Kasai: Reduction Disintegration Behavior of Iron Ore Sinter under High H_2 and H_2O Conditions, ISIJ International 52 (2012), 8, 1447–1453.

[145] Kasai, E., W.J. Rankin, R.R. Lovel and Y. Omori: An Analysis of the Structure of Iron Ore Sinter Cake, Tetsu-to-Hagane 75 (1989), 8, 635–641.

[146] Kasai, E. and F. Saito: Differential Thermal Analysis of Assimilation and Melt-formation Phenomena in the Sintering Process of lron Ores, ISIJ International 36 (1996), 8, 1109–1111.

[147] Bartusch, H., T. Hauck and H.-G. Grabiez: Balancing and behaviour of chlorine in the Blast Furance, Stahl und Eisen 134 (2014), 1, 51-56.

[148] Ende, H.v., K. Grebe, Thomalla and G.E. Hoffman: Alkalien als Ursache von Schwell- und Zerfallsvorgängen bei der Reduktion von Eisenerzpellets, Stahl und Eisen (1970), 13, 667–676.

[149] Hsieh, L.-H. and J.A. Whiteman: Effect of Raw Material Composition on the Mineral Phases in Lime-Fluxed Iron Ore Sinter, ISIJ International 33 (1993), 4, 462–473.

[150] http://de.wikipedia.org/wiki/ISO: Internationale Organisation für Normung. downloaded: 17th Nov. 2013.

[151] International Organization for Standardization: ISO 7215 - Iron ores - Determination of relative reducibility (1995).

[152] International Organization for Standardization: ISO 11258 - Iron ores for shaft direct-reduction feedstocks — Determination of the reducibility index, final degree of reduction and degree of metallization (1995).

[153] International Organization for Standardization: ISO 7992 - Iron ores - Determination of reduction properties under load (1992).

[154] International Organization for Standardization: ISO 11256 - Iron ore pellets – Determination of clustering of feedstock for direct reduction by gas reforming (1998).

[155] International Organization for Standardization: ISO 8371 - Iron ores for blast furnace feedstocks — Determination of the decrepitation index (2007).

[156] International Organization for Standardization: ISO 4698 - Iron ore pellets for blast furnace feedstocks - Determination of the free-swelling index (2007).

[157] International Organization for Standardization: ISO 15967 - Direct reduced iron - Determination of the tumble and abrasion indices of hot briquetted iron (HBI) (2007).

[158] International Organization for Standardization: ISO 3271 - Determination of Tumble Strength (1995).

[159] DIN ISO 9277:2014-05: Bestimmung der spezifischen Oberfläche von Feststoffen durch Gasadsorption nach dem B.E.T.-Verfahren (2014).

[160] Brunauer, S., P.H. Emmett and E. Teller: Adsorption of Gases on Molecular Layers, Journal of the American Chemical Society 60 (1938), 2, 309–319.

[161] Klank, D.: Produktgestaltung in der Partikeltechnologie, Frauenhofer-IRB-Verlag, Stuttgart (2008).

[162] Lowell, S.: Characterization of porous solids and powders: Surface area, pore size, and density, 4th ed., Springer, Dordrecht, the Netherlands (2010).

[163] Jander, G., K.F. Jahr and H. Knoll: Maßanalyse - Theorie und Praxis der klassischen und elektrochemischen Titrierverfahren, 7th ed., De Gruyter (1965).

[164] Jander, G., K.F. Jahr, G. Schulze and J. Simon: Maßanalyse, 16th ed., De Gruyter, Berlin und New York (2003).

[165] International Organization for Standardization: ISO 10835 - Direct reduced iron and hot briquetted iron - sampling and sample preparation (2007).

[166] International Organization for Standardization: ISO 5416 - Direct reduced iron - Determination of metallic iron - Bromine-methanol-titrimetic method (2006).

[167] Turkdogan, E.T.: Blast Furnace Reactions, Metallurgical Transaction B 9B (1978), 2, 163–179.

A Appendix

A-1 List of Figures

Figure 1-1: Worldwide production of crude steel, hot metal and DRI/HBI [1,2] 3

Figure 1-2: Iron making routes [3] 4

Figure 2-1: Schematic picture of a blast furnace [16] 7

Figure 2-2: Classification of direct reduction processes [11] 8

Figure 2-3: Flow sheet of the MIDREX®-process [31] 9

Figure 2-4: Classification of smelting reduction process routes [11] 10

Figure 2-5: Schematic picture of the COREX®-process [9] 10

Figure 2-6: Different aspects of ferrous burden distribution [1,2,44,46] 11

Figure 3-1: Light microscopic picture of a hematitic ore (a) and detail picture (b) 22

Figure 3-2: Light microscopic picture of magnetitic ore (a) and detail picture (b) 22

Figure 3-3: Picture of partly martitized magnetite (a) and fully transformed hematite (martite) (b) 23

Figure 3-4: Mixture of limonite (grey) and hematite (light grey) 23

Figure 3-5: Light microscopic picture of a typical pellet structure, hematite grains with intercrystalline slag phase (glass) and pores 24

Figure 3-6: Different phases in sinter in dependence of the basicity [73,76] 26

Figure 3-7: Typical appearance of spinel (brownish parts) within a sinter grain 27

Figure 3-8: Different types of hematite of different origins 28

Figure 3-9: Secondary hematite due to oxidation on cooling 28

Figure 3-10: Different types of calcioferrites, (a) directly grown from the meld, (b) as a result of dissolution of spinel 29

Figure 4-1: Phase diagram iron and oxygen [82] 32

Figure 4-2: Baur-Glaessner diagram for the system Fe-O-C [86] 35

Figure 4-3: Baur-Glaessner diagram for gas mixtures of H_2/H_2O (grey) and CO/CO_2 (black) 36

Figure 4-4: Different sorts of behaviour of reacting solid particles [87] 39

Figure 4-5: Concentration profiles of the solid reactant according to the progressive-conversion model (a) and the shrinking-core model (b) [87] 40

Figure 4-6: Different steps of the reduction reaction [85] (left) and gas concentration profiles for the reactions according to the shrinking-core model [87] 41

Figure 4-7: Gas concentration profile for mass transport control [87] 42

Figure 4-8: Gas concentration profiles with pore diffusion control of a non-porous solid (left) and a porous solid (right) [87] 43

Figure 4-9: Gas concentration profiles and reaction progress with chemical reaction control of a non-porous solid (left) and a porous solid (right) [87] 44

Figure 4-10: Time dependent conversion according to the different mechanisms (left) [49] and qualitative progress of reduction as a function of the reduction rate [85] (right) 45

Figure 4-11: Regions of different iron metallic iron formation [7,98] 47

Figure 5-1: Temperature dependence of the initial reduction step of hematite to wustite (left) and the final reduction step of wustite to metallic iron (right) [92,119] 49

Figure 5-2: Temperature dependence of the reduction of hematite to magnetite [111] 50

Figure 5-3: Temperature dependence of the reduction of hematite powder, reduction with CO (left), CO/H_2 mixture (middle) and H_2 (right) [41,42,90] 50

Figure 5-4: Influence of different H_2/CO rations on the reduction performance [89] 51

Figure 5-5: Grain Size dependence of the first steps of reduction of hematite to wustite (left) and final reduction step of wustite to metallic iron (right) [92,119] 52

Figure 5-6: Reducibility of different grain sizes of lump ore (upper) and sinter samples (lower) [116,117] 52

Figure 5-7: Effect of total porosity (left) and small pores (right) on the reducibility at 1000 °C [79] 53

Figure 5-8: Pore size distribution (left) and reducibility at different pore diameters [125] 53

Figure 5-9: Reducibility properties of different iron oxides [40] 54

Figure 5-10: Influence of MgO on sinter reducibility [136] 55

Figure 5-11: Influence of CaO/SiO_2 ratio on reduction degree [139] (left), reduction rate on basicity [129] (middle) and reduction degree on basicity [140] (right) 56

Figure 5-12: RDI tendencies of different raw materials [142] 56

Figure 5-13: Comparison of $RDI_{-3.15}$ of different materials at different temperatures for gas composition A (without H_2, left) and B (25 % H_2, right) [143] 57

Figure 5-14: Strength vs. porosity [125] 58

Figure 5-15: Influence of MgO on the stability at room temperature (left) [135] and TI values (middle) [135] and RDI values (right) [77] 59

Figure 5-16: Influence of phases [80] and basicity on cold strength [140] and on the mechanical performance during reduction at weak reduction potentials (RDI) [139] 59

Figure 6-1: Constitutional plan of the vertical reduction aggregate as set in the laboratory 64

Figure 6-2: Photo of the furnace and the reduction tube (left) and the gas mixing unit (right) 65

Figure 6-3: Picture and sketch of the rotating tumbling drum 66

Figure 6-4: Polished sections of a lump ore (left), pellet particles (middle) and sinter pieces (right) 67

Figure 7-1: Example of the recorded data and interpretation of characteristic values 71

Figure 7-2: Gas composition of different modified 72

Figure 7-3: Blast Furnace temperature and gas concentration profiles according to *Biswas* [8] (left) and *Gudenau* [7] (right) 73

Figure 7-4: Example for the developed temperature and gas concentration profiles 74

Figure 7-5: Testing conditions for BF profiles with different GODs 75

Figure 7-6: Baur-Glaessner diagram for gas mixtures of H_2, H_2O, CO, CO_2 with Boudouard equilibrium and reduction testing paths of BF conditions (black), DR1 (dark grey) and DR2 (light grey) 77

Figure 8-1: Light microscopic pictures of different regions of the Hematite ore 84

Figure 8-2: Light microscopic pictures of the Magnetite ore 84

Figure 8-3: Light microscopic pictures of the Limonitic ore 84

Figure 8-4: Hematite grains surrounded by glass and glass inclusions within larger crystals from Pellet Brands 1 (a) and Brand 3 (b) 85

Figure 8-5: Microstructure of a single pellet, residue of magnetite 85

Figure 8-6: Light microscopic pictures of the Pellet Brand 1 (a), Pellets Brand 2 (b) and Pellet Brand 3 (c) 86

Figure 8-7: Exemplary pictures of different phases appearing in Sinter Sample 1 and 2 87

Figure 9-1: Reduction progress of different iron ores according to ISO 4695 90

Figure 9-2: Reduction progress of different pellet brands according to ISO 4695 91

Figure 9-3: Reduction progress of different sinter samples according to ISO 4695 92

Figure 9-4: Graphical (left) and numerical (right) effect of variation of ISO 4695 93

Figure 9-5: Testing conditions within the Baur-Glaessner diagram (left) and results on reducibility as a result of different initial and final GODs (right) 94

Figure 9-6: Effect of pre-reduction step at GOD 0.46-0.10 (left) and GOD 0.54-0.10 (right) 95

Figure 9-7: Effect of hydrogen addition on the reduction performance 96

Figure 9-8: Reduction progress of the investigated iron ores at all different process conditions Hematitic ore (a), Magnetitic ore (b) and Limonitic ore (c) 98

Figure 9-9: Reduction progress of the investigated pellet brands at all different process conditions Brand 1 (a), Brand 2 (b) and Brand 3 (c) 100

Figure 9-10: Reduction progress of the investigated sinter samples at all different process conditions for Sinter 1 (a) and Sinter 2 (b) 102

Figure 9-11: Different reaction fronts at intermediate stages of reduction of a (hematitic) lump ore piece (left) and a pellet (right)....105

Figure 9-12: Morphological evolution of a hematitic ore particle during the testing procedure ISO 4695....106

Figure 9-13: Different stages of metallic iron formation depending on the distance to the surface, outer edge (a) to core part (c), Hematitic ore, RD = ±80 %....106

Figure 9-14: Different kinds of iron formation depending on the morphology of the raw ores RD = ±80 %....107

Figure 9-15: Different kinds of iron formation depending on the morphology of the raw pellets RD = ±80 %....107

Figure 9-16: Different kinds of metallic iron formation depending on the initial phases within sinter....108

Figure 9-17: Formation of metallic iron whiskers at lower final GOD of 0.28, hematitic ore, RD = ± 37 %....109

Figure 9-18: Different types of metallic iron formation depending on the surface distance, comparison between BF1 (a-c) and DR1 (d-f) testing conditions, Pellet Brand 1....109

Figure 9-19: Magnetitic ore reduced at the absence of H_2 (left) and at DR1 conditions (25 % H_2, right)....110

Figure 9-20: Qualitative progress of reduction rate for different rate determining steps [85]....111

Figure 9-21: Reduction curves as a result of the standardized testing procedure (left column) and derived qualitative progress of reduction rate (right column) for iron ores (top row), pellet brands (intermediate) and sinter samples (bottom)....112

Figure 10-1: Comparison of the reduction performance $(dR/dt)_{40}$ of the investigated iron ores....115

Figure 10-2: Reduction performance $(dR/dt)_{40}$ of the investigated pellet brands....116

Figure 10-3: Correlation between slag amount (left) and basicity (right) and the reduction rate of the investigated Sinter Samples....117

Figure 10-4: Reduction performance $(dR/dt)_{40}$ of Sinter Sample 1 and 2....118

A-2 List of Tables

Table 1-I: Classification of the most common iron making process routes: 5

Table 2-I: Guidelines for the requirements of different burden material for different process routes 18

Table 3-I: Excerpt of the various occurring iron minerals [10,47,64–67] 21

Table 4-I: RD and MD of different iron oxide phases 36

Table 5-I: Reducibility properties of different mineral phases [85,139] 55

Table 5-II: Summary of influencing parameters of reducibility and mechanical properties 60

Table 5-III: Standardized testing procedures for determining reducibility parameters 62

Table 5-IV: Standardized testing procedures for different mechanical parameters 62

Table 6-I: Technical data of the vertical reduction aggregate 65

Table 7-I: Gas composition of modified ISO 4695 testing procedures 72

Table 7-II: Gas compositions at every stage of the different BF testing conditions 75

Table 7-III: Gas compositions at every stage of the different BF testing conditions (including H_2) 75

Table 7-IV: Gas compositions and GODs at different stages for all process related testing conditions. 76

Table 8-I: Chemical composition, specific surface and basicity of the raw materials investigated 81

Table 8-II: Different appearing phases within the structure of the different raw materials 83

Table 9-I: Reducibility and mechanical characteristics according to ISO 4695 92

Table 9-II: Reducibility characteristics of different iron ores at industrial scale process conditions 99

Table 9-III: Reducibility characteristics of different pellet brands at industrial scale process conditions 100

Table 9-IV: Reducibility characteristics of different sinter samples at industrial scale process conditions 102

Table 9-V: Mechanical properties after industrial scale process conditions 104

Table 9-VI: Description of different phases in reduced samples 105

A-3 Publications

Contribution to journals and conference proceedings

Hanel, M.B., H. Mali, J.L. Schenk, H. Mali, F. Hauzenberger, H. Stocker, and C. Thaler: Reducibility of Hematitic Lump Ore at different near Blast Furnace Conditions, 1st ESTAD and 31st JSI, Paris, France (2014).

Hanel, M.B, H. Mali, C. Thaler, H. Stocker, F. Hauzenberger, M. Skorianz, and J.L. Schenk: Characterization of burden material for ironmaking by means of reduction tests with morphological characterization, The ISIJ-VDEh-Jernkontoret Joint Symposium, Osaka, Japan (2013), 145 – 153.

Hanel, M.B, M. Skorianz, J.L. Schenk, H. Mali, F. Hauzenberger, H. Stocker, and C. Thaler: Characterization of Different Lump Ore Brands According to Industrial Scale Process Conditions by Means of Reducibility Testing and Morphological Investigation, AISTech, Pittsburgh, USA (2013), 447 – 456.

Kain-Bückner, B., H. Mali, M.B. Hanel, J.L. Schenk, F. Hauzenberger, H. Stocker and C. Thaler: Charakterisierung von Rohmaterialien für die Eisenerzherstellung mit Bildverarbeitung, BHM - Berg- und hüttenmännische Monatshefte 158 (2013), 11, 445 - 446.

Rantitsch, G., J.L Schenk, K. Lünsdorf, A. Bhattacharyya, M.B. Hanel, D. Wallner and H. Kaltenböck: Structural Characterization of Metallurgical Coke by Raman Spectroscopy, BHM - Berg- und hüttenmännische Monatshefte, 158 (2013), 11, 447 - 448.

Skorianz, M., H. Mali, J.L. Schenk, J.F. Plaul, A. Pichler and M.B. Hanel: Mineralogical and structural evolution of iron ore fines reduced in a lab scale fluidized bed reactor, 6th International Congress on the Science and Technology of Ironmaking – ICSTI, Rio de Janeiro, Brasil (2012), 2347 – 2359.

Skorianz, M.; H. Mali, J.L. Schenk, J.F. Plaul, B. Weiss, and M.B. Hanel: Evaluation of reducibility of iron ore fines by reduction tests under fluidized bed conditions and petrographical investigations, Asia Steel Conference, Beijing, China (2012).

Contribution at conferences and scientific boards

Hanel, M.B., H. Mali, J.L. Schenk, H. Mali, F. Hauzenberger, H. Stocker, and C. Thaler: Reducibility of Hematitic Lump Ore at different near Blast Furnace Conditions, 1st ESTAD and 31st JSI, Paris, France (2014), April 7-8th,

Hanel, M.B.: Characterization of iron carriers for use in reduction processes, K1-MET Scientific Exchange Day, Leoben, Austria (2014), March 10th.

Hanel, M.B, M. Skorianz, and J.L. Schenk: Characterization of Different Lump Ore Brands According to Industrial Scale Process Conditions by Means of Reducibility Testing and Morphological Investigatio,. AISTech, Pittsburgh, USA (2013) May 6th-8th.

Hanel, M.B, M. Skorianz and J.L. Schenk: Characterization of burden material for ironmaking by means of reduction tests with morphological characterization, The ISIJ-VDEh-Jernkontoret Joint Symposium, Osaka, Japan (2013), April 15th-16th.

Hanel, M.B and M. Skorianz: Development of methods for the evaluation of iron ore reduction behavior for the optimization of ironmaking processes, European Mineral Resources Conference EUMICON, Austria, Leoben (2012), September 19th-21st.

Hanel, M.B: Characterization of the reducibility / disintegration of lump iron ore carriers, K1-MET Scientific Exchange Day, Vienna, Austria (2011), March 19th.

Research reports (not accessible)

Skorianz, M. and M.B. Hanel: Reduction properties of pellets composed of siderite-manganese ore, Chair of Metallurgy, Montanuniversitaet Leoben, Austria (2013).

Hanel, M.: Bewertung der Reduzierbarkeit und Zerfallsstabilität von unterschiedlichen Phasen in stückigem Erzmöller - Endbericht der ersten Förderphase K1-MET, Chair of Metallurgy, Montanuniversitaet Leoben, Austria (2012).

Hanel, M.: Reduction properties of iron, titanium and vanadium containing ore from EVRAS Highveld Steel and Vanadium, Chair of Metallurgy, Montanuniversitaet Leoben, Austria (2012).

Hanel, M.: Reduktionseigenschaften von Pellets mit unterschiedlichen Mengen an Rücklaufstoffen, Chair of Metallurgy, Montanuniversitaet Leoben, Austria (2012).

Schmidt, L., M.B. Hanel, M. Skorianz and J.L. Schenk: The Optimization of Fluidized Bed Reducing Reactor and Technology for the Use of Ultra-Fine Ores for FINEX®-Process - Interim Report, Chair of Metallurgy, Montanuniversitaet Leoben, Austria (2012).

Thaler, C., M. Skorianz, M.B. Hanel and J.L Schenk: Final Report – Enhancement of Competitiveness of the FINEX® -Technology - Phase 2, Chair of Metallurgy, Montanuniversitaet Leoben, Austria (2011).

A-4 Curriculum Vitae

Personal Information:

Name	Dipl.-Ing. Martina Hanel
Address	Barbaraweg 33 A-8700 Leoben
Phone	0043 (0) 664 59 37 754
E-Mail	martina.hanel@unileoben.ac.at
Date and place of birth:	January 8th, 1985, Leoben
Nationality:	Austria

Education:

2010-2014	**Doctoral Thesis**, Chair of Ferrous Metallurgy *"Characterization of Ferrous Burden Material for Use in Ironmaking Technologies"* (June 2014)
2003-2009	Academic studies at the Montanuniversitaet Leoben, Bachelor and Masterstudy Metallurgy; Master program: Specialization in Iron- and Steelmetallurgy, Casting Resaearch and Non-ferrous Metallurgy **Master Thesis**, Chair of Ferrous Metallurgy: *"Investigation of crack formation during initial solidification of Fe-Ni and Fe-Ni-Cr alloys"* (Sept. 2009) **2nd Bachelor Thesis**, Chair of Ferrous Metallurgy: *"Determination of secondary dendrite arm spacing for steels with varying carbon contents"* (Oct. 2007, Presented at the International Students' Day of Metallurgy in Freiberg in 2008) **1st Bachelor Thesis**, Chair of Non-Ferrous Metallurgy: *"Behaviour of the accompanying elements in the copper pyrometallurgy"* (Sept. 2008)
June 2003	Higher School Certificate**,** passed with distinction
1995-2003	Grammar School, BG/BRG Leoben Neu, Moserhofstraße 7a, 8700 Leoben
1991-1995	Elementary School in Leoben

Work Experience:

2010-today	**Research Assistant**, Montanuniversitaet Leoben, Chair of Ferrous Metallurgy, Working group "Primary Metallurgy"; Doctoral Thesis within the K1-MET metallurgical competence centre and in collaboration with the industrial partners Siemens VAI Metals Technologies GmbH, voestalpine Stahl GmbH and voestalpine Stahl Donawitz GmbH
2009-2010	**Research Assistant**, Montanuniversitaet Leoben, Chair of Ferrous Metallurgy, Working group "Continuous Casting": various projects in collaboration with different industrial partners

2006-08 Internship voestalpine Stahl Donawitz GmbH (Steel plant, Ladle furnace)

2003-05 Internship Austria Systeme und Technologie (AT&S)

Additional Skills and Information:

Languages:
German: Mother tongue
English: Fluent
French: Basic knowledge

IT-skills: MS Office, Corel Draw, AutoCad, LATEX, Clemex Vision, Origin

Memberships:
ASMET (Austrian Society for Metallurgy and Materials)
AIST (Association for Iron and Steel Technologies)

Awards: Poster publication on the „ASMET - Forum für Metallurgie und Werkstofftechnik“, Leoben Austria, 2009 (1st place)

Steelmaking Challenge on the 15th international students‘ day of metallurgy, Freiberg, Germany, 2008 (2nd place)

Leoben, May 14th, 2014